ЖУРНАЛ
ЭКСПЕРИМЕНТАЛЬНОЙ И ТЕОРЕТИЧЕСКОЙ
ФИЗИКИ
АКАДЕМИЯ НАУК СССР

SOVIET PHYSICS

JETP

VOLUME 5 NUMBER 1

A Translation

of the

Journal of Experimental and Theoretical Physics

of the

Academy of Sciences of the USSR

Volume 32

AUGUST, 1957

Published by the

AMERICAN INSTITUTE OF PHYSICS

INCORPORATED

SOVIET PHYSICS
JETP

A translation of the Journal of Experimental and Theoretical Physics of the USSR.

A publication of the

AMERICAN INSTITUTE OF PHYSICS

SOVIET PHYSICS is a monthly journal published by the American Institute of Physics for the purpose of making available in English reports of current Soviet research in physics as contained in the Journal of Experimental and Theoretical Physics of the Academy of Sciences of the USSR. The page size of SOVIET PHYSICS will be 7⅛" x 10¼", the same as other Institute journals.

Transliteration of the names of Russian authors follows the system employed by the Library of Congress.

This translating and publishing project was undertaken by the Institute in the conviction that dissemination of the results of researches everywhere in the world is invaluable to the advancement of science. The National Science Foundation of the United States encouraged the project initially and is supporting it in large part by a grant.

The American Institute of Physics and its translators propose to translate faithfully all the material in the Journal of EXPERIMENTAL AND THEORETICAL PHYSICS OF THE USSR appearing after January 1, 1955. The views expressed in the translated material, therefore, are intended to be those expressed by the original authors, and not those of the translators nor of the American Institute of Physics.

Two volumes are published annually, each of six issues. Each volume contains the translation of one volume of the Journal of EXPERIMENTAL AND THEORETICAL PHYSICS OF THE USSR. New volumes begin in February and August.

Subscription Prices:

Per year (12 issues)

United States and Canada	$60.00
Elsewhere	64.00

Back Numbers

Single copies	$ 6.00

Subscriptions should be addressed to the American Institute of Physics, 335 East 45th Street, New York 17, New York.

SOVIET PHYSICS

JETP

A translation of the Journal of Experimental and Theoretical Physics of the USSR.

SOVIET PHYSICS—JETP VOL. 5, NO. 1, PP 1-155 AUGUST, 1957

Investigation of the (γ, p) Reaction in Zinc

R. M. OSOKINA AND B. S. RATNER

The P. N. Lebedev Physical Institute of the Academy of Sciences USSR

(Submitted to JETP editor June 1, 1956)

J. Exptl. Theoret. Phys. (U.S.S.R.) **32**, 20-26 (January, 1957)

Measurements of the yield and angular and energy distribution of photoprotons emitted from zinc have been carried out at various bremsstrahlung peak energies ranging from 19.8 to 30.7 mev. The results are compared with the statistical theory of nuclear reactions and with the direct photoeffect model. The data obtained with zinc confirm the conclusions regarding the significance of a direct photoeffect and of the influence of shells for nuclei with $Z \sim 30$.

1. INTRODUCTION

THE present work continues the investigation of photoprotons emitted by different nuclei under the action of synchrotron bremsstrahlung with γ-ray energies up to 30 mev[1-3].

As is well known, deviations from the statistical theory in the investigation of photonuclear reactions have been observed in a number of papers (Refs. 4-6 and others). In the investigation of the (γ,p) reaction in copper[1] and in nickel[2] a number of additional facts were discovered which contradict the idea of evaporation of particles from the compound nucleus. These results were qualitatively explained by assuming a direct interaction of the γ-quanta with the individual nucleons in the nucleus (the so-called "direct" photoeffect) with the shell structure of the nucleus taken into account.

In accordance with the shell model[7], the zinc nucleus has a structure analogous to the copper nucleus, with the only difference that outside the filled $4f_{7/2}$ level containing 8 protons, the zinc nucleus in the $3P_{3/2}$ state contains not one but two protons. Therefore, it was expected that investigations carried out with zinc would confirm the sharp change in the proton distribution accompanying a small increase in $E_{\gamma m}$ obtained in the case of copper and explained by assuming that the photoeffect from the $4f_{7/2}$ level begins to be important.

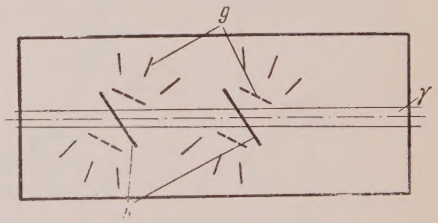

FIG. 1. Positioning of the plates. g – photo plates, h – targets, dotted lines indicate the position of the plates for the measurement of proton yield.

2. THE METHOD OF MEASUREMENT

The experimental method has been described in detail in Ref. 1. The protons were recorded in thick nuclear emulsions NIKFI Ia-2 400μ in thickness. The placing of the plates is shown in Fig. 1. The construction of the chamber in which the plates were situated was altered slightly in order to improve the positioning of the plates and the placement of the chamber with respect to the γ-ray beam. In order to remove soft electrons from

the beam permanent magnets were installed inside the chamber. The proton background was measured with the target removed from the chamber. It was of significant amount (5-10%) in only two plates which were nearest to the γ-beam. In the other plates the proton background did not exceed 1%. The background is primarily due to protons with energies up to 5-6 mev. The target was in the form of a foil of chemically pure zinc of 25 mg/cm^2 in thickness. The energy losses in the half thickness of the target were calculated in accordance with Ref. 8. The emulsions were treated by the dry temperature method using the standard amidol developer. The plates were scanned by means of binocular microscopes MBI-2 with a magnification of 630X. In scanning the plates proton tracks were selected corresponding to proton energies $\epsilon_p \geq 3.0$ mev which started at the surface of the emulsion and proceeded in the required direction. The complete energy spectrum was measured in only two irradiations at energies $E_{\gamma m} = 20.8$ and 28.6 mev. In all the other cases only the energy of the fast protons with $\epsilon_p \geq 9$ mev was determined. The proton energy was determined from the range-energy curve for the Ilford C-2 emulsion[9], which is permissible because of the similarity in the composition of the emulsions NIKFI Ia-2 and Ilford C-2. No identification of deuteron tracks was made.

The dosage was recorded by means of an integrating ionization monitoring chamber. The monitor was calibrated by means of a thickwalled ionization chamber whose sensitivity was calculated according to the data of Ref. 10. The photon spectrum was found in accordance with Ref. 11 taking into account absorption in the walls of the accelerating chamber.

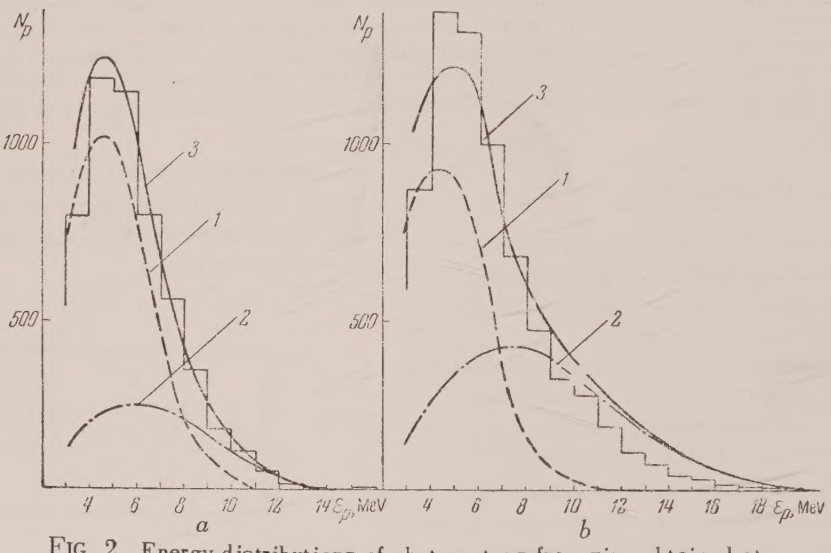

FIG. 2. Energy distributions of photoprotons from zinc obtained at energies $E_{\gamma m}$: *a* – 20.8 mev and *b* – 28.6 mev. *1* – spectra calculated according to evaporation theory; *2* – spectra calculated according to the direct photoeffect model[14] taking shells into account; *3* – the sum of curves 1 and 2.

3. EXPERIMENTAL RESULTS

Figure 2 shows the energy spectra integrated over the angles θ of the photoprotons with energies $\epsilon_p \geq 3$ mev from zinc, obtained at energies $E_{\gamma m} = 20.8$ and 28.6 mev. Curve 1 for $E_{\gamma m} = 20.8$ mev is normalized in accordance with the data on angular distribution on the assumption that its isotropic part (75%) is due to evaporation. For $E_{\gamma m} = 28.6$ mev, the normalization was carried out on the basis of the calculated dependence on $E_{\gamma m}$ of the yield of evaporated protons. The areas under curve 3 and under the experimental histogram are equal. The calculated curves include a correction for finite target thickness. Figure 3 shows energy distributions of photoprotons with energies $\epsilon_p \geq 9$ mev measured for various values of $E_{\gamma m}$. Figure 4 shows the angular distributions of photoprotons with energies $\epsilon_p \geq 3$ and $\epsilon_p \geq 9$ mev. The dependence of the yield

of protons with $\epsilon_p \geq 3$ mev on the maximum γ-ray energy $E_{\gamma m}$ is shown in Fig. 5. The proton yield is normalized to the same ionization in a thick-walled ionization chamber. Figure 6a shows the analogous dependence for photoprotons with $\epsilon_p \geq 9$ mev. obtained by multiplying the yield of protons with $\epsilon_p \geq 3$ mev (Fig. 5) by the ratio of the number of protons with $\epsilon_p \geq 9$ mev to the number of protons with $\epsilon_p \geq 3$ mev, taking the angular distribution into account. The errors shown in the Figures are statistical. Figure 6b shows the cross-section

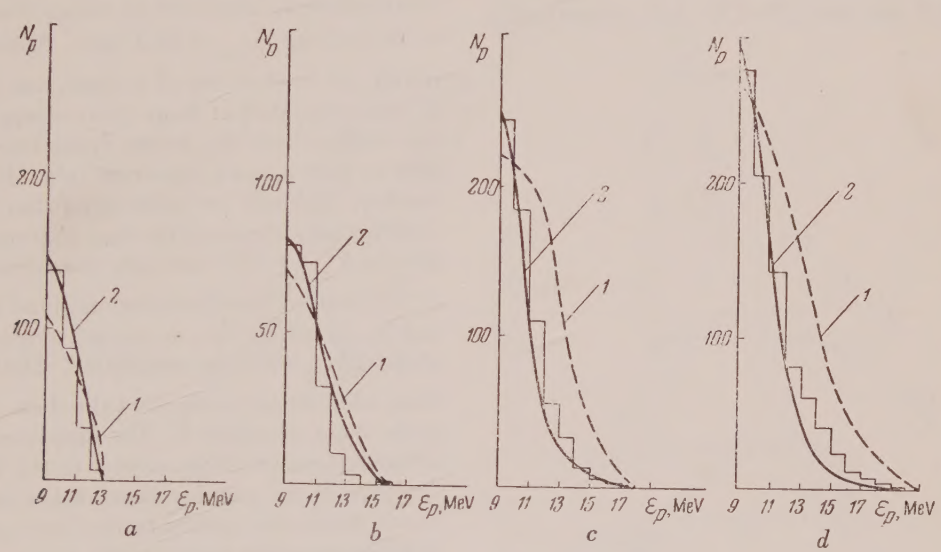

FIG. 3. Energy distributions for protons with energies $\epsilon_p \geq 9$ mev from zinc obtained at $E_{\gamma m}$: a – 20.8; b – 23.3; c – 26.1 and d – 28.6 mev. The spectra have been calculated using the direct photoeffect model taking shells into account and utilizing: *1* – the cross sections from Ref. 14, *2* – the experimental cross-section.

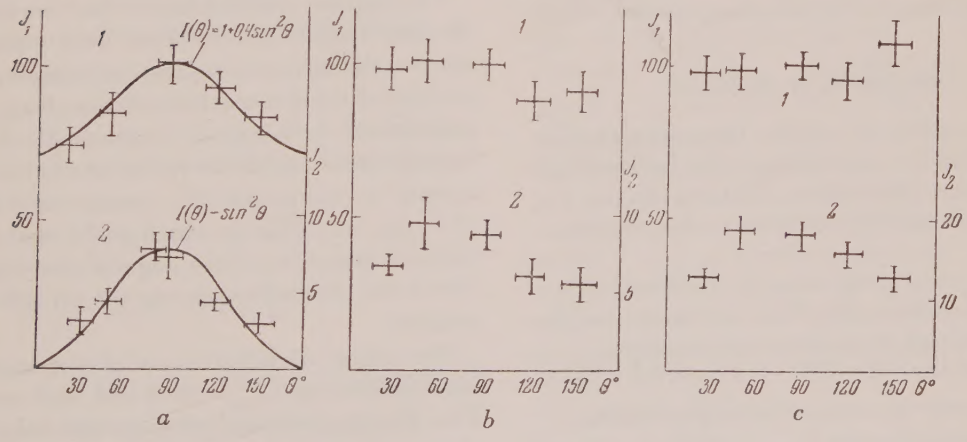

FIG. 4. Angular distributions of photoprotons from zinc obtained at energy values $E_{\gamma m}$: a – 20.8, b – 23.3 and c – 28.6 mev. I_1 and I_2 are the relative numbers of protons per unit solid angle for protons: *1* – with energies $\epsilon_p \geq 3$ mev, *2* – with energies $\epsilon_p \geq 9$ mev.

for the production of photoprotons with $\epsilon_p \geq 9$ mev calculated from the yield curves by the "photon difference" method[12]. An estimate of the integrated cross-section for the emission of photoprotons with energy $\epsilon_p \geq 3$ mev from zinc gives a value equal to 0.46 mev · barn. The ratios for the photoproton yield from zinc, copper and nickel at $E_{\gamma m} = 25.5$ mev are 1.5: 1.0: 1.7, respectively.

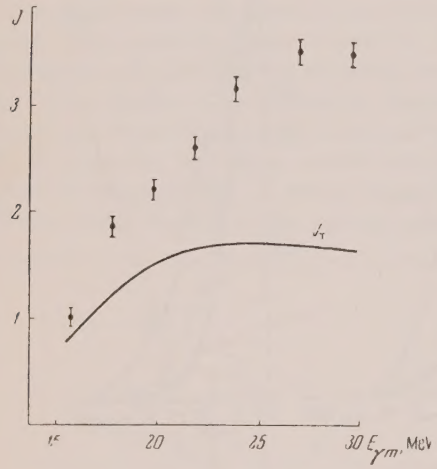

FIG. 5. Dependence on $E_{\gamma m}$ of the yield of photoprotons with energies $\epsilon_p \geq 3$ mev from zinc. I_T is the curve calculated according to evaporation theory and normalized according to the data on angular distribution on the assumption that at $E_{\gamma m} = 20.8$ mev the isotropic part of the yield (75%) is determined by evaporation. I is the yield in relative units reduced to the same ionization in a thick-walled ionization chamber.

4. DISCUSSION OF RESULTS

In the discussion of results, the most attention was devoted to the data obtained for fast protons since the direct photoeffect of interest to us should be particularly prominent in this energy region.

An examination of the angular distributions of photoprotons from zinc (Fig. 4) shows that a marked anisotropy for protons with energies $\epsilon_p \geq 3$ mev of the form $I(\theta) \sim 1 + 0.4 \sin^2 \theta$ for $E_{\gamma m} \leq 20.8$ mev* is replaced by a practically isotropic distribution for $E_{\gamma m} \geq 23.3$ mev. For fast protons with $\epsilon_p \geq 9$ mev the angular distribution for $E_{\gamma m} \leq 20.8$ mev has the form $I(\theta) \sim \sin^2 \theta$. For energies $E_{\gamma m} \geq 23.3$ mev an appreciable isotropic component appears and the maximum in the angular distribution is displaced forward.

Thus in zinc a sharp change in the angular distribution is observed as we go from $E_{\gamma m} = 20.8$ mev to $E_{\gamma m} = 23.3$ mev. Apparently this result, as in the case of copper, can be explained by assuming that at large γ-ray energies the photoeffect from the deeper lying level $4f_{7/2}$ begins to play a more important role. In this connection, it should be pointed out that the angular distributions obtained for fast photoprotons from zinc at $E_{\gamma m} \geq 23.3$ mev are somewhat similar to the angular distributions obtained in nickel[2] and in cobalt[13], i.e., in nuclei where the filling of the $4f_{7/2}$ shell is completed. These distributions also do not contradict the data obtained in the case of copper[1]. The displacement in the forward direction with respect to $\theta = 90°$ of the maximum of the angular distribution in all these cases apparently points to the fact that, for this level, interference between the dipole and the quadrupole absorption of γ-quanta takes place.

It should be noted that in the case of zinc the anisotropy in the angular distributions of fast protons for relatively small values of $E_{\gamma m}$ is too great, just as in the case of copper, in comparison with what is predicted in Refs. 14 and 15 for the photoeffect from the P-shell.

The angular distribution of the form $I(\theta) \sim \sin^2 \theta$ obtained for fast photoprotons from copper and zinc would appear to indicate a considerable transparency of these nuclei for protons from the uppermost level. In this case, however, the following consideration should be taken into account. The transfer by the proton of a considerable amount of energy on collision which could lead to a significant distortion of the angular distribution removes the proton from among the recorded fast protons.

The energy distributions of photoprotons from zinc obtained at $E_{\gamma m} = 20.8$ and 28.6 mev (see Fig. 2) were compared with spectra calculated on the basis of the statistical theory of nuclear reactions[16], and in accordance with the direct photoeffect model proposed in Ref. 14. In making the calculations using the statistical theory it was assumed that the level density of the final nucleus depends on its excitation energy E_R in

* The angular distributions obtained for $E_{\gamma m} = 19.8$ mev which are not shown in Fig. 4 are even more anisotropic than those for $E_{\gamma m} = 20.8$ mev.

accordance with[17] $\omega(E_R) = \text{const} \cdot \exp\{(3.35 \times (A-40)^{1/2} E_R)^{1/2}\}$; $E_R = E_\gamma - \epsilon_p - B_p$ where B_p is the proton binding energy. The calculation was made for the main isotope Zn^{64}. The ratio of the binding energies of the proton and the neutron in the other isotopes is such that their contribution to the total evaporation spectrum is quite small. The binding energies for the proton B_p and for the neutron B_n in Zn^{64} were taken to be 7.7 and 11.8 mev respectively[18].

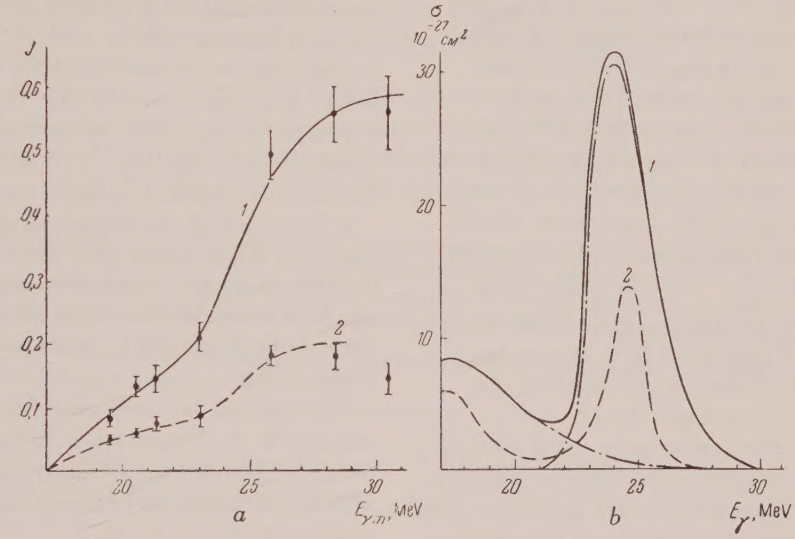

FIG. 6. *a* – dependence on $E_{\gamma m}$ of the yield of fast photoprotons from zinc; *b* – cross-section for the emission of fast protons from zinc. $1 - \epsilon_p \geq 9$, $2 - 8 \leqslant \epsilon_p \leqslant 10$ mev.

The calculation of the energy spectrum using the direct interaction model was carried out on the assumption that the protons in the nucleus are in separate levels with binding energies B_{p1}, B_{p2} etc., and that the total energy of the γ-quantum minus the binding energy is given up to the emitted proton. Transitions $l \to l-1$ and $l \to l+1$ were taken into account. The photoproton spectrum for the given isotope was found using the formula

$$N(\varepsilon_p) = \text{const} \cdot \sum_i n_i \sigma(\varepsilon_p + B_{p_i}) N_\gamma(\varepsilon_p + B_p, E_{\gamma m}) \times [g_{l_i-1} T_{l_i-1}(\varepsilon_p) + g_{l_i+1} T_{l_i+1}(\varepsilon_p)].$$

Here n_i and l_i are respectively the number of protons in the i-th level and their angular momentum in accordance with the model of filling the levels given in Ref. 7; $T_{l_i \pm 1}(\varepsilon_p)$ – the penetrability through the barrier – was calculated using the formulas given in Ref. 16; $g_{l_i \pm 1} = |2(l_i \pm 1) + 1|$ is the statistical factor; $N_\gamma(\varepsilon_p + B_{p_i}, E_{\gamma m})$ is the number of γ-quanta of energy $E_\gamma = \varepsilon_p + B_{p_i}$ in the bremsstrahlung spectrum with maximum energy $E_{\gamma m}$; $\sigma(\varepsilon_p + B_{p_i})$ is the cross-section for the direct photoeffect per nucleon taken from Ref. 14. As may be seen from Fig. 2, for $E_{\gamma m} = 20.8$ mev the experimental spectrum is well described by the sum of the theoretical curves. However, at $E_{\gamma m} = 28.6$ mev, the observed proton distribution shows a deficiency of fast and an excess of slow protons. This deviation may be explained either by assuming that as the energy of the proton increases the probability of it transferring a part of its energy to the other nucleons in the nucleus increases also, or by assuming that the dependence of the cross-section for the direct photoeffect on the energy of the γ-quanta differs from the one given in Ref. 14*. In this connection it is of interest to examine the

* It is of interest to note that a calculation of the direct photoeffect for the nucleus Mo^{100} carried out by B. N. Kalinkin (private communication) showed that the total cross-section is made up of the sum of the resonance cross-sections for individual levels.

data on the cross-section for the emission of fast protons from zinc. As may be seen from Fig. 6b the cross-section for protons with $\epsilon_p \geq 9$ mev has a sharp peak in the region of γ-quanta with energy $E_p \sim 23$-24 mev and falls off towards $E_\gamma \sim 29$-30 mev. Apparently there is also a second maximum at an energy of 17-18 mev but it is less pronounced. The cross-section curve plotted for protons with energy in the range 9-10 mev indicates more clearly the presence of two peaks in the cross-section which are most probably determined by the absorption of γ-quanta by protons in the two outer shells of the zinc nucleus. From the value of the energy of the γ-quanta at which the second rise in the cross-section for the emission of protons with $\epsilon_p \geq 9$ mev is observed it is possible to determine the position of the $4f_{7/2}$ level. The depth of this level is ~ 14 mev from which the value of ~ 6 mev is obtained for the distance between the two upper levels.

In order to check the correctness of the form of the cross-section curve, obtained from the yield curve with considerable errors, this curve was used to calculate the energy distribution of the photoprotons on the assumption of the transfer of the total energy of the γ-quantum minus the binding energy to the proton. The assumed form for the cross-section for the direct photoeffect for each of the upper levels is shown in Fig. 6b. As may be seen from Fig. 3, the spectra of fast photoprotons from zinc calculated using the experimental cross-section agree satisfactorily with the experimental spectra, while Courant's cross-section predicts a much harder proton energy spectrum.

A model for the nuclear photoeffect proposed by Wilkinson[15] has been widely discussed in recent literature. In contrast to the model of collective dipole oscillations of protons with respect to neutrons in the nucleus (Refs. 19, 20 and others), Wilkinson's model explains the "giant" resonance observed in photonuclear reactions in terms of the resonance absorption of γ-quanta by individual nucleons situated within closed shells. In this model the nucleons outside closed shells should play no essential role. However, as indicated by the angular distributions and by the cross-sections for protons obtained in the present work, and also by the results for copper[1], one or two protons in the new unfilled shell play an important role particularly for relatively low values of the energy of the γ-quanta. If the direct photoeffect were determined primarily by the closed shell then one would not expect the experimentally observed sharp change in the form of the angular distributions as the energy of the γ-quanta is varied. Also one would expect that the photoeffect in nickel, copper and zinc should not show appreciable differences.

Thus the results of studying photoprotons from zinc confirm the conclusions reached earlier that the contribution of the direct photoeffect to the proton yield from nuclei with $Z \sim 30$ represents a considerable amount (20-40%) at γ-ray energies used. It seems probable that in the above case the γ-quanta interact with protons situated within individual nuclear shells. Apparently the cross-section for such an interaction has a resonance character.

Indications of the influence of the shells were obtained in the recently published work on the investigation of photoprotons from argon[21]. Unfortunately, the data available for other elements are insufficient to be analyzed in terms of the considerations given above.

The authors are very grateful to R. D. Polukarova and N. A. Ponomareva for their help in scanning the plates, and in analyzing the results, and also to the members of the group operating the synchrotron.

---

1 Leiken, Osokina and Ratner, Dokl. Akad. Nauk SSSR **102**, 245 (1955).

2 Leiken, Osokina and Ratner, Dokl. Akad. Nauk SSSR **102**, 493 (1955).

3 Leiken, Osokina and Ratner, Supp. Nuova Cim. **3**, 105 (1956).

4 O. Hirzel and H. Waffler, Helv. Phys. Acta. **20**, 373 (1947).

5 B. C. Diven and C. M. Almy, Phys. Rev. **80**, 407 (1950).

6 P. R. Byerly and W. E. Stephens, Phys. Rev. **83**, 54 (1951).

7 P. F. Klinkenberg, Rev. Mod. Phys. **24**, 63 (1952).

8 J. Lindhard and M. Scharff, Phys. Rev. **85**, 1058 (1953).

9 J. Rotblat, *Nature* **167**, 550 (1950).

10 Flowers, Lawson and Fossey, Proc. Phys. Soc. (London) **65B**, 286 (1952).

11 G. D. Adams, Phys. Rev. **74**, 1707 (1948).

12 L. Katz and A. G. W. Cameron, Canad. J. Phys. **29**, 518 (1951).

13 M. E. Toms and W. E. Stephens, Phys. Rev. **95**, 1209 (1954).

14 E. D. Courant, Phys. Rev. **82**, 703 (1951).

15 D. H. Wilkinson, Proc. of the 1954 Glasgow Conference on Nuclear Physics.

16 J. Blatt and V. Weisskopf, *Theoretical Nuclear Physics* (Russian translation) 1955.

17 V. Weisskopf, *Statistical Theory of Nuclear Reactions* (Russian translation) 1952.

18 V. A. Kravtsov, Uspekhi Fiz. Nauk **54**, 3 (1954).

19 A. B. Migdal, J. Exptl. Theoret. Phys. (U.S.S.R.) **15**, 81 (1945).

20 M. Goldhaber and E. Teller, Phys. Rev. 74, 1046 (1948).
21 B. M. Spicer, Phys. Rev. 100, 791 (1955).

Translated by G. M. Volkoff
3

SOVIET PHYSICSJETP VOLUME 5, NUMBER 1 AUGUST, 1957

Electron Emission from Dielectric Films Bombarded by Positive Hydrogen Ions

V. Z. SURKOV
Kharkov State University

(Submitted to JETP editor May 18, 1956)
J. Exptl. Theoret. Phys. (U.S.S.R) 32, 14–20 (January, 1957)

An investigation has been made of the electron emission which is produced by bombarding dielectric films with positive ions and which continues after termination of the ion bombardment. The electron emission was excited by hydrogen ions, oxygen ions, and lithium ions. The emission has been observed in films of CaF_2, B_2O_3, Al_2O_3, and in mica sheets. The effect of target temperature on emission was investigated. The potentials at the film surfaces have been measured.

WHEN thin dielectric films deposited on a metal substrate are bombarded by electrons or ions, under certain conditions there is observed an extended electron emission which continues after the bombardment is terminated. The origin of this emission seems to be associated with the positive charge at the surface of the dielectric. Malter [1], who discovered this effect, and other investigators bombarded the surface of a dielectric film with electrons to obtain the emission. Starodubtsev[2] obtained this emission by creating a positive charge at the surface of a B_2O_3 film bombarded by K^+ ions and B_2O^+ ions.

The present work was undertaken to obtain more information on the electron emission from dielectric films, deposited ona metal substrate, which is produced when the films are bombarded by positive ions.

DESCRIPTION OF THE APPARATUS AND METHOD OF MEASUREMENT

The experiments were carried out with the apparatus shown in Fig. 1. The target 6 in the operating chamber 8 is bombarded by positive ions selected by the mass-analyzer 2. The instrument frame is grounded. Ions which leave the mass-analyzer pass through two diaphragms 3 with an aperture diameter of 4 mm. To inhibit secondary-electron emission from diaphragm 3, a negative potential of 300 volts is applied to the cylindrical electrode 4 (inner diameter 12 mm, length 15 mm). The target holder 7, which is insulated from the frame and is in electrical contact with the target 6, can be rotated without breaking the vacuum. The micrometer screw 9 is insulated from the frame and is used to move the probe 10 back and forth without disturbing the vacuum. The probe 10 can touch the target 6, as desired, in which case electrical contact is established between the target and the micrometer screw. It is also possible, without disturbing the vacuum, to position a flat disc-collector (not shown in Fig. 1) between the target and collector 5; this disc-collector is insulated from the frame but is in contact with the collector. The ion current is measured by the galvanometer G in the collector–target circuit when the collector potential $V_c = 0$. The electron emission curve is measured with the same galvanometer G, in the collector–target or disc-collector-target circuit, but with a positive collector potential V_c varying from 0 to 3,000 volts applied to the collector. The dielectric film is deposited on the target by vacuum evaporation in the operating chamber 8 while a vacuum of approximately 10^{-6} mm Hg is maintained. By rotating the rod 7, the targets are set over the evaporator 1, located in the bottom part of the operating chamber 8, and B_2O_3 and CaF_2 are evaporated on to the molybdenum substrate. After the film is evaporated, the target is positioned opposite the collector and subjected to ion bombardment. Before deposition of the film,

the target substrate is heated to 1,000–1,200° C by electron bombardment (the electron–bombardment device is not shown in Fig. 1). The target-substrate heating is carried on until the vacuum in the operating chamber cannot be maintained at 10^{-6} mm Hg. The CaF_2 film was also vacuum evaporated in another chamber with and without substrate baking and then transferred in air to the operating chamber. No noticeable difference in the properties of the targets with the CaF_2 films, prepared in the manner indicated above, was found. The thickness of the film is measured to an accuracy of 1 μ with a multiple –beam interferometer. The targets are bombarded by a beam of positive ions selected by the mass analyzer, with energies ranging from 10 to 40 kev at currents ranging from 2 to 6×10^{-7} amp.

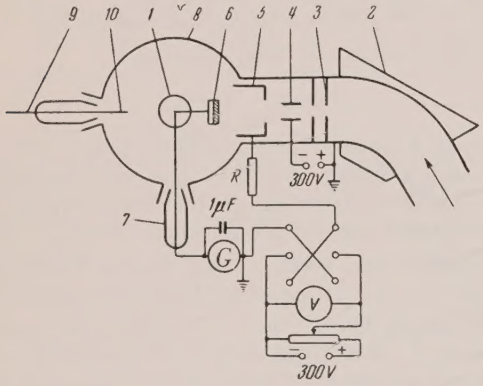

FIG. 1. Diagram of the apparatus.

RESULTS OF THE MEASUREMENTS

Electron Emission from B_2O_3 Films. B_2O_3 was evaporated from a conical tungsten spiral on to the molybdenum substrate. It was found that the vacuum in the operating chamber improved noticeably during intense evaporation of B_2O_3. Following evaporation of the film, the target was heated several times to temperatures of 800–900° C. The thickness of the B_2O_3 film in the experiments being described here varied from 10 to 15 μ. The target was exposed to a beam of protons with an energy of 10 kev.

In Fig. 2 are shown the results of the measurement of electron emission from two targets, I and II, prepared in the same way, and exposed under the same conditions for one minute with $V_c = +400$ volts and an external ballast resistor $R = 1500$ ohms. The distance between the collector and the target was 10 mm.

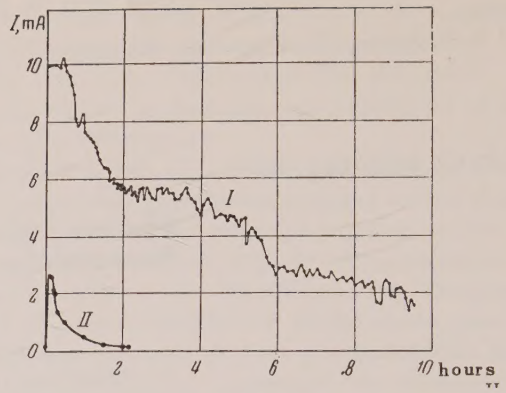

FIG. 2. Electron emission from B_2O_3 films. The time dependence of the emission current I is shown.

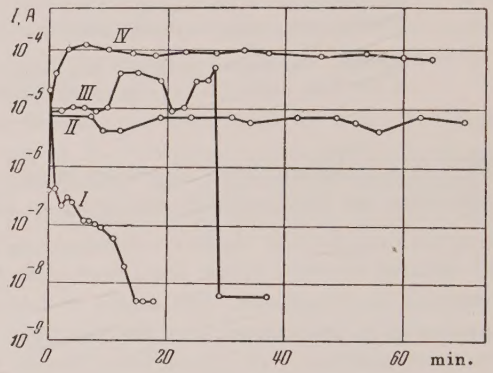

FIG. 3. Electron emission from CaF_2 films. The time dependence for the emission current I is shown for films of various thicknesses: *I*) thickness 20 μ, $V_c = 2{,}500$ volts; *II*–thickness 309 μ, $V_c = 3{,}000$ volts; *III*–thickness 75 μ, $V_c = 2{,}600$ volts; *IV*–thickness 105 μ, $V_c = 1{,}000$ volts.

As is apparent from the data, the emission currents from identical films, exposed to a proton beam under identical conditions, vary by a large factor from one experiment to another. Many such experiments were carried out and the curves shown in Fig. 2 are typical.

Electron Emission from Thin Mica Sheets. Thin cleavage sheets of mica (muscovite) with thicknesses ranging from 3 to 70 μ using substrates of aquadag or vacuum–evaporated silver, were bombarded by beams of H_1^+, H_2^+, H_3^+ and O_2^+ ions with energies from 10 to 40 kev for 1–2 min with V_c ranging from 200 to 3,000 volts and $R = 1{,}500$ ohms. The distance between the col-

lector and target was 10 mm. After bombardment was terminated, electron emissionwas observed in some of the targets, with V_c set at a fixed value.

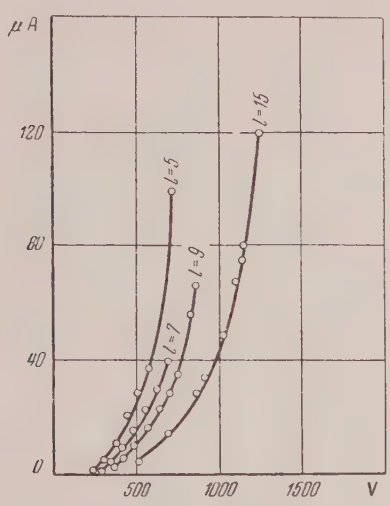

FIG. 4. Electron emission from CaF_2 films. The voltage–current characteristics for the emission are shown for various distances l-between the collector and the target.

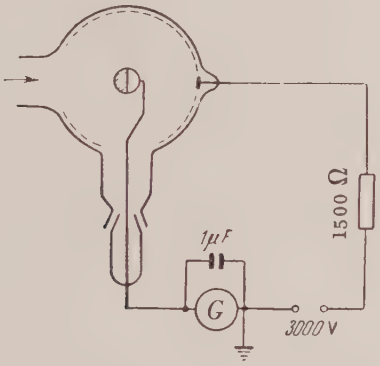

FIG. 5. Diagram of the electron projector.

A total of 118 targets were tested; of these, 29 exhibited electron emission. The emission was observed in sheet thicknesses ranging from 3 to 64 μ, and the highest value of the emission current was 14 μ amp.

In various experiments the time required for the emission to fall from the maxiuum value to the minimum detectable value (10^{-9} amp) varied from several minutes to five hours. It is obvious that one cannot discuss reproducibility of the results. Changing the type of ion or the beam energy, over the region which was investigated, had no effect.

Electron Emission from Al_2O_3 Films. Films of Al_2O_3 were obtained by anodizing polished aluminum in an electrolytic bath (3 percent tartaric acid and ammonium hydroxide, pH = 5.5) for a period of 15 minutes.[3] The thickness of the Al_2O_3 film wasdetermined from the formula

$$t = 13.5\,V,$$

where t is the thickness in Angstroms and V is the voltage in volts.[3] Using this process, transparent non-porous layers of Al_2O_3 with thicknesses from 1.2×10^{-7} to 2.6×10^{-5} cm were obtained on the polished Al.

When these targets were bombarded by beams of H_1^+, H_2^+ and H_3^+ ions with energies from 10 to 40 kev secondary emission was observed. The secondary emission factor was $\sigma \approx 3$. No delayed emission was found in films of this thickness.

TABLE I

Chamber pressure in mm Hg.	Temperature of the container °C.	Cross-sectional resistance, ohms/cm²
760	20	10^5
10^{-5}	20	10^{13}
10^{-5}	60	10^{10}

By passing a current of 1.5 ma for a period of 190 hours to the polished Al in the same electrolytic bath, opaque porous films of Al_2O_3, 5–6 μ in thickness were obtained. The thickness of these films was measured with a multiple-beam interferometer after they were removed from the Al in a $HgCl_2$ solution, washed in distilled water, and dried.

The targets with Al_2O_3 films of theindicated thickness were bombarded with a H_1^+ beam with an energy of 10 kev for 10 seconds with V_c = 2,000 volts and R = 1,500 ohms. Electron emission was observed in these targets after the bombardment was terminated. The emission lasted for 12 min and thelargest value of the emission current was 6 μ amp.

Electron Emission from CaF_2 Films. Calcium fluoride was vacuum evaporated from a molybdenum

container on to the molybdenum substrate. Targets with films of CaF_2 with thicknesses from 2 to 309 μ were bombarded by beams of H_1^+, H_2^+, H_3^+ and O_2^+ ions with energies from 10 to 40 kev and Li_7^+ ions with energies from 2 to 3 kev for a period of 20 sec with V_c ranging from 200 to 3,000 volts and R = 1,500 ohms. 30 targets were tested and in all targets electron emission lasted from several minutes to six hours. The highest emission current was 150 μ amp. In Fig. 3, the time dependence of theelectron emission current for targets with CaF_2 films is shown for films of different thicknesses.

In Fig. 4 the voltage-current characteristics of the electron emission are shown for a target with a CaF_2 film 40–45 μ thick with various distances between the collector and the target l, at room temperature. It should be noted that the voltage-current characteristics will have the form shown in Fig. 4 in each target only if the following conditions are fulfilled: 1) the period of time in which the voltage -current characterisitics are taken must be less than one–two hours; 2) the film must not be punctured. Film punctures are produced when the voltage V_c is too high, at high emission currents with small l (1–3 mm) and when thetarget temperature is increased to 70–80° C. When the film is punctured, circular flashes of light approximately 1–2 mm in diameter are observed at the surface of the target.

Effect of Temperature on Emission from CaF_2 Films. The electron emission of a target with a CaF_2 film, which is produced when thetarget is bombarded by a beam of H_1^+ ions with energies from 10 to 40 kev and which continues after the bombardment, can be observed at temperatures ranging from –195 to + 80°C. The emission was not observed at temperatures above + 80°C. The emission from a target with a CaF_2 film 26–30 μ thick, produced by bombardment with a beam of H_1^+ ions with an energy of 10 kev at a temperature of –195°C, was observed continuously for 6 hours after thebombardment was terminated while the temperature of thetarget was gradually increased to +80°C. At + 80°C the emission current vanished sharply, but after target cooling to below + 80°C. and subsequent bombardment by the beam of H_1^+ ions, the emission was produced again with the same intensity and lifetime.

The results of a measurement of the cross-sectional resistance of a CaF_2 film 20–25 thick are shown in Table I.

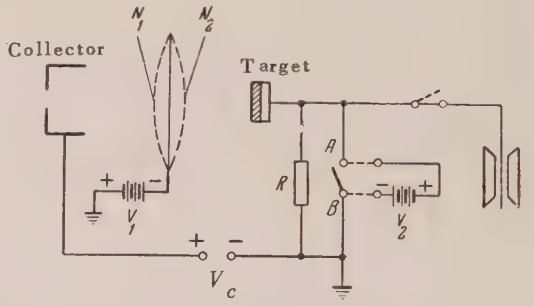

FIG. 6. Diagram of the arrangement used to measure thepotential of thetarget surface.

Observations with an Electron Projector. A film of CaF_2 was vacuum–evaporated on to a steel sphere 4 mm in diameter; the target was placed at the center of a spherical glass bulb, 100 mm in diameter (Fig. 5). The thickness of the CaF_2 film was 10–15 μ. A semi-transparent film of silver was deposited on the inner surface of the sphere; this served as a collector. The silver film was covered with a fine layer of ZnS. When the target of the electron projector was bombarded with a beam of H_1^+ ions with energy of 10 kev, electron emission was produced and continued after the bombardment was terminated. The electrons emitted at the target produced scintillations at the screen of theelectron projector. The luminescence pattern did not cover the entire screen but consisted of separate patches whose shapes kept changing.

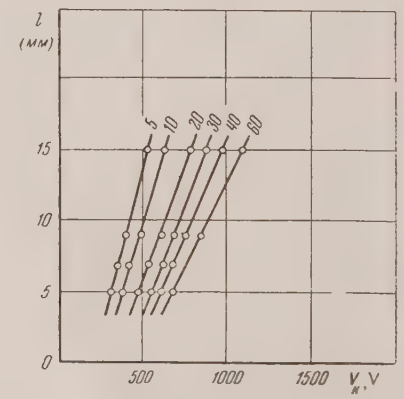

FIG. 7. The dependence of V_c on l for fixed values of I; the values shown on the curves are μ amps.

MEASUREMENT OF THE POTENTIAL AT THE SURFACE OF A TARGET WITH A CaF_2 FILM

A 3 μ Wollaston wire was placed on an insulator in the operating chamber (Fig. 6) between the collector and the target and an image of this wire was projected on the screen along with a scale. A fixed potential, V_1, was applied to the wire. A fixed potential difference, V_c, was set up between the collector and the target, causing the image of the wire on the screen to assume the position N_1. While the target was bombarded the image of the wire assumed the position N_2. After the bombardment of the target was terminated, the image of the wire was gradually restored to the position N_1. After several hours the image of the wire coincided with the original position N_1; then, without removing the potentials V_1 and V_c, the electrometer was disconnected and a potential difference V_2 was applied to the terminals A and B such that the image of the wire assumed the position N_2. The potential V_2 was taken to be the approximate value of the potential at the surface of the target. In various experiments, the potential V_2 varied from 180–220 volts for CaF_2 film thicknesses of 26–30 μ. Inasmuch as the electrons are emitted from a small portion of the target surface, it may be assumed that the potential of the emitting part of the target surface is greater than V_2.

TABLE II

Film thickness, μ	Electron emission current μ amp.	Target surface potential volts	Film thickness, μ	Electron emission current μ amp.	Target surface potential volts
45	5	380	43	25	690
45	20	330	43	18	520
45	25	630	43	20	520
45	30	555	43	20	570
45	22	346	85	2	760
45	51	450	85	2.5	590
45	51	520	85	3	555
45	42.5	450	85	5	830
45	81	520	75	14	330
50	0.7	470	75	19	340
50	0.4	380	75	32	450
			75	46	380

In measuring the potential at the surface of the target with CaF_2 films, use was also made of the method suggested by Dobischek, Jacobs and Treely.[4] It was shown that for a fixed value of the emission current, V_c changes linearly with the distance between the collector and the target l; the potential of the target surface was computed by extrapolating to $l = 0$. The dependence of V_c on l (Fig. 7) computed in the present work for fixed values of the current, using the voltage-current characteristics in Fig. 4, is also linear. In order to change the distance between the collector and the target smoothly, the target was fastened to the probe 10 of the micrometer screw 9 (Fig. 1). After the electron emission had been produced and the bombardment terminated, the disc-collector was positioned between the collector and the target. The diameter of the target was 20 mm and the diameter of the disc-collector was 45 mm. In changing the distance l, in order to maintain any desired fixed value of the electron emission current, it was necessary to vary V_c. Using the curves $V_c = f(l)$ for I = const, the potential at the target surface was calculated by extrapolating to $l = 0$. The surface potentials were measured in several targets and the results are shown in Table II.

I wish to express my sincere gratitude to Prof. K. D. Sinel'nikov for his valuable comments and continued interest.

1 L. Malter, Phys. Rev. 49, 478 (1936); 50, 48 (1936).
2 S. V. Starodubtsev, J. Exptl. Theoret. Phys. 19, 297 (1949); Dokl. Akad. Nauk SSSR 62, 765 (1948).
3 L. Hass, J. Opt. Soc. Am. 39, 532 (1949).
4 D. Dobischek, H. Jacobs and J. Freely, Phys. Rev. 91, 804 (1953).

Translated by H. Lashinsky

Disintegration of Silver and Bromine Nuclei by High Energy Protons

V. I. OSTROUMOV
Radium Institute, Academy of Sciences, USSR
(Submitted to JETP editor May 18, 1956)
J. Exptl. Theoret. Phys. (U.S.S.R.) 32, 3–13 (January, 1957)

We have studied the interaction with heavy nuclei in emulsion of protons with energies 130, 460 and 660 mev. By observing the tracks of recoil nuclei in stars formed as a result of this interaction, we have determined the average number of cascade protons and alpha-particles in stars with different numbers of prongs. The relation between the number of "black" prongs and the mean excitation energy of the nucleus was established for all three energies of the bombarding protons. The distribution of nuclei according to excitation energy was found. The experimentally observed energy spectrum of the protons differs somewhat from an evaporation spectrum.

INTRODUCTION

IT is well known that the process of disintegration of nuclei by fast particles is made up of two stages: cascade and evaporation. The occurrence of the second stage is caused by the fact that as a result of the passage of the primary particle through the nucleus, and the consequent development of a cascade of successive collisions of nucleons, the nucleus is left in an excited state; the excitation energy is usually only a part, small or large, of the initial kinetic energy of the bombarding particle. The excitation energy is one of the most important characteristics of the interaction process. There are several papers in which this quantity has been calculated for different cases of interaction.[1–3] The experimental determination of the excitation energy, for example in work done by radiochemical analysis of the disintegration products, is extremely inexact and is rather in the nature of an estimate. In particular cases estimates have been based on theoretical relations, which in their turn require experimental verification. Lock et al.[4], in studying the interaction of 950 mev protons with nuclei in emulsion, determined the mean excitation energy of the nucleus from the average number of charged particles accompanying each disintegration. In their work they used the relation between the number of charged particles evaporated and the excitation energy, as calculated by Le Couteur.[5] From observations of stars produced in emulsion by high energy cosmic ray particles, Bernardini and co-workers[1] showed that an excitation energy of 35 mev in Ag and Br corresponds on the average to the evaporation of one charged particle (whereas this number is ~ 0.3 according to Ref. 5). The computation of the cascade stage carried out by these authors,[1] as well as the results of their experiments with 400 mev protons, confirm the correctness of the relation they give between number of particles and excitation energy. Stars produced by 450 mev protons were also studied in Reference 6. The authors of this paper came to the conclusion that Le Couteur's curve does not agree with their experimental data, while the relation given in Ref. 1 is in very close agreement.

It would be interesting also to find the distribution function for the nuclear excitation energy. This distribution was computed in the paper of Bernardini et al.,[1] but there are no experimental data on this point.

While the study of fast cascade particles emerging upon disintegration of nuclei by high energy nucleons has been covered in many papers, by using nuclear emulsions, similar investigations of the "black" component of knock-on particles is made difficult by the presence of the evaporation particles. Estimates of the fraction of cascade protons with energy below 30 mev were made[7,8] by observing the angular anisotropy of black tracks in stars on heavy nuclei in emulsion. It comprises 25–30% of the total number of prongs. The Monte Carlo method[1] gives a very similar result. In all these investigations, it was assumed that the "black" cascade particles consist only of protons and of neutrons, (which are not observable in experiments with plates), though there are experimental indications that alpha-particles are present.

The present investigation is devoted to the questions raised above. The method used in this work was described by us in an earlier paper.[9,*] The analysis of tracks of recoil nuclei in stars, on which this method is based, has also been developed by Harding[10] and Grilli and Vitale.[11] In both of these

*The results published in Ref. 9 should be regarded as preliminary, and for purposes of illustration.

papers, it was assumed that the nucleus which produces the recoil track is moving with a velocity whose magnitude and direction are determined by the sum of two independent velocities: 1) the velocity given to the nucleus as a result of the passage of the primary particle which loses part of its kinetic energy in traversing the nucleus (we call this component the transfer velocity), and 2) the velocity acquired by the nucleus during the succeeding evaporation of particles. A similar model of the formation of recoil tracks is also the basis of our method, with the difference that the first component of the momentum of the nucleus is assumed to be equal in magnitude and direction to the change in momentum of the primary particle, which after colliding with the nucleus preserves its initial direction of motion, while the decrease in kinetic energy of the bombarding particle is assumed to be equal to the excitation energy of the nucleus.

EXPERIMENTAL ARRANGEMENT

In our work we used plates with fine-grained emulsion type P–9, prepared in N. A. Perfilov's laboratory, and also plates with NIKFI type K emulsion, on which parallel experiments were done. The emulsion layer was 150 microns in thickness. The emulsion recorded protons with energies up to 30–35 mev, as was established by observing $\pi-\mu$ decay. In the experiment at 140 mev, the NIKFI emulsion was sensitive out to 100 mev. The irradiation was carried out in external, collimated beams of protons, with energy 140, 460, and 660 mev, at the synchrocyclotron of the Institute for Nuclear Problems of the Academy of Sciences of the USSR. The 140 mev protons were obtained by slowing down faster protons in a copper block. When the energy loss in the emulsion layer is included, the effective energy of these protons is set at 130 mev. The beam was incident parallel to the plane of the emulsion within 5°. The number of background stars, as determined from control plates exposed simultaneously but outside the beam, did not exceed 2%. The angles were measured to 1°, the track lengths to 0.3 microns. All the measurements were made under maximum magnification (100 × 20 × 1.5). The small grain size of P–9 emulsion makes it especially valuable for measuring recoil tracks, as was confirmed by comparison data from parallel experiments on K and P–9 emulsions.

The velocities of the recoil nuclei were determined from the range-velocity curves[12] for light fission fragments from uranium, where the conversion coefficient from range in air to range in emulsion was taken as 1760. We selected for measurements those stars which contained recoil tracks which did not deviate by more than 30° from the plane of observation. Only the projection of the track length on this plane was measured. If a star contained alpha-particle tracks shorter than 40 microns while the total number of prongs was less than 6, it was discarded as very probably being the result of disintegration of light nuclei in the emulsion.

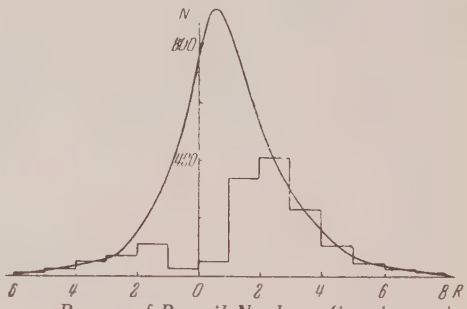

FIG. 1. Distribution of stars according to range of recoil nuclei; "backward" and "forward" refer to direction relative to the bombarding beam. The solid curve is drawn including unobservable cases.

FIG. 2. Distribution of nuclei according to recoil velocity component v. The solid curve is the distribution corrected for unobservable cases, the dashed curve was calculated from formula (2) of the present paper.

EXPERIMENTAL DATA

Figure 1 shows the distribution in range of recoil nuclei, for incident proton energies of 460 and

660 mev (1483) cases). The curve is drawn taking into account cases which are missed because of low velocity of the recoil nucleus (cf. below). Figures 2 and 3 show the distribution of x and y components of the velocity—v and w.* Both these curves are drawn including the correction for unobservable cases. This correction was obtained from the assumption that the true distribution of w is Gaussian. The points for $v = \pm 15 \times 10^7$ cm sec in Fig. 2 were corrected correspondingly. For the points $v = \pm 5 \times 10^7$ cm/sec, the correction was made so that the total number of cases was twice as great as that observed, since the number of stars from Ag and Br which contain recoil tracks is about 50% of all disintegrations of those nuclei. The range correction was made similarly, using the relation between R, v and w.

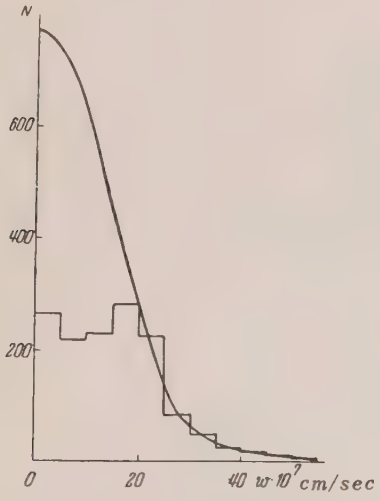

FIG. 3. Distribution of nuclei according to velocity component w. The solid curve is a Gaussian distribution.

The measured values of velocity for stars with different numbers of prongs, and also the velocity of transferred motion of target nuclei calculated from the tracks, $u = v^+ - w$, are shown in Fig. 4. The spread in the individual values for each point is extremely large, and very good statistics are necessary for obtaining more or less smooth curves. For this reason, the experimental points on the graphs are taken as an average for two successive values of the prong number n. In some experiments, the values of w were measured separately in two directions— "up" and "down" with respect to the bombarding beam. The average values obtained were equal within the limits of statistical accuracy, as was to be expected, since evaporation is an isotropic process.

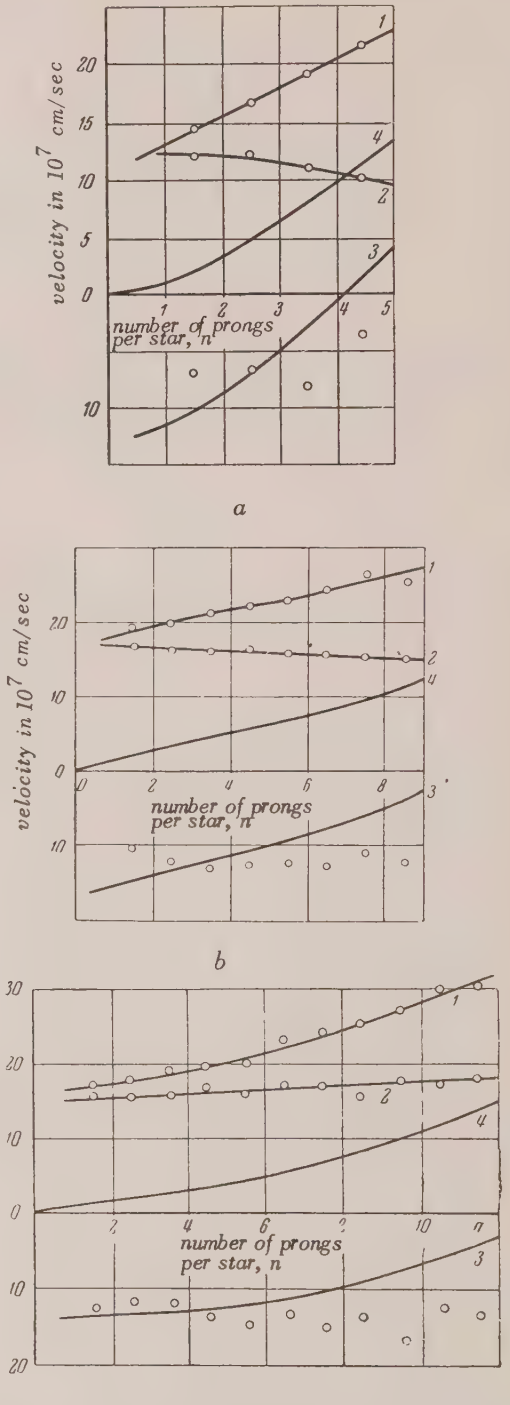

FIG. 4. Average values of the "forward" component of velocity: 1– v^+, 2–w; 3–"Backward" component of velocity v^-; 4–transfer velocity u as a function of prong number, for stars formed by protons with energy: a) 130, b) 460, c) 660 mev.

*Here and throughout the paper we shall stick to the notation used in Ref. 9, where the x-axis is taken along the direction of the incident protons.

Knowledge of the value of u enables us to determine the excitation energy for each type of star from the formula:

$$U + Q = E_0 - [\sqrt{(p_0 - Mu)^2 c^2 - m^2 c^4} - mc^2], \quad (1)$$

where U is the excitation energy, Q is the sum of the binding energies of the ejected particles, M and u are the mass and velocity of the nucleus, m, E_0 and p_0 are the mass, energy and momentum of the impinging proton. In this way we find the dependence of n $(U + Q)$, the number of prongs per star, on the quantity $U + Q$. In order to determine the number of ejected particles, and consequently the value of Q, one can proceed as follows: upon setting some value for the number of charged particles evaporated, n_{evap}, we determine the numbers of alpha-particles and protons evaporated from the theoretical dependence of $(\alpha/p)_{evap}$ on n_{evap} [13] Knowing from the experiment the average number of α-particles and protons in a given type of star and subtracting from the total number of a particular particle the number of evaporation particles, we determine the composition of the charged prompt component. Data concerning the number of fast protons (with energies greater than 30 mev) were obtained from observations on electron-sensitive plates (cf. Table I). We compare the value of U found from (1) with the magnitude of the initial excitation energy necessary for evaporating the given number of particles n_{evap}. If the value of U from formula (1) does not agree with the value of the excitation energy obtained from the theoretical curve of $n_{evap}(U)$, the computation is repeated for a new value of n_{evap}. The ratio of the numbers of cascade neutrons and protons was taken in accordance with Ref. 2 (a check for the case of 460 mev protons showed that n (U) obtained by the method just described changes only slightly if the numbers of neutrons and protons are taken to be equal). In Fig. 5 we show the dependence of the number of black tracks per star on the excitation energy, for all three energies of the bombarding particles.

EXCITATION ENERGY

The curves n (U) enable us to construct the distribution of cases of interaction of fast protons with Ag and Br nuclei according to excitation energy of these nuclei. For this purpose it is necessary to know the prong distribution of stars produced in the emulsion. Disintegrations which are not accompanied by emergence of charged particles of low energy, as well as a considerable number of the one– and two–pronged stars, cannot be counted even in relativistic emulsions, when one is making an area search. Therefore, the experimental data on prong distribution of stars produced by 460 and 660 mev protons were corrected for unobservable cases, in accordance with the data of Bernardini et al.[1] The prong distribution of stars from 130 mev protons was taken as the average of the data of Refs. 3 and 7. The effect of star formation on light nuclei in the emulsion was taken into account by using the results of experiments with high energy neutrons.[8] In Table II we give the prong distributions of stars as obtained from observations of disintegrations in electron-sensitive plates and corrected in the manner just described. For comparison we also give the distribution of stars with more than two prongs, as found in P–9 emulsion and assigned in accordance with our criterion to disintegrations of Ag and Br.

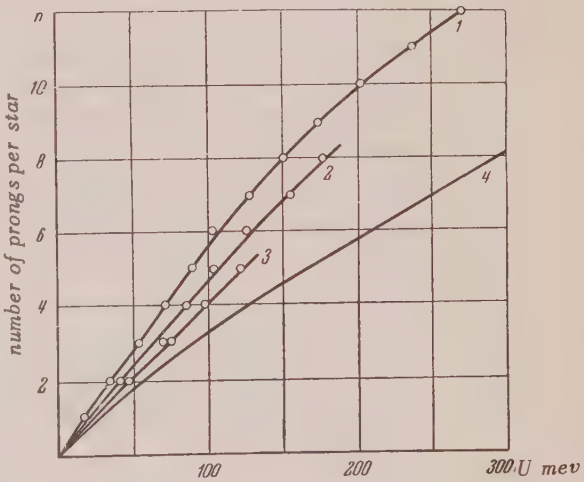

FIG. 5. Relation between number of black prongs per star and excitation energy of Ag and Br nuclei, for proton energies: *1*–660 mev, *2*–460 mev, *3*–130 mev, *4*–theoretical evaporation curve (Ref. 13).

Figure 6 shows the distributions of nuclei according to initial excitation energy, constructed from the data of Fig. 5 and Table II. The distribution found for the case of disintegration by 460 mev protons is in good agreement with the results of computation.[1]

TABLE I

Average Number of Fast Protons ($E > 30$ mev) in stars from Ag and Br

Number of black tracks, n	Energy of incident protons, mev		
	130	460	660
—	0	—	2,1
1	0.76	1,31	1.57
2	0.40	1.08	1.34
3	0.33	1.02	1.21
4	0.27	0.96	1.13
5	0.20	0.78	1.05
6	—	0.66	0,96
7	—	0.49	0,84
8	—	0.40	0.72
9	—	0.27	0.63
10	—	—	0.50
11	—	—	0.33
12	—	—	0.12
average	0.40	0.97	1,13

The average excitation energy can be determined from : 1) the distribution given in Fig. 6; 2) from the transfer velocity u averaged over all stars, using formula 1); 3) from the average number of

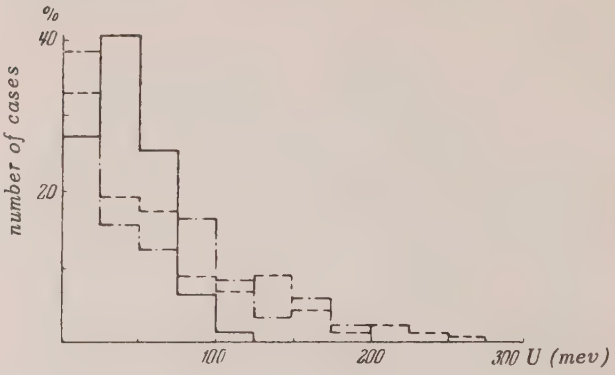

FIG. 6. Distribution of Ag and Br nuclei according to excitation energy from bombardment by protons of energy: 130, solid curve; 460, dash curve; 660 mev, dot–dash curve.

charged evaporation particles, obtained by transforming the curve $n \quad (U + Q)$ to a curve of $n(U)$. All three methods lead to an average value of the excitation energy which is equal, for the case of $E_0 = 130$, $E_0 = 460$ and $E_0 = 660$ mev respectively, to 48 ± 1, 52 ± 4, 58 ± 4 mev. It is obvious that these methods are interdependent, so the errors shown enable one merely to judge the accuracy of computation within the limits of the method used.

On the basis of the data of our experiment, we constructed a curve of nuclear yield from disintegration of silver and bromine by 460 mev protons (Fig. 7). On this same graph are plotted the experimental points obtained in Reference 14 from radiochemical analysis of the products from bombardment of silver by protons of this same energy. It is apparent that the results of the two papers are in agreement. A certain shift of the points is probably caused by the fact that in the experiment with

TABLE II.

Prong distribution of stars in Ag and Br

number of black prongs, n	$E_0 = 130$ mev			$E_0 = 460$ mev			$E_0 = 660$ mev		
	calc.		exp.	calc.		exp.	calc.		exp.
	all stars %	stars with $n \geq 1$ %	stars with $n \geq 1$ %	all stars %	stars with $n \geq 3$ %	stars with $n \geq 3$ %	all stars %	stars with $n \geq 3$ %	stars with $n \geq 3$ %
0	3,1	—	—	20	—	—	17,5	—	—
1	24.4	25.2	18.3	18,7	—	—	15,3	—	—
2	40.6	41.7	37.3	15,5	—	—	13,5	—	—
3	25,1	25.9	31.3	11.7	25,7	27.8	11.3	20,9	16.4
4	5.6	5.8	9.6	11.7	25,7	25,2	10,0	18,5	21.6
5	1,2	1.4	3.5	9.1	19,9	20.7	8,5	15,7	22,2
6	—	—	—	6,1	13,4	13,2	7.3	13,5	16,4
7	—	—	—	4,5	9,8	8,4	6,2	11,5	10,1
8	—	—	—	1,9	4,1	3,2	4,6	8,5	7,2
9	—	—	—	0.6	1,4	1,5	3,1	5,7	3,3
10	—	—	—	—	—	—	2,0	3,7	2,0
11	—	—	—	—	—	—	0,7	1,3	0,7
12	—	—	—	—	—	—	0,4	0,7	0,2

emulsion the average charge of the target nuclei is somewhat less, and consequently the probability of emergence of charged particles is somewhat greater than in the experiment with pure silver.

Starting from our model of the formation of recoil tracks, the distribution function for the quantity v can be written as an integral:

$$F(v) = \int_{-\infty}^{\infty} P(w)\,\Phi(v-w)\,dw, \qquad (2)$$

where $\Phi(v-w) = \Phi(u)$ is the distribution of the velocity u, $P(w)$ the distribution for the velocity w. By solving (2) for $\Phi(u)$, one can, it is true, find the distribution of excitation energy, i.e., the curve of Fig. 6. We have limited ourselves to solving the inverse problem: from $\Phi(u)$ and $P(w)$ we calculated the function $F(v)$, a graph of which is shown as the dashed curve in Figure 2. The agreement of the results of the computation with the observed distribution is satisfactory for positive values v^+. For tracks directed opposite to the incident proton, the two curves differ somewhat. An attempt was made to obtain better agreement of the curves by changing the shape of the curve of $\Phi(u)$ in the region of low values of the argument, where it is determined least accurately. However, this attempt led to no significant improvement.

Possibly the cause of this disagreement lies in the insufficient statistics for the corresponding cases.

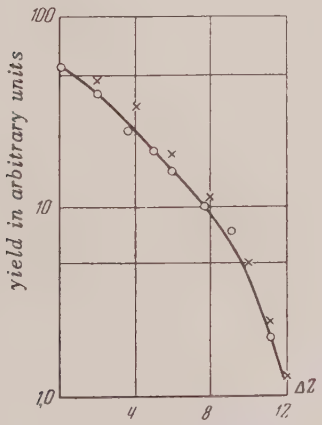

FIG. 7. Yield of nuclei with varying Z from bombardment of Ag and Br by 460 mev protons. The crosses are the results obtained in Ref. 14 and are adjusted to coincide with the present experiment at $\Delta Z = 0$. ($\Delta Z = Z_{in} - Z_{final}$).

PROTON ENERGY SPECTRUM

The energies of protons in the stars were measured from the length of tracks stopping in the emulsion, and the usual geometrical corrections for track yield were made, assuming that their angular distribution is isotropic. This assumption is not completely valid for protons with energy greater than 10 mev, but the observed anisotropy has an insignificant effect on the spectrum shape. The distinguishing of proton tracks from those of α-particles was done visually. This selection is more reliably done with fine-grained emulsion than with type K. The accuracy of selection was checked in a special experiment by a method proposed by Iu. I. Serebrennikov. Along an arbitrarily selected track, starting from its end, in a manner similar to grain-counting, the number of intervals of an ocular scale which were completely covered by developed grains was recorded. The processing of 90 tracks of length 80 μ, carried out by two independent observers, showed that the tracks of α-particles and protons begin to differ significantly after a length of 50 μ, and that visual distinction leads to negligible error (of the 90 tracks, three proton tracks were mistakenly attributed to α-particles).

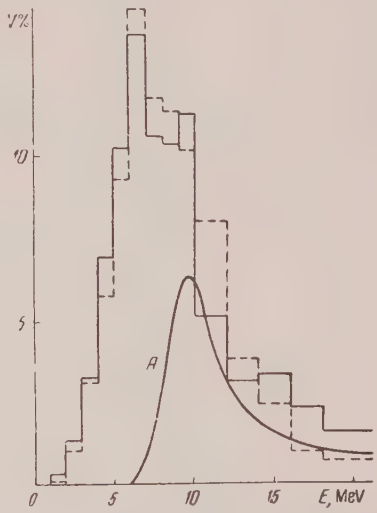

FIG. 8. Energy spectrum of protons emitted from Ag and Br nuclei bombarded by protons of energy: 660, solid line; 460 mev, dashed line. The first distribution was constructed from 6270 tracks, the second from 2500. Curve A shows the spectrum of "black" prompt protons averaged for both beam energies.

The energy spectra of protons (more precisely, singly charged particles) in stars produced by protons of energy 460 and 660 mev, are shown in Fig. 8. If in the first case the spectrum has a single peak due to protons from the evaporation

process (and somewhat broadened by knock-on protons of low energy), in the stars from 660 mev protons there is apparently a second peak associated with direct ejection of a considerable number of protons with energy 8–10 mev. From the dependence of n (U) found in the present work it follows that with increasing excitation energy there is also an increase in the "black" component of directly ejected particles. This is confirmed by the graphs in Fig. 9, which show proton spectra for various initial excitation energies of the nucleus. For comparison, curves are shown for the theoretical evaporation spectra computed with the effect of nuclear cooling included. The difference between the experimental and evaporation spectra gives the energy distribution of prompt protons, whch is shown totaled for all stars in Fig. 8. The difference in shape of the observed and computed evaporation spectra in the energy region up to 4 mev (Fig. 9), can be attributed to inclusion of stars formed on light nuclei in the emulsion, and also to errors in track identification.

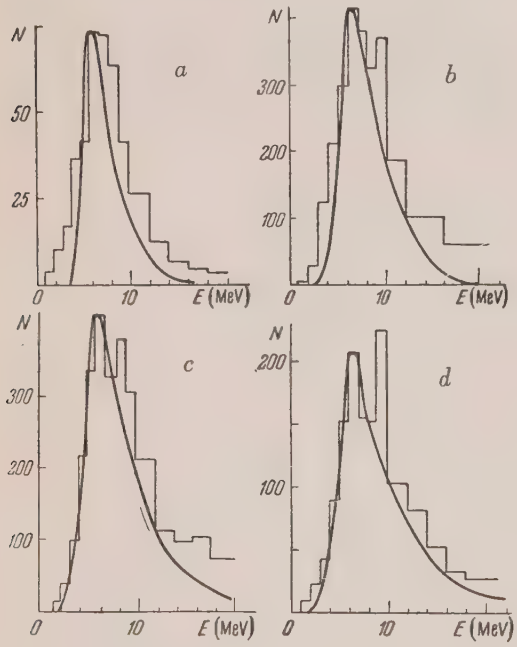

FIG. 9. Energy spectrum of protons for varying initial excitation energy of the nucleus. Computed evaporation spectra are shown for the following nuclear excitations: *a*) 0–50 mev (U_{av} = 25 mev); *b*) 50–100 mev (U_{av} = 75 mev); *c*) 100–150 mev (U_{av} = 125 mev); *d*) 150–200 mev (U_{av} = 175 mev).

A comparison which we have made of the spectra of protons emitted into the forward and backward hemispheres with respect to the beam shows that there is a small excess of particles of low energy (E < 7 mev) emitted backwards. This excess is quantitatively explained by the effect of the motion of the evaporating nucleus. On the other hand, in the high energy region where the direct ejection begins to have an effect, we observe an excess of protons emerging into the forward hemisphere.

KNOCK–ON COMPONENT

The presence of cascade particles of low energy is indicated by the appearance of angular anisotropy of the black tracks in the stars, the anisotropy being the same for protons and α-particles for all three energies of the incident protons in our experiment (56 ± 2% of the prongs are directed into the forward hemisphere).

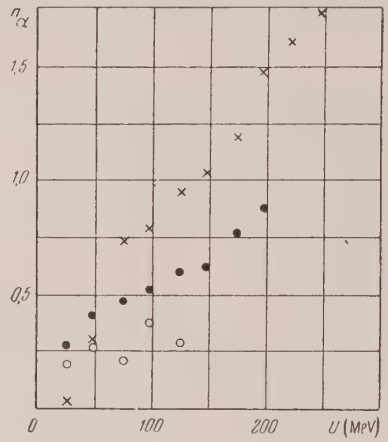

FIG. 10. Dependence of number of cascade α-particles on nuclear excitation energy. Crosses— E_0 = 660 mev; solid circles—E_0 = 460 mev; open circles—E_0 = 130 mev.

The fraction of knock-on particles can be determined from the overall observed anisotropy, by using the angular distribution data and computing by the Monte Carlo method. On the other hand, the average number of charged cascade particles can be found as the difference between the average number of prongs in a star and the number of evaporation particles corresponding to the given excitation energy. A third independent method for determining this quantity consists in observing the proton energy spectrum. As was pointed out above, one can separate the spectrum of cascade protons from the total spectrum observed in the experiment, and thus calculate the number of cascade particles. All three of these methods when applied to disintegrations by 460 and 660 mev protons lead to approximately the same result. Since there are no

corresponding data in the literature concerning cascade α-partcles, the fraction of thelatter was determined only from computations of the n (U) curves, as indicated above. In Table III we present the data for the charged cascade component as obtained in thepresent experiment, and the results of computations in which the effect of α-particles was not included.

Figure 10 shows the relation between the number of cascade α-particles and the excitation energy of the residual nucleus, though the latter quantity should be regarded as a function of the total number of cascade particles.

ACCURACY OF THE METHOD

The internal consistency of the results obtained in the present work, as well as the agreement with corresponding data of other authors, permit us to conclude that the method proposed in Ref. 9, together with all the approximations, is admissible at least for therange of incident proton energies here considered, and is not associated with large errors. We have attempted to estimate the error in the determination of U which is caused by the recoil during ejection of secondary nucleons. By calculating the average angle of emergence of the cascade nucleons from their known angular distribution,[1] and assuming that on the average one nucleon is ejected from the nucleus into each of the energy groups ($E < 30$ mev; $30 < E < 100$ mev, and $E > 100$ mev), we can determine the momentum imparted to the nucleus, and then from formula (1) find the average excitation energy U corresponding to this momentum Mu. On the other hand, U can be determined from the energy balance of the disintegration process. It was found that for a bombarding proton energy of 460 mev, the discrepancy between these two values of U was about 10%, reaching 50% for high excitation energies (~200 mev). However, for high excitation energies the actual error is in all probability smaller, because for a well-developed cascade the angular distribution of "black" prompt nucleons must approach isotropy, which leads to a decrease in the computational error. This is confirmed by the agreement of the maximum value of U (200 mev), as obtained from a Monte Carlo calculation,[1] with the value for the upper limit of U found in our experiment. We estimate the accuracy of the results obtained in the present work to be ~ 20%.

DISCUSSION OF RESULTS

As already pointed out earlier, there are a

TABLE III.

Incident proton energy, mev		Number of particles per disintegration			
		130	460	660	
Cascade Protons	$E < 30$	0.25 (20% of all black protons)	0.57 (30% of all black protons)	0.84 (35% of all black protons)	
	$E > 30$	0.49	0.95	1.03	
	All cascade protons	0.74	1.52	1.87	
Cascade α-particles		0.18 (27% of all α-particles)	0.25 (39% of all α-particles)	0.49 (50% of all α-particles)	
Black knock-ons		0.43	0.82	1.33	
(α/p) in cascades		(21% of all black prongs)	(32% of all black prongs)	(39% of all black prongs)	
All charged knock-ons		0.24	0.47	0.26	
Computed		0.92	1.77	2.36	
		1.19[3]	1.6[1]; 1.9[2]	2.2[2]	

series of papers whose results do not agree with LeCouteur's evaporation theory. The data obtained in our experiment concerning the number of cascade particles, the magnitude of the excitation energy, etc., agree with computations by the Monte Carlo method, if we use Macke's thoretical curve.[13]

The appearance of a second maximum in the energy spectrum of protons from nuclear disintegrations by 660 mev protons appears, at first glance, quite unexpected. There is no indication of this in a single paper published up to the present time. However, one should consider that in these papers, as a rule, the spectrum was studied for all the nuclei in the emulsion lumped together, including the light nuclei, and sometimes even with undefined energy of the bombarding particles (as in experiments with cosmic rays). In addition, in certain experiments the statistics were poor, so that the authors had to take wide energy intervals in constructing a histogram, which led to a coalescence of the two peaks into a single one corresponding to evaporation protons. It is interesting to note that in work[4] done with protons of 950 mev energy, and free of the limitations just mentioned, a second maximum was obtained in the region of 8–10 mev which was even more intense than in our experiment. But the authors themselves[4] apparently regard the appearance of the second maximum as accidental and, wishing to obtain agreement with the experiment, draw the evaporation curve so that the average nuclear excitation turns out to be considerably greater than predicted by the Goldberger model.

The spectrum of cascade protons (Fig. 8) agrees in shape with that calculated by the Monte Carlo method.[1–3] There is no good reason for doubting that the neutral component will have a similar spectrum, shifted toward lower energy because of the absence of a barrier. This means that for practical purposes, the spectra of cascade and evaporation neutrons will be even more indistinguishable than is the case for protons. It seems to us that this last point should be considered when interpreting experiments on the determination of the average nuclear excitation energy from the number of emerging neutrons.

In conclusion, the author expresses his deep gratitude to Prof. N. A. Perfilov for his constant interest in the work and for discussion of results, and to the administrative staff of the laboratory for assistance. The author is grateful to Prof. M. G. Meshcheriakov and Prof. V. P. Dzhelepov, as well as to his co-workers in the Institute for Nuclear Problems, N. P. Bogachev, E. L. Grigor'ev, B. S. Neganov and others, for the great cooperation they have provided him in carrying out the experiment.

1 Bernardini, Booth, and Lindenbaum, Phys. Rev. 88, 1017 (1952).
2 McManus, Sharp, Gellman, Bull. Am. Phys. Soc. 28, No. 6, 20 (1953).
3 Morrison, Muirhead, and Rosser, Phil Mag. 44, 1326 (1953).
4 Lock, March and McKeague, Proc. Roy. Soc. (London) A 231, 368 (1955).
5 J. LeCouteur, Proc. Phys. Soc. (London) A63, 259 (1950).
6 Sprague, Haskin et al, Phys. Rev. 94, 994 (1954).
7 P. E. Hodgson, Phil. Mag. 45, 190 (1954).
8 Blau, Oliver, and Smith, Phys. Rev. 91, 949 (1953).
9 V.I.Ostroumov, Dokl. Akad.Nauk SSSR 103, 413 (1955).
10 J. B. Harding, Phil.Mag.40, 530 (1949).
11 M.Grilli, B.Vitale et al., Nuovo Cimento 12, 889 (1954).
12 Boggild, Brostrom and Lauritsen, Danske Vid. Skelskab. Mat. fys. Medd. 18, No. 4 (1950).
13 *Kosmiche Strahlung*, ed. Heisenberg, 2 Aufl., Berlin, 1953, p. 201.
14 B.V. Kurchatov, V. N. Mekhedov et al., Session of the Academy of Sciences, USSR, on Peaceful Uses of Atomic Energy, July, 1955; Division of Chemical Sciences (transl. U. S.Gov't Printing Office, p. 111).

Translated by M.Hamermesh
1

Angle-Energy Distribution of Photoneutrons from Bi

G. N. Zatsepina, L. E. Lazareva and A. N. Pospelov
P. N. Lebedev Institute of Physics, Academy of Sciences USSR
(Submitted to JETP editor August 3, 1956)
J. Exptl. Theoret. Phys. (U.S.S.R.) **32**, 27-30 (January, 1957)

The angle-energy distribution of photoneutrons emitted from bismuth bombarded by x-rays with a maximum energy E_{max} = 18.9 mev has been investigated using nuclear emulsions. The energy distribution obtained includes a large number of energetic neutrons which cannot be explained in terms of the statistical theory.

In the existing studies of photoneutron angular distributions[1-6], simultaneous measurements of the distribution over angle and energy have not been carried out. In Refs. 1-3, a threshold-detector method was employed; in Refs. 4-6, a scintillation counter was used to detect neutrons with energies above a definite level. In the present work, nuclear emulsions have been used to study the energy distribution of photoneutrons from bismuth, emitted at various angles with respect to the x-ray beam. The measurements were carried out at the 30 mev synchrotron of the Physical Institute, Academy of Sciences, using a maximum x-ray energy E_{max} = 18.9 mev.

In Fig. 1 is shown the arrangement of the sample and the emulsion during irradiation. The bismuth sample, a disc 40 mm in diameter and 5 mm thick (4.91 gm/cm^2), was set up on a light aluminum holder at the center of a collimated x-ray beam. To reduce the neutron background, the collimator was made of graphite and aluminum; a large paraffin block (80 × 80 × 60 cm) with a longitudinal channel, 50 mm in diameter in the direction of the x-ray beam, was placed between the collimator and the sample. NIKFI Ya-2 photoemulsions, 400 μ thick, (3 × 5 cm) were placed at a distance of 16 cm from the center of the sample at angles of 30°, 90°, 150°, and 270° with respect to the x-ray beam. The disposition of the sample and emulsion was chosen (Fig. 1) so as to maintain a uniform solid angle for all emulsions. The uncertainty in the neutron direction due to the finite dimensions of the sample and emulsion was, on the avarage, about 3°.

The x-ray dose was measured with a thin-walled integrating ionization chamber placed in the x-ray beam between the collimator and the paraffin block (the overall thickness of the electrodes and screen, made from aluminum foil, was 300 μ).

To measure the background, the Bi sample at the center of the beam was replaced by a graphite disc 40 mm in diameter and 0.92 gm/cm^2 thick. The number of neutrons in the beam scattered by the graphite disc and by the bismuth sample was the same. The average value of the background

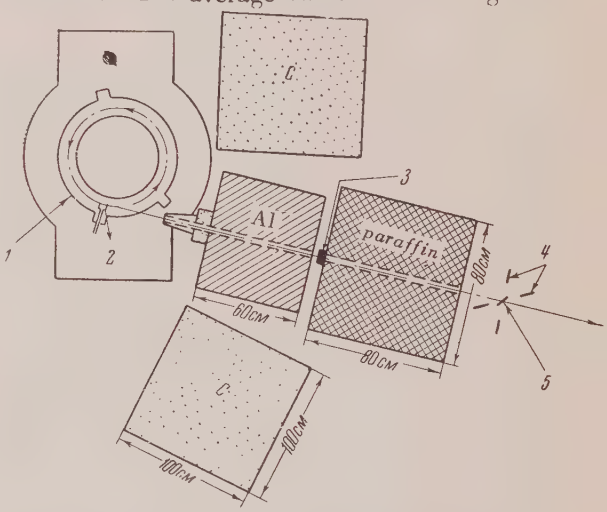

FIG. 1. Arrangement of the sample and emulsion during irradiation: *1* – synchrotron chamber; *2* – external synchrotron target; *3* – thin-walled monitor; *4* – emulsion; *5* – sample.

ranged from 10 to 16 percent as a function of angle.

The developed emulsions were scanned with a MBI-2 microscope with a magnification of 60 in the objective and 5 in the ocular. Only those recoil protons which were scattered at small angles with respect to the direction of neutron motion were recorded. The maximum detection angle in the plane of the undeveloped emulsion was 15°; the maximum in the vertical direction was 24°. Using this selection of tracks the measured proton energy was, on the average, about 8.8 percent smaller than the neutron energy. In converting from the measured recoil-proton spectrum to the photoneutron spectrum, in addition to this correction, corrections were introduced to take account of the energy dependence of the (n-p) scattering cross-section and errors due to tracks which passed out of the emulsion. The range-energy relation for protons was taken from Ref. 7. Less than 9 percent of the Bi photoneutrons were scattered in the sample.

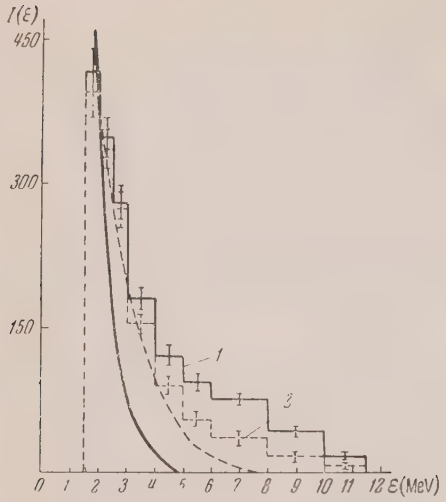

FIG. 2. Energy distribution of photoneutrons from Bi.

After background corrections, the number of protons recorded in the emulsions at angles of 30°, 90°, 150° and 270° was 2605. In Fig. 2 are shown the photoneutron energy spectra, $I(\epsilon)$, obtained at the angles indicated. Histogram *1* represents the energy distribution of neutrons emitted at right angles to the x-ray beam (90° and 270°). Within the error limits, the neutron spectra at 30° and 150° are identical. Histogram *2* represents the summed spectrum for 30° and 150°. Both spectra which are presented are normalized to the same scanned area on the emulsion. The solid curve and the dashed curve refer to neutron energy distributions computed on the basis of the statistical theory, using two different level densities,

$$\omega_1 = C \exp [3.35\,(A-40)^{1/2}(E-E_n-\varepsilon)]^{1/2}$$

and

$$\omega_2 = C \exp [0.7\,(A-40)^{1/2}(E-E_n-\varepsilon)]^{1/2},$$

(C is a constant, A is the mass number, E is the excitation energy, E_n is the binding energy of the neutron and ϵ is the energy of the emitted neutron). The cross-sections for the (γ, n) and $(\gamma, 2n)$ reactions in Bi were taken from Ref. 8. A Schiff spectrum was assumed for the γ-radiation. No account was taken of the change in the x-ray spectrum due to transmission through the Bi sample nor of inelastic neutron scattering in the sample. The introduction of these corrections should tend to increase the relative number of neutrons at the high energies.

Neither spectrum computed on the basis of the statistical theory coincides with the energy distribution observed for the photoneutrons from Bi. The experimental neutron spectra agree roughly with the spectrum calculated using the level density ω_2 only in the region from 1.5 mev to approximately 4 mev. Above 4 mev histograms *1* and *2* exhibit a considerable number of neutrons the yield of which, according to the evaporation model, should be virtually zero. Similar results have been obtained by Byerly and Stephens[9] and Price[3] investigating photoneutrons emitted at 90° to the x-ray beam in photo-disintegration of copper (E_{max} = 24 mev) and bismuth (E_{max} = 22 mev). The number of neutrons with energies above 4 mev is noticeably greater at 90° and 270° than at 30° and 150°. In the Table are shown the relative neutron yields for different energies at 30°, 90° and 150°. It is apparent from this Table that the anisotropy over angle increases sharply with increasing neutron energy. If it is assumed that the neutron yield for energies below 1.5 mev corresponds to that expected on the basis of the statistical theory, neutrons emitted anisotropically with respect to the x-ray beam amount to 8.8 percent of the total number of photoneutrons. It would appear that the data must be analyzed in terms of two different interactions between the γ-quanta and nuclei: the absorption of γ-quanta with the production of a compound nucleus and subsequent evaporation, and a direct photo-effect.

In Fig. 3 the following curve has been plotted for neutrons emitted at right angles to the γ-quanta direction: neutron energy is plotted along the abscissa axis and the function $\ln[I(\epsilon)/\epsilon]$ is plotted

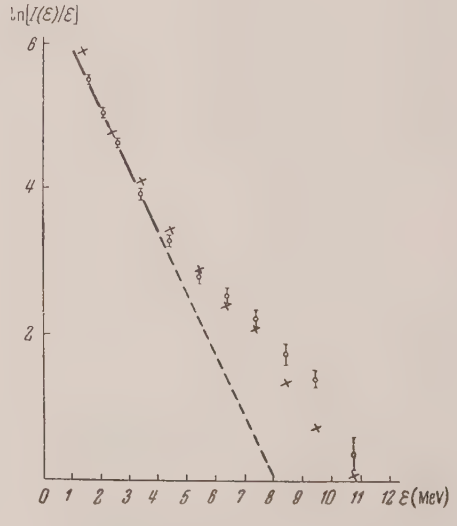

FIG. 3. Spectrum of photoneutrons emitted from Bi at right angles to the direction of the x-ray beam. The crosses refer to the spectrum calculated in accordance with the Courant model.

Relative neutron yields at different energies at 30°, 90° and 150° to the direction of the x-ray beam (per unit solid angle)*.

Energy interval, mev.	30°	90°	150°
1.5—4	0.88 ± 0.04	1 ± 0.04	0.97 ± 0.04
4—7	0.77 ± 0.08	1 ± 0.09	0.66 ± 0.09
7—11	0.17 ± 0.07	1 ± 0.08	0.26 ± 0.06
4—11	0.52 ± 0.06	1 ± 0.06	0.47 ± 0.06
1.5—11	0.74 ± 0.03	1 ± 0.04	0.79 ± 0.04

* The neutron yield at 90° is taken as unity. The errors shown are statistical errors.

along the ordinate axis. The straight segment up to 4 mev yields an average temperature $T = 1.1$ mev. Using a mean excitation energy of about 13 mev, the temperature should be 0.7 mev. The higher value of the temperature is obviously connected with the fact that some of the neutrons with energies below 4 mev are emitted by virtue of a direct interaction. At an energy of approximately 4 mev, above which the neutron yield is obviously due only to the direct photo-effect, a sharp break is observed. The crosses refer to values of $\ln[I(\epsilon)/\epsilon]$ for a neutron spectrum computed under the assumption that the γ-quantum absorbed by the nucleus transfers all of its energy to the ejected neutron. According to Courant[10], in this case the cross-section for the absorption of γ-quanta goes as $\sigma_\gamma \sim 1/E^3$. The value of $\ln[I(\epsilon)/\epsilon]$ computed on this basis is in satisfactory agreement with the experimental data. Other calculations, carried out under the assumption of a small level density at small excitation energies of the residual nucleus, do not yield this type of behavior.

1 H. L. Poss, Phys. Rev. **79,** 539 (1950).
2 Demos, Fox, Halpern and Koch, Bull. Am. Phys. Soc. **27,** 30 (1952).
3 G. A. Price, Phys. Rev. **93,** 1279 (1954).
4 Geller, Halpern and Yergin, Phys. Rev. **95,** 659 (1954).
5 S. A. E. Johansson, Phys. Rev. **97,** 434 (1955).
6 W. R. Dixon, Canad. J. Phys. **33,** 785 (1955).
7 J. Rotblat, Nature **167,** 550 (1951).
8 Halpern, Nathans and Mann , Phys. Rev. **88,** 679 (1952).
9 P. R. Byerly and W. E. Stephens, Phys. Rev. **83,** 54 (1951).
10 E. D. Courant, Phys. Rev. **82,** 703 (1951).

Translated by H. Lashinsky
4

Investigation of Conversion Lines in the β-Spectrum of a Eu^{152}-Eu^{154} Mixture

V. M. Kel'man, V. A. Romanov, R. Ia. Metskhvarishvili and V.A. Koliunov
Leningrad Physical-Technical Institute, USSR Academy of Sciences

(Submitted to JETP editor June 23, 1956)
J. Exptl. Theoret. Phys. (U.S.S.R.) **32**, 39-47 (January, 1957)

Internal conversion lines in the *K* shells and *L* and *M* subshells of Sm^{152} and Gd^{154} were measured with a high resolution β-spectrometer. The ratios of the conversion coefficients were determined for 122 and 123.2 kev transitions. The energy intervals between the conversion lines were measured with high precision.

THE spectrum of a mixture of the long-lived Eu^{152} and Eu^{154} isotopes shows many conversion lines, the most intense of which are due to transitions of Sm^{152} and Gd^{154} nuclei from the first excited states to the ground states[1]. The first excited levels of Sm^{152} and Gd^{154} are 122 and 123.2 kev respectively[2]. The small energy difference between these levels places the corresponding internal-conversion lines of like shells of Sm and Gd very close together, complicating their separation considerably .

To separate the spectrum of the Sm^{152} and Gd^{154} and to find the ratios of the internal-conversion coefficients in the shells and subshells of each of these elements, it is necessary to employ a β-spectrometer of very high resolution. In this investigation we employed for this purpose the prism spectrometer described in Ref. 3, after first increasing its resolution (line half-width 0.04% and in some cases 0.02%)*. In addition, the β-spectrometer was modified to permit accurate measurement of conversion-line energy differences, facilitating considerably the identification of the conversion lines. This β-spectrometer was used to determine the intensity ratios and the energy differences of the strongest conversion lines of Sm^{152} and Gd^{154}.

A mixture of long-lived Eu^{152} and Eu^{154} isotopes was obtained by irradiating natural europium with neutrons. After irradiation, the europium was deposited electrolytically on 5-micron thick aluminum foil. A solution of europium chloride in ethyl alcohol was subjected to electrolysis to obtain a series of sources of various thicknesses 10 mm long and 1 mm wide. The source selected from among these was thin enough to provide good resolution and yet give sufficient intensity. This source was approximately several hundredths of a milligram per square centimeter thi

* The relative half-width of the line is expressed everywhere in this article on a momentum scale.

DESCRIPTION OF β-SPECTROMETER

To increase the resolution of the prism β-spectrometer used in this investigation[3], it was modified as follows.

1. The spectrometer tubes were shielded. The shield construction was the same as used in the Siegbahn spectro-goniometer[4]. Iron rings and shields (Fig. 1) were placed over the spectrometer tubes to reduce the effects of extraneous magnetic fields on the electrons moving in the tubes. In addition, the shields prevented (to some extent) the iron cover of the spectrometer deflecting magnet from disturbing the axial symmetry of the fields of the lenses.

2. Instead of using a straight slit in the recording equipment, the slit was slightly curved to agree in shape with the image of a line source. To determine the shape of the image, the receiving slit was replaced with a photographic plate, which was exposed to the particles passing through the spectrometer. The source used in this case was a deposit of active RdTh on a 10×1 mm strip of aluminum foil; the spectrometer was tuned to the F line.

3. Some modifications were made to the magnet power supply and to the spectrometer lenses. Power was supplied from a storage battery. The current in the main winding *1* (Fig. 2) and in the lenses *2* was regulated with two slide-wire drum-type resistors (each resistor had a drum approximately 1 m long and approximately 40 cm in diameter). The ratio of the currents in the main winding and in the lenses, and also the current in the auxiliary windings *4* (located above the main winding) and *5* (located on the plates) were varied with ordinary rheostats *6*. There was no need to vary this ratio or this current in the auxiliary windings when measuring the group of the peaks corresponding to the conversions in the *L* and *M* subshells. Null methods were used to measure the values of all the currents (using a PPTV-1 potentiometer *7* and standard resistors *8*).

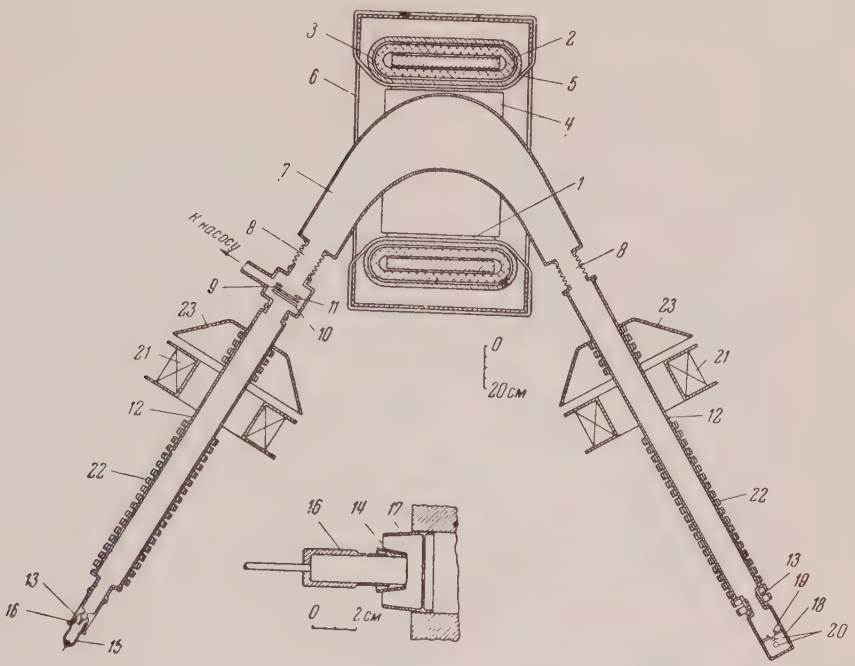

FIG. 1. General view of prism β-spectrometer: *1* – plate of magnet yoke; *2* – main winding; *3* – auxiliary winding, placed over the main one; *4* – auxiliary winding on the plate; *5* – demagnetizing winding; *6* – screen; *7* – spectrometer chamber; *8* – sylphons (bellows); *9* – diaphragm with round hole; *10* – slit diaphragm restricting the beam vertically; *11* – slit diaphragm restricting the beam horizontally; *12* – tubes; *13* – ground edge; *14* – source; *15* – glass insulator; *16* – source holder; *17* – electrode; *18* – counter chamber; *19* – receiver slit; *20* – counters; *21* – magnetic lens; *22* – iron rings; *23* – lens shields.

The currents in the main winding and in the lenses were stabilized by two selenium photocells *9* connected in a bridge circuit and exposed to light reflected from the mirror of sensitive galvanometers *10*. A change in current deflects the galvanometer mirror and causes the corresponding photocell, through an amplifier and a relay system *11*, to actuate motor *12*, which turns the drum of the rheostat so as to return the mirror to its previous position. To reset the equipment to another value of current it is merely necessary to reset the knob of the bridge-circuit potentiometer. The resulting displacement of the mirror causes the rheostat motor to rotate until the required current is established in the circuit.

The electric-bias method was used to measure accurately the energy differences of the conversion lines. A positive voltage, which can be varied in small steps, was applied to a suitably-insulated radioactive source (Fig. 1), and all the currents in the β-spectrometer windings were kept absolutely constant. The number of counts n was then plotted as a function of the voltage U applied to the radioactive source. The distance between the conversion peaks could then be read directly in volts from the curve $n = f(U)$. The electric-bias method was used in its time by Lewis and Bowden[5] to measure the absolute energy difference of monochromatic groups of α-particles. This method was proposed for use in β-spectrometry by Siegbahn[6] for accurate determination of the n/e ratio.

Voltage was applied to the radioactive source from dry cells connected in series. The voltage was determined by conventional measurement of the current in a 3.0062 (sometimes 4.0061) megohm wire-wound resistor. This scheme makes it easy to set and measure voltages up to 5 kv with

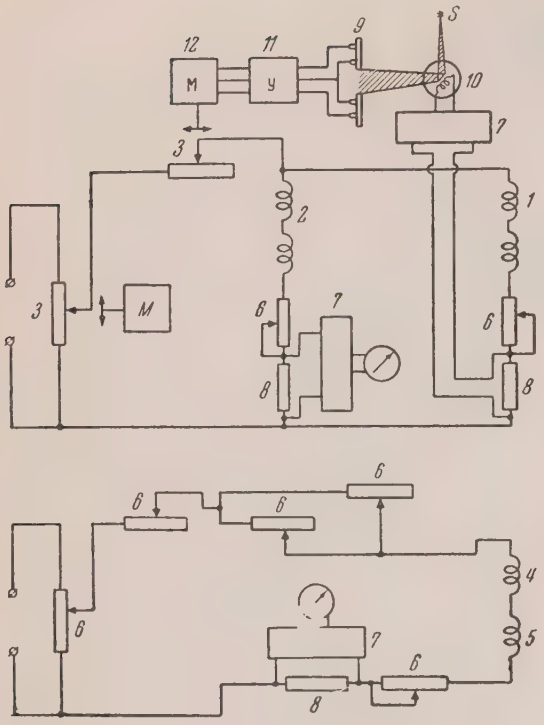

FIG. 2. Power supply circuit of β-spectrometer.

an accuracy to within 1 volt.

Because it has turned out to be much more convenient to plot small portions of the β-spectrum by electric bias rather than measure the current in the main windings and in the lenses, this method is now used also to plot spectra of conversion electrons in the determination of the internal-conversion coefficient ratios. It was established first that within the range of bias used in this investigation, the value of the bias does not effect the areas of the conversion lines. To check this, the F line of an active deposit of RdTh was plotted at various values of bias and the line areas, obtained in different measurements, were compared. They proved to be equal, within the limits of statistical dispersion.

L SUBSHELLS OF Sm^{152} AND Gd^{154}

Figure 3 shows a portion of the spectrum of the mixture of Eu^{152} and Eu^{154}, with the lines formed by internal-conversion electrons of 122 and 123.2 kev gamma rays in the L subshells of Sm^{152} and Gd^{154}. The half-width of the lines is approximately 0.05%. The spectrum was plotted under the following conditions: source dimensions 1 × 10 mm; slit of receiving equipment 1 mm wide, 28 mm long; slit diaphragm *10* (Fig. 1) that limits the vertical divergence of the beam fully open (the only vertical limitation on the beam is diaphragm 9 with a round hole 7 cm in diameter); slit diaphragm *11* which limits the horizontal divergence, cuts a beam 5 cm wide; distance from the source or from the receiving slit to the middle of the corresponding lens 120 cm; aperture ratio of the spectrometer approximately 0.02% of 4π.

The lines could be readily identified by measuring the conversion-line energy differences and comparing these differences with the corresponding energy differences of the electron levels, known from roentgenoscopic measurements[7].

When measuring the energy difference of two conversion lines (even those that were not adjacent), one line was first plotted, followed directly by the second; the first was then repeated and the two energy differences averaged. To some extent, this eliminated the effect of small systematic changes in the intensity of the deflecting magnetic field, which sometimes occurred and which could introduce an error, albeit small, in the measurement. These changes are apparently due to the slow variation in the spectrometer-magnet temperature. The position of the line was established from that of its peak.

Using the measured energy differences of the Sm and Gd conversion electrons and using the electron-level differences given in Ref. 7, it is possible to determine with great accuracy the energy differences of the converting gamma quanta. Thus, for example, the measured energy difference of the conversion electrons from the L_{III} Gd and L_{II} Sm subshells is 1,357 ± 4 ev, from which it follows that the energy difference of the converting gamma quanta in Gd and Sm is 1,292 ev. The error with which the last quantity is determined depends both on the accuracy of our measurements as well as on the accuracy of the data given in Ref. 7.

As can be seen from the drawing, the L_{III}Sm and L_{II}Gd lines did not separate. The distances between these lines and other lines could therefore at first not be established and only the distances from the peak representing the sum of the two lines were measured. To separate the L_{III}Sm and L_{II}Gd lines, the resolution of the β-spectrometer was increased still further in the following manner. An aluminum diaphragm with a slit of 0.5 mm width was placed over the source, thus restricting the width of the source. In addition, diaphragms *10* and *11* (Fig. 1), which limit the divergence of the beam, were so mounted as to form a 4 × 4 cm

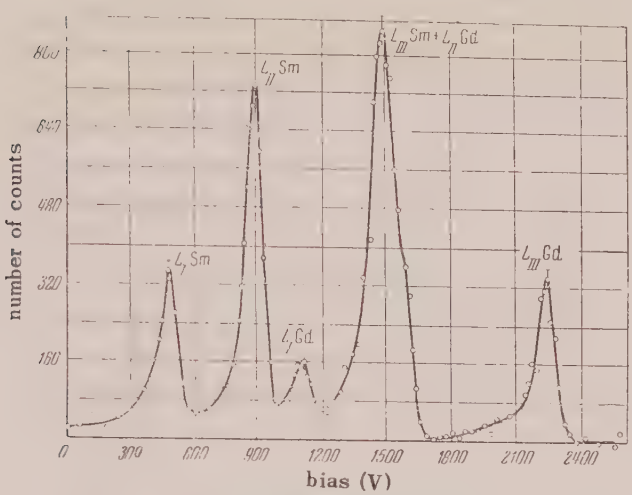

FIG. 3. Portion of β-spectrum of a mixture of Eu^{152} and Eu^{154} isotopes with internal-conversion lines in L subshells of Sm^{152} and Gd^{154}.

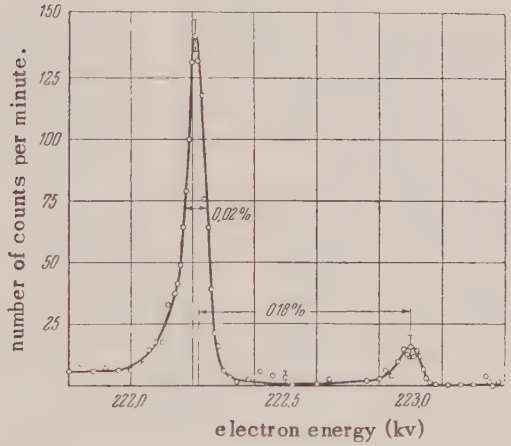

FIG. 4. Conversion lines I and I_a of deposits of active RdTh.

square window (the aperture ratio of the instrument was reduced thereby to 0.01% of 4π).

A check on the resolution of the β-spectrometer for the I and Ia conversion lines of a deposit of active RdTh (Fig. 4) has shown that under these conditions the instrument line half width was 0.02%.

The $L_{III}Sm$, $L_{II}Gd$, and $L_{III}Gd$ lines, plotted with this value of instrument resolution, are shown in Fig. 5. As can be seen, the lines became partly separated. Using graphic line separation, the ratio of the areas (intensities) was found to be $L_{III}Sm/L_{II}Gd = 1.96 \pm 0.05$. The distance between the lines is 76 ± 2 volts. These data were also used to separate graphically the $L_{III}Sm$ and $L_{II}Gd$ lines on Fig. 3, after which it became possible to obtain the distance between each of the $L_{III}Sm$ and $L_{II}Gd$ lines and the other lines, and also to find the ratios of the internal-convergence coefficients in all the L-subshells.

Table 1 compares the electron-level energy differences E obtained from the roentgenoscopic data given in Ref. 7 with the results of our measurements.

To obtain the ratios of the areas of the Sm and Gd conversion lines, the spectrum of the conversion electrons was plotted both by varying the voltage applied to the source (6 times), as well as by the usual method of varying the current in the principal windings and in the lenses (4 times). The first method of plotting the spectrum yielded the following area ratios: for samarium $L_{II}/L_I = 2.25 \pm 0.07$, $L_{III}/L_I = 2.26 \pm 0.07$; for gadolinium

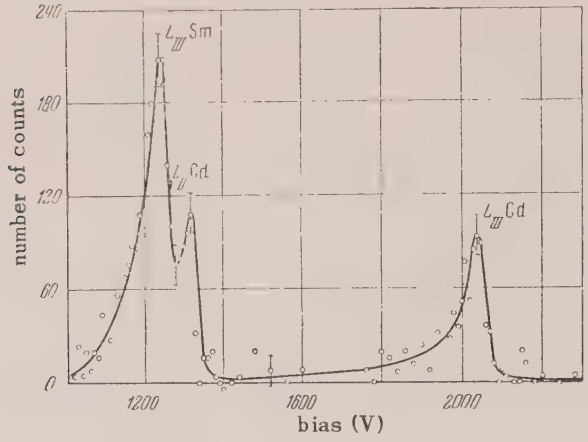

FIG. 5. Conversion lines L_{III} Sm, L_{II} Gd and L_{III} Gd, plotted at increased resolution.

TABLE 1

	Differences in electron energy levels of Sm, ev			Differences in electron energy levels of Gd, ev		
	$E_{L_{II}}-E_{L_I}$	$E_{L_{III}}-E_{L_{II}}$	$E_{L_{III}}-E_{L_I}$	$E_{L_{II}}-E_{L_I}$	$E_{L_{III}}-E_{L_{II}}$	$E_{L_{III}}-E_{L_I}$
From Ref. 7	426	596	1022	441	691	1132
From our work	424±2	597±1	1021±2	443±4	691±4	1131±2

$L_{III}/L_I = 2.80 \pm 0.10$, $L_{III}/L_I = 2.52 \pm 0.07$. The second method yielded for samarium $L_{II}/L_I = 2.20 \pm 0.05$, $L_{III}/L_I = 2.07 \pm 0.07$; for gadolinium $L_{II}/L_I = 2.51 \pm 0.13$; $L_{III}/L_I = 2.30 \pm 0.13$. As can be seen, the ratios of the conversion-line areas obtained by different methods fluctuate within the limits of statistical error. The area ratios deduced on the basis of all the measurements are $L_{II}/L_I = 2.22 \pm 0.04$ L_{III} $L_I = 2.16 \pm 0.05$ for samarium and $L_{II}/L_I = 2.69 \pm 0.08$, $L_{III}/L_I = 2.46 \pm 0.06$ for gadolinium. It follows therefore that the conversion-coefficient ratios are $L_I:L_{II}:L_{III} = 1:$ (2.22 ± 0.04)½ (2.16 ± 0.05) for Sm and $L_I:L_{II}:L_{III} = 1:$ $(2.69 \pm 0.08):$ (2.46 ± 0.06) for Gd.

The experimental values of the ratios of the internal conversion coefficients were compared with theoretical values obtained interpolating the data given by Rouse in Ref. 8. The interpolation was performed graphically. To interpolate by energies, the logarithms of the coefficient of conversion ratios were plotted against the logarithm of the transition energy was plotted. To interpolate by atomic number, a plot was made of the logarithm of the conversion-coefficient ratio vs. the atomic number at the transition energy of interest to us. Comparison of the theoretical values of the ratios of the internal-conversion coefficients, obtained in this manner, with the measured values establishes this transition, as expected to be of the electric quadrupole (E2) type for both Sm^{152} and Gd^{154}. For this type of transition, the theoretical values of the conversion-coefficient ratios (with transition energies expressed in m_0C^2 units, $k = 0.24$) are $L_I:L_{II}:L_{III}$ $= 1: 2.3: 2.2$ for samarium and $L_I:L_{II}:L_{III} = 1:$ $2.7: 2.5$ for gadolinium. This agrees with the measured ratios of the conversion coefficients.

M-SUBSHELLS OF SAMARIUM

Figure 6 shows a portion of the β-spectrum with the lines formed by the internal-conversion electrons in the *M* subshells of Sm (transition energy 122 kev). By measuring the energy intervals between the *M* lines, and also between *M*

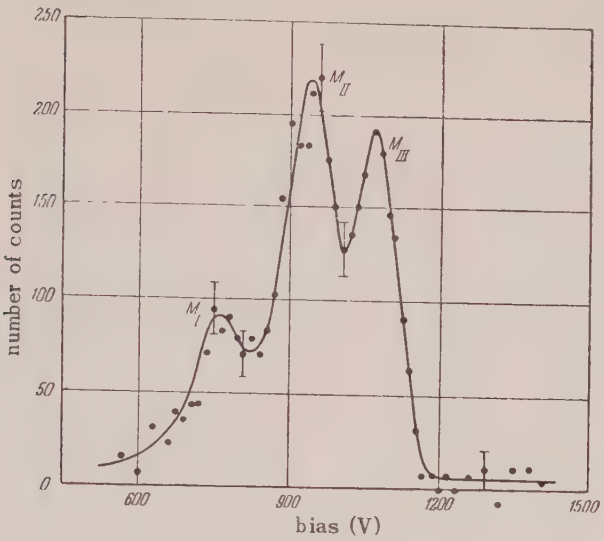

FIG. 6. Internal conversion lines in M subshells of Sm^{152}.

lines and the nearest lines of the L group ($L_{III}Gd$), it is possible to identify them uniquely, as shown in the diagram. The lines M_{IV} and M_V are apparently considerably weaker than those shown on the drawing, and were not noted.

The ratio of the conversion coefficients in the M subshells obtained in this investigation is $M_I:M_{II}:M_{III} = 1:\ (3.4 \pm 0.1):\ (3.3 \pm 0.2)$ (average of eight measurements). The striking fact is that conversion occurs principally in the M_{II} and M_{III} subshells. This agrees with the deductions made on the basis of approximate (non-relativistic, without allowances for shielding) calculations of the relative conversion coefficients in the M subshells[9].

The ratio of the total conversion coefficient in the L subshell to the total conversion coefficient in the M subshell of Sm was measured. The value obtained was $L/M = 4.5 \pm 0.1$ $(L = L_I + L_{II} + L_{III};\ M = M_I + M_{II} + M_{III})$.

MEASUREMENTS OF RATIOS OF CONVERSION COEFFICIENTS IN K AND L SUBSHELLS OF Sm AND Gd.

The K lines of Sm^{152} and Gd^{154}, corresponding to the above transition energies, are shown in Fig. 7. The energy difference of these conversion lines, measured by applying an electric bias to the source, was 2,117 ± 1 ev.

To find the ratios of the coefficient in the K shells to the total conversion coefficients in the L shells of Sm and Gd, the lines were plotted both by using electric bias, as well as by varying the current in the principal windings. When plotting the groups of K lines or groups of L lines by means of electric bias, the current in the spectrotrometer windings was adjusted to correspond approximately to the energy of the plotted group of lines. The value of the potential difference applied to the source was therefore small in all cases (it should have insured the plotting of a spectrum within the limits of a single group). Using this method of measurement, the correction for the value of the energy interval (expressed in ev) should be introduced when changing from one group of lines to the other.

When plotting the spectrum by varying the current in the main windings, the number of counts of the recording device were plotted vs. the value I of this current. Here, therefore, in addition to the usual correction for the width of the pulse interval, a correction was introduced for the non-linear dependence of the spectrometer magnetic field on I. The magnitude of this correction could be obtained without difficulty from the known differences between the momenta of the electrons belonging to different lines in the measured groups of conversion lines. In view of the considerable energy difference between the K and L electrons, a correction was also introduced for the difference in their absorption in the counter films. The curves given in Ref. 10 were used to determine this correction. Inasmuch as the film over the windows of the recording installation

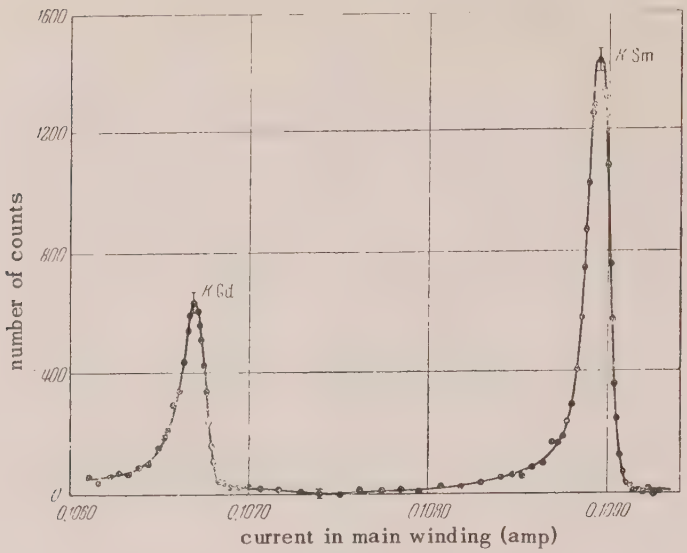

FIG. 7. Internal conversion lines in K shells of Sm^{152} and Gd^{154}.

was relatively thin (the counter chamber was separated from the evacuated portion of the spectrometer by a colloidal film 0.23 mg/cm^2 thick and the total thickness of the colloidal film covering the output opening of the first counter and the input opening of the second counter was 0.1 mg/cm^2), this correction amounted to merely 3% of the K/L ratio.

After processing all the measured data, the following values were obtained for the conversion coefficient ratios: for Sm (transition energy 122 kev) – $K/L = 1.76 \pm 0.04$; for gadolinium (transition energy 123.2 kev) – $K/L = 1.51 \pm 0.03$.

In determining the theoretical values of K/L, we employed the K shells conversion coefficients calculated by L. A. Sliv and I. M. Band (private communication), making allowances for the shielding and for the finite dimensions of the atomic nucleus. The L shell conversion coefficients were obtained by interpolation from the data of Ref. 8. The theoretical relationships obtained in this manner for an E2 transition and a transition energy $k = 0.24$ were $K/L = 2.2$ for samarium and $K/L = 1.9$ for gadolinium.

It must be noted that the small number of the computed L subshells conversion coefficients did not permit sufficiently accurate interpolation. On the other hand the experimentally-obtained K/L ratios are also subject to noticeable systematic errors, owing to the relatively large energy difference between the K and L electrons. These factors apparently explain also the sufficiently large discrepancy between the experimental and theoretical values of the K/L ratios.

1 Slattery, Lu and Wiedenbeck, Phys. Rev. **96**, 465 (1954).

2 Cork, Keller, Rutledge and Stoddard, Phys. Rev. **77**, 848 (1950).

3 Kel'man, Kaminskii and Romanov, Izv. Akad. Nauk, Ser. Fiz. SSSR, **18**, 209 (1954).

4 K. Siegbahn, Ark. for Fys. **4**, 223 (1952).

5 W. B. Lewis and B. V. Bowden, Proc. Roy. Soc. (London) **A145**, 235 (1934).

6 K. Siegbahn, Appl. Sci. Res. **B4**, 25 (1954).

7 Hill, Church and Mihelich, Rev. Sci. Instr. **23**, 523 (1952).

8 K. Siegbahn, *Beta-and Gamma-Ray Spectroscopy*, Amsterdam, 1955, p. 905.

9 E. L. Church and J. E. Monahan, Phys. Rev. **98**, 718 (1955).

10 D. Saxon, Phys. Rev. **81**, 639 (1951).

Translated by J. G. Adashko
6

Charge and Momentum Analysis of Relativistic Particles by the Nuclear Emulsion Technique in Pulsed Magnetic Fields

V. M. Likhachev and Iu. P. Merekov
P. N. Lebedev Physical Institute of the U.S.S.R. Academy of Sciences
(Submitted to JETP editor August 3, 1956)
J. Exptl. Theoret. Phys. (U.S.S.R.) 32, 31-38 (January, 1957)

Strong pulsed magnetic fields (1.2×10^5 gauss) were used in experiments to observe particles from an electron accelerator in nuclear emulsions. The method was applied to measure the energy spectrum of bremsstrahlung from a synchrotron target, and to observe the annihilation of positrons in flight.

As was reported earlier[1], strong pulsed magnetic fields synchronized with the working cycle of an accelerator can be used to obtain a charge and momentum analysis of particles observed in nuclear emulsions.

We have exposed electron-sensitive emulsions [NIKFI type "R"] to γ-rays in a magnetic field of 1.2×10^5 gauss, the emulsions being situated inside a pulsed magnetic field generator (Fig. 1).

FIG. 1. Sketch of the experiment. *1*, γ-rays. *2*, Magnetic field of 7000 gauss. *3*, Pulsed magnetic field generator. *4*, Nuclear emulsion. *5*, Collimator.

The electron-positron pairs were analyzed by momentum and charge, the annihilation of positrons in flight was studied, and the energy spectrum of bremsstrahlung from the synchrotron of the Physical Institute of the Academy of Sciences was measured.

1. METHODOLOGICAL INVESTIGATIONS

1. *Method of measuring magnetic curvature and multiple scattering of particles in emulsion.*

There exist several methods[2-4] for measuring the scattering of particles in emulsion. We adapted and used one of the variants of the angle method.

The track of the particle in the emulsion was divided, as in other methods, into equal intervals (boxes) of length 100μ. Using the eye-piece scale shown in Fig. 2, the angles between consecutive chords were measured. The procedure was as follows: by fine adjustment of the microscope stage, the center of one grain in the particle track is placed at the center of the scale 0. Let the reading α_1 on the scale correspond to the track position 1-2 shown in Fig. 2. After the point 2 on

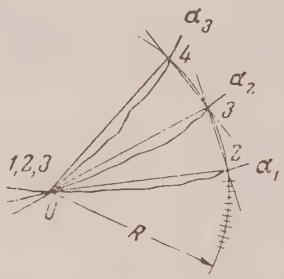

FIG. 2. Eye-piece scale, used for measuring the angles of magnetic deflection and multiple scattering of particles.

the track is moved to the center of the scale, the track occupies position 2-3 and the reading on the scale is α_2, and so on. In this way the track is divided into equal intervals of length R_μ equal to the radius of the scale, and the difference $\alpha_{i+1} - \alpha_i = \Delta_i$ between two consecutive readings represents the angle between consecutive chords. This method is simple to use and can be applied successfully to particles with large scattering. To measure the scattering of high-energy particles, when the intervals must be chosen to be longer than R_μ, the procedure is slightly modified. In this case we consider differences of the form $\alpha_{i+2} - \alpha_i = {}^{(2)}\Delta_i$, or more generally $\alpha_{i+k} - \alpha_i = {}^{(k)}\Delta_i$. If the track is divided into n intervals of length R, then the angle of magnetic deflection in each box is*

$$M = \bar{\Delta}_i \pm (\pi/2)^{1/2} < |S_i| > / \sqrt{n}. \quad (1)$$

* All readings are supposed statistically independent.

Here $\langle|S_i|\rangle=(1/n)\Sigma_i n_i|\Delta_i-\bar{\Delta}_i|$ is the mean value of the random deflection, and the mean square deviation of $\langle|s_i|\rangle$ is

$$\sigma_{\langle|S_i|\rangle}=\langle|S_i|\rangle\sqrt{(\pi-2)/2n}.$$

The results of a calculation of the ratio of the magnetic deflection M to the multiple scattering angle $\langle|s_i|\rangle$, for electrons and positrons, are shown in Fig. 3. The abscissa is the length of the observed track, and results are shown for various values of H. The average number of boxes ($R \approx 100\mu$) per track in our experiment was about 15. From Eq. (1) the error in the determination of the energy of a particle from the magnetic curvature at $H = 1.2 \times 10^5$ gauss was about 30 percent, while the error in a determination by multiple scattering was about 20 per cent. The error in a measurement of the energy of an electron-positron pair was smaller by roughly a factor $2^{-1/2}$, i.e., equal to 21 per cent and 14 per cent by the two methods.

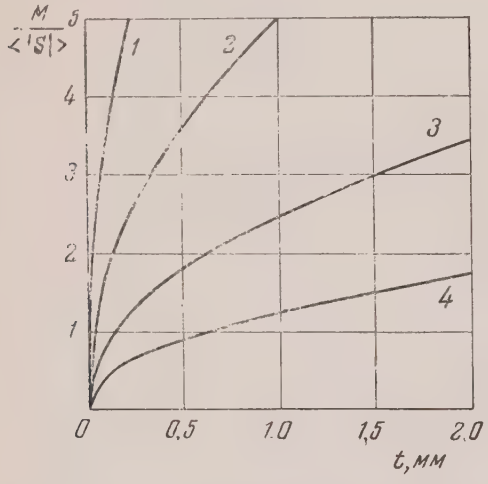

FIG. 3. Results of a calculation of the ratio of the magnetic deflection M to the multiple scattering angle $\langle|S|\rangle$ for an electron or positron. The abscissa is the length of the observed track. Curves are shown for various values of H. *1*, $H = 4.8 \times 10^5$. *2*, $H = 2.4 \times 10^5$. *3*, $H = 1.2 \times 10^5$. *4*, $H = 0.6 \times 10^5$ gauss.

There are two ways to reduce the error in a measurement of magnetic curvature. One is to increase the strength of the magnetic field. The other is to use diluted emulsions**. A rough estimate of the increase in accuracy obtainable from diluted emulsions is made as follows. An emulsion which is diluted twofold gives a reduction of 15 per cent in the average angle of multiple scattering, while the density of grains along a track is hardly affected. An eightfold diluted emulsion gives a reduction of 50 per cent in multiple scattering and a reduction by a factor of 3 in the grain-density[5].

** By diluted emulsions we mean emulsions in which the ratio of gelatin to silver halide is higher than normal.

2. *Questions of Distortion and Spurious Scattering.* The experiments were carried out with NIKFI type "R" emulsions, 200 microns thick. The development was done by the NIKFI staff using the temperature method. After drying, the surfaces of the emulsion were coated with shellac. The following steps were taken to reveal and to measure distortions:

a). The emulsions were exposed twice, first with and then without magnetic field. Between the two exposures the plates were rotated through 180° about an axis perpendicular to their own plane. The tracks of electron-positron pairs produced in the second exposure were used to detect and measure distortions. The scattering of 100 tracks of average length 1.6 mm was measured. In each case the algebraic mean deflection $\langle S_i\rangle$ and the mean absolute deflection $\langle|S_i|\rangle$ were determined. It was found that the algebraic mean deflections lay within the limits of their statistical uncertainty $\pm(\pi/2)^{1/2}\langle|S_i|\rangle/\sqrt{n}$. . A part of the results of these measurements is shown in the following table.

b). From the theory of multiple scattering it is known that, in the absence of distortion, the probability $P(+)$ of a plus sign and the probability $P(-)$ of a minus sign in the first (or second) differences are equal to 0.5. We define the quantity K, which we call the coefficient of distortion, by

$$K = 1 - [P(+)/P(-)]. \qquad (2)$$

In the absence of distortion, and for a track with a sufficiently large number of measurements, $P(+) = P(-) = 0.5$ and $K = 0$. If there is a C-shaped distortion, $P(+) \neq P(-)$, and the probability for a plus or minus sign to appear takes the form

$$P(+) = \int_0^\infty \frac{1}{\sqrt{2\pi D(\theta)}} \exp\left\{-\frac{(\theta-\theta_0)^2}{2D(\theta)}\right\} d\theta = g \neq 0.5;$$

$$P(-) = 1 - g,$$

№	t, μ	$<\lvert s_i \rvert>^\circ$	$<s_i>^\circ$	$\pm(\pi/2)^{1/2}<\lvert s_i \rvert>/\sqrt{n}$
1	1720	0.30	0.02	±0.09
2	1260	0.37	0.05	±0.13
3	2300	0.43	0.06	±0.11
4	1150	0.48	0.01	±0.19
5	1380	0.77	0.01	±0.27
97	1610	0.36	0.08	±0.12
98	1960	0.25	0.03	±0.07
99	1000	1.25	0.05	±0.45
100	1000	0.95	0.10	±0.37

and the coefficient of distortion is

$$K = 1 - [g/(1-g)] \neq 0.$$

If track number i contains N_i measurements (boxes), then the probability that the number of observed positive deflections should be n_i is, in the absence of distortion,

$$P[n_i,\ (N_i - n_i)] = \left(\frac{1}{2}\right)^{N_i} C_{N_i}^{n_i}, \qquad (3)$$

and in the presence of distortion

$$P[n_i,\ (N_i - n_i)] = g^{n_i}(1-g)^{N_i - n_i} C_{N_i}^{n_i}. \qquad (4)$$

In Fig. 4, the theoretical distribution curve of the number of plus signs per track is shown by the continuous line. The experimental points are shown as crosses. The theoretical curve is obtained by adding together curves of the form of Eq. (3), one corresponding to each of the 100 tracks upon which measurements were made. The resultant curve is unsymmetrical because the different tracks have different lengths and different values of N_i.

The theoretical expectation for the probability (or the number of cases) that the number of plus signs in a track should not exceed 5 is 0.54 ± 0.05, i.e., 54 tracks in the observed sample. In this estimate the variance is calculated according to the formula $D(n_i) = Np(1-p)$, with $N = 100$, $p = 0.54$. The experimental value is 53 tracks.

c). "Spurious scattering" includes errors σ_1 arising from non-parallel movement of the microscope stage, the so-called "stage-noise", errors σ_2 arising from the scatter of grains in a particle track away from the true trajectory, and errors of measurement σ_3. Our measurements were made with a MBI-8 microscope. The variance due to "spurious scattering" is the sum of the variances σ_1^2, σ_2^2, σ_3^2. The mean square error produced by spurious scattering in our experiment did not exceed 0.07°.

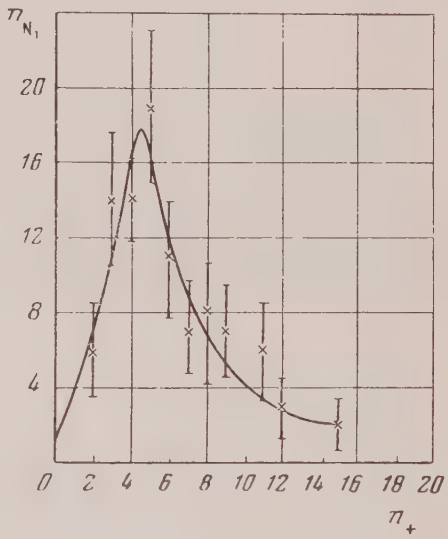

FIG. 4. Theoretical distribution curve for the number of plus signs per track in the 100 tracks which were measured. The crosses are the experimental values.

3. *Charge-Analysis of Particles.*

If the direction of motion of a particle is known, the determination of the sign of the charge depends on measuring the deflection in the magnetic field. Figure 5 shows the probability that a positively charged particle traversing t microns of emulsion in a magnetic field of strength H should be identified as negative. It is assumed that positive and negative particles have the same *a priori* probability and the same momentum distribution.

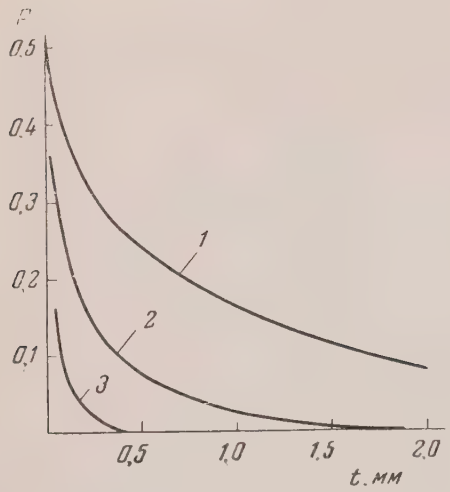

FIG. 5. Curves showing the probability of an incorrect determination of the sign of the charge. *1*, $H = 0.6 \times 10^5$ gauss; *2*, $H = 1.2 \times 10^5$; *3*, $H = 2.4 \times 10^5$.

The determination of the sign of the charge from magnetic deflection in weaker fields (10-30 kilogauss) is made difficult by the presence of strong multiple scattering. However, if the momentum of the particle can be measured, either from the multiple scattering itself or otherwise, then the sign of the charge can be fixed with reasonable certainty[6].

4. *Methodological Deductions.*

Some 800 electron-positron pairs, in which the track-length of each particle was greater than 540μ, were chosen for measurement. The total track-length measured was 230 cm. Figure 6 shows microprojections of electron-positron pairs seen in the emulsion exposed in a magnetic field of 1.2×10^5 gauss. By measuring simultaneously the angle of magnetic deflection M and the angle of multiple scattering S, we can deduce the scattering constant for electrons and positrons of NIKFI type R emulsion. We used the formula

$$K_{100\mu} = \overline{|S|E_M},$$

where E_M is the particle energy determined from the magnetic deflection. The scattering constant derived from 2700 measurements was

$$K_{100\mu} = 23.4 \pm 0.7 \text{ degree MeV}/(100\ \mu)^{1/2}.$$

In measuring the scattering constant we cut off the large-angle single scattering by requiring that each observed scattering angle should not exceed four times the average angle. The mean energy per particle deduced from the magnetic deflection of the 1600 tracks was 43 ±3 mev, and from the multiple scattering measurements 46 ±2 mev.

2. BREMSSTRAHLUNG SPECTRUM AND POSITRON ANNIHILATION IN FLIGHT

The continuous curve in Fig. 7 shows the result of a calculation of the energy-spectrum of bremsstrahlung produced by the synchrotron of the Physical Institute of the Academy of Sciences. The synchrotron target was a tungsten

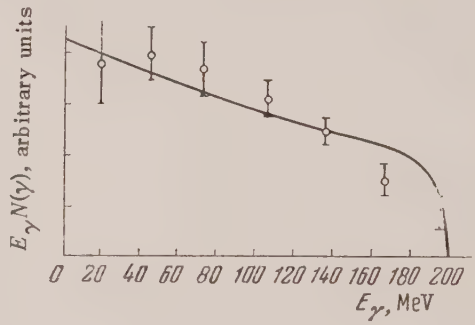

FIG. 7. Experimental values of photon intensity $E_\gamma N(\gamma)$ plotted against photon energy E_γ.

wire of diameter 1 mm. The effective target thickness was 0.16 radiation lengths. The calculation was made from the Bethe-Heitler formula, including effects of absorption of γ-rays in the target and of double radiation by electrons. At such thicknesses the spectrum of photons emitted in the forward direction is rather accurately the same as the complete spectrum from a single atom.

To deduce the number of photons from the number of observed electron-positron pairs, one needs to know the effective cross-section for pair creation by nuclei of the emulsion. We calculated the effective cross-section from the Bethe-Heitler formulas. We used the correction factor*

$$[1 + 0.12\,(Z/82)]^{1/2}.$$

* *Translators note.* This formula is incorrectly quoted and should read $[1 - 0.12\,(Z/82)^2]$.

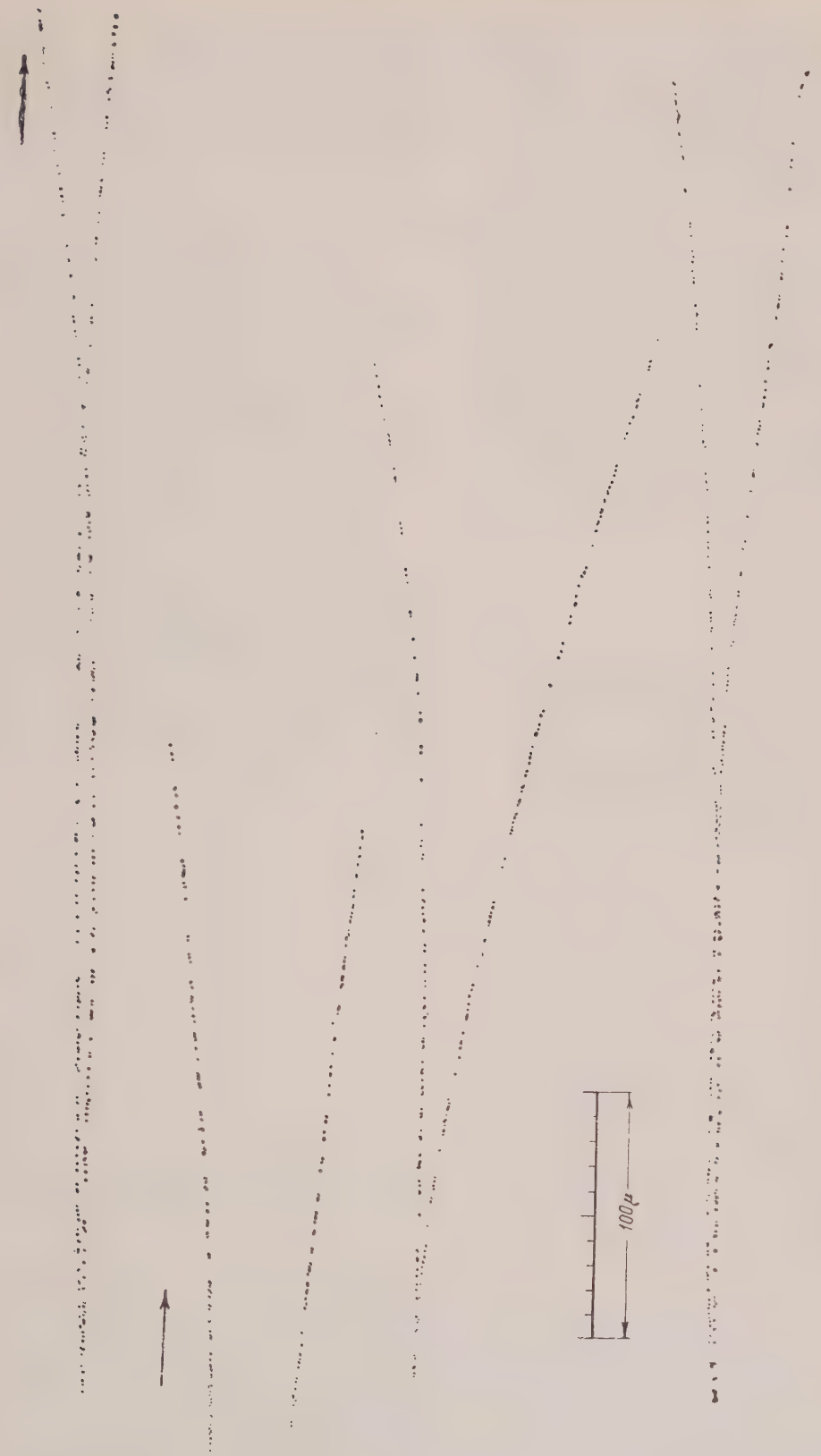

FIG. 6. Microprojections of electron-positron pairs observed in emulsions which were exposed in a magnetic field of 1.2×10^5 gauss.

which has been shown by various authors[7-10] to be required in order to convert the Born approximation Bethe-Heitler cross-sections to true cross-sections. For Ag($Z = 47$) and Br($Z = 35$), which are the worst emulsion nuclei for using the Born approximation, the correction does not exceed 4 per cent.

In making a histogram of the spectral distribution of electron-positron pairs, we accepted only those pairs in which each particle had a track-length in emulsion greater than 540μ. This selection discriminated against low-energy pairs, because the components of low-energy pairs are more likely to leave the emulsion, and it was necessary to correct the observed spectrum accordingly.

The probability that neither component of a positron-electron pair of energy E_0 should leave the emulsion before travelling a distance t microns is

$$Q(E_1, E_0 - E_1, t, d) = [1 - P(E_0, E_1, t, d)]\,[1 - P(E_0, E_0 - E_1, t, d)],$$

Here $P(E_0, E_1, t, d)$ is the probability that one component (electron or positron) with energy E_1 should leave the emulsion of thickness d before travelling t microns. To find the value of Q averaged over the energies of the components we must evaluate an expression of the form

$$\int_0^{E_0 - 2mc^2} \Psi(E_0, E_1)\, Q(E_1, E_0 - E_1, t, d)\, dE_1 \Big/ \int_0^{E_0 - 2mc^2} \Psi(E_0, E_1)\, dE_1,$$

where $\Psi(E_0, E_1)$ is the probability for a photon of energy E_0 to produce a pair with component energies E_1, $E_0 - E_1$. The integration was performed graphically. This correction was calculated, including the effects of multiple scattering and of the deviation of the angles of emission of positron and electron from the direction of the photon[11]. The results of the calculation* are shown in Fig. 8.

The determination of the energy of a pair from the magnetic deflection is made with an average error of 21 per cent. This large experimental error causes a redistribution of points in the observed pair spectrum. The redistribution must be taken into account when the experimental results are compared with theory. Figure 9 shows a histogram of the experimental pair spectrum (full lines), and a histogram obtained from the theoretical spectrum by introducing random "errors of measurement" by a Monte Carlo technique (dotted lines). The two histograms coincide within the statistics.

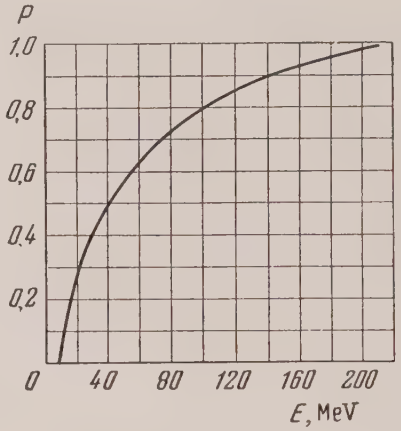

FIG. 8. Calculated correction factor to determine the "true" number of pairs from the number observed in emulsion.

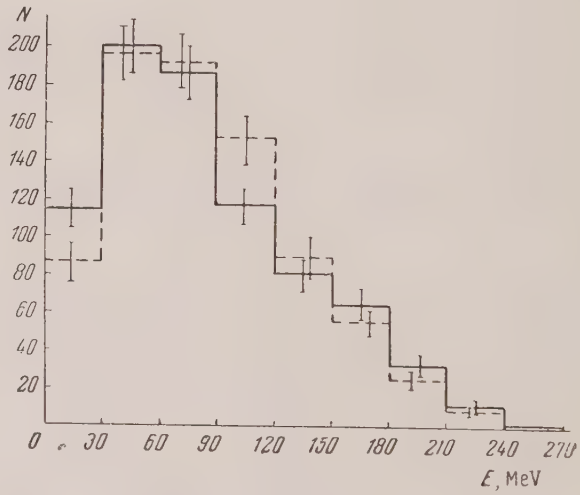

FIG. 9. Histograms of the pair energy spectrum. The full lines are the experimental values. The dotted lines are theoretical values with "errors of measurement" introduced by a Monte Carlo technique.

Experimental values of the photon intensity as a function of photon energy are shown in Fig. 7. These are deduced from the pair spectrum. The experimental errors in the measurement of the pair energies prevent a detailed investigation of the form of the spectrum, especially at the high-energy end where a departure from the Bethe-Heitler theory might most reasonably be expected.

In scanning the emulsions we observed four cases of particle annihilation in flight. A charge measurement showed that in each case the vanishing particle was a positron. In the extreme relativistic limit, the probability for this process is[12]

$$\Phi = \pi r_0^2 \frac{mc^2}{E} [\lg (2E_+ / mc^2) - 1].$$

The annihilation probability for a particle of average energy (43 mev) passing through a length 1400 μ (the average track length) of emulsion is 1.7×10^{-3}. The experimental frequency of annihilation is 1.5×10^{-3}, obtained by dividing the total track-length of the annihilating particles (1795μ) by the total track-length of all positrons ($118 \times 10^4 \mu$).

In conclusion the authors express their deep gratitude to Professors V. I. Veksler and M. P. Podgoretskii for their constant attention and help.

---

* *Note added in proof.* More detailed calculations of the correction were completed after this manuscript went to press. The maximum deviation from the preliminary results was not greater than 15 per cent, and for positron-electron pairs with energy above 100 mev the deviation was not greater than 4 per cent.

1 Likhachev, Kutsenko and Voronkov, J. Exptl. Theoret. Phys. (U.S.S.R.) **29**, 894 (1955).
2 Goldschmidt-Clermont, King, Muirhead and Ritson, Proc. Phys. Soc. (London) **61**, 183(1948).
3 S. Lattimore, Nature, **161**, 518 (1948).
4 P. H. Fowler, Phil. Mag. **41**, 169 (1950).
5 E. C. Dodd and C. Waller, *Fundamental Mechanisms of Photographic Sensitivity* (Butterworths, London 1951), page 266.
6 Dilworth, Goldsack, Goldschmidt-Clermont and Levy, Phil. Mag. **41**, 1032 (1950).
7 H. A. Bethe and L. C. Maximon, Phys. Rev. **93**, 768 (1954).
8 R. L. Walker, Phys. Rev. **76**, 527 (1949).
9 J. L. Lawson, Phys. Rev. **75**, 433 (1949).
10 DeWire, Ashkin and Beach, Phys. Rev. **83**, 505 (1951).
11 M. Stearns, Phys. Rev. **76**, 836 (1949).
12 P. A. M. Dirac, Proc. Camb. Phil. Soc. **26**, 361 (1930).

Translated by F. J. Dyson
5

On the Shape of Resonance Paramagnetic Absorption Curves in Crystals

G. IA. GLEBASHEV
Kazansk State University
(Submitted to JETP editor November 2, 1955)
J. Exptl. Theoret. Phys. (U.S.S.R.) 32, 82–86 (1957)

The 6th order moment of the resonance paramagnetic absorption curve in crystals at high frequency has been calculated. Comparison of the computed 4th and 6th order moments with the experimental values confirms the theory of exchange narrowing. The exchange interaction coefficients thus obtained are smaller than those which are obtained by comparing the Van Vleck and Opechowski formulas for magnetic specific heat and Curie temperature with static susceptibility measurements.

THE calculation of moments of the resonance absorption curve in crystals at high frequencies (spin relaxation) was first carried out by Van Vleck[1]. He determined the 2nd and 4th moments considering dipole and exchange interactions of magnetic ions. It turned out that, with the existence of solely a dipole interaction, the resonance absorption curve has approximately a Gaussian shape. The experimentally observed absorption curves, however, are considerably narrower.

Taking exchange forces into consideration does not change the 2nd moment and strongly raises the 4th order moment. This shows that the exchange interaction of magnetic ions must lead to a narrower resonance absorption curve than is obtained in its absence. Consequently, through the effect of the exchange interaction, one can explain the shape of the experimental absorption curves. In the present work, the question of the adequacy of the narrowing effect of exchange forces is examined. To this end, the 6th moment of the resonance absorption curve is calculated for large static fields.

1. 6th MOMENT

Let us direct a static magnetic field H along the z axis and a high frequency field of frequency ν along the x axis.

For purposes of convenience one calculates the moments not of the curve $\chi''(\nu)$ (χ'' is the imaginary part of the complex magnetic susceptibility), but of the curve

$$f(\nu) = 2kT\chi''(\nu)/\pi\nu,$$

where T is the absolute temperature. In the calculation of moments of the resonance absorption curve in large static fields in a region far from a state of saturation, $f(\nu)$ can be represented in the form (see Ref. 2):

$$f(\nu) = g^2\beta^2(2S+1)^{-N} \times \sum_{n,m} |S_{xnm}|^2 \delta(|\nu_{nm}| - \nu). \quad (1)$$

Here, n and m are indices of eigenvalues of the operator

$$\mathcal{H}' = g\beta H \sum_j S_{zj} + \sum_{j>k} B_{jk} S_{zj} S_{zk} + \sum_{j>k} (A_{jk} - {}^1/_3 B_{jk})(\mathbf{S}_j \mathbf{S}_k),$$

S_{xnm} is a matrix element of the projection of the spin of the system on the x axis, g is the Lande′ factor, β is the Bohr magneton, S is the spin quantum number of a magnetic particle, and

$$A_{jk} \text{ and } B_{jk} = -(3g^2\beta^2/2r_{jk}^3)[3\cos^2(\widehat{Hr}_{jk}) - 1]$$

are the coefficients of the exchange and dipole interactions of the ions j and k, $\overline{\mathbf{S}}_j$ and $\overline{\mathbf{S}}_k$ their spins and r_{jk} the distance between them.

From Eq. (1) one obtains the expression

$$\nu_{2n} = \nu_{2n}/\nu_0 = (-1)^n \operatorname{Sp} U_{2n}^2 / h^{2n} \operatorname{Sp} S_x^2 \quad (2)$$

$$U_{2n} = \mathcal{H}' U_{2n-2} - U_{2n-2}\mathcal{H}' \quad (U_2 = \mathcal{H}' S_n - S_x \mathcal{H}')$$

for the normalized moment of order $2n$ of the resonance absorption curve. In this way the normalized 6th order moment is determined by the formula

$$\overline{\nu}_6 = -\operatorname{Sp} U_6^2 / h^6 \operatorname{Sp} S_x^2. \quad (3)$$

In view of the unwieldiness we cannot completely work out the expression Sp U_6^2 within the confines of the present appper. Briefly, the 6th

order moment can be written in the form

$$\nu_6 = \nu_z^6 + 15\nu_z^4\Delta\nu_2 + 15\nu_z^2\Delta\nu_4 + \Delta\nu_6,$$

where $\overline{\Delta}\,\nu_2$, $\overline{\Delta}\,\nu_4$ and $\overline{\Delta}\,\nu_6$ are the normalized moments of second, fourth and sixth orders relative to the Larmor frequency $\nu_z = g\beta H/h$. The numerical value of the 6th order moment relative to the Larmor frequency was determined for a crystal in which the magnetic ions form a simple cubic lattice, with the direction of the magnetic field H along a principal crystal axis.

The calculation for an arbitrary direction of the field H relative to the crystal axis and also for other crystal lattice types becomes highly complicated. For this reason the value of $\overline{\Delta}\,\nu_6$ averaged over direction of the field H, applicable for absorption curves in powders, was not calculated.

The exchange interaction, owing to the rapid decrease of exchange forces with distance, was considered only for neighboring particles. After rather laborious calculations, the numerical value of the 6th order moment was obtained equal to

$$\begin{aligned}\overline{\Delta\nu_6} = h^{-6}\,[&\varepsilon^2A^4\,(520\lambda^3 - 230\lambda^2 - 14\lambda)\\ &+ \varepsilon^3A^3\,(-31\lambda^3 + 18\lambda^2 - \lambda)\\ &+ \varepsilon^4A^2\,(1080\lambda^3 - 312\lambda^2 + 4\lambda)\\ &+ \varepsilon^5A\,(57\lambda^3 - 21\lambda^2 + 2\lambda)\\ &+ \varepsilon^6\,(665\lambda^3 - 181\lambda^2 + 2\lambda)],\end{aligned} \tag{4}$$

where $\epsilon = -3\,g^2\,\beta^2\,/\,2d^6$, d is the lattice constant, A is the exchange coefficient for neighboring particles and $\lambda = S\,(S+1)$.

2. COMPARISON WITH EXPERIMENT AND DISCUSSION OF RESULTS

For the demonstration of the adequacy of the exchange narrowing let us determine the exchange coefficients from a comparison of the calculated 4th and 6th order moments with experimental values. Insofar as the numerical value of the 4th moment determined by Van Vleck is approximate, its value was calculated under the same assumptions as used for the 6th order moment. The 4th and 2nd moments come out equal to:

$$\begin{aligned}\overline{\Delta\nu_4} = h^{-4}\,[&\varepsilon^2A^2\,(24.22\,\lambda^2 - 3.6\lambda)\\ &+ 3h^4\,(\overline{\Delta\nu_2})^2\,(0.74 - 0.021\,\lambda^{-1})],\end{aligned} \tag{5}$$

$$\overline{\Delta\nu_2} = 4.44\lambda\varepsilon^2/h^{-2}.$$

It is more convenient to compare the ratios

$$X = \overline{\Delta\nu_4}\,/\,(\overline{\Delta\nu_2})^2$$

and

$$Y = \overline{\Delta\nu_6}\,/\,(\overline{\Delta\nu_2})^2.$$

rather than the moments. In our case, these ratios are equal to:

$$\begin{aligned}X &= (A/\varepsilon)^2\,(1.228 - 0,183\lambda^{-1})\\ &\quad + 2.22 - 0,6\lambda^{-1},\\ Y &= (A/\varepsilon)^4\,(5.94 - 2,63\lambda^{-1} + 0.16\lambda^{-2})\\ &\quad + (A/\varepsilon)^2\,(12.34 - 3.65\lambda^{-1} + 0.05\lambda^{-2})\\ &\quad + 7.60 - 2,07^{-1} + 0.02\lambda^{-2}\end{aligned} \tag{6}$$

if the odd powers of A/ϵ with small coefficients are thrown away.

Most often we have to deal with experimental absorption curves in substances for which the spin of the particles $S = 1/2,\ 3/2,\ 5/2$. We give the ratios X and Y for these values of S:

$$S = {}^1/_2:$$

$$X = (A/\varepsilon)^2 + 2.13; \tag{7}$$

$$Y = 2.72\,(A/\varepsilon)^4 + 7.67\,(A/\varepsilon)^2 + 4.88,$$

$$S = {}^3/_2:$$

$$X = 1.18\,(A/\varepsilon)^2 + 2.21;\ Y = 5.25\,(A/\varepsilon)^4 + 11.39\,(A/\varepsilon)^2 + 7.05,$$

$$S = {}^5/_2:$$

$$X = 1.21\,(A/\varepsilon)^2 + 2.21;\ Y = 5.66\,(A/\varepsilon)^4 + 11.94\,(A/\varepsilon)^2 + 7.36.$$

It should be kept in mind that experiment gives the curves $\chi''(H)$, measured with a contant frequency ν of the high frequency field by means of the variation of the static intensity H. However, if one takes into account the smallness of the zero absorption at high frequencies, the weak thermal

dependence $\chi''(T)$, and the invariance of the structure of the bands of the energy spectrum of the spin system in a large static field H under its variation, one can regard that $\chi''(H)$ (especially its side to the right of the peak) is a good approximation of the course of the curve $f(\nu)$. The ratios X and Y were determined from the experimental absorption curves for the various substances.

TABLE

Substance	S	$(A/\varepsilon)_4$	$(A/\varepsilon)_6$	ΔA, %
$Cu(NH_3)_4SO_4 \cdot H_2O$	1/2	1.490	1.481	0,6
$Cu(NH_3)_4SO_4 \cdot H_2O$	1/2	2,486	2.218	10,8
$CuCl_2 \cdot 2H_2O$	1/2	1,166	1.103	5,4
$CuBr_2$	1/2	0.900	0.955	4,4
CuF_2	1/2	0.990	0.980	1
$CuCl_2 \cdot 2(NH_4Cl) \cdot 2H_2O$	1/2	2,445	2,280	6,8
$Cu(C_5H_7O_2)_2$	1/2	1,300	1.265	2,7
$Cu(CHO_2)_2 \cdot 4H_2O$	1/2	1,386	1,301	6,1
$VOCl_2$	1/2	1.221	1.155	5,4
$VO_3(C_6H_4)_3N_2(CH)_2$	1/2	1,506	1,422	5,6
$VOSO_4$	1/2	1.900	1.830	3.7
$CrCl_3$	3/2	1.236	0.981	20.6
$CrCl_3$	3/2	1.603	1.276	20,4
$CrK(SO_4)_2 \cdot 12H_2O$	3/2	1.488	1.349	9,4
$CrK(SO_4)_2 \cdot 12H_2O$	3/2	1.438	1.283	10.8
$CrK(SO_4)_2 \cdot 12H_2O$	3/2	1.363	1.142	16.7
$Cr(C_7H_5O_3) \cdot H_2O$	3/2	0.911	0,731	19.8
$Cr(NH_3)_6Cl_3 \cdot H_2O$	3/2	1.062	0,890	16,2
$CH_2(NH_3)_2 \cdot Cr[N(CS)(CO)SCN_2]$	3/2	0.503	0,336	33.5
$MnCO_3$	5/2	1.030	0.816	14
$MnCO_3$	5/2	1.290	1.11	20.2
$MnSO_4$	5/2	1.61	1.36	15.5
$MnSO_4 \cdot 4H_2O$	5/2	1.648	1.431	13.2
$MnSO_4 \cdot 4H_2O$	5/2	1.739	1.468	15.6
$MnSO_4 \cdot 4H_2O$	5/2	1.009	0.813	19.6
$(FeF_3)_2 \cdot 9H_2O$	5/2	1.613	1.290	20
$Fe(C_5H_7O_2)_3$	5/2	1.126	0.910	19.2

The exchange coefficients $(A/\epsilon)_4$ and $(A/\epsilon)_6$ were determined from the comparison of their calculated and experimental values. The results are given in the Table. The values of the ratio $(A_4 - A_6)/A_4$ are also given (in percent). The scatter of the values of A/ϵ, determined from various measurements for one and the same substance, on the average can be put within ± 15%.

It follows from the tabulated data that for substances whose atoms have spin $S = 1/2$, the percent deviation of the exchange coefficient A_6 from A_4 does not exceed experimental error, and in the majority of cases is considerably less. Thus, a rather satisfactory agreement of the magnitudes of the exchange coefficients A_4 and A_6 is observed between themselves. For other substances ($S > 1/2$), the difference between these quantities is more substantial and for the most part goes beyond the limits of experimental error. This was to be expected as a consequence of neglecting the effect of the crystalline electric field on the shape of the curve. Thus, the facts show that, within the limits of admissible experimental accuracy, the exchange interaction of the magnetic ions of a crystal explains the observed narrowing of the curves of paramagnetic resonance absorption quite satisfactorily.

Such results attract attention: For substances with a considerable density of magnetic ions, the exchange coefficients A/ϵ are smaller than for substances with a small density of magnetic ions. This can imply that substances with small magnetic density have such crystal structure in which two or more closely spaced magnetic ions are contained per unit cell; however, the same result could arise from another source. Actually in substances with a large magnetic density, the absorption curve is disposed to the edges to a greater extent than in substances with a small density of magnetic ions. Experiment does not

permit measurement of the limits of the curves to a sufficient degree, since the curve breaks off early. Therefore, a reduction of the magnitudes of the exchange coefficients can occur, but for the first substances it is strong, and for the second, weak.

The obtained exchange coefficients for paramagnetic substances are not large. They are significantly less than the exchange coefficients determined by Wright [3] from a comparison of the experimental values of the magnetic specific heat and of the Curie temperature Θ with VanVleck's and Opechowski's formulas for them. To what extent should one expect a reduction of the size of the exchange coefficient from a comparison of the moments?. One can point out at least three sources as a reserve for a possible increase of the exchange coefficient: 1) Consideration, in the calculation of the moments, of the correct crystal structure of the substance, 2) Averaging of the moments over the direction of the static magnetic field (for powders) and 3) Use of the exact form of the experimental absorption curve.

Taking account of the actual crystal structure of a substance cannot lead to an essential change of the moments, since the sums which enter in them depend chiefly on the interaction of neighboring magnetic ions.

The use of the averaged 2nd and 4th order moments:

$$\Delta\nu_{2\,av} = {}^{3}/_{5}\, h^{-2} g^4 \beta^4 \lambda \Sigma r_{jk}^{-6},$$

$$\overline{\Delta\nu_{4\,av}} = h^{-4}\left[\varepsilon^2 A^2 (110.1\lambda^2/9 - 4.32\lambda/3) + 3h^4 (\overline{\Delta\nu_{2\,av}})^2 (0.835 - 0.019\lambda^{-1})\right]$$

for the determination of the exchange coefficient (4th order moment determined by the authors of the present paper) gives values of the exchange coefficients smaller by 30–40% than those quoted above.

To obtain Wright's exchange coefficients through the consideration of the exact shape of the experimental absorption curve is also difficult. For this, (no longer speaking about the ratio Y), the ratio X determined from the exact shape of the absorption curve must exceed the available experimental values by hundreds of times, which is difficult to expect.

Thus, the exchange coefficients are not large. With such values of the exchange coefficients, the formulas of Van Vleck [4] and Opechowski [5] for the magnetic specific heat and Θ are unable to explain the experimental values of these quantities.

In conclusion, I express my appreciation to S. A. Al'tshuler for his valuable suggestions.

---

1 J. H. VanVleck, Phys. Rev. 74, 1168 (1948).
2 G. Ia. Glebashev, Reports Kazan State University, 116, 121 (1956).
3 A. Wright, Phys. Rev. 76, 1826 (1949).
4 J. H. VanVleck, J. Chem. Phys. 5, 320 (1937).
5 W. Opechowski, Physica 4, 181 (1937).

Translated by R. L. Eisner
11

Dependence of the Taper Length of Emulsion Tracks on Particle Charge

D. V. VIKTOROV AND M. Z. MAKSIMOV

(Submitted to JETP editor November 23, 1955)
J. Exptl. Theoret. Phys. (U.S.S.R.) 32, 135-138 (January, 1957)

Proceeding from Freier's hypothesis that the tapering of tracks is due to the increase of specific energy losses, it is suggested that an increase of the quantum yield of developed grains with increasing energy absorbed by the photographic layer takes place in nuclear as well as in x-ray emulsions. The energies at which this phenomenon begins are approximately the same. The dependence of the taper length on the particle charge has been computed. The calculations satisfactorily agree with the available experimental data.

IN the past few years, a method has been devised which enables us to identify, by the length of the taper part of the track, the charge of the multiply-charged particles of the heavy component of the primary cosmic radiation which stopped in the emulsion.

Protons and α-particles are relatively easily identified by the grain density in the track, because the tracks of these particles are developed in the film in the form of a discrete chain of grains. The tracks of multiply-charged particles are in the form of a continuous colony of grains, the counting of which is practically impossible. One can, however, utilize another property of such particles: the track of these particles thins down appreciably towards its end. The utilization of the taper length for the determination of the charge has been first considered in the work of Freier[1] who gave a qualitative relationship. It was assumed there that the thinning down is due to the decrease of the specific losses because of electron capture by the ionized nucleus while it is slowing down. The probability of capture or loss of an orbital electron is determined by the velocity of the particle and depends also on the number of already captured electrons; the thinning down becomes noticeable after the capture of the first k-electron.

The experimental taper lengths obtained later[2] do not agree with the theoretical calculations. In addition to some inaccuracy in the calculation pointed out by Perkins[3], a more serious argument against the working hypothesis of the calculation is, according to Lonchamp[4], the discrepancy between the calculated and experimental energy of the residual paths of the particle.

New data became recently available, on the basis of which one can carry out a more exact calculation of the taper length, depending on the particle charge. One can also make some remarks about the mechanism of the thinning down.

It is known that during transition through matter, charged particles spend a substantial part of their energy on the ionization of the matter atoms. The energy losses are determined by the following relations[5]:

$$-dE/dx = (4\pi Z^2 e^4/mv^2) N_A Z_A \ln(2mv^2/I_A), \quad (1)$$

where m is the electronic mass, v – the velocity of the particle, I_A – the mean ionization potential for the atoms of the matter, N_A and Z_A – the number of atoms per cm^3 and the atomic number of the atoms with mass number A, and Z the charge of the impinging particle. This formula is obtained in the Born approximation, by averaging over all the ionization potentials (when the velocity of the particle is greater than that of the orbital electrons and also for matter having a not too large atomic number).

If the velocity of the particle is of the order of the velocity v_e of the orbital electrons, then the dependence of the charge of the particle on its velocity starts to appear. Then one should write [in Eq. (1)] $Z = Z_{\text{eff}}(v_e)$. For the investigation of this dependence, let us use the Thomas-Fermi method[6,7]. In the calculations below, the Thomas-Fermi method is used only up to the K-shell. For the K-shell, we use formulas derived on a quantum-mechanical basis:

$$mv_e^2/2 \approx 13.5\, Z_{\text{eff}}^{4/3}(\text{eV});\quad 1 \leqslant Z_{\text{eff}} \leqslant (Z-2), \quad (2a)$$

$$mv_e^2/2 = 13.5\, Z_{\text{eff}}^2(\text{eV});\quad (Z-2) \leqslant Z_{\text{eff}} \leqslant Z. \quad (2b)$$

As mentioned above, Eq. (1) is obtained after summing over all the electrons of the atoms in the matter. In the transition of charged particles through matter with high atomic number, not all the electrons contribute to the slowing down, but only a part proportional to $Z_A^{1/3} v_s \hbar/e^2$,

where v_s is the velocity of the orbital electrons of the matter. Taking this into account, Eq. (1) will take the form[8]

$$-\frac{dE}{ax} = \frac{4\pi Z_{\text{eff}}^2 e^4 \gamma^2}{mv_e^2} N_A Z_A^{1/3} \times \frac{v_e}{\gamma v_0}\left[3\left(\frac{v_e}{2Z_{\text{eff}}\gamma v_0}\right)^{1/3} - \frac{v_e}{2Z_{\text{eff}}\gamma v_0}\right], \quad (3)$$

where $v_0 = e^2/\hbar$; $v_e = \gamma v$. We will call taper length L the length of the residual path, from the point where the velocity of the ion is of the order of the velocity of the orbital K-electron, to the end of the path:

$$L = -\int_{v=0}^{v=v_e Z/\gamma} dx \quad (4)$$

$$= \int_0^{E_{\text{CI}}} \frac{dx}{dE} dE = \int_{Z_0}^{Z} \frac{dE_{\text{CI}}}{dZ_{\text{eff}}}\left(\frac{dx}{dE}\right) dZ_{\text{eff}}$$

where γ is a coefficient expressing the relationship between the velocity of the orbital electrons and the velocity for which the electron capture is most probable; $mv_e^2/2$ is determined by Eq. (2a) and (2b); Z_0 is determined from the expression (3) when $dE/dx \approx 0$, taking (2a) into account; a is the mass number of the impinging particle;

$$E_{\text{CI}} = \left(\frac{Mav^2}{2}\right)_{v=v_e/\gamma} = 1836\, a \frac{mv_e^2}{2}\frac{1}{\gamma^2}.$$

Substituting (3) and the expression of E_{cr} [(using (2a) and (2b)] into (4), we get the following relation for the taper length:

$$L = k \frac{0.11\ a}{\gamma^3 \rho (Z_A^{1/3}/A)_{\text{av}}} \times [1 + 0.33 \ln (Z-2)]\, 10^{-4}\ (\text{cm}),$$

where ρ is the emulsion density; the subscript av means averaging over all the emulsion atoms; k is a coefficient taking into account the approximate character of the relationship (3).

For a photoemulsion, $\rho (Z_A^{1/3}/A)_{\text{av}} \approx 0.17$; substituting this value (and letting $k \approx 1$; $a \approx 2Z$; $\gamma = 0.65$[9,10]), we get

$$L \approx 4{,}7\ Z[1 + 0.33 \ln (Z-2)] \quad (5)$$

(in microns). This formula is good, generally speaking, for $Z > 2$, which is indicated by the presence of the logarithmic term which appears because of electrons above the K-shell (for $Z = 2$, the second term of (5) should be deleted).

Taper lengths computed from Eq. (5) will be somewhat underestimated for large Z's because in this case $a > 2Z$.

The results of the calculations from formula (5) are presented in the Table and can be compared with the calculations by Freier (from the formula $L \approx 0.72Z^2$ for $Z < 9$) and with the experimental data. The data for $Z = 2$ is taken from Ref. 11; it follows that the charge of the helium ion is unstable at an energy of 2.5 mev (corresponding to the 8.4μ path in the photoemulsion). For $Z = 3$, the data are taken from Ref. 10 (measurements on $_3Li^8$). The calculation is however carried out for $a = 2Z$, and it is therefore necessary to recompute the taper length for $a = 8$, which gives 19.6μ. For $Z = 6$, the data are taken from Ref. 12 – (artificial acceleration of carbon nuclei). The remaining data are taken from Ref. 2.

The taper length computed from formula (5) is in better agreement with the experimental data than the result of Freier's calculations.

The above calculations are carried out with the assumption (the same as Freier's) that the width of the track is determined by the magnitude of the specific energy losses. An experimental confirmation of this point of view is given in Ref. 13, where it is shown that the width of the track of multiply-charged particles from the heavy component of a cosmic radiation is proportional to the specific energy losses up to relativistic energies, if these losses do not exceed 50-60 kev/μ in the emulsion.

In addition, if the dimensions of the developed grains do not depend on the specific energy losses after the mentioned limit, then the external increase of the grain density with the rise of the specific energy losses reminds the effect of change in quantum occurrence of developed grains with the rise of the energy of the quanta, in an x-rays emulsion. (By quantum occurrence, we mean the number of emulsion grains which have gotten the possibility to be developed, per absorbed quantum). It follows from Ref. 14, that the quantum occurence is unity in the range of wavelengths from 1.5 to 0.3 A, and is proportional to the energy of the quanta if the wavelength is decreased from 0.3 to 0.01 A.

It follows from the comparison of specific losses with the energy of the radiation quantum that, in nuclear emulsions, the proportionality of the track's width to the specific energy losses starts to appear starting from somewhat larger magnitudes

TABLE

Dependence of the taper length on the particle charge

Z	Taper length (in microns)		
	Experimental data.	According to Freier	Using formula 5
2	8.4	3	9.4
3	19	6	14.7 (19.6 for $a=8$)
6	50	18	41
9	75	48—58	70
10	90	48—66	80
12	130	64—88	100
13	140	66—114	110
14	130	78—130	121
16	160	100—160	141
20	190	145—240	184
25	240	250—340	241

than in the x-ray emulsions. The rise of the number of developed grains is , in the latter case, due to the secondary electrons. The same mechanism determines apparently the thickening of the multiple charge particle tracks.

The discrepancy between the theoretical and the experimental taper lengths led Perkins[3], and later Lonchamp[4] , to the assumption that the thickening of the particle track is due to δ-electrons. It is known that the number of δ-electrons increases with the decrease of the particle energy, and that the energy decreases – hence their path is shortened. The capture of orbital electrons by a nucleus starts for particle velocities of the order of 10^9 cm/sec; therefore, the maximum electron energy, determined by the relation $w_{max} = 2mv^2$ (where w and m are the energy and mass of the electron and v – the velocity of the particle), is equal to 11 ev.

The paths of electrons with such a small energy have been poorly investigated and although one can determine their number for a given interval of energy, a quantitative estimation of their influence on the track's width is difficult.

In order to check the assumption that the taper length is determined by the increase in the specific energy losses by capture of orbital electrons, one has to measure the change in the specific energy losses for multiply-charged particles. Kuznetsov, Perfilov and Lukirskii[10] have measured the specific energy losses of Lithium ions from explosive nuclear fission, on the basis of the linear dependence of the specific energy losses on the darkening. They show that the specific energy losses almost do not change when the charge of the particle is decreased. This result is confirmed by the experiment with artificially accelerated nitrogen ions[15]. Let us note that the nitrogen ion energy was not sufficient for a total ionization, i.e., the measurement was carried out only in a taper region where the ionic charge was known to be less than seven. Therefore, on this basis one cannot reach the conclusion of independence of the specific energy losses on the energy for nitrogen nuclei, i.e., for nitrogen atoms with charge seven.

After what was said, it is obvious that the difficulty of the taper length measurement for particles with $Z < 6$ does not come from the fact that the length is small, but from the fact that specific energy losses vary negligibly with the electron capture by the slowing down particle, and that the width of the track is practically constant, i.e., there is no visible taper. Further experiments with artificially accelerated multiple charge ions of sufficient energy losses on the width of the particle track.

1 Freier, Lofgren, Ney and Oppenheimer, Phys. Rev. **74**, 1818 (1948).

2 Hoang-Tchang-Fong and D. Mortellet, Compte rendus **231**, 695 (1950).

3 D. H. Perkins, Proc. Roy. Soc. (London) **203**, 399 (1950).

4 S. P. Lonchamp, J. Phys. Rad. **14**, 433 (1953).

5 N. Bohr, Phys. Rev. **58**, 654 (1940); **59**, 270 (1941).

6 J. Knipp and E. Teller, Phys. Rev. **59**, 695 (1941).

7 N. Mott and G. Massey, *Theory of atomic collisions.*

8 N. Bohr, *Transition of charged particles through matter.*

9 K. C. Stephens and D. Walker, Phil. Mag. **45**, 543 (1954).

10 Kusnetsov, Likurskii and Perfilov, **100**, 665 (1955).

11 P. L. Kapitza, Proc. Roy. Soc. **106**, 602 (1924).

12 J. F. Miller, Phys. Rev. **83**, 1261 (1951).

13 M. Ceccarelli and G. T. Zorn, Phil. Mag. **43**, 356 (1952).

14 D. Bramley and R. H. Herz, Proc. Phys. Soc. **638**, 90 (1950).

15 Reynolds, Scott and Zucker, Phys. Rev. **95**, 671 (1954).

Translated by E. S. Troubetzkoy
18

Excitation of Betatron Oscillations by Synchrotron Momentum Oscillations in a Strong Focusing Accelerator

IU. F. ORLOV

(Submitted to JETP editor November 15, 1955)
J. Exptl. Theoret. Phys. (U.S.S.R.) **32**, 130-134 (January, 1957)

The occurrence of resonances between the synchrotron oscillations of the momentum p and the amplitude beats near resonance on magnetic field perturbations is demonstrated. Resonances occur if the ratio between the beat frequency (for $\Delta p/p = 0$) and the frequency of synchrotron oscillations is an integer. Transitions through these resonances are examined in the linear and non-linear approximations.

1. EQUATIONS OF MOTION AND RESONANCES

LET us examine the simultaneous effect of the perturbation of the magnetic field and of the betatron frequency, due to the synchrotron oscillations of the momentum. The simultaneous effect of a parametric resonance is not important here. Let us consider, for example, the radial oscillations. The initial equations have the form

$$\frac{d^2r}{d\theta^2} - \left(\frac{l}{2\pi}\right)^2 \frac{\partial H/\partial r}{P_0} r + \left(\frac{l}{2\pi}\right)^2 \frac{\partial H/\partial r}{P_0} \frac{\Delta p}{p} r = \left(\frac{l}{2\pi}\right)^2 \frac{\Delta H}{P_0}, \tag{1}$$

where $1/p_0 = e/cp_0 = 1/\rho_0$; ρ_0 is the radius of the unperturbed closed orbit; l is the length of the periodic sector; $\theta = (2\pi/l)s$; s is the coordinate along the unperturbed closed orbit. The small synchrotron oscillations of the momentum are described by the term $\Delta p/p$. The gradient of the magnetic field $\partial H_0/\partial r$ has a period of 2π.

The general solution of the unperturbed equation ($\Delta p/p = \Delta H = 0$) has the form

$$r = a\varphi^* + a^*\varphi, \quad \varphi(\theta) = f(\theta)\exp(i\nu\theta), \quad f(\theta) = f(\theta + 2\pi) \tag{2}$$

(φ is the Floquet function and ν the known betatron quasi-frequency). As usually, we seek a solution of Eq. (1) in the form

$$r = x\varphi^* e^{-i\nu\theta} + x^*\varphi e^{i\nu\theta}, \quad r' = x\varphi'^* e^{-i\nu\theta} + x^*\varphi' e^{i\nu\theta}. \tag{3}$$

For x we have the equation

$$\frac{dx}{d\theta} + i\nu x = -i\left(\frac{l}{2\pi}\right)^2 \frac{1}{w} f(\theta) \frac{\partial H/\partial r}{P_0} (xf^* + x^* f) \frac{\Delta p}{p} - i\left(\frac{l}{2\pi}\right)^2 \frac{1}{w} f(\theta) \frac{\Delta H}{H}, \quad w = i(\varphi\varphi'^* - \varphi^*\varphi'). \tag{4}$$

In the linear approximation,

$$\Delta p/p = (\Delta p/p)_{\max} \sin \Omega\theta, \tag{5}$$

where Ω is the synchrotron frequency in appropriate units.

Equation (4) can be solved in the usual way, by finding the general solution for $\Delta H = 0$ and then the solution of the complete equation (4). If $\epsilon_1 \ll 2\Omega$, then

$$\frac{\varepsilon_1}{2\Omega} \ll 1, \quad \varepsilon_1 = \frac{1}{2\pi}\left(\frac{\Delta p}{p}\right)_{\max} \times \left(\frac{l}{2\pi}\right)^2 \int_0^{2\pi} |\varphi|^2 \frac{\partial H/\partial r}{P_0} d\theta, \tag{6}$$

and the solution for $\Delta H = 0$ has the form

$$x_0 \approx Ae^{-i\nu\theta}\left(1 + 2\sum_k \frac{1}{k!}\left(\frac{i\varepsilon_1}{2\Omega}\right)^k \cos k\,\Omega\theta\right). \tag{7}$$

This solution can be obtained by expanding all the terms of the right hand side of (4) in Fourier series. In the expansion (7), we are interested in $k \sim 3$-5. For such k's the following strong equality is true.

$$1 > \nu \gg k\Omega. \tag{8}$$

Hence the only term which contributes appreciably to the right hand side of (4) is

$$-i\left(\frac{l}{2\pi}\right)^2 \frac{1}{\omega} < |\varphi|^2 \frac{\partial H/\partial r}{P_0} > \frac{\Delta p}{p} x = -i\varepsilon_1 (\sin \Omega\theta) x. \tag{9}$$

The remaining linear terms are small corrections for x_0 and have, furthermore, such frequencies which are of no interest.

For $\epsilon_1/2\Omega \gtrsim 1$ the expansion (7) is not adequate. Let us note, however, that Ω being small, we can speak of an "instantaneous" frequency

$$\nu_\theta = \nu + \varepsilon_1 \sin \Omega\theta. \tag{10}$$

Formula (10) is obtained in correspondence with (4) and (9). Instead of (7) we get

$$x_0 \approx A \exp\left\{-i\int_0^\theta \nu_\theta d\theta\right\} \tag{11}$$

$$= A \exp\left\{-i\nu\theta + i\,\frac{\varepsilon_1}{\Omega}(\cos\Omega\theta - 1)\right\}.$$

It is easy to see that (7) is a Fourier expansion of the function

$$\exp\left[-i\nu\theta + i\,(\varepsilon_1/\Omega)(\cos\Omega\theta - 1)\right]$$

for $\epsilon_1/2\Omega \ll 1$. Hence (11) is the general solution of (4) for $\Delta H = 0$.

Let us note that, according to (7) and (11), we can speak of an approximate Floquet function for Eq. (4), namely:

$$\Phi(\theta) = F(\theta)\exp(i\nu\theta), \tag{12}$$

$$F(\theta) = F(\theta + \tau)$$

$$= f(\theta)\exp\{i(\varepsilon_1/\Omega)(\cos\Omega\theta - 1)\},$$

$$\Phi(\theta) = \varphi(\theta)\exp\{(i\varepsilon_1/\Omega)(\cos\Omega\theta - 1)\}, \tag{13}$$

where τ is the period of the synchrotron oscillations.

We seek the solution of the complete equation (4) in the form

$$x = a\Phi^* + a^*\Phi. \tag{14}$$

For a we have

$$a = \text{const} + \frac{i}{w\rho_0}\left(\frac{l}{2\pi}\right)^2 \int_0^\theta f(\theta)\,\frac{\Delta H}{H_0} \tag{15}$$

$$\times \exp\left[i\nu\theta + \frac{i\varepsilon_1}{\Omega}(\cos\Omega\theta - 1)\right] d\theta.$$

The frequency ν is always chosen within the limits

$$k/M - 1/2M < \nu < k/M, \tag{16}$$

where k is an integer and M is the number of periodic sectors. For $\nu = k/M$ we have two resonances: the so-called outside resonance (usual resonance on magnetic field perturbations) and the parametric one; for $\nu = k/M - 1/2M$ we have only the parametric resonance (resonance on the gradient perturbation).

Let us consider only a single resonant harmonic in the integral of Eq. (15):

$$he^{-i(k\theta/M+\gamma)} = \left[\frac{i}{w\rho_0}\left(\frac{l}{2\pi}\right)^2 \frac{1}{2\pi M} \right. \tag{17}$$

$$\left. \times \int_0^{2\pi M} f(\theta)\,\frac{\Delta H}{H}\exp(ik\theta/M)\,d\theta\right] e^{-ik\theta/M}.$$

then

$$a = \text{const} + he^{-i\gamma_1}\int_0^\theta \exp\left[i\varepsilon_0\theta + \frac{i\varepsilon_1}{\Omega}\cos\Omega\theta\right] d\theta, \tag{18}$$

$$\gamma_1 = \gamma + \varepsilon_1/\Omega;$$

$$\varepsilon_0 = \nu - k/M. \tag{19}$$

where ϵ_0 is the distance to the outside resonance for $\Delta p/p = 0$. The integral in (18) describes, for $E_1 = 0$ the amplitude beat of an equilibrium orbit with a frequency ϵ_0*. For $\epsilon_1 \neq 0$, $\Omega \to 0$, $\epsilon_0/\Omega \neq n$. (n is an integer), Eq. (18) describes the change of the equilibrium orbit for an adiabatic change of ϵ

$$\varepsilon = \varepsilon_0 + \varepsilon_1 \sin\Omega\theta,$$

$$a = \text{const} + (h/\varepsilon)\exp(i\varepsilon\theta + i\gamma_2). \tag{20}$$

Resonances occur when the equalities $\epsilon = n\Omega$ are satisfied[1]. According to (18),

$$a \approx \text{const} + \frac{h}{\varepsilon}\exp(i\varepsilon\theta + i\gamma_2)$$

$$+ \theta h J_n\left(\frac{\varepsilon_1}{\Omega}\right) e^{-i\gamma_1}. \tag{21}$$

2. TRANSITION THROUGH RESONANCES IN THE LINEAR APPROXIMATION

As it is known, Ω changes in time. In a slow transition through a resonance, the main contribution to the integral

$$\int_0^{t=\Omega\theta} \frac{1}{\Omega}\exp\left(i\,\frac{\varepsilon_0}{\Omega}t + i\,\frac{\varepsilon_1}{\Omega}\cos t\right) dt \tag{22}$$

comes from the variation of the coefficient ϵ_0/Ω in the exponential. The resonance being very sharp, the variation of Ω does not practically affect the factor $(1/\Omega)\exp\{i\epsilon_1/\Omega)\cos t\}$; the variation of ϵ_0/Ω is, however, quite appreciable because the resonance occurs only if ϵ_0/Ω is an integer.

Writing ϵ_0/Ω in the form

$$\varepsilon_0/\Omega = n - \frac{n}{\Omega}\,\frac{d\Omega}{dt}(t - t_0), \quad t_0 \sim t \tag{23}$$

---

* The sign of $\epsilon_0 = \nu - k/M$ is irrelevant for the effect under consideration. We put $\epsilon_0 > 0$.

we must make the usual substitution

$$\frac{\varepsilon_0}{\Omega} t \to \int_0^t \frac{\varepsilon_0}{\Omega} dt = \left(n + \frac{n}{\Omega}\frac{d\Omega}{dt} t_0\right) t - \frac{n}{2\Omega}\frac{d\Omega}{dt} t^2 \quad (24)$$

in the exponent of the integral (22). During a single period of synchrotron oscillations, Ω changes only slightly; therefore,

$$\int_0^t \frac{1}{\Omega} \exp\left(\frac{i\varepsilon_0}{\Omega} t + \frac{i\varepsilon_1}{\Omega} \cos t\right) dt \quad (25)$$

$$\approx J_n\left(\frac{\varepsilon_1}{\Omega}\right) \int_0^\theta \exp\left(i\beta\vartheta - \frac{n}{2}\frac{d\Omega}{d\vartheta}\vartheta^2\right) d\vartheta, \quad \beta = n\frac{d\Omega}{d\vartheta}\vartheta_0.$$

the quantity $J_n(\epsilon_1/\Omega)$ falls off rapidly as $n = \epsilon_0/\Omega$ increases. Hence only the transitions through the first resonances $n = 2, 3, 4, 5$ are appreciable. In the initial period, the acceleration changes according to the law $\Omega \approx \Omega_0 p_0/p$; hence

$$\left|\frac{nd\Omega}{d\vartheta}\right| \approx \left|\frac{\varepsilon_0}{2\pi M}\frac{dT/dN}{2T}\right|, \quad T = \frac{p^2}{2m}, \quad (26)$$

where dT/dN is the kinetic increase per revolution. Substituting this into (25) we get

$$a \approx \text{const} + (h/\varepsilon)\exp(i\varepsilon_0\vartheta + i\gamma) + 2\pi h J_n(\varepsilon_1/\Omega)\, e^{i\delta}\,(C(u) - iS(u)) \times \sqrt{MT/(\varepsilon_0 dT/dN)}; \quad (27)$$

$$u = u_0 + \vartheta\sqrt{\frac{n}{\pi}\frac{d\Omega}{d\vartheta}} = u_0 + \vartheta\sqrt{\frac{\varepsilon_0 dT/dN}{4\pi^2 MT}}, \quad (28)$$

where $C(u)$ and $S(u)$ are the Fresnel integrals.

According to (14) and (17), the maximum increase of r after the transition through a resonance is equal to

$$(\Delta r)_{\max} = 4\pi |\varphi|_{\max} h J_n\left(\frac{\varepsilon_1}{\Omega}\right) \times (C^2 + S^2)^{1/2}_{\max}\left(\frac{MT}{\varepsilon_0 dT/dN}\right)^{1/2} \approx 4\pi |\varphi|_{\max} h J_n\left(\frac{\varepsilon_1}{\varepsilon_0} n\right)\left(\frac{MT}{\varepsilon_0 dT/dN}\right)^{1/2}. \quad (29)$$

Assuming a static independence of the perturbations in the various magnets, we have for $\sqrt{\langle h^2\rangle}$, according to (17)

$$\sqrt{\langle h^2\rangle} = \frac{1}{w\rho_0}\left(\frac{l}{2\pi}\right)^2 \frac{1}{2\pi M^{1/2}} \times \sqrt{\left\langle\left(\frac{\Delta H}{H}\right)^2\right\rangle}\left(\left|\int_0^\pi \varphi dt\right|^2 + \left|\int_\pi^{2\pi} \varphi dt\right|^2\right)^{1/2}. \quad (30)$$

The following approximate equality is usually satisfied:

$$\partial H_\cdot(\vartheta)/\partial r \approx -\partial H(\vartheta + \pi)/\partial r. \quad (31)$$

Hence

$$\varepsilon_1 \approx \frac{1}{2\pi}\left(\frac{\Delta p}{p}\right)_{\max}\left(\frac{l}{2\pi}\right)^2 \frac{1}{b\rho_0} \left|\int_0^\pi |\varphi|^2 dt - \int_\pi^{2\pi} |\varphi|^2 dt\right|, \quad (32)$$

$$b = H/(\partial H(\partial r). \quad (33)$$

The order of magnitude of ϵ_0 is $1/8\,M$ -$1/4\,M$. Equation (29) can be written in another form. Let us denote by r_0 the amplitude of the equilibrium orbit for $\Delta p/p = 0$:

$$r_0 = 2|\varphi|_{\max} h/\varepsilon_0. \quad (34)$$

Then

$$\frac{(\Delta r)_{\max}}{r_0} \approx 2\pi\varepsilon_0 J_n\left(n\frac{\varepsilon_1}{\varepsilon_0}\right)\left(\frac{MT}{\varepsilon_0 dT/dN}\right)^{1/2}. \quad (35)$$

And we have an analogous formula for the vertical oscillations.

3. EFFECT OF NONLINEARITY IN THE TRANSITION THROUGH RESONANCES

The effect of nonlinearity can be taken into account by making the substitution

$$\varepsilon \to \varepsilon + \alpha a^2, \quad (36)$$

$$\alpha = \pm\frac{l^2}{8\pi^2 w}\frac{1}{H_0\rho_0}\frac{1}{2\pi}\int_0^{2\pi} |\varphi|^4 \frac{\partial^3 H}{\partial r^3} d\vartheta$$

[a from Eq. (18)]; if the plus sign is taken for r, z -oscillations, then the minus sign is taken for the z, r-oscillations. This is related to the fact that, usually,

$$\partial^3 H(0)/\partial r^3 \approx -\partial^3 H(\vartheta + \pi)/\partial r^3.$$

During the transition through resonance, a^2 contains a constant term, an oscillating term and a slowly increasing term. The constant term changes only the magnitude ϵ_0, and the oscillating term has no effect. As far as the slowly increasing term is concerned, when the inequality $\alpha(\nu - k/M) < 0$ is satisfied, the increase of a^2 lead to the situation where the ratio $(\nu - k/M + \alpha a^2)/\Omega$ remains constant as Ω decreases. This will lead to particle loss.

For this not to happen, it is obviously sufficient that the following inequality be satisfied.

$$nd\Omega/d\theta \gg \alpha (da^2/d\theta)_{\max},$$

where $(da^2/d\theta)_{max}$ has to be taken in a region of monotonic increase of a, according to (27). In this region,

$$\frac{dC}{d\theta} \approx \frac{dS}{d\theta} = \frac{dS}{du}\frac{du}{d\theta} \approx 0.7\,\frac{1}{2\pi}\left(\frac{\varepsilon_0\, dT/dN}{MT}\right)^{1/2}.$$

Therefore

$$\alpha\left(\frac{da^2}{d\theta}\right)_{\max} \approx 3.6\pi\alpha h^2 J_n^2\left(n\,\frac{\varepsilon_1}{\varepsilon_2}\right)\left(\frac{MT}{\varepsilon_0\, dT/dN}\right)^{1/2}.$$

And we finally get the safety factor condition

$$150\alpha h^2 J_n^2\left(n\,\frac{\varepsilon_1}{\varepsilon_0}\right)\left(\frac{MT}{\varepsilon_0\, dT/dN}\right)^{2/3} \ll 1 \qquad (37)$$

or

$$\frac{\alpha\,(\Delta r)^2_{\max}}{|\varphi|^2_{\max}}\left(\frac{MT}{\varepsilon_0\, dT/dN}\right)^{1/2} \ll 1. \qquad (38)$$

This condition is not difficult to satisfy. It is automatically satisfied for the usual specifications on $\partial^3 H/\partial r^3$ and $(\Delta r)_{max}$

1 Hammer, Pidd and Terwilliger, Rev. Sci. Instr. 26, 555 (1955).

Translated by E. S. Troubetzkoy
17

SOVIET PHYSICS JETP VOLUME 5, NUMBER 1 AUGUST, 1957

On the Construction of the Scattering Matrix. II. The Theory with Non–Local Interaction

B. V. MEDVEDEV
Mathematical Institute, Academy of Sciences, USSR

(Submitted to JETP editor July 28, 1955)
J. Exptl. Theoret. Phys. (U.S.S.R.) 32, 87–98 (January, 1957)

N. N. Bogoliubov's method for constructing the scattering matrix is generalized to the case of a theory with non–local interaction. For such a theory, a scattering matrix is constructed which satisfies the physically necessary requirements.

1. INTRODUCTION

ATTEMPTS, having their origin in the "struggle with divergences", to avoid the use of point interactions in the quantum theory of fields and to replace it by an extended interaction, are as old as quantum electrodynamics itself.[1–3] However, elaborate investigations of such theories,[4–5] undertaken within the framework of the description of a many–electron system by means of the many–time formalism or the Tomonoga–Schwinger equation in the interaction representation, have shown that the introduction of a form factor violates the conditions for solvability of the equations of motion, since the Hamiltonians at points with space–like separation no longer commute. Consequently, the non–local theory is incompatible with the Hamiltonian method. The physical reason for this is that the introduction of a form factor actually results in propagation of signals (at least, in the small) with super–light velocity. Thus the requirement that there exist a wave function describing the state of the system at a definite time loses its meaning.

In the hope of avoiding the difficulties of the Hamiltonian method, attempts have been made to go directly to the Euler–Lagrange integro–differential equations which follow from the variational principle with non–local interaction.[6] In quantum theory this procedure leads to the considera-

tion of the equation of motion of the field operators in the Heisenberg representation. More recently, there has been undertaken a further development of one of the variants of such a theory[7-8], which is characterized by the action function for the interaction:

$$S_{\text{int}} = \int dx'\, dx''\, dx'''\, \Lambda(x', x'', x''') \qquad (1)$$

with the "Lagrangian"

$$\Lambda(\xi) = \Lambda(x', x'', x''') \qquad (2)$$

$$= gF(x', x'', x''')\bar{\psi}(x')\, u(x'')\, \psi(x'''),$$

where $\bar{\psi}$, ψ and u are the Heisenberg operators of Dirac and scalar fields, $F(x', x'', x''')$ is the form factor, and ξ denotes the triplet of points x'. x'' and x''' (in the sequel $d\xi$ will denote the product $dx'\, dx''\, dx'''$).

However, more detailed investigation[9-11] has shown that Bloch's proof[8] of the unitary of the S-matrix is incorrect, and that with this method for constructing a non-local theory one obtains (except, possibly, for a very restricted class of special Lagrangians) a non-unitary S-matrix, which is physically inadmissible. One may surmise that the difficulties with unitarity which occur in the Heisenberg representation are a direct consequence of the failure to satisfy the conditions for solvability of the Tomonaga-Schwinger equation in the interaction representation.

This idea prompts one to introduce the non-local interaction not into the theory of the equation of motion, but rather into the theory of the S-matrix, whose framework is much broader, and in which the formulation of the problem is more natural for a non-local theory. The present paper is devoted to the generalization to a non-local theory of Bogoliubov's method. [12,13] * where it will be convenient to use the form of the theory presented in Ref. 14. ** The starting point for the construction will be the physically obvious requirements I, *A-D* which are imposed on the S-matrix.

As in the local case, in order to give an explicit description of the operation of switching on and switching off the interaction, we replace (cf. B. S. and I) the actual Lagrangian (2)*** by $g(\xi)\Lambda(\xi)$ where $g(\xi)$ here is a function of the three space-time points x', x'' and x'''. The full switching on of the interaction over all space will, of course, correspond to $g(\xi) = 1$. The expansion of $S(g)$ in series can be written in the form:

$$S(g) = 1 \qquad (3)$$

$$+\sum_{n=1}^{\infty} \frac{1}{n!} \int S_n(\xi_1, \ldots, \xi_n)\, g(\xi_1) \ldots g(\xi_n)\, d\xi_1 \ldots d\xi_n.$$

It is clear that the conditions of correspondence to classical theory and relativistic invariance (B. S. 3.17 and 4.4) are taken over into the non-local theory with practically no change:

$$S_1(\xi) = i\Lambda(\xi), \qquad (4)$$

$$U_L S_n(L\xi_1, \ldots, L\xi_n)\, U_L^+ = S_n(\xi_1, \ldots, \xi_n). \qquad (5)$$

(In the last formula, $L\xi$ in an obvious way denotes the aggregate of the three points Lx', Lx'' and Lx'''.) No new points come up in the formulation of the condition of unitarity; one can immediately write:

$$S_n(\xi_1, \ldots, \xi_n) + S_n^+(\xi_1, \ldots, \xi_n) \qquad (6)$$

$$+ \sum_{k=1}^{n-1} P(\xi_1, \ldots, \xi_k / \xi_{k+1}, \ldots, \xi_n)$$

$$\times S_k(\xi_1, \ldots, \xi_k)\, S_{n-k}^+(\xi_{k+1}, \ldots, \xi_n) = 0.$$

The situation is different for the causality condition. Formally it is impossible in a non-local theory to satisfy the causality condition in its classical sense, because of the very basic physical ideas--the presence of a form factor will always lead to propagation of the interaction, at least in the small, with a velocity greater than the velocity of light. Physically, this is not inadmissible since,[15] so long as such violations are limited to regions of the order of "elementary lengths", they will be unobservable in a reasonable theory, and will mean only that the "mathematical" points x' . . . which serve as variables of integration do not signify physical points.

In fact, the introduction of a form factor in the interaction Lagrangian (2) means physically that we drop the usual picture of point elementary particles, and go over to a picture of extended elementary particles which are, so to speak, smeared

*Cited as B. S. in the sequel. We shall use the notation of this and the next paper.

**The starting point for the construction will be the physically obvious.

***For purposes of concreteness, we shall consider the non-local theory with Lagrangian (2). However, all the results will, of course, be valid in a theory with any Lagrangian of similar type.

out in space and time. But as soon as we drop the notion of point elementary particles, we are left without any way of assigning a physical meaning to the assertion: "something happens at a definite space–time point", and all physical quantities and concepts must now refer, not to points, but to (small) space–time regions. The use of "points" $x' \ldots$ is only as a mathematical tool, and it would be altogether unnatural to require the fulfillment of any physical conditions with regard to them, such as, for example, that there be no propagation of the interaction from the point x to point y if y does not occur later than x.

It is obvious that, in place of such requirements of formal causality, in a non–local theory we should impose requirements which result in satisfying the principle of causality for macroscopic distances (compared to the "elementary length" when it has a real physical meaning. The conditions which must be imposed on form factors, in order to restrict to macroscopic distances the breakdown of strict causality in expressions where $F(\xi)$ appears once, have been analyzed in detail recently; [16] as a result of this analysis, a set of sufficient conditions were found, which we shall assume to be satisfied.

However, in the expressions for the operator functions S_n in the scattering matrix, the form factor $F(\xi)$ will occur repeatedly. Therefore the criteria found in Ref. 16 are not enough, and we must now, dropping the strict causality condition I–2, formulate a weakened condition which should eliminate the possibility of adding to the breakdown of formal causality, due to the presence of the form factor, new violations caused by unsatisfactory construction of the S–matrix. Such a condition is found in a natural way if we try to generalize the integral causality condition formulated in I to the case of the non–local interaction (1).

2. THE CONDITION OF ALMOST–CAUSALITY

Again, as in I, let us consider two regions, G_1 and G_2, situated so that $G_1 \geq G_2$ and generalize the definition of classes of functions $g_1(x)$ and $g_2(x)$, introduced in I–3, to the case where each of the functions depends, not on one, but on three points x', x'', x'''. We shall define these classes in the strictest sense, namely we shall require that:

$$\begin{array}{l} g_1(\xi)\neq 0, \text{ only if simultaneously } x_1' \in G_1,\ x_1'' \in G_1 \text{ and } x_1''' \in G_1, \\ g_2(\xi)\neq 0, \text{ only if simultaneously } x_2' \in G_2,\ x_2'' \in G_2 \text{ and } x_2''' \in G_2. \end{array} \tag{7}$$

With such a definition, the principle of causality will require that, despite the presence of the form factor $F(\xi)$, the interaction $g_2(\xi)\Lambda(\xi)$ shall act on the system as if the interaction $g_1(\xi)\Lambda(\xi)$ were not present, while the effect of the interaction $g_1(\xi)\Lambda(\xi)$ shall not depend on the specific nature of the interaction $g_2(\xi)\Lambda(\xi)$, but only on the state of the system which develops as a result of the latter's action. In fact, what we want is that formally "acausal" interactions be associated only with triples of points x', x'', x''' appearing in the argument of a single form factor, i.e., referring to the same "point" ξ, while the possibility of meeting pairs of such points in the arguments of different functions $g_1(\xi)$ and $g_2(\xi)$ is precisely what is excluded by the conditions (7) and $G_1 \gtrsim G_2$.

Considerations which are completely analogous to those used in the derivation of condition (6) of Reference I give, as the mathematical expression of this requirement, the condition

$$S(g_1 + g_2) = S(g_1)\,S(g_2), \text{ if } G_1 \geqslant G_2, \tag{8}$$

which we shall name the *condition of almost–causality*, in order to distinguish it from the strict causality conditions which occur in the local theory. It satisfies the principle of correspondence to local theory in an obvious fashion – when we make the limiting transition

$$F(x', x'', x''') \to \delta(x' - x'') \times \delta(x'' - x''')$$

it becomes the integral causality condition I–6 of the local theory.

The fact that the condition of almost–causality is weaker than the integral causality condition I–6 manifests itself graphically in the fact that it is impossible to go over from it to a differential formulation analogous to I–2. Actually, there is no difficulty in deriving, from equation (8), a condition analogous to condition I–9 for a class of functions analogous to the special class I–8. However, in the non–local theory it turns out that it

is not possible to approximate an arbitrary function $g(\xi)$ by functions of this special class, since for this purpose we would require the regions G_1 and G_2 to not merely touch, but rather to interpenetrate.

In order now to translate condition (8) into the language of the operator functions $S_n(\xi_1 \ldots \xi_n)$ we must, as in the derivation of I–7 use for $S(g_1)$, $S(g_2)$ and $S(g_1 + g_2)$ the expansions (3). After exactly the same algebraic transformations, we arrive at the condition: *

$$S_n(\xi_1, \ldots, \xi_n) = S_l(\xi_1, \ldots, \xi_l)\, S_{n-l}(\xi_{l+1}, \ldots, \xi_n), \tag{9a}$$

$$\text{if} \quad \{\xi_1, \ldots, \xi_l\} \gtrless \{\xi_{l+1}, \ldots, \xi_n\}. \tag{9b}$$

Thus the condition of almost–causality (8) leads, in the same way as the integral causality condition I–6, to a multiplicative representation for the operator functions S_n of separable (cf. I) aggregates of arguments $(\xi_1 \ldots, \xi_n)$.* We now proceed to investigate the compatibility of this condition with the other conditions, IA–C, which are imposed on the S–matrix.

3. COMPATIBILITY OF CONDITIONS IMPOSED ON THE SCATTERING MATRIX

We note first that if the set of variables $\{\xi_1 \ldots, \xi_n\}$ splits into a sum of two space–like aggregates $\{\xi_1 \ldots, \xi_l\}$ and $\{\xi_{l+1} \ldots, \xi_n\}$, then, as in the local case, we obtain from (9) the requirement of commutability of the operator functions of the space–like sets of arguments:

$$S_l(\xi_1, \ldots, \xi_l)\, S_{n-l}(\xi_{l+1}, \ldots, \xi_n) = S_{n-l}(\xi_{l+1}, \ldots, \xi_n)\, S_l(\xi_1, \ldots, \xi_l), \tag{10}$$

$$\text{if} \quad \{\xi_1, \ldots, \xi_l\} \sim \{\xi_{l+1}, \ldots, \xi_n\}.$$

Like the corresponding condition I–10 of the local theory, (10) will be fulfilled automatically if the elementary commutators (anticommutators) of the free field operators vanish for space–like intervals. The fact that (10) cannot be satisfied, if the elementary commutators differ from zero, even if only for extremely small space–like intervals, is apparent from the fact that (10) must, in particular, be valid when all the arguments in each set $\{\xi_1 \ldots, \xi_l\}$ and $\{\xi_{l+1} \ldots, \xi_n\}$ coincide.

The situation which we have just described can be regarded as the mathematical formulation of the fact that we are dealing with a field theory with non–local interaction: the commutators of free fields must vanish outside the light cone; in this sense we may say that we are dealing with a theory in which the free fields have local character. Therefore condition (10) also has the significance of a condition on the local nature of the theory of the free fields (here we have in mind the fact that the fields must appear in the Lagrangian as a whole, without being split into positive and negative frequency parts).

In I the theorem was proved that, if in a local theory the set of arguments of the operator function S_n separates in several ways, the representations of S_n which, by virtue of I-7, result from these splittings will differ from one another only by a transposition of functions S_ν, $S_{\nu'}$ of space-like sets of arguments. It is easy to see that the proof of this theorem carries over verbatim to the non–local theory, so that it remains valid there. Since, by virtue of (10), operator functions of space–like sets of arguments also commute in the non–local theory, the compatibility of the requirements imposed on each S_n by the condition of almost–causality is proven if this condition can be applied repeatedly.

The situation is similar for the theorems concerning unitarity which were demonstrated in I. In fact, their proofs were based entirely on certain algebraic relations for which the nature of the symbols $x_1 \ldots, x_n$ or $\xi_1 \ldots, \xi_n$ was completely

---

*The notation $\{\xi_1, \ldots, \xi_l\} \gtrless \{\xi_{l+1}, \ldots, \xi_n\}$ means that $\{x_1', x_1'', x_1''', \ldots, x_l', x_l'', x_l'''\} \gtrless \{x_{l+1}', \ldots, x_n'''\}$. One should also keep in mind the remark (cf. I, footnote 3) concerning the order of enumeration of the variables.

*We note that for separability of the aggregate $\{\xi_1, \ldots, \xi_n\}$ it is not sufficient to have the aggregate $\{x_1', x_1'', x_1''', \ldots, x_n', x_n'', x_n'''\}$ be separable, i.e., to have at least one cut through it; it is neccesary, in addition, that this cut not go through any one of the sets of points $\{x_i', x_i'', x_i'''\}$, referring to the same composite "point" ξ_i.

irrelevant; it was required only that the separation I–7a follow from the relation I–7b, and this remains true when we replace all the x_i by ξ_i, because of (9).

Thus if the set of arguments $\{\xi_1 \ldots, \xi_n\}$ of the operator function S_n is separable (only in this case is the condition of almost–causality applicable to S_n), and if the unitarity-condition is satisfied for $S_1 \ldots S_{n-1}$ for arbitrary values of the arguments, then the representation (9) for S_n which results from the condition of almost–causality will automatically satisfy the unitarity condition. So the compatibility of conditions D and C for the S–matrix is demonstrated.

Since the mutual compatiblity of the remaining conditions imposed on S_n is obvious from the same considerations as in the local theory, all four conditions A–D imposed by us on the S–matrix are consistent with one another.

From this it follows immediately that we can always find a sequence of operator functions $S_1 \ldots S_n$ all of whose terms will satisfy conditions A–D.

In fact, let us assume that the operator functions $S_1 \ldots S_n$ have been constructed. We shall show that we can always construct an S_{n+1} which, together with the already constructed $S_1 \ldots S_n$ will satisfy all the conditions A-D. The manifold of all possible values of the arguments $\xi_1 \ldots \xi_{n+1}$ of the operator functions S_{n+1} separates into two classes: arguments forming an inseparable set, and arguments forming a separable set.

If a certain set of arguments belongs to the second class, then from the condition of almost–causality the corresponding value of S_{n+1} will be represented as a product of already known operator functions of lower index, so that according to our earlier remarks all the conditions A–D will be satisfied.

If a certain set of arguments belongs to the first class, then the condition of almost–causality in general imposes no limitations on the corresponding value of the operator function. As we see from (6), the unitarity condition uniquely determines the Hermitean part of S_{n+1} in terms of the already known $S_1 \ldots S_n$. The anti–Hermitean part of S_{n+1} remains arbitrary.

So if we are given operator functions $S_1 \ldots S_n$ satisfying A–D, we can always construct an operator function S_{n+1} which together with them satisfies the same conditions. On the basis of the principle of complete induction, we then arrive at the possibility of constructing a sequence of operator functions $S_1 \ldots S_n \ldots$ satisfying all the requirements A–D, i.e., we get the theorem of the existence of the scattering matrix (cf. Ref. 6 in I).

4. THE CONSTRUCTION OF THE OPERATOR FUNCTIONS OF THE S–MATRIX

In order to formulate the method of successive construction of the operator functions of the S–matrix and to get compact and symmetrical expressions which appear in it, we shall investigate the structure of the operator functions S_n $(\xi_1 \ldots, \xi_n)$ in more detail. From the theorem of the complete separability of separable aggregates, which was proven in I, it follows that, for any combination of arguments of the function S, the points $\xi_1 \ldots, \xi_n$ can always be divided into m $(1 \leq m \leq n)$ groups $\{\xi_{\lambda_i} \ldots, \xi_{\lambda_{\nu_1}}\}; \ldots; \{\xi_{\lambda_{\nu_i + \ldots + \nu_{m-1}+1}} \ldots, \xi_{\lambda_m}\}$, which are separated from one another, while the group of points in each set are inseparable. In the local theory, this separation led to a division into m groups of points, such that the points within each group coincided, while the points in different groups were distinct. Since we here want to maintain the analogy with this formulation, we shall say that the ν points $\xi_{\lambda_1} \ldots, \xi_{\lambda_\nu}$ of one inseparable group "coalesce" and form a composite point Ξ^{ν}, consisting not of three, but of 3ν ordinary points $x'_{\lambda_i} \ldots\ldots, x'''_{\lambda_\nu}$.

Here we introduce the concept of an almost–local operator. We shall say that the operator expression $N_\nu(\xi_{\lambda_i} \ldots, \xi_{\lambda_\nu})$, depending on the field operators at the "points" $\xi_{\lambda_1} \ldots, \xi_{\lambda_\nu}$, is an *almost–local operator* if

$$N_\nu(\xi_{\lambda_1}, \ldots, \xi_{\lambda_\nu}) = 0 \qquad (11)$$

for an arbitrary separable set of arguments, and if the conditions of relativistic invariance, (5) and (10), are satisfied for N_ν. It is clear that the almost-local operator is a direct generalization of the concept of quasi–local operator, introduced in B. S.; in fact, in a local theory the set of arguments $x_1 \ldots x_\nu$ can, as already mentioned, be inseparable if and only if all the points $x_1 \ldots, x_\nu$ coincide.

Comparing the definition of almost–local opera-

tor with the definition of a composite point, we see that the set of arguments of an almost–local operator always forms a composite point Ξ^{ν}; we may threfore say that each almost–local operator will depend, not on several composite points (of third order) ξ, but on one composite point Ξ^{ν}. $= \{\xi_{\lambda_1} \ldots, \xi_{\lambda_\nu}\}$ of order 3ν. Since the composite points ξ, consisting of triplets of ordinary points (so that they are composite points of third order) are in no way physically distinguished from composite points of n'th order, the Lagrangian $\Lambda(\xi)$, "depending only on a single point" ξ, loses its special position among almost–local operators.

Using the concept of a composite point, we may say that the n arguments of S_n always break up (uniquely) into m $(1 \leq m \leq n)$ mutually separated composite points $\underset{1}{\Xi}^{\nu_1}, \ldots, \underset{m}{\Xi}^{\nu_m}$ $(\nu_1 + \ldots + \nu_m = n)$. From the theorem demonstrated in I, concerning the possibility of representing a sum of inseparable sets as an ordered sequence, it will now follow that the "points" $\underset{1}{\Xi}^{\nu_1}, \ldots, \underset{m}{\Xi}^{\nu_m}$ can always (not in general, uniquely) be ordered in time, maintaining the relation (cf. Ref. 6 in I):

$$\Xi^{\nu_{\lambda_1}}_{\lambda_1} \succcurlyeq \Xi^{\nu_{\lambda_2}}_{\lambda_2} \succcurlyeq \ldots \succcurlyeq \Xi^{\nu_{\lambda_m}}_{\lambda_m}. \tag{12}$$

Now applying the condition (9) of almost–causality to each of the sections occurring in (12), we get for S_n the representation

$$S_n(\xi_1, \ldots, \xi_n) = S_{\nu_{\lambda_1}}(\Xi^{\nu_{\lambda_1}}_{\lambda_1}) \ldots S_{\nu_{\lambda_m}}(\Xi^{\nu_{\lambda_m}}_{\lambda_m}), \tag{13}$$

similar to the representation I–25 of the local theory. If the "points" $\underset{1}{\Xi}^{\nu_1}, \ldots, \underset{m}{\Xi}^{\nu_m}$ can also be ordered in some other way, we obtain for S_n a representation differing in form from (13). However, because of the uniqueness of the resolution of a separable aggregate into a sum of inseparable aggregates, and the self–consistency of the condition of almost–causality, it can differ from (13) only by transpositions of commuting S_ν's of space–like separated pairs of "points" Ξ^{ν}, — consequently all such representations will be equivalent; they can threfore be combined into the symmetric expression:

$$S_n(\xi_1, \ldots, \xi_n) = T\,[S_{\nu_1}(\Xi_1^{\nu_1}) \ldots S_{\nu_m}(\Xi_m^{\nu_m})], \tag{14a}$$

if

$$\{\xi_1, \ldots, \xi_n\} = \Xi_1^{\nu_1} + \ldots + \Xi_m^{\nu_m}; \tag{14b}$$

$$1 \leqslant m \leqslant n; \quad \Sigma \nu_i = n.$$

Here it is implied that the T-ordering applies only between "points" $\underset{i}{\Xi}^{\nu_i}$ while the operator functions of individual "points" enter as a whole in (14). As a consequence of the theorems concerning separation and ordering of aggregates, which we have just quoted, the meaning of the T-products which occur in (14a) is completely obvious and unique: the expression (14) simply denotes the representation (13) for all possible orderings (12) with the separation (14b); in addition, it shows explicitly the symmetry of S_n with respect to all its arguments.

Formula (14) reduces the problem of determining S_n for arbitrary sets of arguments to the determination of the operator functions S_ν for the individual arguments Ξ^{ν} which are composite "points", i.e., for the inseparable sets $\{\xi_1 \ldots, \xi_\nu\}$.

We have already noted that the condition of almost–causality in general imposes no limitations on the value of S_ν for such arguments, that the unitarity condition uniquely determines the Hermitean part of such S_ν in terms of the operator functions $S_1 \ldots S_{\nu-1}$ of lower index, while the anti–Hermitean part of such S_ν remains arbitrary [of course, within the limitations of the requirements arising from the conditions of relativistic invariance (5) and (10)]. Since these quantities can be regarded as almost–local operators,

$$\tilde{N}_\nu(\xi_1, \ldots, \xi_\nu) = \tilde{N}_\nu(\Xi^{\nu}) = \tilde{M}_\nu(\Xi) + i\tilde{\Gamma}_\nu(\Xi^{\nu}) \tag{15}$$

($\tilde{M}_\nu$ and $\tilde{\Gamma}_\nu$ are Hermitean), we may say that (14) completely (and uniquely) determines all the operator functions $S_1(\xi), \ldots, S_n(\xi_1 \ldots \xi_n)$ in terms of the sequence of Hermitean almost–local operators

$$\Lambda(\xi) = \Gamma_1(\Xi^1), \quad \Gamma_2(\Xi^2), \ldots, \quad \Gamma_n(\Xi^n), \ldots, \tag{16}$$

which are assigned completely arbitrarily, and to-

gether determine the physical system whose theory is being constructed. Thus the problem of construction of the S-matrix in the non–local theory is solved in principle.

The representation (14) for S_n has, however, an essential defect from the practical point of view: it does not give a single expression for the operator function $S_n(\xi_1 \ldots, \xi_n)$ for all values of its arguments––for combinations $\xi_1 \ldots, \xi_n$, in which the points ξ are coupled differently, (14) gives for S_n different expressions, which do not automatically go over into one another. Thus, for example, according to (14), we must use for S_2 the expression $T[S_1(\xi_1) S_1(\xi_2)]$, if ξ_1 and ξ_2 are unconnected, and the expression $\tilde{N}_2(\xi_1, \xi_2)$ if they are connected.

In order to eliminate this defect, we must, obviously, represent the value of S_n for a coupled set of arguments as a sum of expressions which continuously extend its meaning for uncoupled arguments plus some additional term which automatically vanishes if the arguments are uncoupled. To do this we must first extend continuously the definition of the T–product, which so far exists only for T–products of functions of uncoupled points Ξ_1, $\ldots \Xi_k$, to the case where the points are coupled, when the T–product in its usual intuitive sense does not exist, and we must take refuge in additional arbitrary conventional definitions.

One possible convention is the definition of the T–product according to Wick's theorem as the sum of all possible normal products with all possible chronological contractions. It is easy to see that this definition is equivalent to the independent time ordering of the individual free field operators appearing in the operator function. In the local theory (cf. I) this definition was a completely natural one, since it led (for suitable choice of the regularization) to the automatic fulfillment of the unitarity condition when the points were coupled. It is easy to see by direct computation that this way of extending the definition of the T–product in the non–local theory leads to violation of unitarity.

Another possibility would be a definition of the T–product which would not lead to a violation of unitarity for coupled points. Such a definition would be preferable from the point of view of the general theory, but it would be much less convenient for calculation, since there would clearly be no analog of Wick's theorem.

We shall therefore assume that we have a definition of the T–product for coupled points which does not necessarily achieve unitarity, and split up the value of S_n for completely uncoupled arguments $\xi_1 \ldots, \xi_n$ into a sum

$$S_n(\xi_1, \ldots, \xi_n) = S_n^T(\xi_1, \ldots, \xi_n) + N_n(\Xi^n) \quad (17)$$

of quantities S_n^T, consisting of a sum of T–products of operator functions with a smaller number of arguments, extended in accordance with some chosen convention, and the almost–local operator

$$N_n(\Xi^n) = M_n(\Xi^n) + i\Gamma_n(\Xi^n)$$

(M and Γ are Hermitean). The operator M_n will again be uniquely determined via the unitarity condition in terms of the operator functions S_k of lower index, while its form will of course depend on the way the T–product definition is extended (in particular, if the second method suggested above is used, it will be zero).

Substituting the resolution (17) in (14) and making some combinational transformations, we get an expression for $S_n(\xi_1 \ldots, \xi_n)$ as a sum

$$S_n(\xi_1, \ldots, \xi_n) = \sum_{\left(\Xi_1, \ldots, \Xi_m;\ 1 \leqslant m \leqslant n\right)}^{\prime} T[N_{\nu_1}(\Xi_1^{\nu_1}) \ldots N_{\nu_m}(\Xi_m^{\nu_m})], \quad (18)$$

in which it is assumed that the summation is extended over all possible separation of the set $\{\xi_1 \ldots, \xi_n\}$ into a sum of "points" $\Xi_1^{\nu_1}$, $\ldots, \Xi_m^{\nu_m}$, where the points Ξ, consisting of different points ξ, are assumed to be different, while the order of the points Ξ in the entries $N_{\nu_1} \ldots N_{\nu_m}$ is irrelevant.*

The summation in (18) is carried out first over the number m of points Ξ_i; second, over all possible distributions of the ν_i variables ξ in each point $\Xi_i^{\nu_i}$, and third, over all possible assignments of the variables $\xi_1 \ldots \xi_n$ among the m groups with $\nu_1 \ldots \nu_m$ in each group. We can therefore write the expression in more detail in the form

*We emphasize once more that the almost–local operators N_{ν_i} are assumed to enter into the T–product as a whole; the T–ordering is done only between different Ξ_i, and not inside them.

$$S_n(\xi_1, \ldots, \xi_n) = T(N_1(\xi_1) \ldots N_1(\xi_n)) \tag{19}$$
$$+ \sum_{\left(\substack{2 \leqslant m \leqslant n-1 \\ \sum \nu_i = n}\right)} \frac{1}{m!} P(\xi_1, \ldots, \xi_{\nu_1} | \xi_{\nu_1+1}, \ldots, \xi_{\nu_1+\nu_2} | \ldots | \xi_{\nu_1+\ldots+\nu_{m-1}+1}, \ldots, \xi_n)$$
$$\times T[N_{\nu_1}(\xi_1, \ldots, \xi_{\nu_1}) N_{\nu_2}(\xi_{\nu_1+1}, \ldots, \xi_{\nu_1+\nu_2}) \ldots N_{\nu_m}(\xi_{\nu_1+\ldots+\nu_{m-1}+1}, \ldots, \xi_n)]$$
$$+ M_n(\Xi^n) + i\Gamma_n(\Xi^n).$$

The factor $1/m!$ appears here because each specific subdivision occurs $m!$ times in the sum (19), differing only in an irrelevant order of arrangment of the factors under the sign of the T–product.

Formulas (18) or (19) give us the desired representation of the operator functions $S_n(\xi_1, \ldots, \xi_n)$ valid for any values of the arguments. They express S_n in terms of the sequence of almost-local operators

$$N_1(\xi) = i\Lambda(\xi), \tag{20}$$

$$N_2(\xi_1, \xi_2), \ldots, N_n(\xi_1, \ldots, \xi_n), \ldots,$$

in each of which the Hermitean part M_n is uniquely determined by the functions S_k (i.e., in the last analysis, by the operators N_k) of lower index, while the anti–Hermitean part $i\Gamma_n$ remains arbitrary and must be given in the formulation of the theory. Formula (19) is completely analogous in structure to the expression I–30 of the local theory.

Combinatorial transformations, which are the same as those used in the local theory (cf. B. S. 4.30–4.34) ebable us to convert the expansion (3) with the operators functions (19) to the concise formula:

$$S(g) = T\left(\exp\left\{\int N(\xi; g)\, g(\xi)\, d\xi\right\}\right) \tag{21}$$
$$= T\left(\exp\left\{i\int \Lambda(\xi; g)\, g(\xi)\, d\xi + \int M(\xi; g)\, g(\xi)\, d\xi\right\}\right),$$

if we define the almost–local Hermitean functionals $M(\xi; g)$ and $M(\xi; g)$ by the expansions:

$$\Lambda(\xi; g) = \Lambda(\xi) + \sum_{\nu=2}^{\infty} \frac{1}{\nu!} \int \Gamma_\nu(\xi, \xi_1, \ldots, \xi_{\nu-1})\, g(\xi_1) \tag{22}$$
$$\ldots g(\xi_{\nu-1})\, d\xi_1 \ldots d\xi_{\nu-1},$$

$$M(\xi; g) = \sum_{\nu=2}^{\infty} \frac{1}{\nu!} \int M_\nu(\xi, \xi_1, \ldots, \xi_{\nu-1})\, g(\xi_1) \tag{23}$$
$$\ldots g(\xi_{\nu-1})\, d\xi_1 \ldots d\xi_{\nu-1}.$$

The functional $\Lambda(\xi; 1)$ can now be regarded as the total Lagrangian of the system. Its individual terms, which are determined by the almost–local operators

$$\Lambda(\xi) = \Gamma_1(\Xi^1), \quad \Gamma_2(\Xi^2), \ldots, \Gamma_n(\Xi^n), \ldots,$$

differ from one another only in the manner of "turning on the interaction" (cf. the discussion in B. S. at the end of Section 4), which we are free to choose, and differ also in the number of simple points $x \ldots$ which are contained in a single composite point Ξ. Therefore there is no basic physical distinction between them, so that combining them in the total Lagrangian $\Lambda(\Xi; 1)$, which must be given in order to characterize the physical system, is entirely natural.

The functional $M(\xi; g)$, on the other hand, has no direct physical relation to the system under consideration. Its appearance is due to the arbitrariness discussed above in the definition of the continuation of T–products into the domain of coupled arguments: if we use a definition which does not maintain unitarity, for coupled arguments then we must correct things by adding to the Lagrangian the "anti–Hermitean added term" $-iM(\xi; g)$.

It should be emphasized that in order to construct the S–matrix according to formula (21), we must first of all give some definite method for extending the definition of the T–product into the domain of coupled arguments. As soon as such a definition is made, we can assign a definite total Lagrangian $\Lambda(\xi; 1)$. The functional $M(\xi; 1)$ is then uniquely determined from the condition of unitarity,* so that (21) gives us the value of the S-matrix. If we now shift from this definition of the T–product to some other, then to get the same S-matrix we must change the form not only of the functional $M(\xi; 1)$ but also of the functional $\Lambda(\xi; 1)$. Thus the total Lagrangian $\Lambda(\xi; 1)$ determines the S–matrix uniquely only with respect to a fixed method of defining the T–product in the region of coupled arguments.

*In practise, the functional $M(\xi; 1)$ can only be determined by successive use of the unitarity requirement in order to find the almost–local operators $M_2 \ldots M_n, \ldots$

Such a situation is completely analogous to that which occurs in the local theory; there, too, the form of the total Lagrangian $L(x; 1)$ determines the S–matrix only with respect to some given fixed method of regularization; in order to get the same S–matrix with different methods of regularization requires the use of different total Lagrangians $L(x; 1)$.**

5. DISCUSSION

The fundamental result obtained above is the proof that, by generalizing the method of Bogoliubov and Stueckelberg to the non–local theory, one can construct for any Lagrangian an S–matrix satisfying the physically obvious conditions A–D. We have succeeded in overcoming the difficulty with the unitarity of the S–matrix which arises in constructing the theory in the Heisenberg representation.

Physically, this progress proved possible, apparently, because of the more consistent application of the non–local point of view. In fact, the introduction of a form factor means in descriptive terms the assignment to the elementary particles of a certain internal structure. Since we avoid defining it, and regard the form factor as something put into the theory from outside, this means that we avoid – at least at this stage of the theory, the study of the laws which govern the internal structure of elementary particles, and regard it as given; all our equations refer essentially only to processes in which the internal structure of the particles does not change.

But from this point of view it appears unnatural to require of the equations of the theory that they answer the question: what happens if, roughly speaking, the particles "penetrate on another"; to this there corresponds mathematically not only the attachment of several points $x' \ldots$ to one point ξ, but also the case of coupling of arguments. This information must be put into the theory from outside, just as is done for the form factor and the "fundamental Lagrangian $\Lambda(\xi)$, in such a way, of course, that it does not come into conflict with the latter.

The method of solution of the equation in Heisenberg representation[7,8] taking the form factor and the quantity $\Lambda(\xi)$ as given, assigned a completely definite meaning to the operator functions of the S–matrix for coupled arguments, while starting coupled "points" ξ. Thus, from our point of view, this method gave a more detailed description than is admissible for a non–local system, and it was just this which gave rise to the difficulty with unitarity.

In our method for constructing the S–matrix, this defect does not occur: to define the theory completely we require the assignment of the values of all the operator functions of the S–matrix (15) for completely coupled sets of arguments; then the requirement of mutual compatibility of these values (the unitarity condition) determines their Hermitean parts, while their anti–Hermitean parts (16) must be assigned in formulating the theory, and together determine the assumed internal structure of the particles. Such a procedure for constructing the theory, in which in a certain sense we separate the "domains of essential non–locality" and the domains of the more or less customary space–time description (cf. Reference 17), naturally follows from our condition of almost- causlity.

The "total Lagrangian" (22) is the operator which in our case defines the theory. This may serve as an argument in support of the position that, in a consistent non–local theory, we must not limit ourselves to the consideration, of non–local interactions of just one specific kind, such as (1), (2), but must consider general non–local interactions, expressed in terms of Lagrangians which are general functionals of the field operators, like the Lagrangian (22). Since, in addition, one may hope that the introduction of a form factor will make it possible to avoid divergences, in such a non–local theory the demarcation between renormalizable and unrenormalizable theories is erased.

In conclusion, we should like to point out that the theory we have constructed should not necessarily be regarded as complete. Here we have in mind that the possibility is not excluded of establishing some additional limitations on the choice of the set of almost–local operators $\Gamma_n(\Xi^n)$, starting from some additional physical requirements. Here we are thinking of gauge invariance conditions, which in the light of recently obtained results[18] requires further serious investigation, and also of conditions of the type of the "reality condition."[19] We shall not enter into a discussion of these questions here.

The author takes this opportunity to express his deep gratitude to N.N. Bogoliubov for continual

**We note that the entire procedure developed for constructing the non–local S–matrix suggests the idea that the coupling of arguments in the non–local theory can be regarded as an unusual method for evaluating the indeterminate forms which occur for coupled (coincident) arguments in the local theory, which is usually accomplished by means of regularization. Obviously, therefore, one could arrive at the non–local theory from a "formalistic" point of view, not attributing any physical meaning to the non–local character, but regarding it merely as a method of regularization before making the limiting transition to the local theory. It is not out of the question that such a method of regularization might be of some interest, in view of its close connection with the space–time description.

attention to this work and for many suggestions and valuable advice, and also to D. V. Shirkov and V. L. Bonch–Bruevich for fruitful discussion.

[1]G. Wataghin, Z. Physik 88, 92 (1934); 92, 547 (1934).

[2]O. Scherzer, Ann d. Physik 34, 585 (1939).

[3]M. A. Markov, J. Exptl. Theoret. Phys. (U.S.S.R.) 10, 1311 (1940).

[4]M. A. Markov, J. Exptl. Theoret. Phys. (U.S.S.R.) 16, 790 (1946); Usp. Fiz. Nauk 29, 269 (1946).

[5]M. A. Markov, J. Exptl. Theoret. Phys. (U.S.S.R.) 25, 527 (1953).

[6]D. I. Blokhintsev, J.Exptl. Theoret. Phys. (U.S.S.R.) 18, 566 (1948).

[7]P. Kristensen and C. Moller, Danske Vid. Selskab. Mat. fys. Medd. 27, No. 7 (1952).

[8]C. Bloch, Danske Vid. Selskab. Mat. fys. Medd. 27, No. 8 (1952).

[9]C. Hayashi, Progr. Theor. Phys. 10, 533 (1953); 11, 226 (1954).

[10]B. V. Medvedev, Dokl. Akad. Nauk SSSR 100, 433 (1955).

[11]B. V. Medvedev, Dissertation, Mathematical Institute, Academy of Sciences USSR, 1955.

[12]N. N. Bogoliubov, Dokl. Akad. Nauk SSSR 81, 757, 1015 (1951); 82. 217 (1952).

[13]N. N. Bogoliubov and D. V. Shirkov, Usp. Fiz. Nauk 55, 149 (1955).

[14]B. V. Medvedev, J. Exptl. Theoret. Phys. (U.S.S.R.) 31, 791 (1956); Soviet Phys. JETP 4, 671 (1957).

[15]D. I. Blokhintsev, J. Exptl. Theoret. Phys. (U.S.S.R.) 16, 480 (1946).

[16]M. Chretien, and R. E. Peierls, Nuovo Cimento 19, 668 (1953).

[17]M. A. Markov. J. Exptl. Theoret. Phys. (U.S.S.R.) 21, 11 (1951).

[18]M. Chretien and R. E. Peierls, Proc. Roy. Soc. (London) A223, 468 (1954).

[19]V. L. Bonch–Bruevich, Dokl. Akad. Nauk SSSR 98, 561 (1954).

**Cited as I in thesequel.

Translated by M. Hamermesh

Stability of Plasma in a Strong Magnetic Field

IU.A. TSERKOVNIKOV
Mathematical Institute, Academy of Sciences, USSR
(Submitted to JETP editor September 20, 1956)
J. Exptl. Theoret. Phys. (U.S.S.R.) 32, 69–74 (January, 1957)

The stability of an inhomogeneous plasma with respect to small perturbations in a strong magnetic field is investigated. The plasma density and temperature and also the magnetic field strength are considered as given functions of space coordinates and as parameters on which the plasma stability is dependent.

THE study of plasma stability is of interest to physicists and astrophysicists in connection with gaseous discharges. In the past few years, various types of plasma instability have been considered in a number of articles. Kruskal and Schwarzchild[1] have examined the instability of a plasma contained by a magnetic field in a gravitational field; they have also considered the instability of a plasmatic fiber resulting from small kinks. These authors describe the behavior of the plasma through hydrodynamical equations. This is only justified, however, when the collision frequency is large with respect to the frequency which characterizes the time rate of change of the disturbance. Brueckner and Watson[2] have considered some forms of instability arising when the plasmatic density is small and collisions may be neglected; the perturbed functions which describe the distribution of the plasma components were then assumed to satisfy a linearized Boltzmann equation with no collisions. Such equations are also used in the present article, as it is assumed that the processes which generate instability take place in a time considerably smaller than that required for a particle to travel through a mean free path.

It is further assumed that the initial disturbance arises in a volume which is small with respect to the dimensions of the system, and sufficiently far from the boundaries of the plasma. This allows us to neglect boundary conditions. Thus we limit ourselves to the consideration of a local instability which may be due to velocities and to inhomogeneities in density, temperature and magnetic fields.

1. THE DISTRIBUTION FUNCTION FOR THE STATIONARY STATE

The state of the plasma whose stability is to be examined is described through the distribution function of its components f_i (v, x), and by the electric and magnetic fields E and H. The index i denoting the plasma component (we assume the plasma consists of ions and electrons) will be left out whenever possible in order to simplify the notation. Assuming that E and H are constant in time, f_i is found to satisfy the equation

$$\mathbf{v}\partial f_i/\partial \mathbf{x} + (e_i\mathbf{E}/m_i + [\mathbf{v}\omega_{Hi}])\,\partial f_i/\partial \mathbf{v} = \partial_e f_i/\partial t, \tag{1}$$

where m_i is the mass of the particles, e_i is their charge, and $\omega_{Hi} = e_i H/m_i c$ is the Larmor frequency.

Equation (1) is coupled with Maxwell's equations by the well known expressions for the current and charge density

$$\mathbf{j} = \sum_i e_i n_i \mathbf{u}_i, \quad \rho = \sum_i e_i n_i, \qquad n_i\mathbf{u}_i = \int \mathbf{v} f_i d\mathbf{v}, \quad n_i = \int f_i d\mathbf{v}. \tag{2}$$

We shall consider later the case of a strong magnetic field, when the principal term in equation (1) becomes the term containing ω_H. This means that the Larmor radius $\lambda_L = \sqrt{T/m}\, mc/|e|H$ is much smaller than the dimensions of the system, the mean free path and the distance in which a particle receives an increment of velocity $v_T = \sqrt{T/m}$ from the action of the electric field E.

Assume[3] that the solution of Eq. (1) can be obtained in the form of an expansion in inverse power, of ω_H

$$f = f_0 + \omega_H^{-1} f_1 + \omega_H^{-2} f_2 + \cdots \tag{3}$$

The first two terms of the series are then found to obey the following equations

$$[\mathbf{vl}]\frac{\partial f_0}{\partial \mathbf{v}} = 0,$$

$$\mathbf{v}\frac{\partial f_0}{\partial \mathbf{x}} + \frac{e}{m}\mathbf{E}\frac{\partial f_0}{\partial \mathbf{v}} + [\mathbf{vl}]\frac{\partial f_1}{\partial \mathbf{v}} = \frac{\partial_e f_0}{\partial t}, \quad (4)$$

where $\mathbf{l} = \mathbf{H}/H$ is in the direction of thetangent to the magnetic lines of force. Let v_1 and v_2 be the components of the velocity along the coordinates perpendicular to l, and let $\theta = \arctan(v_2/v_1)$; the first of equations (4) may then be written as $\partial f_0/\partial\theta = 0$. This implies

$$f_0 = F_0(\mathbf{x}, v_l, v_\perp),$$
$$v_l = \mathbf{vl}, \quad v_\perp = \sqrt{v_1^2 + v_2^2}. \quad (5)$$

We can integrate the second of equations (4) over θ from 0 to 2π. Making use of the facts that f_1 is periodic in θ, while F_0 and $\partial_e F_0/\partial t$ are independent of θ, we obtain the equation

$$v_l(\mathbf{l}\partial F_0/\partial \mathbf{x}) + E_l \partial F_0/\partial v_l = \partial_e F_0/\partial t, \quad (6)$$

where E_l is the component of the electric field E along the direction l. One must keep in mind that in general v_l and $v_\perp$ are themselves functions of $\mathbf{x}$. In view of Eq. (6), f_1 may easily be obtained from Eq. (4). The function f_1 will contain the unknown functions F_1 which may be determined like F_0 from periodicity conditions in the next approximation.

In order not to complicate any further formulas which are already complex enough, we shall limit ourselves to investigating the stability of cylindrically symmetrical plasma. We introduce cylindrical coordinates r, φ, z, assuming that the function f depends only upon r. We assume further that the current flows along the z-axis, giving rise to a magnetic field H in the φ direction, and that $E_\varphi = 0$. Equation (6) then yields

$$F_0 = n(m/2\pi T)^{3/2} e^{-mv^2/2T}, \quad (7)$$

where n and T are the density and temperature, which are the same for the two plasma components (the temperature is given in energy units). The function f_1 has the form

$$f_1 = \left\{\frac{eE_r}{T} - \frac{1}{n}\frac{\partial n}{\partial r} - \left(\frac{mv^2}{2T} - \frac{3}{2}\right)\frac{1}{T}\frac{\partial T}{\partial r}\right\} v_\perp \sin\theta F_0 + F_1, \quad (8)$$
$$v_\perp = \sqrt{v_r^2 + v_z^2}, \quad \theta = \operatorname{arc\,tg}(v_z/v_r).$$

where F_1 is an undetermined function which we shall not need later. We also set $E_z = 0$ in the first approximation (7), since in the static case, the electromagnetic drift in the r-direction is compensated by diffusion which is only considered in the next approximation. Substituting (8) into (2) and applying Maxwell's equations, we find the following relation between the magnetic field H and the pressure $p = 2nT$:

$$\frac{1}{r}\frac{\partial rH}{\partial r} = -\frac{4\pi}{H}\frac{\partial p}{\partial r}. \quad (9)$$

Equations (7) to (9) will be required to investigate the stability of the system. The quantities H, n and T will be considered as given functions of r and will be treated as parameters on which the plasma stability depends.

2. THE FORM OF THE EQUATION FOR SMALL DISTURBANCES

We shall describe small disturbances δf_i, δ E, and δH in the stationary quantities f_i, E and H by a system of equations consisting of Maxwell's equations and the linearized Boltzmann equation

$$\frac{\partial \delta f_i}{\partial f} + \mathbf{v}\frac{\partial \delta f_i}{d\mathbf{x}} + \frac{e_i}{m_i}\left(\mathbf{E} + \frac{1}{c}[\mathbf{vH}]\right)\frac{\partial \delta f}{\partial \mathbf{v}} = -\frac{e_i}{m_i}\left(\delta\mathbf{E} + \frac{1}{c}[\mathbf{v}\delta\mathbf{H}]\right)\frac{\partial f_i}{\partial \mathbf{v}}, \quad (10)$$

where collision terms are neglected.

Equation (10), which contains on its right-hand side the function f_i determined in the previous Section, is a homogeneous equation in the perturbations, with coefficients depending on r. As stated above, the initial disturbance, produced at a time $t = 0$, occupies a small volume with respect to the dimensions of the system. The expansion of small scale disturbances δa into Four-

ier series of a complete set of normalized functions, $\delta a = \Sigma\, a_m \psi_m\ (x)$, must include terms of large m. But then for large m, the functions ψ_m can be written as

$$\psi(\mathbf{x}) = \bar{\psi}(\mathbf{x})\, e^{iS(\mathbf{x})}, \qquad (11)$$

where ψ and $\mathbf{k}(\mathbf{x}) = \partial S/\partial \mathbf{x}$ change only slightly over a distance $\lambda = 2\pi/k$. Accordingly we shall assume that the initial disturbance is of the form (11), and we shall seek solutions of the form

$$\delta f_i = g_i(\mathbf{xv})\, e^{i(\omega t + S)}, \qquad (12)$$

$$\delta \mathbf{E} = \mathbf{e}(\mathbf{x})\, e^{i(\omega t+S)}, \qquad \delta \mathbf{H} = \mathbf{h}(\mathbf{x})\, e^{i(\omega t+S)}.$$

For simplicity, we assume harmonic time dependence $e^{i\omega t}$. It is, however, well known that such solutions of the kinetic equation with no collision integral lead to the appearance of divergent integrals. We shall therefore assume that the imaginary part of ω has a sign which insures the growth of the disturbance ($Im\omega < 0$). This specification corresponds to a Laplace transform. The resulting dispersion equation may be extended if needed in the upper half-plane, and determines the poles ω_k of the Laplace transforms of the functions δf, $\delta \mathbf{E}$ and $\delta \mathbf{H}$. For large values of t, the solution of Eq. (10) and Maxwell's equation has the form

$$A(t) \approx \sum A_k e^{i\omega_k t}, \qquad (13)$$

where $A(t)$ is one of the functions representing the disturbance; therefore the existence of roots of the dispersion equation in the lower half-plane implies instability. Substituting (12) into 10) we obtain the following equation

$$i(\omega + \mathbf{kv})\, g + \mathbf{v}\frac{\partial g}{\partial \mathbf{x}} + \frac{e}{m}\left(\mathbf{E} + \frac{1}{c}[\mathbf{vH}]\right)\frac{\partial g}{\partial \mathbf{v}} = -\frac{e}{m}\left(\mathbf{e} + \frac{1}{c}[\mathbf{vh}]\right)\frac{\partial f}{\partial \mathbf{v}}. \qquad (14)$$

Since the size of the initial disturbance is much smaller than the dimensions of the system, the quantities g, $\mathbf{h}$, $\mathbf{e}$, n and T change only slightly over a distance $\sim \lambda$. The assumption of large magnetic field H implies that these quantities also change slightly over a distance equal to the Larmor radius λ. Terms containing $\partial g/\partial \mathbf{x}$ and the field $\mathbf{E}$ in Eq. (14) may therefore be assumed to be small, and Eq. (14) may be solved by the method of successive approximations.

In the zero approximation we have, instead of Eq. (14),

$$i(\omega + \mathbf{kv})\, g + [\mathbf{v}\omega_H]\frac{\partial g}{\partial \mathbf{v}} = -\frac{e}{m}\left(\mathbf{e} + \frac{1}{c}[\mathbf{vh}]\right)\frac{\partial F_0}{\partial \mathbf{v}}, \qquad (15)$$

where F_0 is the Maxwell function (9). The second term of expansion (3) is included in the next approximation. If the quantity λ is smaller than the Larmor radius, which may happen for sufficiently weak magnetic field, then the magnitude of the velocity $\mathbf{u}$ will enter as a parameter in Eq. (15). N. N. Bogoliubov and S. L. Sobolev have shown that the plasma is then stable if u does not exceed a critical value u_{crit}. The condition $u < u_{crit}$ may also be fulfilled in a strong magnetic field. But in this case it does not necessarily follow that the plasma is stable as the Laplace transforms of the solutions of the basic equations have poles in the ω-plane — which are proportional to the first power of the gradients of the stationary quantities. In order to find these poles one must neglect the frequency ω in Equation (15) and take it into account in the next approximation.

Considering the above analysis, and assuming the geometry of the stationary state, we obtain from equation (15)

$$g = \frac{4\pi e \rho}{k^2 m v_\perp}\frac{\partial F_0}{\partial v_\perp} + G(r, v_\varphi v_\perp)\exp\left\{i\frac{v_\perp k}{\omega_H}\sin(\theta - \alpha)\right\}, \qquad (16)$$

where $\rho = \Sigma e_i \int g_i\, d\mathbf{v}$.

It is assumed here that the wave vector $\mathbf{k}$ is perpendicular to the magnetic field, i.e., the initial disturbance does not depend on the angle φ; k is then given by

$$k = \sqrt{k_r^2 + k_z^2}, \quad \alpha = \operatorname{arc\,tg}(k_z/k_r).$$

In that case

$$S(\mathbf{x}) = \int^r k_r(r)\, dr + k_z z,$$

where k_z is independent of the coordinates.

The function G is determined in the next approximation from the condition of periodicity with respect to θ and is found to be

$$G = \frac{4\pi}{k^2 H} \frac{\left\{\frac{1}{n}\frac{\partial n}{\partial r} + \left(\frac{mv^2}{2T} - \frac{3}{2}\right)\frac{1}{T}\frac{\partial T}{\partial r} + \frac{\Omega}{k_z}\frac{eH}{cT}\right\}\left\{c\rho J_0(w) - \frac{v_\perp}{c} j J_0'(w)\right\}}{\frac{\Omega}{k_z} - \frac{v_\perp^2}{2}\frac{\partial}{\partial r}\left(\frac{1}{\omega_H}\right) - \frac{v_\varphi^2}{r\omega_H}} F_0,$$

$$\Omega = \omega - \frac{cE_r}{H} k_z, \qquad j = \frac{k}{ik_z}\sum e_i \int v_\perp \cos\theta g_i \, dv,$$

$J_0(\omega)$ and $J_0'(\omega)$ are the zero order Bessel function and its derivative; $\omega = v_\perp k/\omega_H$

Substituting (16) into (12) and eliminating the unknown quantities j and ρ, we obtain the dispersion equation. If it is assumed that the wave length λ is larger than the Debye and Larmor radii

$$(k_0^2 = k^2 T / 4\pi e^2 n \ll 1$$

and

$$k_L^2 = k^2 T mc^2 / e^2 H^2 \ll 1),$$

the dispersion equation becomes

$$\left(2 - \sum_i Q_i^{(0)}\right)\left(4\eta + \sum_i Q_i^{(2)}\right) \tag{17}$$

$$+ \left(\sum_i \varepsilon_i Q_i^{(1)}\right)^2 + \left(k_0^2 + \sum_i k_L^2 Q_i^{(1)}\right)\left(4\eta + \sum_i Q_i^{(2)}\right)$$

$$- \frac{1}{2}\sum_i k_L^2 Q_i^{(3)}\left(2 - \sum_i Q_i^{(0)}\right)$$

$$- \frac{3}{2}\sum_i \varepsilon_i k_L^2 Q_i^{(2)} \sum \varepsilon_i Q_i^{(1)} = 0,$$

where

$$\eta = H^2/8\pi p, \quad p = 2\pi T, \quad \varepsilon_i = \pm 1$$

for ions and electrons respectively, and

$$Q_i^{(n)} = \frac{1}{\sqrt{\pi}} \int_0^\infty \xi^n e^{-\xi} d\xi \int_{-\infty}^\infty e^{-\tau^2} \tag{18}$$

$$\times \frac{\frac{\Omega}{k_z}\frac{e_i H}{cT} + \frac{\partial \ln nT^{-3/2}}{\partial r} + (\xi + \tau^2)\frac{\partial \ln T}{\partial r}}{\frac{\Omega}{k_z}\frac{e_i H}{cT} + \frac{\partial \ln H}{\partial r}\xi - \frac{2}{r}\tau^2} d\tau.$$

Formula (18) determines $Q_i^{(n)}$ in the lower half of the complex ω-plane. If $Im\omega \geq 0$, the contour of integration must be suitably deformed.

3. THE DISPERSION EQUATION

A. *Small Curvature of the Magnetic Field*

Let $\partial H/\partial r >> H/r$. The last term in the denominator of (18) can then be neglected. Equation (17) then splits up into two equations. One of these is a second degree algebraic equation which admits the solution

$$z \equiv \frac{H^2}{2\pi p}\frac{\Omega}{k_z v_{dr}} = \left(\frac{1}{2} - \frac{H^2}{8\pi p}\right) \tag{19}$$

$$\pm \sqrt{\left(\frac{1}{2} + \frac{H^2}{8\pi p}\right)^2 - \frac{\partial \ln T}{\partial \ln H}},$$

$$v_{dr} = \frac{c}{enH}\frac{\partial p}{\partial r},$$

where v_{dr} is the drift velocity of the electrons with respect to the ions. The second equation has the following form:[5]

$$F(z) \equiv -2 + (z + \gamma)\Phi(z) + (-z + \gamma)\Phi(-z) = 0, \tag{20}$$

$$\Phi(z) = \int_0^\infty \frac{e^{-\xi}}{z + \xi} d\xi, \qquad \gamma = \frac{\partial \ln nT^{-1}/\partial \ln H}{1 - \partial \ln T/\partial \ln H}, \tag{21}$$

where γ is a parameter on which depends the plasma stability.

One of the stability conditions turns out to be that the radicand in equation (19) be positive. Since the function $F(z)$ has no singularities below the real axis, the number of roots N of equation (20) in the lower half-plane is equal to

$$N = \frac{1}{2\pi i}\int_C \frac{dF}{dz}\frac{dz}{F}. \tag{22}$$

The contour of integration, C, is shown in Fig. 1.

For large z, the function $F(z)$ takes the form

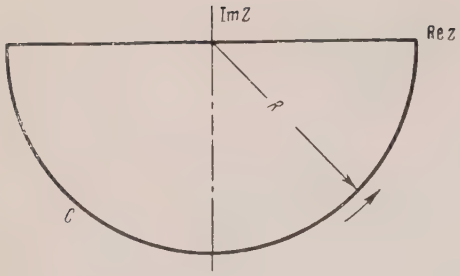

FIG. 1

$$F(z) = \frac{2(2-\gamma)}{z^2} + \frac{12(4-\gamma)}{z^4} + O\left(\frac{1}{z^6}\right). \quad (23)$$

The value of the integral (22) over the infinite semi-circular path is then $-2\pi i$. Since $F(z)$ is an even function of z, the integral along the real axis equals $2i$ times the increment in the argument of $F(z)$ as z goes from infinity to zero. Therefore

$$N = -1 - [\arg F(\infty) - \arg F(0)]/\pi. \quad (24)$$

For real values of z, the imaginary part of $F(z)$ differs from 0,

$$\operatorname{Im} F(z) = i\pi e^{-|z|}(|z| - \gamma)\operatorname{sign} z, \quad (25)$$

since the contour of integration for (21) must be deformed when the real axis is approached from the lower half-plane. If γ is positive, Im $F(z)$ vanishes for $z = \pm\gamma$ and Re $F(\pm\gamma) < 0$. Therefore equation (20) has no real roots. For small values of z, $F(z)$ may be taken as

$$F(z) = -2\gamma \ln z - 2(1 + C\gamma) - i\pi\gamma, \quad (26)$$

where $C \approx 0.577$ is Euler's constant.

The increase in the argument of $F(z)$ as z moves along the real axis can easily be obtained from Eqs. (23), (25), and (26). Thus when

$$0 < \gamma < 2 \quad (27)$$

the function $F(z)$ transforms the real axis into the contour shown in Fig. 2, in accordance with the formula obtained for it. It follows from Fig. 2 that the increase in the argument of $F(z)$ equals -2π and the number of roots N is then equal to 1. Therefore when condition (27) is satisfied, the plasma is unstable.

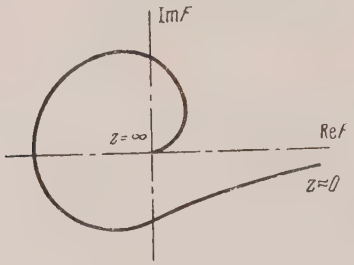

FIG. 2

One may verify in a similar fashion that for other values of γ, the number of roots N is zero, i.e., the plasma is stable. If instead of γ we introduce the parameter $\partial \ln T/\partial \ln H$, then in view of equation (19) we obtain the following condition for the plasma stability in a magnetic field of small curvature:

$$-\frac{H^2}{8\pi p} < \frac{\partial \ln T}{\partial \ln H} < \left(\frac{1}{2} + \frac{H^2}{8\pi p}\right)^2. \quad (28)$$

Condition (28) resembles the condition for convectional stability of an inhomogeneously heated gas in a gravitational field.[6] Note that the component $k_r(r)$ of the wave vector does not enter in Eqs. (19) and (20). This shows that when the wave length exceeds the Larmor and Debye radii, the solution is independent of the form of the initial disturbance along the radius r. When γ is close to 2 or 0, the expressions (23) and (26) approach zero, and the roots of Eq. (20) can be obtained in the explicit form

$$z = -i\sqrt{\frac{12}{2-\gamma}}, \quad \gamma \approx 2, \quad (29)$$

$$z = -ie^{-(1/\gamma)-C}, \quad \gamma \approx 0.$$

As expected, the real part of z is small in the first case and large in the second.

B. Intermediate Curvature of the Magnetic Field

Let us now assume that the current density and plasma temperature are constant over a cylindrical cross section. Then (see Ref. 7)

$$H = H_0 q,$$
$$n = (H_0^2/8\pi T)(1 - q^2) \quad \text{for} \quad q = r/a < 1, \quad (30)$$

where a is the radius of the cylinder which contains the plasma, $H_0 = 2I/ca$ and J is the total current. The dispersion equation then takes the form

$$F(z) \equiv \{2 + (\gamma - z)\,\Phi^{(0)}(z) + (\gamma + z)\,\Phi^{(0)}(-z)\} \times \{\gamma - (\gamma - z)\,\Phi^{(2)}(z) - (\gamma + z)\,\Phi^{(2)}(-z)\} + \{(\gamma - z)\,\Phi^{(1)}(z) - (\gamma + z)\,\Phi^{(1)}(-z)\} = 0, \tag{31}$$

$$\Phi^{(n)}(\pm z) = \frac{1}{\sqrt{\pi}} \int_0^\infty \xi^n e^{-\xi} d\xi \int_{-\infty}^{+\infty} \frac{e^{-\tau^2} d\tau}{\pm z + \xi - 2\tau^2},$$

$$n = 0,\ 1,\ 2,$$

$$\gamma = 2q^2/(1 - q^2),$$

$$z = (\Omega |e| 2I/k_z c^2 T)\, q^2, \quad q = r/a.$$

For large values of z,

$$F(z) = 4\frac{(\gamma - 2)(\gamma + 5/2)}{z^2} + 4\frac{13\gamma^2 - 25\gamma/2 - 198}{z^4} + O\left(\frac{1}{z^6}\right). \tag{32}$$

As in the previous case, the imaginary part of $F(z)$ differs from zero along the real axis. For large real values of z

$$\operatorname{Im} F(z) = \frac{\sqrt{2\pi}}{3} e^{-|z|/2} \left\{ -(\gamma + 4)\sqrt{|z|} + \frac{\gamma^2 + 5\gamma/2 - 4/3}{\sqrt{|z|}} + O\left(\frac{1}{|z|^{3/2}}\right) \right\} \operatorname{sign} z. \tag{33}$$

For small values of z, the function $F(z)$ takes the form

$$F(z) = -1.61\,(1 + 0.76\gamma) - \frac{4\pi^2}{27}\gamma^2 + 1.61\sqrt{\pi}\,(1 + i)\,\gamma^2 \left(\frac{z}{2}\right)^{1/2} + \frac{4\pi i}{9\sqrt{3}}\,(6 + 11.08\gamma - 5.08\gamma^2)\,\frac{z}{2} + O(z^{3/2}). \tag{34}$$

When γ is close to 2, the roots of Eq. (31) may be obtained in explicit form by making use of expansion (32). Setting (32) equal to zero, we find

$$z = -i\sqrt{38/(2 - \gamma)} \quad \gamma \approx 2. \tag{35}$$

It follows from Eq. (35) that the plasma is unstable for values of γ to the left of the point $\gamma = 2$, while it is stable for values of ν to the right of that point. We shall show that the plasma is unstable over the whole interval $\gamma = 0$ to $\gamma = 2$, or, what amounts to the same thing, for all values of $q = r/a$ which fulfill the condition

$$0 < r/a < 1/\sqrt{2}. \tag{36}$$

Indeed when γ is close to 2, the number of roots N may be found from equation (35). When $\gamma < 0$, equation (24) and equations (32) to (35) may be used to find the number of roots N, and it may be easily verified that the real axis is transformed by the function $F(z)$ into the contour shown in Fig. 3. Fig. 4 shows this contour for $\gamma > 2$, when the number of roots N in the lower half-plane is zero. We now vary continuously the value of γ from 2 to 0 and from 2 to ∞. If the contour intersects the origin during this variation, the number of turns changes by $\pm 2\pi m$ (where m is an integer) and the number of roots changes by $\pm 2m$. But in region (36) the number of roots can only increase, for otherwise the number N would be negative. Therefore the plasma is unstable over the whole interval (36).

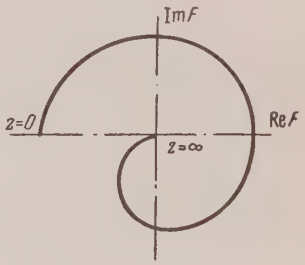

FIG. 3

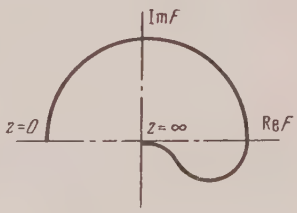

FIG. 4

If the system of equations,

$$\operatorname{Im} F(zq) = 0, \quad \operatorname{Re} F(zq) = 0 \quad (\operatorname{Im} z = 0), \tag{37}$$

which determines the real roots of Eq. (31) admits of solutions for values of the parameter q lying outside of the interval (36), then there may appear regions of instability in the interval $1/\sqrt{2} < q < 1$.

If $r < a/\sqrt{2}$, then instability may generally cause a redistribution of currents over the cross-section of the cylinder.

The dependence of n, T and H upon r may similarly be obtained in other cases.

In conclusion the author wishes to express his profound gratitude to N. N. Bogoliubov for his assistance in this analysis.

1 M. Kruskal and M. Schwarzchild, Proc. Roy. Soc. (London) A223, 348 (1954).

2 K. A. Brueckner and K. M. Watson, Phys. Rev. 102, 19 (1956).

3 This is similar to the method used by Watson, Phys. Rev. 102, 12 (1956), to obtain the distribution function for a low density plasma.

4 L. D. Landau, J. Exptl. Theoret. Phys. (U.S.S.R.) 16, 574 (1946)

5 Equation (20) was obtained and analyzed by N. N. Bogoliubov.

6 L. D. Landau and E. M. Lifshitz, *The Mechanics of Continuous Media*, Moscow, 1953.

7 A Schlüter, Z. Naturforsch. 5a, 72 (1950).

Translated by M. A. Melkanoff
9

SOVIET PHYSICS JETP VOLUME 5, NUMBER 1 AUGUST, 1957

Quantum Corrections to the Thomas–Fermi Equation

D. A. KIRZHNITS
P. N. Lebedev Physical Institute, Academy of Sciences, USSR

(Submitted to JETP editor January 16, 1956)
J. Exptl. Theoret. Phys. (U.S.S.R.) 32, 115–123 (January 1, 1957)

The operator form of the Hartree–Fock equation is considered. The Thomas–Fermi and the Thomas–Fermi–Dirac equations are obtained in the zeroth approximation in terms of $\hbar$. Quantum corrections were found by the operator method for the Thomas–Fermi equations of 2nd and 4th order in $\hbar$. The correction of 2nd order is compared with the Weizsacker correction and it is shown that the latter is 9 times larger than the quantum theory value. The resultant equations are applied to the computation of the total energy of the atom.

1. INTRODUCTION

THE Thomas–Fermi method[1] is one of the methods of the statistical description of systems consisting of a large number of identical particles, and finds wide application in different areas of physics. On the basis of this method, the idea is presented of electrons (if an atom is under discussion) moving classically but with the additional condition that in each cell of phase space there be located no more than two particles. Interaction of particles is considered here by the introduction of the self–consistent field (with or without exchange).

The method under consideration is approximate, for which reason attempts have repeatedly been made at making it more precise in various ways by the introduction of corresponding corrections.[1] In their number we include the quantum correction (or, what amounts to the same thing, the correction for heterogeneity) which reflects the fact of the smearing out of the trajectory of the particle. This correction was first found by Weizsacker[2] by a variational method; however, in its quantitative behavior, it has been subjected to criticism, both in principle and in a comparison of its value with experiment.[3–7]. It was established that the Weizsacker correction was too large a quantity, in which connection, it was improved in a series of researches[3,6] by the introduction of a constant coefficient less than unity. In the present work, a stepwise quantum–mechanical derivation of the quantum corrections of second and fourth order in $\hbar$ is deduced from the Hartree–Fock equation. In this case it is appropriate to use the operator formulation of the problem. A study of the non–relativistic equation of Hartree–Fock in operator form is given in Sec. 2. This form is especially convenient in the relativistic case, and also for interactions which depend on the spin or on the isotopic spin. In the neglect of the non–commutability of the operators for the potential and kinetic energies, we obtain the Thomas–Fermi and the Thomas–Fermi–Dirac equations.

The quantum corrections correspond to a consideration of the commutators of these operators,

in which the corrections of higher order areconnected with the more complicated commutators. This problem is considered in Sec. 3 and in the Appendix.

In Sec. 4, the resultant correction is used for evaluation of the total energy of the atoms of the noble gases. In this case, the disagreement with experiment is reduced from 25–35% (without account of quantum corrections) and 20–35% (with account of the Weizsacker correction) down to 5–7%.

2. OPERATOR FORMULATION OF THE HARTREE–FOCK EQUATION

The quantum–mechanical equations of particles interacting according to the potential $V(|q'-q''|)$ have, in the Hartree–Fock approximation, the form:[8]

$$\int dq''' \{(q'|U+B-A|q''')(q'''|\rho|q'') - (q'|\rho|q''')(q'''|U+B-A|q'')\} = 0. \quad (1)$$

Here ρ is the density matrix

$$(q'|\rho|q'') = \sum_n \rho_n \psi_n(q') \bar{\psi}_n(q''), \quad (2)$$

where ρ_n is the average occupation number; U is the total kinetic and potential energy in the external field; B is the potential energy of the direct interaction of the particles:

$$(q'|B|q'') = \int V(|q'-q'''|)\cdot(q'''|\rho|q''')\,dq'''\cdot\delta(q'-q''); \quad (3a)$$

A is the exchange energy[1]:

$$(q'|A|q'') = {}^1/_2 V(|q'-q''|)(q'|\rho|q''). \quad (3b)$$

Equation (1) corresponds to the stationary case.

It is appropriate to formulate the problem in operator form, starting out from the matrix elements for the corresponding operators. The advantage of such an approach is connected with the independence of the resultant equation of the type of representation, and also with a significant simplification of the computations. The transition to the operators is brought about with the help of the following equivalent relations:

$$\hat{Q} f(q') = \int (q'|Q|q'') f(q'')\,dq'', \quad (4a)$$

$$(q'|Q|q'') = \frac{1}{(2\pi\hbar)^3} \times \int \hat{Q}\left(q', p - i\hbar\frac{\partial}{\partial q'}\right)\exp\left[\frac{ip}{\hbar}(q'-q'')\right]dp, \quad (4c)$$

which, if we neglect the differential operator in $\hat{Q}$ [and also carry out the substitution $q' \to (q'+q'')/2$], goes over into the well known equation of compound representation.

To find the operator which corresponds to the density matrix, we introduce the filling–factor operator, whose spectrum is the mean value of the filling factor:

$$\hat{\rho}(q, \hat{p})\psi_n(q) = \rho_n \psi_n(q). \quad (5)$$

Then (2) has the form:

$$(q'|\rho|q'') = \hat{\rho}(q', \hat{p}') \times \sum_n \psi_n(q')\bar{\psi}_n(q'') = \hat{\rho}(q', \hat{p}')\delta(q'-q''). \quad (6)$$

The latter equation follows from the completeness theorem. It follows from Eq. (6), along with (4b), that the filling–factor operator $\hat{\rho}$ is precisely the operator whose matrix elements coincide with the density matrix.

As far as the operators which correspond to the different parts of the Hamiltonian are concerned, the operator which yields $(q'|U|q'')$ is simply

$$\hat{U} = \hat{p}^2/2M + V_e(q), \quad (7)$$

where V_e is the potential for the external field. For $(q'|B|q'')$, we get from Eqs. (4b), (4c) and (6):

$$\hat{B}(q') = \int V(|q'-q'''|)(q'''|\rho|q''')\,dq''' = \frac{1}{(2\pi\hbar)^3}\int V(|q'-q'''|)\,dq''' \int \hat{\rho}\left(q''', p - i\hbar\frac{\partial}{\partial q'''}\right)dp. \quad (8)$$

Finally, we get for A, by means of several transformations,

$$\hat{A}(q', p') = \frac{1}{2}\int \hat{\rho}\left(q', p - i\hbar\frac{\partial}{\partial q'}\right)V_{(p'-p)/\hbar}\,dp, \quad (9)$$

where V_k is the Fourier component of the function $V(|q' - q''|)$.

Equation (1) takes the following form in operator notation:

$$[\hat{H}, \hat{\rho}] = 0, \quad \hat{H} = \hat{U} + \hat{B} - \hat{A} \qquad (10)$$

and represents the condition for stationarity of the distribution. It then follows that $\hat{\rho}$ ought to be a function of operators which commute with the Hamiltonian, i.e., of integrals of the motion.

For a system in which all the degenerate states which correspond to a given energy value have their indentical filling factors (for example, for an atom with all shells filled), we can consider that

$$\hat{\rho} = \hat{\rho}(\hat{H}). \qquad (11)$$

Concrete form of this function should be given additionally. Thus, if we are interested in a non–degenerate Fermi gas, then

In the case of a degenerate gas, which will be considered below,

$$\hat{\rho} = 2\left[\exp\left(\frac{\hat{H} - E_0}{kT}\right) + 1\right]^{-1}. \qquad (12)$$

Here E_0 is the upper limit of filling, which is determined by the total charge of the system; moreover, the possibility is considered of two spin orientations.

Going on to the case of electrostatic interaction of the particles $V(|q' - q''|) = e^2/|q' - q''|$, $V_e = -e\varphi_e$, we get operator equations equivalent to (1):

$$\Delta\Phi(\mathbf{r}) = -4\pi\rho_e(\mathbf{r}) + \frac{4\pi e^2}{(2\mu\hbar)^3}\int \hat{\rho}[\hat{H}]\, d\mathbf{p}, \qquad (13)$$

$$\hat{A}(\mathbf{r}, \mathbf{p}) = \frac{e^2}{2\pi\hbar}\int \hat{\rho}[\hat{H}']\frac{d\mathbf{p}'}{|\mathbf{p} - \mathbf{p}'|^2},$$

$$\hat{H} = \frac{\hat{p}^2}{2M} - e\Phi(\mathbf{r}) - A(\mathbf{r}, \mathbf{p});$$

$$\hat{\rho}[\hat{H}] = \hat{\rho}[\hat{H}(\mathbf{r}, \mathbf{p} - i\hbar\nabla)].$$

Here Φ is the self-consistent field: $\Phi = \varphi_e - B/e$, ρ_e is the external charge.

The system (13) is an explicit solution of Eq. (1); the ease of obtaining it is compensated by the fact that the argument $\hat{\rho}$ is itself the sum of non–commuting quantities. The center of difficulty of the calculation is thus transferred to the realization of the function from the sum of non–commuting arguments. In cases in which we can neglect this lack of commutation, i.e., in the quasi– classical case, the Thomas–Fermi and the Thomas–Fermi–Dirac equations follow from the system (13) [in place of a proof, we refer to Ref. 1, Sec. 16, where the equations are written in c–numbers which coincide with (13) in the quasi–classical case].

3. QUANTUM CORRECTIONS TO THE THOMAS–FERMI EQUATION OF ORDER $\hbar^2$ AND $\hbar^4$

In the computation of the quantum corrections by means of the expansion of $\hat{\rho}[\hat{H}]$ in Eq. (13) in a series of the commutator components of the Hamiltonian use is made of the formula (see Appendix E):

$$f(\hat{a} + \hat{b}) = f(\overline{a + b}) \qquad (14)$$
$$+ f''(\overline{a + b})\cdot[ab]/2 + f'''(\overline{a + b})\cdot[[ab]\, b]/6$$
$$+ f'''(\overline{a + b})\cdot[a\,[ab]]/6 + f^{IV}(\overline{a + b})\,[ab]^2/8,$$

where the bar over $a + b$ signifies that a and b must be considered as commuting (i.e., $i\hbar\nabla$ is to be omitted in the argument). Considering the degenerate gas (12), and expanding the operator $\epsilon[(\mathbf{p} - i\hbar\nabla)^2 - 2Me\Phi]$ in Eq. (13), we take

$$a = (\mathbf{p} - i\hbar\Lambda)^2, \quad b = -2Me\Phi$$

which gives for the commutators

$$[ab] = -4i\hbar eM\,\mathbf{p}\nabla\Phi \qquad (15)$$
$$+ 2\hbar^2 eM\,\Delta\Phi + 4\hbar^2 M(\nabla\Phi\nabla),$$
$$[ab]^2 = -16\hbar^2 e^2 M^2(\mathbf{p}\nabla\Phi)^2 + \ldots,$$
$$[[ab]\, b] = -8\hbar^2 e^2 M^2(\nabla\Phi)^2 + \ldots,$$
$$[a\,[ab]] = -8\hbar^2 M(\mathbf{p}\nabla)^2\Phi + \ldots$$

Consideration of more complicated commutators in this approximation is unnecessary since it gives terms $\sim \hbar^3$ and higher. Upon substitution of (14) and (15) in the first equation of (13), and after integration of the δ–function and its derivatives arising here, we get the Thomas–Fermi equation with the quantum corrections*

$$\Delta\Phi + 4\pi\rho_e = 4\pi e\rho(\Phi, \nabla\Phi, \Delta\Phi \ldots) \qquad (16)$$
$$= (4e/3\pi\hbar^3)[2M(e\Phi + E_0)]^{3/2}$$
$$- (e^3M^2/6\pi\hbar)[2M(e\Phi + E_0)]^{-3/2}$$
$$\times [(\nabla\Phi)^2 - 4(\Phi + E_0/e)\Delta\Phi].$$

*As has been pointed out by the author, Eq. (16) was also obtained by A. S. Kompaneets and E. S. Pavlov by means of a method essentially different from that given in the present work.

Here ρ is the density of the electron cloud; E_0 must be taken equal to zero in the case of a neutral system. Equation (16) is simplified in the case

$$e\Phi + E_0 < 0,$$

since here the functions

$$1 - \varepsilon, \ \delta, \delta'$$

and so forth are identically equal to zero. This gives for any finite order of $\hbar$

$$\Delta\Phi + 4\pi\rho_e = 0. \tag{16a}$$

Correction terms of the order of $\hbar$ (and generally of any odd order) are absent, as also follows from the real nature of ρ.

Let us find the correction to the energy which is determined by quantum effects. According to the general formula for the approximation of a self–consistent field,

$$E = \sum_n E_n - E_{\text{int}},$$

$$E_{\text{int}} = \frac{e^2}{2}\int \frac{\rho(\mathbf{r}_1)\rho(\mathbf{r}_2)}{|\mathbf{r}_1 - \mathbf{r}_2|} d\mathbf{r}_1 d\mathbf{r}_2$$

we get

$$E = \frac{1}{(2\pi\hbar)^3}\int\left(\frac{\hat{p}^2}{2M} - e\Phi\right) \times \left[1 - \varepsilon\left(\frac{\hat{p}^2}{2M} - e\Phi - E_0\right)\right] d\mathbf{p}\, d\mathbf{r} - E_{\text{int}}, \tag{17}$$

where

$$\hat{p} = p - i\hbar\nabla.$$

Instead of taking (17) into account and using Eqs. (14) and (15), we can establish the connection between the energy corrections and the density ρ. For this purpose, we note that for any order of $\hbar$ (f is an arbitrary function),

$$\int_0^\infty f\left(\frac{\hat{p}^2}{2M} - A\right)p^2 dp, \quad A = e\Phi + E_0,$$

is represented in the form of an expansion only in half–integer (positive and negative) powers of A [in this connection, see Eq.(23)]. This statement is based on the parity of the half–integral expression relative to p and $\hat{p}$, and can be proved by induction. Let us transform (17) to the form

$$E = E_1 + E_0\int \rho\, d\mathbf{r} - E_{\text{int}}.$$

$$E_1 = \frac{1}{(2\pi\hbar)^3}\int (\hat{H} - E_0)\,[1 - \varepsilon(\hat{H} - E_0)]\, d\mathbf{p}\, d\mathbf{r}. \tag{18}$$

Differentiating E_1 with respect to E_0 we obtain

$$\partial E_1/\partial E_0 = -\int \rho \cdot d\mathbf{r}$$

Integrating this expression, we take it into account that ρ depends only on the combination

$$e\Phi + E_0$$

and on commutators which do not contain E_0. Therefore, we can carry out the integration with E_0 over $e\Phi$, taking the commutators to be constant.

This gives for the energy correction

$$\delta E = -e\int^{\Phi} d\Phi \int \delta\rho\,(\Phi, \nabla\Phi \ldots)\, d\mathbf{r} + E_0\int \delta\rho\,(\Phi, \nabla\Phi \ldots)\, d\mathbf{r}. \tag{19}$$

The arbitrary constant of integration ought to be so chosen that the result did not contain any powers of

$$e\Phi + E_0,$$

$e\Phi + E_0$ beside the half- integral ones, and in particular, that $e\Phi + E_0$ be absent in the zeroth power.

In the second order of $\hbar$, with account of (16), we get (for $E_0 = 0$):

$$\delta_2 E = -\frac{e^2 M}{24\pi^2\hbar}\int d\mathbf{r}\,(2Me\Phi)^{-1/2}[(\nabla\Phi)^2 + 4\Phi\Delta\Phi]. \tag{20}$$

Transforming to atomic units $e = M = \hbar = 1$ we express $\delta_2 E$ in terms of ρ by Eq.(16). This gives, in the approximation under consideration

$$\delta_2 E = \frac{1}{72}\int d\mathbf{r}\,\frac{(\nabla\rho)^2}{\rho} - \frac{\pi}{3}\lim_{\varepsilon\to 0}\frac{\partial\rho}{\partial r} r^2\Big|_{\varepsilon}^{\infty}. \tag{21}$$

The first term of this expression coincides in form with the well known correction of Weizsacker[2] for the inhomogeneity of the density, but is numerically smaller by a factor of 9. The second term is not important if we put in (21) the density distribution of Hartree–Fock (or a distribution with a suitable behavior at zero; see below, Sec.4).

In conclusion, let us establish the dependence on Z of the quantum correction for an atom with a nuclear charge Z. Starting out from the estimates

$$r \sim Z^{-1/3}, \quad \rho \sim Z/r^3 \sim Z^2,$$

we find

$$\delta_2 E \sim Z^{7/3}, \tag{22}$$

while in the quasi-classical case,

$$E_0 \sim Z^{7/3}.$$

Thus, expansion in $\hbar^2$ is at the same time an expansion in $Z^{-1/3}$*. This corresponds to the fact that the Thomas–Fermi equation is the more accurate the larger the value of Z.

Let us proceed to the quantum corrections of fourth order. The technique of computation in this case is the same as above, but in place of (14) we use a formula which contains more complicated commutators [see Appendix, Eq. (1)]. In the process of calculation, the relation

$$\int_0^\infty \left(\frac{p^2}{2M}\right)^m \frac{\partial^n}{\partial (p^2/2M)^n} \varepsilon\left(\frac{p^2}{2M} - e\Phi\right) p^2 dp \tag{23}$$

$$= \frac{(-1)^{n-1}}{2^{n-1}} (2M)^{3/2} (2m+1)(2m-1)$$

$$\ldots (2m-2n+5)(e\Phi)^{m-n+3/2}.$$

is useful. As a result, we obtain the following expression for the correctness of fourth order to the density:

$$\delta_4 \rho = (32e^4 M^4 \hbar / 15\pi^2)(2Me\Phi)^{-3/2} \tag{24}$$

$$\times \{64\Phi^3 \Delta^2 \Phi - 192\Phi^2 \nabla\Phi \cdot \nabla\Delta\Phi$$
$$- 64\Phi^2 (\nabla_i \nabla_k \Phi)^2 - 80 (\Delta\Phi)^2 \Phi^2$$
$$+ 200\, \Phi\, \Delta\Phi \cdot (\nabla\Phi)^2$$
$$+ 240\Phi \nabla_i \Phi \cdot \nabla_i \nabla_k \Phi \cdot \nabla_k \Phi - 175 (\nabla\Phi)^4\}.$$

Expressing the energy correction in terms of ρ, we obtain in the given approximation [taking also into consideration the terms of the same order from Eq. (20)],

$$\delta_4 E = -\frac{1}{4320 (3\pi^2)^{2/3}} \tag{25}$$

$$\times \int \frac{dr}{\rho^{11/3}} \{8 (\nabla\rho)^4 - 27\rho (\nabla\rho)^2 \Delta\rho + 24\rho^2 (\Delta\rho)^2\}.$$

The estimate of the dependence of Eq. (26) on Z gives

$$\delta_4 E \sim Z \tag{26}$$

corresponding to the fact that the $Z^{-3/2}$ appears as the expansion parameter.

In conclusion, we note that consideration of the quantum corrections of fourth order to the Thomas-Fermi equation requires, generally speaking, a simultaneous consideration of the corrections of second order to the Thomas–Fermi–Dirac equation, i.e., to quantum corrections in the exchange. This problem has a whole series of specific peculiarities and will be set forth in a separate paper.

4. ENERGY OF THE ATOM IN THE STATISTICAL MODEL

It is known from experiment, and from quantum-mechanical calculations, that the total energy of an atom E is a monotonic function of the ordinal number Z. This bears witness to the weak dependence of E on the details of the internal structure of the atom, and permits us to hope for a successful application of the semi-classical statistical model to the calculation of E. However, calculation of E by means of the Thomas–Fermi model, which leads to the expression $E = -0.769\, Z^{7/2}$ gives much too large a value (in absolute magnitude) to the energy. This is connected with the fact that the density in the Thomas–Fermi model varies as $r^{-2/3}$ at the origin while qunntum mechanics leads to a finite value of ρ at $r \sim 0$. In view of this fact, there is an excess of electrons in the neighborhood of the nucleus in the given model in comparison with their actual distribution. This fact leads to a lower value of the kinetic energy of the electron cloud and to a higher value (in absolute magnitude) of the total energy*. The reason for this is clear and is contained in the inapplicability of the quasi-classical Thomas–Fermi equation in the vicinity of

*The dimensionless parameter

$$\hbar^2 / p^2 r^2$$

has the order of

$$\rho^{-2/3} r^{-2} \sim Z^{-2/3}.$$

the nucleus, since the quantum effects in this region must be especially strong. Therefore, we can hope that calculation of the Weizsacker quantum correction improves the position with respect to the energy of the atom. This is evident if only from the fact that for $\rho \sim r^{3/2}$, the integral (21) tends to ∞, i.e., the energy is each case does not have a minimum. (a growth of ρ at zero that is weaker than r^{-1} is acceptable). However, calculations of N. Sokolov[3] have shown that although the Weizsacker correction also leads to a decrease (in absolute value) of the total energy of the atom, this decrease is so great that divergence from experiment is obtained just as in the quasi–classical case, but with different sign. This, and also a series of other considerations [3–7] leads to the conclusion that the Weizsacker correction has too large a value. One of the reasons is the circumstance that the test function chosen by Weizsacker in the variational method was excessively rough and therefore gives a higher value of the energy.

It was established above that quantum–mechanical considerations lead to a quantum correction of second order which is 9 times smaller than that of Weizsacker. The correction we found has been used by us in the calculation of the total energy of the atom by the Lenz–Jensen method. This method, in application to the present problem, has been described in Ref. 3, where the calculations are carried out with the Weizsacker correction: therefore the details of the calculation are omitted below.

The method just mentioned is not connected with the solution of the differential equation for the potential Φ, but derives from the expression for the energy which is expressed in terms of the density ρ:

$$E = \frac{3}{10}(3\pi^2)^{2/3}\int \rho^{5/3}\,d\mathbf{r} - Z\int \frac{\rho}{r}\,d\mathbf{r} + \frac{1}{2}\int \frac{\rho(\mathbf{r}_1)\,\rho(\mathbf{r}_2)}{|\mathbf{r}_1 - \mathbf{r}_2|}\,d\mathbf{r}_1\,d\mathbf{r}_2 - \frac{3}{4}\left(\frac{3}{\pi}\right)^{1/3}\int \rho^{4/3}\,d\mathbf{r} + \delta_2 E + \ldots \qquad (27)$$

Here the first term is the kinetic energy, the second and the third are potential terms, the fourth is exchange (without quantum corrections), and, finally, the remaining terms are the quantum corrections of the 2nd, 4th, . . . orders. Carrying out the calculations for second order in $\hbar$, we limit ourselves to writing down five terms and seek a minimum of (27) by substitution of different test functions of ρ. Here it is shown (see also Ref. 3) that, within an accuracy of 3–4% of the quantity E, this minimum is realized by the class of functions

$$\rho(r) = c\exp\{-(\lambda r)^{1/\beta}\}, \qquad (28)$$

where λ and β are variation parameters and C is determined by normalization. Upon substitution of Eq. (28) in $\delta_2 E$, we can discard the second term in (21) and the Weizsacker correction, decreased by a factor of 9, will figure in (27).

Departure of the total energy,

$$\delta = (E - E_{\text{emp}})\,E_{\text{emp}}\%$$

from the empirical (and semi–empirical) values which are taken from Ref. 4, and also the values of the parameters are listed in the Table where, moreover we give the values of δ for the Thomas–Fermi and Thomas–Fermi–Dirac equation with the Weizsacker correction.

For argon ($Z = 18$), we have carried out estimates of the fourth order corrections of (26). In this connection, it is important to note that just as the density obtained from the solution of the Thomas–Fermi equation cannot be used for estimating the second order correction because of the notably higher divergence, the density (28) is unsuitable, for the same reason, for estimating the fourth order correction. It is necessary to set up the variational problem for the function included in (26), and we must limit the class of test functions to functions which do not lead to the divergencies of (26). Moreover, for an approximate estimate, we must substitute in Eq. (26) the exact solution of the Hartree equation.[9] This leads to the estimate

$$\delta_4 E \approx -3\%.$$

It is evident from the Table above that the second order quantum correction contributes a term to the energy ~ 20–30%; this bears witness to the excellent convergence of the approximation process. In addition, for accurate determination of the fourth order correction, it is necessary to take into account quantum–exchange corrections (see the end of Sec. 3) and also to make use of a much wider class of test functions with the purpose of improving the accuracy of the result.

I express my deep gratitude to Corresponding Member of the Academy of Sciences, USSR, V. L. Ginzburg for his interest in the work and for his valued remarks, to A. S. Kompaneets for his judgment on a number of problems involved in the research, and also to L. Ia. Trendelev who carried out a great deal of the computational work.

REALIZATION OF A FUNCTION FROM NON–COMMUTING ARGUMENTS

In a number of problems of quantum theory, one deals with functions of the sum of non–commuting operators, the rule of operation with which has recently been clarified by a number of researches.[10] These methods, which appear to be sufficiently general, can be applied to the problem considered above of the expansion in powers of $\hbar$, but have a much more useful special property which stems from the fact that an expansion in powers of $\hbar$ is simultaneously a computation of more complicated commutators.

As early as 1933, the first terms of an expansion of functions of the sum of operators were described by Peierls but the method used by him in the problem of finding the coefficients of expansion was extremely crude. A much simpler method is considered below, with the help of which an expansion up to four commutators was obtained.

For a sufficiently wide class of functions $f(a+b)$, where $\hat{a}$ and $\hat{b}$ are non–commuting arguments, we can use a Fourier expansion* and thus work with exponential functions $\exp[i(a+b)\tau]$

Let us represent it in the form

$$\exp[i(a+b)\tau] = \exp(ib\tau)\, K \exp(ia\tau), \quad \text{(a)}$$

here K depends on the commutators of $\hat{a}$ and $\hat{b}$ on τ, and is determined by an equation which is obtained upon differentiation of Eq. (a) with respect to τ:

$$\partial K/\partial\tau = i\exp(-i\tau[b)a]\; K - iKa$$

$$\exp(-i\tau[b)a] \equiv e^{-i\tau b}\, a e^{i\tau b} \quad \text{(b)}$$

$$= \sum_{n=0}^{\infty} \frac{(-i\tau)^n}{n!} [\overbrace{b[b\ldots[ba}^{n}]\ldots].$$

Starting out from $K_0 = 1$, we find

$$\partial K_1/\partial\tau = \tau[ba], \quad K_1 = \tau^2[ba]/2.$$

Similarly, limiting ourselves to two commutators and to the square of one of them, we get the expression

(c)

$$K_2(\tau) = (i\tau^3/6)\{[a[ba]] - [b[ba]]\} + (\tau^4/8)[ba]^2.$$

In Eq. (a), the operators K and $e^{ia\tau}$ no longer act on $e^{ib\tau}$, as a consequence of which the latter can be moved to the right:

$$\exp[i(a+b)\tau] = K(\tau)\exp[i(\overline{a+b})\tau], \quad \text{(d)}$$

where the bar denotes that a and b must be considered as commuting operators, and $K(\tau)$ ought not to act on the function following it. Transforming from the Fourier form to the initial function, we get*

$$f(a+b) = f(\overline{a+b}) + f''(\overline{a+b})[ab]/2 + f'''(a+b)\{[[ab]b] + [a[ab]]\}/6 + f^{IV}(\overline{a+b})[ab]^2/8. \quad \text{(e)}$$

Consideration of more complicated commutators is carried out similarly. Introducing the notation

$$Q_n^m = [\underbrace{a[a\ldots[a}_{m}[\underbrace{b[b\ldots[ba}_{n}]\ldots], \quad \text{(f)}$$

we obtain the reamining terms of the expansion $K(\tau)$ up to four commutators inclusively in the form:

$$K_3(\tau) = (\tau^4/24)(Q_2^1 - Q_1^2 - Q_3^0) + (i\tau^5/120)(7Q_1^0Q_1^1 - 4Q_1^0Q_2^0 - 6Q_2^0Q_1^0 + 3Q_1^1Q_1^0) + (\tau^6/48)(Q_1^0)^3,$$

$$K_4(\tau) = (i\tau^5/120)(Q_4^0 + Q_2^2 - Q_1^3 - Q_3^1) + (\tau^6/720)(-3Q_1^2Q_1^0 - 10(Q_1^1)^2 - 12Q_1^0Q_1^2 + 4Q_1^1Q_2^0 + 9Q_1^0Q_2^1 - 5Q_1^0Q_3^0 + 16Q_2^0Q_1^1 - 10(Q_2^0)^2 - 10Q_3^0Q_1^0 + 6Q_2^1Q_1^0) + (i\tau^7/1680)(5Q_1^1(Q_1^0)^2 + 11Q_1^0Q_1^1Q_1^0 + 19(Q_1^0)^2Q_1^1 - 8(Q_1^0)^2Q_2^0 - 12Q_1^0Q_2^0Q_1^0 - 15Q_2^0(Q_1^0)^2) + (\tau^8/384)(Q_1^0)^4\ldots \quad \text{(g)}$$

(h)

*For the functions $\epsilon(a+b)$, we must use the discontinuous integral of Dirichlet.

*The quantity τ plays the role of the differentiation operator with respect to $\overline{a+b}$.

[1] P. Gombas, *Statistical Theory of the Atom*, IIL, Moscow, 1951 (Russian translation).
2 C. Weizsacker, Z. Physik 96, 431 (1935).
3 N. Sokolov, J. Exptl. Theoret. Phys. (U.S.S.R.) 8, 365 (1938).
4 P. Gombas, Acta. Phys. Huang. 3, 105, 127 (1953).
5 A. S. Kompaneets, J. Exptl. Theoret. Phys. (U.S.S.R.) 25, 540 (1953); 26, 153 (1954).
6 R. Berg and L. Willets, Proc. Phys. Soc. (London) 68 A, 229 (1955).
7 W. Theis, Z. Physik 142, 503 (1955).
8 P. Dirac, *The Principles of Quantum Mechanics*
9 D. Hartree and W. Hartree, Proc. Roy. Soc. (London) 166A, 450 (1938).
10 R. Feynman, Phys. Rev. 84, 108 (1951); I. Fujiwara, Progr. Theoret. Phys. 7, 433 (1952); K. Yamazaki, Progr. Theoret. Phys. 7, 449 (1952); R. Blauber, Phys. Rev. 84, 395 (1951).
11 R. Peierls, Z. Physik 80, 771 (1933).

Translated by R. T. Beyer
15

SOVIET PHYSICS JETP VOLUME 5, NUMBER 1 AUGUST, 1957

Capture of Conduction Electrons by Charged Defects in Ionic Crystals

IU. E. PERLIN
Kishinev State University

(Submitted to JETP editor October 25, 1955)
J. Exptl. Theoret. Phys. (U.S.S.R.) 32, 105–114 (January, 1957)

Capture of conduction electrons by charged defects of an ionic crystal lattice is regarded as a one-quantum thermal transition from the continuous spectrum to an excited state of the discrete spectrum. The role of the perturbation is played by the nonconfigurational interaction which in an ideal crystal leads to ordinary polaron scattering. The capture probability as a function of polaron velocity has been computed and the temperature dependence of current–carrier lifetime has been established.

1. INTRODUCTION

IN the phenomenological theory of semiconductors, the recombination coefficients of conduction electrons with "impurity centers" such as ion vacancies or excess interstitial ions) are usually regarded as parameters to be determined by comparing the theory with experiment. The large number of such parameters endows the formulas of the phenomenological theory with excessive approximational flexibility so that the comparison of the theory with experiment is sometimes inconclusive. Therefore, calculation of the probability of electron capture by an impurity center using the methods of a microscopic theory is of considerable interest.

We shall not in this article attempt a complete review of the theortical work on this problem. We shall, however, indicate that a treatment of the problem very similar to ours was first published by Adirovich,[1] who regarded electron capture as a quantum transition induced by the nonconfigurational interaction of an electron with ion motions (the violation of adiabaticity). Adirovich's proposed model of a pulsating double layer enabled him to make a qualitative estimate of capture probability.

A theoretical formula for the reombination coefficient which does not contain undetermined parameters and which permits comparison of the theory with experiment was obtained by Pekar,[2] who divided the process of electron capture by an impurity center into the diffusion of an electron to a lattice defect and direct thermal transition to a discrete energy level. In crystals where conduction electron mobility is low, the first part of the process can play the deciding role.

Pekar and the present author[3] made a comparison of the recombination coefficient calculated on this hypothesis with experimental data on electron capture by F centers in alkali halide crystals and obtained satisfactory results. Nevertheless, without a quantum mechanical calculation of the thermal transition probability (of an electron) to a discrete level, the "diffusion" theory of recombinations is of uncertain applicability. There are undoubtedly cases in which the second stage of the process rather than the first, plays the deciding role.

The present article attempts a quantum mechanical calculation of the probability for electron capture by a positively charged ionic crystal lattice defect (such as a negative ion vacancy). Such a

process occurs in connection with the coloring of ionic crystals by x–rays. The captured electrons form F centers.

In a number of recently published investigations of the theory of thermal ionization of F centers (see, for example, the articles by O'Rourke and by Vasileff [4]), thewave functions of the continuous spectrum are given in the form of the product

$$\chi(\mathbf{r}) \prod_{\varkappa} \Phi_n(q_\varkappa)$$

of the purely electronic function and the wave functions Φ_{n_k} of undisturbed normal lattice oscillators. These articles thus ignore the effect of inertial polarization of the ionic crystal on the electron states of the continuous spectrum as well as the shift of the equilibrium positions of the phonon field oscillators which results from interacions with electrons. Such an approximation is unacceptable since at large distances from a defect , a conduction electron forms a polaron and its state is described by the dampedwave function

$$\psi(\mathbf{r} - \xi),$$

belonging to the discrete spectrum, where ξ is the translational radius vector of the polaron which characterizes the location of the center of symmetry of the polarized potential well.

Confining ourselves to strong coupling between an electron and the longitudinal phonon field we shall use as a basis the Hamiltonian of Pekar's theory of polarons:

$$\hat{H} = -(\hbar^2/2\mu)\Delta + V(\mathbf{r}) \qquad (1.1)$$

$$+ \sum_{\varkappa} A_\varkappa(r)\, q_\varkappa + {}^1/_2\hbar\omega \sum_{\varkappa} (q_\varkappa^2 - \partial^2/\partial q_\varkappa^2).$$

Here μ is the effective electron mass in the conduction aand, $V(\mathbf{r})$ is the interaction potential between an electron and a lattice defect, q_k are the normal coordinates of the phonon field, ω is the frequency limit of longitudinal optical oscillations (whose small dispersion we neglect);

$$A_\varkappa(r) = -\frac{e}{\varkappa}\sqrt{\frac{c\hbar\omega}{4\pi}}\int \frac{(\varkappa,\ \mathrm{grad}\ \chi_\varkappa(\mathbf{r}'))\, d\tau'}{|\mathbf{r} - \mathbf{r}'|}, \qquad (1.2)$$

where $c = 1/n^2 - 1/\epsilon$ is the inertial polarization constant of the crystal. The functions

$$\chi_\varkappa(\mathbf{r}) = \sqrt{\frac{2}{L^3}} \begin{cases} \cos(\varkappa\mathbf{r}) & \text{for } \varkappa_x \geqslant 0, \\ \sin(\varkappa\mathbf{r}) & \text{for } \varkappa_x < 0 \end{cases} \qquad (1.3)$$

form a complete orthomormal set in the space L^3.

Keeping in mind that a weakly coupled electron is a fast subsystem while the lattice oscillators comprise a slow subsystem, we can employ an adiabatic method, that is, we can obtain an approximate eigenfunction of the operator (1.1) as the product

$$\Psi(\mathbf{r}, \ldots q_\varkappa \ldots) \qquad (1.4)$$

$$= \psi(\mathbf{r}, \ldots q_\varkappa \ldots)\, \Phi(\ldots q_\varkappa \ldots),$$

where the electronic function satisfies the equation

$$\Big[-(\hbar^2/2\mu)\Delta + V(\mathbf{r}) \qquad (1.5),$$

$$+ \sum_{\varkappa} A_\varkappa(\mathbf{r})\, q_\varkappa\Big]\psi(\mathbf{r}, q) = E(q)\,\psi(\mathbf{r}, q),$$

and the eigenvalues of

$$\Big[E(q) + {}^1/_2\,\hbar\omega \sum_{\varkappa}(q_\varkappa^2 - \partial^2/\partial q_\varkappa^2)\Big]\Phi = H\Phi \qquad (1.6)$$

are approximate values of the energy of the entire system. In deriving (1.6) we omitted terms resulting from the action of the kinetic energy operator of the slow subsystem on the electronic function ("nonadiabatic "terms).

In our case of strongly excited states the electron moves in a quasi-classical orbit of large radius. In this case, the field of the defect affects the electronic wave function less than the polaron effect in a perfect crystal. This means that the center of localization of the function ψ will not coincide with the center of the defect Coulomb field (the coordinate origin) and we are justified in setting

$$\psi(\mathbf{r}, \ldots q_\varkappa \ldots) = \psi_0(\mathbf{r} - \xi, \ldots q_\varkappa \ldots). \qquad (1.7)$$

Following the traditional method, we can calculate ψ_0 on the assumption that the potential energy of the slow subsystem differs little from its equilibrium (minimum) value in the configuration

$$(q_\varkappa)_{\min} = q_{\varkappa\xi} = -A_{\varkappa\xi}/\hbar\omega, \qquad (1.8)$$

where

$$A_{\varkappa\xi} = \int A_\varkappa(\mathbf{r})\,|\psi_0(\mathbf{r} - \xi)|^2\, d\tau. \qquad (1.9)$$

If we limit ourselves to a first-order perturbation

calculation of $E(q)$ from (1.5), then (1.6) becomes

$$\left\{I[\psi_0] + W(\xi) + {}^1/_2\hbar\omega \times \sum_\varkappa [(q_\varkappa - q_{\varkappa\xi})^2 - \partial^2/\partial q_\varkappa^2]\right\}\Phi = H\Phi; \quad (1.10)$$

$$I[\psi_0] = (\hbar^2/2\mu)\int |\nabla\psi_0|^2 d\tau - {}^1/_2\hbar\omega\sum_\varkappa q_{\varkappa\xi}^2 \quad (1.11)$$

is independent of ξ and

$$W(\xi) = \int V(\mathbf{r})\,|\psi_0(\mathbf{r}-\xi)|^2 d\tau. \quad (1.12)$$

Proceeding to an examination of the final form of ψ_0, we note that in the limiting case $\xi \to \infty$ this function describes the state of the electron in a polaron. However the field of the defect destroys the spherical symmetry of ψ_0 and the radius of the electronic state is changed. The first of these effects can be regarded as the polarization of the electronic "ψ cloud" in the polaron by the Coulomb field of the defect. The author's method of calculating the polarizability of an F center[5] enables us to show that when

$$\xi > 6.19/\alpha\sqrt{\varepsilon c} = 1.24\, r_p/\sqrt{\varepsilon c}, \quad (1.13)$$

where

$$\alpha = \mu e^2 c/2\hbar^2,$$

and

$$r_p = 5/\alpha$$

is the so-called polarization radius of the polaron, the deformation of ψ_0 can be neglected.

In Ref. 6 it was shown that when

$$\xi > 5/\alpha = r_p, \quad (1.14)$$

which practically coincides with (1.13), it is also possible to neglect the change of radius of the electronic state in the polaron. Assuming that (1.13) and (1.14) are satisfied at all points of the quasi-classical orbits of strongly excited states we can therefore take ψ_0 in the form of the usual electronic wave function in a polaron[2]:

$$\psi_0(r) = \sqrt{\alpha^3/7\pi}\,(1+\alpha r)\,e^{-\alpha r}. \quad (1.15)$$

We note, finally, that according to Ref. 6, for a Coulomb impurity center subject to condition (1.14), W is approximated with sufficient accuracy by a Coulomb potential.

The eigenfunction of (1.10) will be sought in the form

$$\text{equation} \quad \Phi(\xi, \ldots q'_\varkappa \ldots),$$

where

$$q'_\varkappa = q_\varkappa - q_{\varkappa\xi}, \quad (1.16)$$

and ξ is a function of the variables q_k. The choice of this function is to some extent arbitrary. According to Pekar[2], the dependence of ξ on q_k is given implicitly by

$$\sum_\varkappa q_\varkappa \partial q_{\varkappa\xi}/\partial\xi_i = 0 \quad (i = 1, 2, 3). \quad (1.17)$$

The insertion of

$$\Phi(\xi,\ q'_\varkappa)$$

after transformations which are entirely analogous to the corresponding transformations in polaron theory changes (1.10) to the form

$$\left\{I[\psi_0] + W(\xi) - (\hbar^2/2M)\Delta_\xi + {}^1/_2\sum_\varkappa \hbar\omega\,(q'^2_\varkappa - \partial^2/\partial q'^2_\varkappa)\right. \quad (1.18),$$

$$\left. (q_\varkappa)_{\min} = q_{\varkappa\xi} = -A_{\varkappa\xi}/\hbar\omega,\right.$$

where M is the effective mass of the polaron,

$$\hat{H}' = (\hbar^2/2M)\sum_\varkappa \Delta_\xi\, q_{\varkappa\xi}\,\partial/\partial q'_\varkappa; \quad (1.19)$$

$$\hat{H}'' = (\hbar^2/2M) \times \sum_\varkappa\sum_\lambda (\nabla_\xi q_{\varkappa\xi},\ \nabla_\xi q_{\lambda\xi})\,\partial^2/\partial q'_\varkappa \partial q'_\lambda. \quad (1.20)$$

Equation (1.18) differs from the analogous equation of the polaron theory not only because of the presence of the term $W(\xi)$ but also in that the number of variables including the vector ξ exceeds by 3 the number of degrees of freedom of the lattice. Therefore, (1.18) must in general be interpreted along with the supplementary relations (1.17).

However, it is possible to consider the more general problem described by (1.18), where ξ and

q'_k are independent variables. Insertion of the dependence of ξ on q'_k into the solution of this general problem leads to a solution of our special problem. This substitution can be performed in the last stage of the calculations, thus including, in particular, the entire perturbation theory in the generalized stage. Therefore the transition matrix elements can be calculated from the zero–approximation eigenfunctions of the generalized equation (1.18).

The zero–approximation generalized functions are obtained from (1.18) if the operators $\hat{H}'$ and $\hat{H}''$, which in the polaron theory lead to one-quantum and two-quantum scattering, respectively, are regarded as small perturbations. When these operators are omitted, the variables in (1.18) are separable and the eigenfunctions and energies of the zero–order stationary states are:

$$\Phi^0_{n,n_\varkappa}(\xi, \ldots q'_\varkappa \ldots) = \varphi_n(\xi) \prod_\varkappa \Phi_{n_\varkappa}(q'_\varkappa), \quad (1.21)$$

$$H^0_{n,n_\varkappa} = I[\psi_0] + E_n + \hbar\omega \sum_\varkappa (n_\varkappa + 1/2). \quad (1.22)$$

Here φ_n nnd E_n satisfy the Schrödinger equation

$$-(\hbar^2/2M)\Delta_\xi \varphi_n + W(\xi)\varphi_n = E_n \varphi_n, \quad (1.23)$$

which describes the motion of a quasi–particle (polaron) in a Coulomb field. The Φ_{nk} are the wave functions of the harmonic oscillators. The criterion for the applicability of our approximation to strongly excited discrete F–center levels can be derived from the virial theorem and the inequality (1.14):

$$n^2 > 10ZM/\varepsilon C\mu, \quad (1.24),$$

where n is the principal quantum number of the hydrogen-like term.

In the present article we confine ourselves to an examination of one–quantum transitions between zero–order stationary states resulting from the perturbation $\hat{H}'$. It is assumed that the initial polaron state belongs to the continuous spectrum and that its energy is given by

$$E_n = E(\mathbf{k}) = \hbar^2 k^2/2M \ll \hbar\omega. \quad (1.25)$$

Then a transition with emission of a phonon takes place to one of the discrete states, and therefore represents the localization of the conduction electron close to the impurity center. This transition will be regarded as electron capture.

The captured electron can subsequently be ejected into the continuous spectrum again by absorption of a phonon, but there is a much greater probability (when the temperature is not high) that it will "drop" to the ground state of the F-center in a thermal or optical transition. Thermal transitions between discrete levels were investigated by Huang and Rhys.[7]

The single–phonon capture proposed here is, of course, not the only possible mechanism. A possible competing mechanism is a "multi–phonon" transition associated with deformation of the electronic wave function ψ by the field of the impurity center. As a result of this deformation, the equilibrium values of the normal coordinates q_k of the phonon field differ in the various electronic states, and the corresponding oscillator wave functions

$$\Phi_{n_\varkappa}(q_\varkappa - q_{\varkappa\xi})$$

and

$$\Phi_{n'_\varkappa}(q_\varkappa - q_{\varkappa\xi'})$$

become nonorthogonal. A probability of a multiphonon transition exists in the first perturbation approximation. We intend to investigate such transitions in one of our future articles.

2. MATRIX ELEMENT OF A SINGLE PHONON TRANSITION

For the succeeding calculations we introduce the unit of length

$$a_0 = \varepsilon\hbar^2/Me^2. \quad (2.1)$$

In the formulas which follow all quantities having the dimension of a length or a reciprocal length will be expressed in units of a_0 and a_0^{-1}, respectively.

If we neglect the small dispersion of the longitudinal optical vibrations of the crystal and use Pekar's expressions[2] for M and $q_{k\xi}$ the perturbation operator becomes

$$\hat{H}' = -\frac{\sqrt{\pi}}{100}\hbar\omega\,(\varepsilon C)^{1/2}\left(\frac{A}{\hbar\omega}\right)^{1/2} \times \sum_\varkappa \frac{\varkappa(1+\varkappa^2/28\alpha^2)}{(1+\varkappa^2/4\alpha^2)^4}\chi_\varkappa(\xi)\,\partial/\partial q'_\varkappa, \quad (2.2)$$

where all of Pekar's notation[2] has been retained. In particular

$$A = \mu e^4 / 2\hbar^2\varepsilon^2, \tag{2.3}$$

$$\alpha = 21.6\,(\varepsilon c)^{-3}\,(\hbar\omega / A)^2. \tag{2.4}$$

The transition between stationary states

$$k, \ldots n_\varkappa \ldots \rightarrow n, \ldots n'_\varkappa \ldots$$

corresponds to the matrix element

$$(k, \ldots n_\varkappa \ldots \mid \hat{H}' \mid n, \ldots n_\varkappa \ldots) \tag{2.5}$$
$$= \int \varphi^*_k(\xi) \prod_\varkappa \Phi_{n_\varkappa}(q'_\varkappa)\, \hat{H}'\, \varphi_n(\xi) \prod_\varkappa \Phi_{n'_\varkappa}(q'_\varkappa)\, dq'_\varkappa\, d\xi.$$

For the quantum transition with emission of a phonon $\hbar\omega_\varkappa$, integration over the variables $q'_\varkappa$ gives

$$\prod_\varkappa \int \ldots dq'_\varkappa = \sqrt{(n_\varkappa + 1)/2} \tag{2.6}$$

for an allowed transition; one term of the sum in (2.2) remains, corresponding to the emitted phonon $\hbar\omega_\varkappa$.

In proceeding to integrate over the variables ξ we make the following simplifying assumptions:

1) We limit ourselves to a consideration of a transition between *s*-states of the Coulomb field, setting

$$\varphi_n(\xi) = R_n(\xi) / 4\pi, \tag{2.7}$$

where $R_n(\xi)$ is the radial function

2) We consider a transition to a strongly excited state of the discrete spectrum with a principal quantum number which satisfies the inequality

$$n^2 > 10\, M / \varepsilon c\mu \gg 1. \tag{2.8}$$

In this state the most probable value of ξ for the polaron is $\sim n^2 >> 1$ and, consequently, the principal role in the Laguerre polynomial is played by a higher term. Consequently, we shall use the following approximate radial function for the discrete spectrum:

$$R_n(\xi) \cong (2/n)^{n+1/2} \xi^{n-1} e^{-\varepsilon/n} / \sqrt{(2n)!}\,. \tag{2.9}$$

3) The wave function of the continuous spectrum will be replaced by its asymptotic expression, which is valid for large ξ [8]:

$$R_k(\xi) \cong \sqrt{2/L}\, \xi^{-1} \sin(k\xi + \ln(2k\xi)/k + \delta), \tag{2.10}$$

$$\delta = \arg \Gamma(1 - i/k). \tag{2.11}$$

The wave function $R_k(\xi)$ is normalized in a sphere of radius $L \rightarrow \infty$.

4) We assume $Z = 1$. For $Z \neq 1$ ϵ in the final result can be replaced by ϵ/Z.

Using the wave functions (2.9) and (2.10), we obtain after some calculation:

$$(k, n_\varkappa \mid \hat{H}' \mid n, n_\varkappa + 1) \tag{2.12}$$
$$= 7{,}06 \cdot 10^{-3} \sqrt{2\pi}\, L^{-2} \hbar\omega_\varkappa\, (\varepsilon c)^{1/2}$$
$$\times \left(\frac{A}{\hbar\omega}\right)^{1/2} \sqrt{n_\varkappa + 1}\, \frac{(1 + \varkappa^2/28\alpha^2)\, 2^n \mid \Gamma(n + i/k)\mid}{(1 + \varkappa^2/4\alpha^2)^4 n^{n+3/2} \sqrt{(2n)!}}$$
$$\times \operatorname{Re}\{f(-\varkappa) - f(\varkappa)\} e^{i(\gamma + \ln(2k)/k)},$$

where

$$\varkappa_x \geqslant 0 \text{ and } f(\varkappa) \tag{2.13}$$
$$= [1/n - i\,(k - \varkappa)]^{-(n+i/k)},\ \gamma = \sum_{t=1}^{n-1} \arg\,(t + i/k).$$

The dimensionless parameters k and n in (2.12) are related to each other under energy conservation by

$$\hbar^2 k^2 / 2M a_0^2 = -Me^4 / 2\hbar^2\varepsilon^2 n^2 + \hbar\omega_\varkappa \tag{2.14}$$

or

$$k^2 + 1/n^2 = p^2, \tag{2.14a}$$

$$p = 6.56\,(\varepsilon c)^{-2}\,(\hbar\omega/A)^{3/2} \ll 1$$

for the majority of ionic crystals.

From (2.14) and (2.14*a*) it follows that capture is possible only for small values of the dimensionless wave number k. This enables us to introduce an approximate formula for γ, with the sum in (2.13) replaced by an integral:

$$\gamma = \sum_{t=1}^{n-1} \operatorname{arc\,ctg}\, kt \tag{2.15}$$
$$\cong (n - 1)\operatorname{arc\,ctg}\, k(n - 1) + \frac{1}{2k} \ln[1 + k^2 (n - 1)^2].$$

3. THE PROBABILITY OF ELECTRON CAPTURE BY A DEFECT

The probability per unit time of a transition from a state of the continuous spectrum to a discrete level can be calculated from the familiar formula

$$w_\varkappa(k) = (2\pi/\hbar)\,\rho(E)\,|(k, n_\varkappa|H'|n, n_\varkappa+1)|^2, \quad (3.1)$$

where $\rho(E)$ is the density of states in the energy range of the continuous spectrum. For the wave functions of the continuous spectrum which we have normalized in a sphere of radius L

$$\rho(E) = (L/2\pi)(43.1/Ak)(\varepsilon c)^{-4}(\hbar\omega/A)^2. \quad (3.2)$$

The expression for the transition probability which is obtained after inserting (2.12) and (3.2) in (3.1) contains the wave number $\varkappa$ of the emitted phonon. When account is taken of the dispersion law of optical vibrations, this quantity is determined with complete accuracy from energy conservation. If, however, we neglect dispersion and replace all longitudinal optical frequencies by the frequency limit ω, the magnitude of $\varkappa$ becomes indeterminate. In order to eliminate this uncertainty, the expression obtained for the probability can be averaged over all values of $\varkappa$ by the formula

$$w(k) = \frac{1}{z}\int w_\varkappa(k)\,dz(\varkappa), \quad (3.3)$$

$$dz(\varkappa) = L^3\varkappa^2 d\varkappa/2\pi^2,$$

where $dz(\varkappa)$ is the number of normal frequencies in the interval $d\varkappa$ and $z = L^3/\Omega$, where Ω is the volume of a unit crystal cell, is the total number of normal frequencies in the fundamental region.

The probability (3.3) must furthermore be multipled by the total number NL^3 of defects in the fundamental crystal region. The probability of electron capture then becomes

$$w(k) = 1{,}07\cdot 10^{-3} N\Omega(\varepsilon c)^9\,\omega\left(\frac{A}{\hbar\omega}\right)^6 \quad (3.4)$$

$$\times\ \frac{2^{2n}|\Gamma(n+i/k)|^2}{\pi k n^{2n+1}(2n)!}$$

$$\times(\bar{n}_\varkappa+1)\int_0^\infty R_k^2(\varkappa)\,\frac{\varkappa^2(1+\varkappa^2/28\alpha^2)^2\,d\varkappa}{(1+\varkappa^2/4\alpha^2)^8}.$$

In deriving this last formula, n_k was taken outside of the summation over $\varkappa$ (integration in $\varkappa$ space) and given its average equilibrium value

$$\bar{n}_\varkappa = (e^{\hbar\omega/\Theta} - 1)^{-1}, \quad (3.5)$$

where Θ is the statistical temperature.

In accordance with (2.2)

$$R_k(\varkappa) = \mathrm{Re}\{f(-\varkappa) - f(\varkappa)\}\,e^{i(\gamma+\ln(2k)/k)}. \quad (3.6)$$

We have not been able to calculate the complicated integral in (3.4) in finite form. However, approximate values of the integral can be obtained by investigating the integrand.

It is easily seen that the function

$$f(\varkappa)^2 = (1+y^2)^{-n} n^{2n} e^{-(2/k)\,\mathrm{arc\,tg}\,y}, \quad (3.7)$$

$$y = n(k-\varkappa)$$

has the character of a δ function with its maximum at

$$y = y_m = -1/nk;\quad \varkappa_m = p^2/k. \quad (3.8)$$

The maximum of $|f(-x)|$ lies in the region of negative $\varkappa$, i.e., outside the limits of integration in (3.4), and the greatest value of this function in the integration interval (for $\varkappa = 0$) is many orders smaller than the maximum of $|f(\varkappa)|$. On this basis we set

$$R_k(\varkappa) \cong \mathrm{Re}\,e^{i(\gamma+\ln(2k)/k)} f(\varkappa) \quad (3.9)$$

$$= (1+y^2)^{-n/2} n^n e^{-(1/k)\,\mathrm{arc\,tg}\,y}\cos\vartheta_\varkappa,$$

$$\vartheta_\varkappa = \gamma + \ln(2k)/k \quad (3.10)$$

$$-\ln(1+y^2)/2k + n\,\mathrm{arc\,tg}\,y.$$

The other factor of the integrand in (3.4) is

$$f_1(\varkappa) = \varkappa^2(1+\varkappa^2/28\alpha^2)^2(1+\varkappa^2/4\alpha^2)^{-8}, \quad (3.11)$$

which is also expressed by a curve with its peak at $\varkappa = \varkappa_1 \approx 0.8\,\alpha$. However, by comparison with (3.7) this function changes very smoothly.

Let us consider the two limiting cases.

a) The case of relatively fast electrons, when

$$k \sim p;\ kn \gg 1. \tag{3.12}$$

In this case $\varkappa_m \sim p$ and since as usual in ionic crystals $p \gtrsim$ a the main part of the δ curve (3.7) corresponds to the region of smooth decrease of $f_1(\varkappa)$. Therefore $f_1(\varkappa)$ can be taken outside the integral sign in (3.4) using $\varkappa = \varkappa_m = p^2/k$. We note, furthermore, that as a result of (3.8) $|y| << 1$ in the vicinity of the maximum of (3.7), so that, in accordance with (3.10),

$$\vartheta_\varkappa \approx \vartheta_m + ny.$$

This indicates that $\cos^2 \vartheta_\varkappa$ oscillates extremely rapidly in the indicated region ($n \to \infty$!) and can be taken outside the integral sign with an average value of 1/2. Thus, in the limiting case under consideration,

$$\int_0^\infty R_k^2(\varkappa) f_1(\varkappa)\, d\varkappa \tag{3.13}$$

$$\approx (p^4/2k^2)(1 + p^4/28\alpha^2k^2)^2 (1 + p^4/4\alpha^2k^2)^{-8}$$

$$\times n^{2n} \int_{-\infty}^{nk} (1 + y^2)^{-n} \cdot e^{-(2/k)\,\mathrm{arc\,tg}\,y} dy.$$

The integral in (3.13) with the substitution $y = \tan z$ reduces to

$$I(n, k) = \int_{-\pi/2}^{z_0} e^{-2z/k} \cos^{2(n-1)} z\, dz,$$

where $z_0 = \arctan nk \sim \pi/2$ can be replaced by infinity because of the rapid decrease of the integrand. In this case $I(n,k)$ reduces to the tabulated integral [9]

$$I(n, k) \approx e^{\pi/k} \int_0^\infty e^{-2x/k} \sin^{2(n-1)} x\, dx \tag{3.14}$$

$$= ke^{\pi/k} (2n - 2)!\, |\Gamma(1 + i/k)|^2 / 2^{2n-1} |\Gamma(n + i/k)|^2.$$

By using the well-known properties of the Γ function we easily obtain

$$k\,|\Gamma(1 + i/k)|^2 = \pi/\mathrm{sh}(\pi/k) \approx (2\pi/k) e^{-\pi/k},$$

since $k << 1$. Collecting the results we arrive in this limiting case at the formula

$$w(k) = N\Omega k\omega\varepsilon c (\bar{n}_\varkappa + 1) \tag{3.15}$$

$$\times \left(\frac{p^2}{k^2} - 1\right)^2 \frac{(1 + p^4/28\alpha^2k^2)^2}{(1 + p^4/4\alpha^2k^2)^8}.$$

b) The case of slow electrons, when

$$k \ll p;\ n \sim 1/p. \tag{3.16}$$

In this case, $\varkappa_m >> \varkappa_1$ and the maximum of the δ function (3.7) is located in the region where $f_1(\varkappa)$ decreases rapidly to zero. A numerical tabulation shows that in this case the most important region of the integral in (3.4) is nevertheless the "half width" of the δ curve since in this region $f_1(\varkappa)$ is approximated very closely by

$$f_1(\varkappa) \approx (2\alpha)^{12} n^{10}/49 (1 + y^2)^5. \tag{3.17}$$

When $\cos^2 \vartheta_\varkappa$ is replaced by its average value, just as in case a), we can obtain

$$w(k) = \frac{4.45 \cdot 10^{16} N\Omega\omega}{2\pi k (\varepsilon c)^{2.7}} \left(\frac{\hbar\omega}{A}\right)^{18} (\bar{n}_\varkappa + 1) \tag{3.18}$$

$$\times \frac{2^{2n} |\Gamma(n + i/k)|^2 n^8}{(2n)!} I(n + 5, k).$$

The insertion of $I(n + 5, k)$ from (3.14) leads in the considered case of slow-electron capture to

$$w(k) = 1.97 \cdot 10^8 N\Omega\omega (\varepsilon c)^{-7} (\hbar\omega/A)^3 \tag{3.19}$$

$$\times (\bar{n}_\varkappa + 1) L(n) k^3 (p^2/k^2 - 1)^{-3},$$

$$L(n) = \prod_{i=1}^{8} (1 + i/2n) \sim 1. \tag{3.20}$$

As a numerical example we took a KCl crystal, for which [2] $\epsilon c = 1.2$; $A = 1.10$ ev; $\hbar\omega = 0.026$ ev and $p = 0.0166$. Figure 1 shows the dependence of the probability for single-phonon capture on polaron velocity (wave number). The curve was plotted for "large" and small k according to (3.15) and (3.19) and was extrapolated graphically into the region of intermediate values of $\varkappa$. We note that the peak of the curve lies in the region of "large" k to which (3.15) applies.

4. TEMPERATURE DEPENDENCE OF CAPTURE PROBABILITY

The temperature dependence of capture probability can be obtained by statistical averaging of

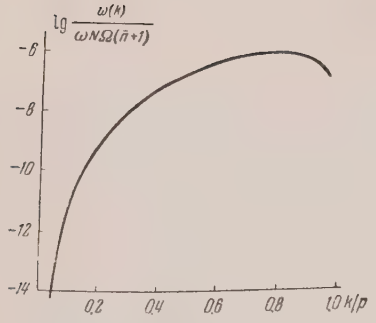

Fig. 1

the foregoing expressions. We assume that free polarons are in thermal equilibrium with the lattice. The Maxwellian distribution of the polarons is

$$F(k)\,dk = 4p^{-3}\sqrt{\beta^3/\pi}\,e^{-\beta k^2/p^2}k^2dk, \qquad (4.1)$$

where $F(k)$ is the distribution function over the wave numbers and $\omega = \hbar\omega/\Theta$. The statisitically averaged probability is

$$\bar{w} = 4\sqrt{\beta^3/\pi}\int_0^1 w(p\xi)\,e^{-\beta\xi^2\xi^2}d\xi,\quad \xi = k/p. \qquad (4.2)$$

We were not able to calculate $\bar{\omega}$ from (4.2) in general form. We therefore confined ourselves to tabulating the dependence of $\bar{\omega}$ on β for a KCl crystal by numerical integration. The results of the calculations are shown in Fig. 2. The capture probability is extremely small at low temperatures but increases rapidly with heating and reaches its peak at $T \sim 120°$ K. With further heating the

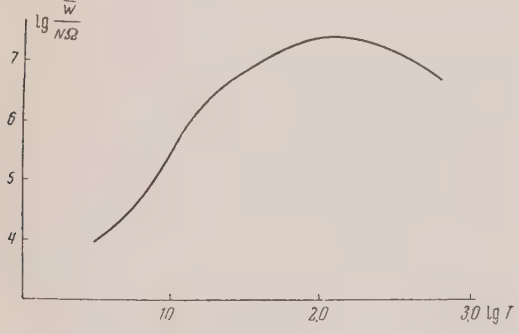

Fig. 2

probability decreases relatively slowly (by a factor of about 4 between 120° and 600°K.).

The minimum lifetime of polarons in a KCl crystal ($\Omega \approx 6.2 \cdot 10^{-23}$ cm^3) with reference to one-quantum capture is

$$\tau_{min} \sim 5\cdot 10^{14}N^{-1}\ \text{sec}. \qquad (4.3)$$

In Pekar's diffusion theory the polaron lifetime against capture by Coulomb centers is calculated from the formula[2]

$$\tau = \varepsilon/4\pi e u N, \qquad (4.4)$$

where u is the polaron mobility, which according to Ref. 2 is given by the relation $u = u_0(e^{\beta}-1)$

For KCl $u_0 = 463$ abs. units. For $T = 122°$ K ($\beta = 2.5$) formula (4.4) gives $\tau \sim 1.5 \cdot 10^5 N^{-1}$ sec. Comparison with (4.3) shows that, in the case considered polaron diffusion to lattice defects is not a "bottleneck" in the recombination process. The diffusion theory will hardly be applicable at very low temperatures also. We emphasize that our conclusion does not refer to capture by neutral centers when, as was noted above, the diffusion theory leads to satisfactory agreement with experiment.

We propose in the future to make a comparison of the theory with experimental findings, especially with reference to the kinetics of the thermal bleaching of colored crystals. At the present stage of our investigation such a comparison would be premature since, in addition to what has been presented above, we require a theoretical calculation for multi-phonon capture and thermal ionization of F-centers. Subsequent articles will be devoted to these calculations.

In conclusion the author wishes to acknowledge his indebtedness to Professor S. I. Pekar, who made a number of very valuable comments.

---

1 E. I. Adirovich, *Some Problems of the Theory of Luminescence in Crystals*, Gostekhizdat, Moscow, 1951.
2 S. I, Pekar, *Investigations in the Electron Theory of Crystals*, Gostekhizdat, Moscow. 1951.
3 S. I. Pekar and Iu. E. Perlin, J. Exptl. Theoret. Phys. (U.S.S.R.) 20, 271 (1950).
4 R. S O'Rourke, Phys. Rev. 91, 265 (1953); N. D. Vasileff, Phys. Rev. 96, 603 (1954).
5 Iu. E. Perlin, J. Exptl. Theoret. Phys. (U.S.S.R.) 20, 274 (1950).
6 Iu. E. Perlin, Uch. Zap. Kishinev, Un. 17, 91 (1955).
7 K. Huang and A. Rhys. Proc. Roy. Soc. A204, 406 (1950); A. S. Davydov, J. Exptl. Theoret. Phys. (U.S.S.R.) 24, 397 (1953); M. A. Krivoglaz, J. Exptl. Theoret. Phys. (U.S.S.R.) 25, 191 (1953).
8 L. D. Landau and E. M. Lifshitz, *Quantum Mechanics*, Gostekhizdat, Moscow, 1948.
9 I. M. Ryzhik, *Tables of Integrals, Sums, Series and Products*, Gostekhizdat, Moscow, 1948.

Translated by I. Emin
14

The Exciton State of an Imperfect Molecular Crystal

A. S. SELIVANENKO
P. N. Lebedev Physical Institute, Academy of Sciences, USSR
(Submitted to JETP editor July 12, 1955)
J. Exptl. Theoret. Phys. (U.S.S.R.) 32, 75–81 (1957)

The Schrödinger equation is solved in a semi–infinite molecular crystal. Exciton states localized at the surface are found. The energy spectrum of surface excitons is obtained.

I. INTRODUCTION

A. S. DAVYDOV[1] investigated the excited states (given the name "excitons" by Ia. I. Frenkel') of an ideal molecular crystal. If the number of elementary cells in the perfect crystal is large, it is obviously permissible to regard the crystal as infinite and to impose periodic boundary conditions.

It has been shown theoretically[2] that in a large crystal the finiteness of the volume, if taken into account accurately, does not lead to a noticeable disturbance of the normal motions. But the assumption that a crystal is infinite necessarily makes it impossible to investigate physical phenomena occurring at the surface. Very few papers[3] have been written on this subject, mainly because the disturbance produced by the free crystal surface is not small compared with the molecular interaction energy, and therefore ordinary perturbation theory is inapplicable. I. M. Lifshitz's theory of regularly degenerate perturbations[4–7] makes possible some significant progress in this direction.

Our problem is to study the behavior of an excited state (exciton) at the surface of a molecular crystal. For simplicity we consider a cubic lattice with one molecule per unit cell. We neglect the molecular motions, i.e., we study a "free" exciton. The equation for a stationary state of a molecular crystal can be written in the form

$$\Big(\sum_n \hat{H}_n + \frac{1}{2}\sum_{nm}{}' \hat{V}^0_{nm} - \mathcal{E}\Big)\Phi = 0, \qquad (1)$$

where $\hat{H}_n$ is the energy operator of the molecule in the n'th cell of the lattice, $\hat{V}^0_{nm}$ the interaction operator between the m'th and n'th molecules, $\mathcal{E}$ the eigenvalue, and Φ the wave–function of the crystal. The summation extends over all molecules in the crystal, and the prime means that the terms with $n = m$ are omitted. The molecules are bound by Van der Waals forces, and the binding energies are much smaller than the dissociation energy of a molecule. These properties are indicated by the fact that, when a molecular crystal sublimes, the molecules evaporate without dissociation. The weak binding of the molecules in the crystal preserves to some extent the individuality of each molecule and allows us to use the most powerful method of calculation, perturbation theory.

Since $\hat{V}^0_{nm}$ is small, an approximate wave-function for the crystal can be expressed in the form

$$\Phi = \varphi_{-N}\cdots\varphi_{-1}\varphi_0\varphi_1\cdots\varphi_N = \prod_m \varphi_m.$$

Here $(2N_1 + 1)(2N_2 + 1)(2N_3 + 1) = 2N + 1$ is the number of molecules in the crystal, and φ_m is the eigenfunction of a single molecule.

Suppose that the nth molecule absorbs a photon and makes a transition to an excited state. Then $\varphi_n \to \varphi_n{}^f$, where $\varphi_n{}^f$ is the molecular wave–function of the excited state. The wave–function of the crystal will be a superposition

$$\Phi^f = (2N+1)^{-1/2} \times \sum_{n=-N}^{N} a^0_n \chi^f_n, \qquad \chi^f_n = \varphi^f_n \prod_m \varphi_m. \qquad (2)$$

Here $|a^0_n|^2$ is the statistical weight of the state in which the excitation is carried by the nth molecule. From the definition of an ideal crystal it follows that this quantity should be independent of n. The antisymmetrization of the wave–functions gives rise to very complicated formulas without significantly changing the results, and will for the sake of simplicity be omitted in our analysis. We substitute Eq. (2) into Eq. (1), multiply by χ^f_m and integrate over the internal variables of the molecular wave–functions. The result is

$$\sum_n{}' M^f_{nm} a^0_n - \varepsilon^f a^0_m = 0, \qquad (3)$$

$$M^f_{nm} = \int \varphi_m \varphi^f_m \hat{V}^0_{nm} \varphi^f_n \varphi_n \, d\tau, \tag{4}$$

where ϵ_f represents all the remaining terms, including the eigenvalue $\mathcal{E}$ (see Ref. 1, in which the same notations are used).

The matrix element M^f_{nm} determines the probability for transferring the excitation from the nth molecule to the mth. The formula shows that the greater the interaction energy, the more rapidly the exciton will migrate. Hence when we go from molecular to ionic crystals the migration velocity will in general increase. Further, the exciton will migrate with highest probability and therefore with highest velocity along those crystallographic directions in which the interaction is strongest.

If the interaction is due to a dipole–dipole force, then the transfer probability is $W \sim |M^f_{nm}|^2 \sim R^{-6}$, where R is the molecular separation. Any vibration of the crystal, even if the changes in the molecular separations are small, will produce a strong effect on the interaction, on the migration velocity, and finally on the line widths in the optical spectrum.

II. THE SEMI–INFINITE CRYSTAL

In an ideal crystal $|a^\circ_n|^2$ is independent of the index n, since all molecules in the crystal are equivalent. In a finite crystal the molecules at the surface are distinguished from molecules inside the crystal, and the values of $|a^\circ_n|^2$ will be different.

Suppose that a crystal is cut by a plane and the interaction between molecules on opposite sides of the plane ceases to exist. Between the molecules in each half of the crystal we suppose the interaction to be the same as in the infinite crystal. The lattice is supposed to be undisturbed, except for molecules close to the cutting plane where the interactions are different and some disturbance of the lattice may occur.

The equation for the semi–infinite crystal is

$$\Big(\sum_n \hat{H}_n + {}^1\!/_2 \sum_{nm}{}' \hat{V}_{nm} - \mathcal{E}\Big)\Phi = 0. \tag{5}$$

The operator $\hat{V}_{nm}$ differs from $\hat{V}^\circ_{nm}$. Equation (5) may be written in the form

$$\Big(\sum_n \hat{H}_n + {}^1\!/_2 \sum_{nm}{}' \hat{V}^0_{nm} - {}^1\!/_2 \sum_{nm}{}' \hat{\Lambda}_{nm} - \mathcal{E}\Big)\Phi = 0, \tag{6}$$

$$\sum_{nm}{}' \hat{\Lambda}_{nm} = \sum_{nm}{}' \hat{V}^0_{nm} - \sum_{nm}{}' \hat{V}_{mn}, \tag{7}$$

where $\hat{\Lambda}_{nm}$ is a perturbation operator. If the nth and mth molecules are on opposite sides of the cutting plane, then by definition $\hat{V}_{nm} \equiv 0$. If the molecules are on the same side of the plane, then $\hat{V}_{nm} \equiv \hat{V}^\circ_{nm}$, and the perturbation operator is zero, except for molecules at the surface. Thus it is assumed that the perturbation does not penetrate deeply into the crystal.

We substitute Eq. (2) into Eq. (6), multiply by χ^f_m, and integrate over the internal molecular variables. The result is

$$\begin{aligned} &\sum_n{}' a_n \int \varphi_m \varphi^f_m \hat{V}^0_{nm}\, \varphi_n \varphi^f_n d\tau + \sum_n{}' a_n \Big(\int \varphi_m \varphi^f_m \hat{V}_{nm}\, \varphi_n \varphi^f_n d\tau \\ &\qquad - \int \varphi^f_m \varphi_m \hat{V}^0_{nm}\, \varphi^f_n \varphi_n d\tau\Big) - a_m \varepsilon^f_1 = 0, \\ &\sum_n{}' a_n M^f_{mn} - \sum_n{}' a_n \Lambda_{nm} - \varepsilon^f_1 a_m = 0, \end{aligned} \tag{8}$$

where ϵ^f_1 denotes all the remaining terms, as before. The index n may be represented as a vector $n = n_1 \mathbf{i} + n_2 \mathbf{j} + n_3 \mathbf{k}$, where i, j, k are generators of the cubic lattice. The cutting plane is parallel to the plane of the vectors j, k and passes through the point $n_1 = 0$.

The problem can now be reduced to one dimension. Since the crystal remains periodic in the plane of the vectors j, k, we can write

$$a_n = a_{n_1 n_2 n_3} = a_{n_1} e^{i(n_2 k_2 + n_3 k_3)} = a_{n_1} e^{i \mathbf{n}_\tau \mathbf{k}_\tau},$$

$$\mathbf{k}_\tau = \sum_{i=2}^{3} (\pi / N_i)\, \mathbf{b}_i^{-1} \nu_i, \qquad -N_i \leqslant \nu_i \leqslant N_i,$$

$$\mathbf{n}_\tau = n_2 \mathbf{b}_2 + n_3 \mathbf{b}_3,$$

Here $\mathbf{b}_i^{-1}$ is a vector of the reciprocal lattice, and $\mathbf{b}_2$, $\mathbf{b}_3$ are vectors of the physical lattice defining a plane cell.

This *ansatz* for the amplitudes means physically that we resolve the exciton wave into three directions and let these three component waves propagate independently of each other. The probability of finding the exciton at a given position (molecule) n_1, n_2, n_3, is then the product of the

probabilities for finding it in the three planes passing through that position perpendicular to the lattice axes i, j, k.

We sum separately over the variables n_2, n_3,

$$\sum_n{}' a_n M^f_{nm} = \sum_{n_1} a_{n_1} M^f_{n_1 m}(\mathbf{k}_\tau);$$

$$M_{n_1 m}(\mathbf{k}_\tau) = \sum_{n_2 n_3} e^{i\mathbf{n}_\tau \mathbf{k}_\tau} M^f_{n_1 m n_2 n_3}.$$

In the same way we write

$$\sum_n{}' a_n \Lambda_{nm} = \sum_{n_1} a_{n_1} \Lambda_{n_1 m}.$$

This summation means physically that we are considering the interaction of the mth molecule with a whole plane, say the $(m+g)$ th, of lattice–sites. The interaction of the mth molecule with the lattice plane in which it itself lies will not be disturbed by the cutting plane, and this interaction therefore does not affect the amplitude a_m or the energy level. Pictorially, we may say that the cutting of the crystal, with the assumptions which we have made, changes its properties only in the n_1 direction. Now n_1 may coincide with m.

The equation for a one–dimensional chain may be written

$$\sum_{n_1} a_{n_1} M^f_{n_1 m}(\mathbf{k}_\tau) - \sum_{n_1} a_{n_1} \Lambda_{n_1 m} - \varepsilon^f_1 a_m = 0. \quad (9)$$

Henceforth we shall write n instead of n_1. In matrix notation, the system of equations (9) becomes

$$(M - \Lambda - \varepsilon^f_1 E)\,\mathbf{a} = 0, \quad (10)$$

Here M is the matrix with elements M^f_{nm}, E is the unit matrix, Λ has elements Λ^f_{nm} and a is a column –matrix.

We consider the case in which the molecules interact not only with nearest neighbors but also weakly with next–nearest neighbors. Since we are now interested only in one half of the crystal (with $n_1 \geq 1$), the perturbation operator may be written

$$\frac{1}{2}\sum_{nm}(\Lambda_{nm}\delta_{n0}\delta_{m1} + \Lambda_{nm}\delta_{n1}\delta_{m0} + l\Lambda_{nm}\delta_{n2}\delta_{m1} + l\Lambda_{nm}\delta_{n1}\delta_{m2} + \Lambda_{nm}\delta_{n0}\delta_{m2} + \Lambda_{nm}\delta_{n2}\delta_{m0});$$

To avoid writing the factor 1/2, we suppose it henceforth included in the definition of each matrix element.

The first two terms represent the perturbation acting between the first layer of molecules of the left half of the crystal ($n \leq 0$) and the first layer of molecules of the right half. This perturbation must be assumed a little larger than $\hat{V}^{\circ}_{01}$, since in our model there is some interaction between the first layer of the right half and the second layer on the left. To avoid having additional terms in the operators, we suppose this perturbation of the first layer on the right by the second layer on the left to be already included at the beginning of the calculation. The magnitude of this perturbation will affect the numerical values but not the form of our results. The third and fourth terms represent the change in the interaction between the layers $n = 1$ and $n = 2$. The surface layers of the crystal will be compressed in the direction normal to the surface, and l is a measure of the magnitude of this effect. The fifth and sixth terms are the perturbation of the layer $n = 2$ by the layer $n = 0$. The δ_{ik} are Kronecker sybols.

III. THE PERTURBATION OPERATOR

We consider the one–dimensional perturbation operator as it was before the transition to matrix notation:

$$\hat{\Lambda} = \sum_{nm}{}' \hat{\Lambda}_{nm} = \sum_m \sum_n \hat{\Lambda}_{nm}.$$

First we transform it as follows:

$$\sum_n \hat{\Lambda}_{nm} = \sum_n (\hat{\Lambda}_{nm}\delta_{n0}\delta_{m1} + \hat{\Lambda}_{nm}\delta_{n1}\delta_{m0} + l\hat{\Lambda}_{nm}\delta_{n2}\delta_{m1} + l\hat{\Lambda}_{nm}\delta_{n1}\delta_{m2} + \hat{\Lambda}_{nm}\delta_{n0}\delta_{m2} + \hat{\Lambda}_{nm}\delta_{n2}\delta_{m0} =$$

$$= \sum_n \sum_{i=1}^{2} (\alpha_{ni}\delta_{n0} + \beta_{ni}\delta_{n1} + \varkappa_{ni}\delta_{n2}) \times (\gamma_{mi}\delta_{m0} + \mu_{mi}\delta_{m1} + \eta_{mi}\delta_{m2}). \quad (11)$$

The coefficients α, β, γ, etc. in Eq. (11) are determined by requiring that the final expression after expanding the brackets becomes identical with the preceding expression. In matrix notation the operator (11) becomes

$$\Lambda = \sum_{nm} \sum_{i=1}^{2} a_n L_n^i L_m^i; \tag{12}$$

$$L_n^i = \int \varphi_n \varphi_n^f (\alpha_{ni}\delta_{n0} + \beta_{ni}\delta_{n_1} + \varkappa_{ni}\delta_{n2})\, d\tau, \tag{13}$$

$$L_m^i = \int \varphi_m \varphi_m^f (\gamma_{mi}\delta_{m0} + \mu_{mi}\delta_{m_1} + \eta_{mi}\delta_{m2})\, d\tau.$$

Eq. (10) may be written

$$\mathbf{a} = (M - \varepsilon_1^f E)^{-1} \Lambda \mathbf{a}.$$

We express the vector Λ a as a superposition of eigenvectors of the unperturbed system, Λ a $= \Sigma \mathfrak{L}_n$ a $_n{}^\circ$, the vectors a $_n{}^\circ$ being orthogonal to each other. The orthogonality condition implies

$$\begin{aligned} \mathscr{L}_n &= \mathbf{a}_n^0 \Lambda \mathbf{a}, \\ \mathscr{L}_0 &= \sum_{i=1}^{2} a_0^0 (L_0^i L_1^i a_1 + L_0^i L_2^i a_2), \\ \mathscr{L}_1 &= \sum_{i=1}^{2} a_1^0 (L_1^i L_0^i a_0 + L_1^i L_2^i a_2), \\ \mathscr{L}_2 &= \sum_{i=1}^{2} a_2^0 (L_2^i L_0^i a_0 + L_2^i L_1^i a_1). \end{aligned} \tag{14}$$

All the remaining coefficients are zero, since in the perturbation operator only three matrix elements are different from zero. We now let the operator $(M - \epsilon_1{}^f E)^{-1}$ act upon Λ a :

$$\mathbf{a} = (M - \varepsilon_1^f E)^{-1} \Lambda \mathbf{a} = \frac{\mathscr{L}_0}{\lambda_0 - \varepsilon_1^f}\, \mathbf{a}_0^0 + \frac{\mathscr{L}_1}{\lambda_1 - \varepsilon_1^f}\, \mathbf{a}_1^0 + \frac{\mathscr{L}_2}{\lambda_2 - \varepsilon_1^f}\, \mathbf{a}_2^0 \tag{15}$$

The coefficient $\mathfrak{L}$ in the expansion of the vector Λ a in terms of the a $_n{}^\circ$ are c—numbers, and therefore commute with the operator $(M - \epsilon_1{}^f E)^{-1}$. The vector a $_n{}^\circ$ is an eigenvector of the unperturbed problem, i.e., it is an eigenvector of the operator M and λ_n is the corresponding eigenvalue.

The absolute square $|a_i|^2$, $-N \leq i \leq N$, of the ith component of the (in general infinite—dimensional) vector a in Eq. (10) is the probability of finding the exciton at the ith molecule. The vectors of the unperturbed and perturbed system are constructed in our model from the same basic states (the unit matrix is the same). From Eq. (15) it appears that the perturbed vector a has only 3 components different from zero, indicating that the exciton is localized close to the surface. In the expansion coefficients of the vector a [Eq. (15)] there appear the coefficients $\mathfrak{L}_0$, $\mathfrak{L}_1$, $\mathfrak{L}_2$ defined by the expansion (14). To complete the solution of the problem we must calculate $\mathfrak{L}_0$, $\mathfrak{L}_1$, $\mathfrak{L}_2$.

By operating with $L_n{}^1$ on Eq. (15), we obtain

$$L_0^1 a_0 + L_1^1 a_1 + L_2^1 a_2 = \frac{\mathscr{L}_0}{\lambda_0 - \varepsilon_1^f}\, L_0^1 a_0^0 + \frac{\mathscr{L}_1}{\lambda_1 - \varepsilon_1^f}\, L_1^1 a_1^0 + \frac{\mathscr{L}_2}{\lambda_2 - \varepsilon_1^f}\, L_2^1 a_2^0.$$

The operation of $L_n{}^2$ gives the analogous result

$$L_0^2 a_0 + L_1^2 a_1 + L_2^2 a_2 = \frac{\mathscr{L}_0}{\lambda_0 - \varepsilon_1^f}\, L_0^2 a_0^0 + \frac{\mathscr{L}_1}{\lambda_1 - \varepsilon_1^f}\, L_1^2 a_1^0 + \frac{\mathscr{L}_2}{\lambda_2 - \varepsilon_1^f}\, L_2^2 a_2^0.$$

These equations reduce to the form

$$\begin{aligned} a_1 (L_0^1 + L_1^1 - T_1 - T_2 - T_3 - T_3') \\ + a_2 (L_2^1 - T_1' - T_2') = 0, \\ a_1 (L_0^2 + L_1^2 - T_1 - T_2 - T_3 - T_3') \\ + a_2 (L_2^2 - T_1' - T_2') = 0; \end{aligned} \tag{16}$$

$$T_1 = \frac{L_0^1 |a_0^0|^2}{\lambda_0 - \varepsilon_1^f} \sum_{i=1}^{2} L_0^i L_1^i, \qquad T_1' = \frac{L_0^1 |a_0^0|^2}{\lambda_0 - \varepsilon_1^f} \sum_{i=1}^{2} L_0^i L_2^i,$$

$$T_2 = \frac{L_1^1 |a_1^0|^2}{\lambda_1 - \varepsilon_1^f} \sum_{i=1}^{2} L_1^i L_0^i, \qquad T_2' = \frac{L_1^1 |a_1^0|^2}{\lambda_1 - \varepsilon_1^f} \sum_{i=1}^{2} L_1^i L_2^i,$$

$$T_3 = \frac{L_2^1 |a_2^0|^2}{\lambda_2 - \varepsilon_1^f} \sum_{i=1}^{2} L_2^i L_0^i, \qquad T_3' = \frac{L_2^1 |a_2^0|^2}{\lambda_2 - \varepsilon_1^f} \sum_{i=1}^{2} L_2^i L_1^i,$$

Using the condition that the two halves of the crystal are identical, we have put $|a_0| \equiv |a_1|$.

In order that Eq.(16) should have a non—zero solution, the determinant must vanish, and this gives a quadratic equation for $\epsilon_1{}^f$ .. When $\epsilon_1{}^f$ is

known, the coefficients can be calculated from Eq. (15), and hence $\mathfrak{L}_0$, $\mathfrak{L}_1$, $\mathfrak{L}_2$, and finally the eigenvalue $\mathfrak{E}$, can be determined.

IV. CONCLUSIONS

The solution which we have found [Eq. (15) et seq.] extends only over the region of the crystal which is disturbed by the surface. We saw that $a_{n_1} = a_{n_1}\delta_{n_1 2} + a_{n_1 2}$, i.e., the amplitude is non–zero only at the surface. Such a solution, obtained by writing Eq. (10) in the form

$$\mathbf{a} = (M - \varepsilon_1^f E)\,\Lambda \mathbf{a}$$

exists only where the operator Λ is different from zero. Inside the crystal, where the surface has no effect on the molecular interactions, Davydov [1] has shown that solutions have the form of a plane exciton wave $e^{i(\mathbf{kn}-\omega t)}$. Using Davydov's terminology, we may call the solution (15) a surface exciton wave, as opposed to a volume wave.

The surface exciton wave, which we call for brevity a surface exciton, occupies levels distinct from the levels of volume excitons. The number of lattice planes, into which the surface exciton penetrates, is fixed by the depth of penetration of the surface perturbation. The number of levels of a surface exciton in turn cannot exceed the number of lattice planes into which the exciton penetrates. Or if there are not one but α molecules in each plane cell (b_2 b_3), then each level splits into α bands. Each band finally has a continuous structure connected with the variation of the surface wave–vector k_τ of the exciton.

To observe a surface exciton spectroscopically, one must use a crystal with a large inter–molecular interaction. The heat of sublimation should be of the order of 10 kilo–calories per mole. The experiment must be done at the lowest possible temperature, and the specimen must have a large surface–to–volume ratio, (for example, a powder). Mosaic structure and microscopic cracks in a crystal should also cause surface excitons to appear at internal surfaces.

The method of calculation which we have used can also be successfully applied to problems connected with any kind of lattice irregularity in molecular crystals.

In conclusion, the author expresses his thanks to V. L. Levshin for his interest in the work, and to A. S. Davydov and I. V. Obreimov for valuable advice and criticism.

---

1 A. S. Davydov, *Theory of Light Absorption in Molecular Crystals*, Ukrainian Academy of Sciences Press, Kiev, 1951).

2 W. Ledermann, Proc. Roy. Soc. (London) A182, 362 (1944).

3 I. M. Lifshitz and S. I. Pekar, Usp. Fiz. Nauk 6, 531 (1955).

4 I. M. Lifshitz and L. N. Rosentsveig, J. Exptl. Theoret. Phys. (U.S.S.R.) 18, 1013 (1948).

5 I. M. Lifshitz, Dokl Akad. Nauk SSSR 58, 83 (1945).

6 I. M. Lifshitz, J. Exptl. Theoret. Phys. (U.S.S.R.) 17, 1016 (1947).

7 I. M. Lifshitz, J. Exptl. Theoret. Phys. (U.S.S.R.) 17, 1077 (1947).

Translated by F. J. Dyson
10

Multiple Interaction Hamiltonians in Quantum Electrodynamics

G. F. FILIMONOV AND IU. M. SHIROKOV
Moscow State University

(Submitted to JETP editor November 13, 1955)
J. Exptl. Theoret. Phys. USSR 32, 99-104 (January, 1957)

A method is described for constructing electromagnetic interaction Hamiltonians of a many-particle system, based on the usual Hamiltonian formalism. For illustration the Hamiltonian for the pair interaction of spinor particles is derived.

INTRODUCTION

THE exact solution of problems connected with the many body problem in quantum electrodynamics is confronted by considerable difficulties both of principle and of technique. An approximate treatment of this problem is possible by means of representing complicated motions of a system of N charged particles as a superposition of simpler processes, in each of which $N'(N' = 2, 3. . ., N)$ real and a certain number of virtual particles take part, and by separately investigating each of these processes. Due to the work of Schwinger it is now known how to obtain the Green's function, and also how to obtain and to solve (approximately) the corresponding equation for each of these simpler systems.

In this article we propose a different method of describing the elementary interactions of which the complex motion of the system of N particles is composed. In place of a set of Green's functions we shall make the system of N particles, corresponding to a set of interaction Hamiltonians of different orders. Each of these corresponds to a process with a strictly defined number of real and virtual particles. As will be seen below, it will be possible, by using this method, to calculate in a simpler way the relativistic and field corrections to the optical spectra of atoms which have their origin in the multiple interactions of the particles.

An explicit expression for the Hamiltonian of the N-th order which also contains the term representing N-fold interactions (N real particles participate simultaneously) can be obtained from the usual equation of quantum electrodynamics

$$(\hat{E} - \hat{\mathcal{H}})\,\psi(x) = 0;$$
$$\hat{\mathcal{H}} = \sum_{j=0}^{\infty} \hat{H}_j, \qquad (1)$$

written, for example, in the Schrödinger or the Tomonaga-Schwinger representation. In order to do this, it is necessary to assume all the processes of lower multiplicity (1, 2, . . ., $N-1$th orders), to be virtual, and to exclude the terms corresponding to them from the equations of motion (1) by means of unitary transformations. A summation over the intermediate states of the 1, 2, . . ., $(N-1)$-th orders is carried out in Eq. (1). The result then describes correctly electromagnetic processes in systems with $N'(N' \geq N)$ real and virtual particles, and its Hamiltonian will contain explicit expressions of $N' = N, N+1, \ldots, 2N-1$ orders which can be directly used to describe processes in which N' real and virtual particles participate.

The representation of the Hamiltonian of the N-th order by summing the processes with all possible intermediate states possesses a number of advantages which make this method convenient for the solution of specific problems.

First of all, in each approximation (in each H_N) the relativistic invariance of the method is guaranteed, since the terms are classified only according to the number of particles which they describe. This allows one to obtain correct nonrelativistic approximations for the interaction Hamiltonians of all orders, even in the Schrödinger representation, which is quite useful in view of the fact that until now a number of authors[1,2] have attempted unsuccessfully to obtain them from Breit's equation.

In the second place, a "preliminary" summation over the intermediate states of the interaction Hamiltonian makes it unnecessary to calculate higher approximations of the interaction energy by means of perturbation theory, and consequently a knowledge of the complete sets of eigenfunctions of the system under consideration in the zeroth approximation is not required. The energy corrections of the required order to the energy terms of the atom will be simply determined by the matrix elements of the corresponding Hamiltonians.

In the third place, in this case, just as in the case of the expansion of the S-matrix in a power series, a "term by term" regularization is possible

since the removal of the field divergences from each Hamiltonian of the N-th order means their removal from the corresponding approximations of the theory.

1. SETTING UP THE N-TH ORDER HAMILTONIANS

The basic equation of electrodynamics (1) has the following form in the Schrödinger representation:

$$[(i\partial/\partial t) - \mathcal{H}]\psi(\mathbf{r}, t) = 0; \qquad \mathcal{H} = H_0 + H_1^{tr} + H_2^l. \tag{1.1}$$

Here $\psi(\mathbf{r}, t)$ is the wave function of a certain system of particles in configuration space, H_0, H_1^{tr}, H_2^l — are respectively the Hamiltonians of the free fields, of the interaction of transverse photons with particles, and of the Coulomb interaction between particles. We assume all fields to be quantized and we do not introduce a potential of an external field*.

Let us carry out the unitary transformation

$$\psi(\mathbf{r}, t) = e^{iS_1}\psi'(\mathbf{r}, t), \tag{1.2}$$

by means of which (1.1) is brought into the form

$$[(i\partial/\partial t) - \mathcal{H}_1]\psi(\mathbf{r}, t) = 0; \tag{1.2a}$$

$$\mathcal{H}_1 = e^{-iS_1}\mathcal{H}e^{iS_1} = \sum_{m=0}^{\infty}\frac{(-i)^m}{m!} \times [S_1, [S_1, \ldots [S_1, H_0 + H_1^{tr} + H_2^l]\ldots]]. \tag{1.3}$$

If one demands that

$$H_1^{tr} - i[S_1, H_0] = 0, \tag{1.4}$$

then the Hamiltonian of Eq. (1.3) will be free of the interaction term of the first order (see also Ref. 3). But, as has been noted already above, it will contain explicit expressions for the Hamiltonians of the 2-nd and the 3-rd orders

$$H_2 = H_2^l - {}^1/_2 i[S_1, H_1^{tr}]; \tag{1.5}$$

$$H_3 = -i[S_1, H_2^l - {}^1/_3 i[S_1, H_1^{tr}]]. \tag{1.6}$$

Carrying out in turn the 2, 3, . . ., k, . . ., $(N-1)$th unitary transformations of the type (1.2) and imposing on the operators S_k the conditions

$$H_k - i[S_k, H_0] = 0, \tag{1.7}$$

analogous to (1.4) we shall obtain as a result the equation

$$[(i\partial/\partial t) - \mathcal{H}_{N-1}]\psi(\mathbf{r}, t) = 0; \qquad \mathcal{H}_{N-1} = \exp\{-iS_{N-1}\}\mathcal{H}_{N-2}\exp\{iS_{N-1}\}, \tag{1.8}$$

which correctly describes processes in which N' ($N' \geq N$) real and virtual particles take part. In its Hamiltonian explicit expressions occur for the interaction Hamiltonians of the N, $N+1$, . . ., $(2N-1)$-th orders.

The Hermitian nature of the operators $\mathcal{H}_N$ occurring in (1.8) and of the individual terms H_k which they contain is a direct consequence of the Hermitian nature of the original Hamiltonian $\mathcal{H}$ and of its terms (1.3), and may be easily proved by the method of induction with the aid of relations (1.2) - (1.8). We shall not go into this, but shall directly state a rule according to which the operators S_k should be constructed to satisfy condition (1.7). In order to do this we shall represent the operator H_k in the form

$$H_k = \int d\mathbf{p}\{h_k(\mathbf{p}) + h_k^*(\mathbf{p})\}. \tag{1.9}$$

Then S_k turns out to be equal to

$$S_k = -i\int d\mathbf{p} \times \left(h_k(\mathbf{p}) - h_k^*(\mathbf{p})\right)\Big/\left(\sum_n E_i(\mathbf{p}_j) - \sum_p E_i(\mathbf{p}_j)\right), \tag{1.10}$$

where $\sum_n E_i\left(\sum_p E_i\right)$ is the sum of the free energies of particles of the i-th kind with momenta $\mathbf{p}_j$, absorbed (created) by the absorption (creation) operators occurring in $h_k(\mathbf{p})$; p is the set of all the three dimensional momenta occurring in the integrand of (1.9). $E_i(\mathbf{p}_j)$ stands for the diagonalized operator for the free energy which in the case of Bose-particles is defined by equation

$$E_i^B(\mathbf{p}_j) = e_{ij} = +\sqrt{\mathbf{p}_j^2 + m_i^2} \tag{1.11a}$$

and in the case of Fermi-particles is defined by equation

$$E_i^F(\mathbf{p}_j) = \varepsilon_{ij} = \pm\sqrt{\mathbf{p}_j^2 + m_i^2}. \tag{1.11b}$$

It follows from (1.10) that S_k is a self-conjugate quantity. The verification of this formula presents no difficulties and may be carried out by substituting into (1.7) formula (1.10) and the expressions H_0 and $h_k(\mathbf{p})$ which have the form of a product of certain cœfficient functions by the product of field operators.

* The introduction into (1.1) of the interaction of the particles with an external field does not change the following calculations.

In the Tomonaga-Schwinger representation the Hamiltonians H_N are obtained in the same way as in the Schrödinger representation and have the same appearance. For example, the terms H_2, H_3 in the Tomonaga-Schwinger representation are identical with (1.5) and (1.6). The difference arises only in the explicit expression for the operators H_k and S_k, which in the Tomonaga-Schwinger representation are defined on an arbitrary space-like hypersurface $\sigma = \sigma(x_\mu)$, which passes through a fixed point in four-dimensional space (x_μ)

$$H_k = H_k(x_\mu), \qquad S_k = S_k[\sigma(x_\mu)], \qquad \text{(B)}$$

where S_k is a functional. At the same time the expressions which define $S_k[\sigma]$ also take on a different form. Thus, to Eq. (1.7) in the Tomonaga-Schwinger representation there corresponds (in complete agreement with Ref. 4, where the expression $S_1[\sigma(x_\mu)]$ is investigated) the equation

$$-\frac{\delta}{\delta\sigma(x)} S_k[\sigma(x)] = H_k(x), \qquad (1.7a)$$

by integrating which we shall obtain an explicit expression for S_k

$$S_k[\sigma(x)] = -\frac{1}{2}\int_{-\infty}^{\infty} H_k(x')\,\varepsilon[\sigma(x),\ \sigma(x')]\,d^4x', \qquad (1.10a)$$

where

$$\varepsilon[\sigma(x),\ \sigma(x')] = \pm 1 \quad \text{for} \quad x_0 - x_0' \gtrless 0. \qquad \text{(C)}$$

It may easily be seen that with the aid of the transformations (1.10) one may eliminate all the effects from the equation of motion with the exception of the self-energy parts. The reason for this is that S_k commutes here with H_0 and does not lead to the appearance in the equation of a corresponding counter term with a negative sign. Therefore, the self-energy effects should be eliminated from the equations of motion (1.8) with the aid of subtraction devices used in the regularization procedure.

2. EXAMPLE. PAIR INTERACTION OF SPINOR PARTICLES

The term corresponding to pair interaction of particles (for example, of electrons) in the first order in $e^2(H_{2ee})$ is contained in the Hamiltonian H_2 [see Eq. (1.5)]. The expressions for this term, and also for S_1 were first obtained by Snyder[3] who investigated in detail the general covariance properties of H_{2ee}, and who also attempted to obtain an expression for the electromagnetic mass of the electron in this approximation. The formula (1.5) was also utilized in the investigation of the problem of positronium[5] and the results obtained in that case agreed with those of other authors[6,7]. Therefore, we shall not investigate expression (1.5) in detail, but shall show how it can be written, and shall compare it with certain well-known formulas.

In the simplest case of electromagnetic interaction of spinor particles of the same mass, the Hamiltonian of Eq. (1.1) consists of the following terms:

$$\mathcal{H} = H_{0e} + H_{0\gamma} + H_{1e}^{tr} + H_{2ee}^{l}, \qquad (2.1)$$

where

$$H_{0e} = \int d\mathbf{p}\,\psi^*(\mathbf{p})(\alpha\mathbf{p} + \beta m)\,\psi(\mathbf{p}), \qquad (2.2)$$

$$H_{0\gamma} = \int d\mathbf{k}\,k\,a_j^*(\mathbf{k})\,a_j(\mathbf{k}), \qquad (2.3)$$

$$H_{1e}^{tr} = \frac{-q}{4\pi^{3/2}}\int d\mathbf{p}_1\,d\mathbf{p}_2\,d\mathbf{k}\,k^{-1/2}\delta(\mathbf{k} - \mathbf{p}_{12})\,[a_j(\mathbf{k}) + a_j^*(-\mathbf{k})]\,\psi_1^*\alpha_j\psi_2, \qquad (2.4)$$

$$H_{2ee}^{l} = \frac{q^2}{2(2\pi)^3} \times \int d\mathbf{p}_1\,d\mathbf{p}_2\,d\mathbf{p}_3\,d\mathbf{p}_4 p_{12}^{-2}\cdot\delta(\mathbf{p}_{\cdot 2} + \mathbf{p}_{34})\,\psi_1^*\psi_2\psi_3^*\psi_4 \qquad (2.5)$$

are, respectively, the Hamiltonians for the free electrons, for the free protons, for the interaction between electrons and free protons, and for the Coulomb interaction; α_j, are the Dirac matrices; $\psi_\alpha(\mathbf{p}_k) = \psi_{k\alpha}$ is the absorption operator for an electron with momentum $\mathbf{p}_k$; $a_j(\mathbf{k})$ is the absorption operator for a transverse photon with momentum $\mathbf{k}$;

$$\mathbf{p}_{ab} = \mathbf{p}_a - \mathbf{p}_b; \qquad p_\alpha = |\mathbf{p}_\alpha|; \qquad \mathbf{p}_\alpha^0 = \mathbf{p}_\alpha / p_\alpha; \qquad \text{(D)}$$

p, k are three-dimensional momenta, and the system of units is used in which $\hbar = c = 1$, $q = \sqrt{4\pi/137}$

In accordance with expression (1.10)

$$S_1 = \frac{-q}{4i\pi^{3/2}} \times \int \frac{d\mathbf{p}_1\,d\mathbf{p}_2\,d\mathbf{k}}{\sqrt{k}}\,\delta(\mathbf{k} - \mathbf{p}_{12})\,\frac{a_i(\mathbf{k})\,\psi_1^*\alpha_i\psi_2 - a_i^*(\mathbf{k})\,\psi_2^*\alpha_i\psi_1}{k - \varepsilon_1 + \varepsilon_2}. \qquad (2.6)$$

Now substituting (2.5), (2.6) into (1.5) and retaining there only terms not containing photon operators, we obtain for H_{2ee}

$$H_{2ee} = \frac{q^2}{2(2\pi)^3}$$

$$\times \int dp_1\, dp_2\, dp_3\, dp_4 \hat{\delta}(p_{12} + p_{34}) \cdot \psi^*_{1\alpha}\psi_{2\beta}\psi^*_{3\mu}\psi_{4\nu}$$

$$\times \left\{ \frac{\delta_{\alpha\beta}\delta_{\mu\nu}}{p_{12}^2} - \frac{\delta_{ij} - p^0_{12i}p^0_{12j}}{2p_{12}} \right.$$

$$\left. \times \left(\frac{\alpha_{i\alpha\beta}\alpha_{j\mu\nu}}{p_{12} - \varepsilon_1 + \varepsilon_2} + \frac{\alpha_{i\alpha\beta}\alpha_{j\mu\nu}}{p_{12} - \varepsilon_4 + \varepsilon_3} \right) \right\} \quad (2.7)$$

– an expression which describes pair forces between two electrons. Its covariant nature finds its expression in particular in the fact that in the case of scattering it reduces to the well-known formula due to Möller**

$$H^{\text{рас.}}_{2ee} = \frac{q^2}{2(2\pi)^3} \quad (2.8)$$

$$\times \int dp_1\, dp_2\, dp_3\, dp_4 \hat{\delta}(p_{12} + p_{34}) : \frac{\psi^*_1\alpha_i\psi_2\psi^*_3\alpha_i\psi_4 - \psi_1\psi_2\psi^*_3\psi_4}{p_{12}^2 - (\varepsilon_1 - \varepsilon_2)^2} :$$

In the case of bound states the first non-relativistic approximation (2.7) corresponds to the non-exchange part of pair interactions and agrees with Breit's formula

$$H_{2ee} = \frac{q^2}{2(2\pi)^3} \quad (2.9)$$

$$\times \int dx_1\, dx_2 \frac{2\delta_{\alpha\beta}\delta_{\mu\nu} + \alpha_{\alpha\beta}\alpha_{\mu\nu} + (\alpha_{\sigma\beta}x^0_{12})(\alpha_{\mu\nu}x^0_{12})}{2x_{12}}$$

$$\times : \psi^*_\alpha(x_1)\,\psi_\beta(x_1)\,\psi^*_\mu(x_2)\,\psi_\nu(x_2) :.$$

It follows from (2.9) [or from (2.7)] that Breit's formula for the interaction energy is equally applicable to the description of non-exchange interaction between electrons, between positrons and between electrons and positrons:

$$:H^{\text{non-exch}}_{2ee}: \varphi_{ab}(p_1, p_2) = (L^+_{1a}L^+_{2b} + L^-_{1a}L^-_{2b} + 2L^+_{1a}L^-_{2b})$$

$$\times \int dp'_1\, dp'_2\, G^{\text{sym}}_{ab}(p_1, p_2; p'_1, p'_2)\, \varphi_{ab}(p'_1, p'_2). \quad (2.10)$$

Here $\varphi_{ab}(p_1p_2)$ is the wave function in configuration space for a system of two particles; G^{sym}_{ab} is the expression for the interaction energy which occurs inside { } in (2.9) or in (2.7);

$$L^{\pm}_k = \frac{e_k \pm (\alpha p_k + \beta m)}{2e_k}$$

are projection operators. This result does not agree with the "exact three-dimensional equation" (13) of Ref. 8.

$$:H_{2ee}:\varphi_{ab}(p_1, p_2) = (L^+_{1a}L^+_{2b} - L^-_{1a}L^-_{2b}) \quad (2.11)$$

$$\times \int dp'_1\, dp'_2\, G^{\text{сим}}_{ab}(p_1, p_2; p'_1; p'_2)\, \varphi_{ab}(p'_1, p'_2),$$

obtained in the Bethe-Salpeter theory. As may be seen from (2.11) the "exact three-dimensional equation" of Salpeter excludes first of all any possibility of interaction between electrons and positrons, and secondly leads to different signs for the interaction between pairs of electrons and between pairs of positrons. Both these facts contradict reality, and therefore the "exact three-dimensional equation" (13) of reference 8 can be used only to describe processes occurring between electrons.

The covariant nature of (2.7) also manifests itself in the fact that it contains a covariant expression for the electromagnetic mass of the electron. In order to obtain it we must calculate the matrix element $\langle a| : \hat{H}_{2ee} : |a\rangle$, which turns out to be equal to

$$\delta m = \frac{q^2}{4m(2\pi)^4} \quad (2.12)$$

$$\times \int dp_2 \left\{ \frac{1}{p_{12}} - \frac{1}{e_2} + \frac{1}{e_2} \frac{m^4}{(p_1p_2 - e_1e_2)^2 - m^4} \right\}$$

and contains only a logarithmic divergence as $p_2 \to \infty$.*

The calculation of δm represents a very laborious and painstaking effort, and therefore the explicit formulation of the Hamiltonians of the N-th orders

** According to Wick's theorem

$$H_{2ee} = :H_{2ee}: + :\hat{H}_{2ee}:$$

is equal to the sum of its normal product which describes pair interactions and the normal product with one pairing which describes the effect of the electron self-energy.

* In (2.12) the matrix element was calculated for only the diagonal part of the operator: $\widehat{H}_{2ee}$:, since the matrix element of its non-diagonal part is identically equal to zero due to the violation of the law of conservation of parity.

in the Schrödinger representation may be considered to be worth while only in those cases when the process under investigation is not connected with field divergences and does not require the regularization of the equations. In such cases if we write the equations of motion in the Schrödinger representation we shall obtain expressions of simpler structure which do not require integration over the fourth coordinates. However, in order to investigate field processes in quantum electrodynamics it is more convenient to write the equation of motion in the Tomonaga-Schwinger form. This guarantees a manifestly covariant form for the Hamiltonian of each order, and allows the equations of motion to be regularized directly.

1 G. Breit, Phys. Rev. **74**, 1278 (1948); **76**, 1299 (1949).
2 W. Perl and V. Hughes, Phys. Rev. **91**, 842 (1953).
3 H. S. Snyder, Phys. Rev. **78**, 98 (1950).
4 J. Schwinger, Phys. Rev. **75**, 651 (1949).
5 K. A. Tumanov and Iu. M. Shirokov, J. Exptl. Theoret. Phys. (U.S.S.R.) **24**, 369 (1953).
6 A. A. Sokolov and V. N. Tsytovich, J. Exptl. Theoret. Phys. (U.S.S.R.) **24**, 253 (1953).
7 V. B. Berestetskii and L. D. Landau, J. Exptl. Theoret. Phys. (U.S.S.R.) **19**, 673 (1949).
8 E. E. Salpeter, Phys. Rev. **87**, 328 (1952).

Translated by G. M. Volkoff
13

SOVIET PHYSICS JETP VOLUME 5, NUMBER 1 AUGUST, 1957

Some Sum Rules for the Cross Sections of Electric Quadrupole Transitions in the Nuclear Photoeffect

IU. K. KHOKHLOV
The P. N. Lebedev Physical Institute, Academy of Sciences, USSR

(Submitted to JETP editor February 6, 1956)
J. Exptl. Theoret. Phys. (U.S.S.R.) **32**, 124-129 (January, 1957)

Two parameters which characterize the cross sections for quadropole transitions in the nuclear photoeffect are estimated [formulas (22), (25)]. Other (known) parameters which characterize the dipole transition cross section are used for this purpose. The estimates indicate that, in intermediate and heavy nuclei, the "center of gravity" of the quadropole transition cross section is situated at energies exceeding 10-20 mev.

THE previous theoretical estimates[1-3] of the parameters which characterize the total cross sections for electric quadropole transitions in the nuclear photoeffect are based on the liquid drop model of the nucleus (let us denote this total cross section by $\sigma_{E2}(\nu)$, where ν is the photon energy).

These estimations allow us to assume that the cross section σ_{E2} has at least two maxima. The first maximum is in the range of energies of the order of 1 mev, which correspond to the eigenfrequency of nuclear surface vibration. The second maximum takes place on the right of the dipole resonance energy, at energies of the order of 20-40 mev – which correspond to the lowest eigenfrequency of the nuclear matter polarization quadropole vibrations. The cross section area under the second maximum is appreciably larger than the cross section area under the first one.

In order to obtain a model-independent confirmation of the conclusion of Danos and Steinwedel[2-3] on the existence and on the role of the second maximum, we will consider two sum rules which characterize the cross section for quadropole transitions. These sum rules [see formulas (19), (20) and also (22), (25)] relate the cross sections $\sigma_{E2}(\nu)$ with some constants (with respect to ν) which depend on the nuclear structure. For the calculation of one of these constants (the calculation of the other one is trivial), we make use of that phenomenological expression for the coordinate distribution of two protons in a nucleus which is experimentally confirmed in the case of dipole transitions. For this purpose, the first step of this work consists in reconsidering two known sum rules which correspond to the cross section for dipole transitions.

1. DIPOLE TRANSITIONS

In the present section, we are interested in the

two following sum rules which have been considered previously[4-8]

$$\int_0^\infty \sigma_{E1}(\nu)\, d\nu = 2\pi^2 \frac{\hbar}{c} \frac{1}{i\hbar} \langle D\dot{D} - \dot{D}D \rangle, \tag{1}$$

$$\int_0^\infty \sigma_{E1}(\nu) \frac{d\nu}{\nu} = \frac{4\pi^2}{\hbar c} \langle D^2 \rangle. \tag{2}$$

$\sigma_{E1}(\nu)$ is the total cross section for dipole transitions and the symbol $< >$ means averaging over the ground state of the nucleus; D is any of the components of the dipole moment operator in the long wave length approximation. To be specific, let $D \equiv D_z = \sum_\alpha e_\alpha z_\alpha$, where e_α and z_α are the charge and the z-component of the coordinate $\mathbf{q}_\alpha$ of the α-th nucleon. The dot above the operator stands for $i/\hbar$ times the commutator with the Hamiltonian of the nucleus.

The coordinates $\mathbf{q}_\alpha$ are related by the condition

$$\sum_\alpha \mathbf{q}_\alpha = 0, \tag{3}$$

which expresses the fact that we are dealing with the relative coordinates subspace.

Using Eq. (3) and after some transformations, we get

$$\int_0^\infty \sigma_{E1}(\nu)\, d\nu = 2\pi^2 \frac{\hbar e^2}{mc} \frac{NZ}{A} (1 + \Delta). \tag{4}$$

where N and Z are the neutron and proton numbers; m is the nucleonic mass; Δ is a positive quantity for the calculation of which it is necessary to know 1) the ground state wave function of the nucleus, and 2) the exchange part of the nuclear potential; in the absence of exchange, $\Delta = 0$.

The theory[4,5] gives the following estimate for Δ:

$$\Delta \approx 0.1 A^2/NZ \approx 0{,}4. \tag{5}$$

This estimate is in excellent agreement with a more exact investigation which can be carried out in the case of photofission of the deuteron.

The right hand side of the sum rule (2) is computed in Ref. 7. (See also Refs.6 and 8). In the present Section, we are going to consider the sum rule (2) from a somewhat different, phenomenological point of view.

Let us introduce the functions $n_p(\mathbf{r})$ and $n_{2p}(\mathbf{r}, \mathbf{r}')$ describing the coordinate distribution of two protons in a nucleus

$$n_{2p}(\mathbf{r}, \mathbf{r}') = [Z(Z-1)]^{-1} \times \sum_{p_1 \neq p_2} \sum \langle \delta(\mathbf{r} - \mathbf{q}_{p_1})\, \delta(\mathbf{r}' - \mathbf{q}_{p_2}) \rangle, \tag{6}$$

$$n_p(\mathbf{r}) = \int n_{2p}(\mathbf{r}, \mathbf{r}')\, d\mathbf{r}'. \tag{7}$$

Using the distributions n_p and n_{2p} the expression $< D^2 >$ can be rewritten in the form

$$\langle D^2 \rangle = \frac{e^2}{3} [Z \langle r^2 \rangle_p + Z(Z-1) \langle \mathbf{r}\mathbf{r}' \rangle_{2p}], \tag{8}$$

$$\langle r^2 \rangle_p = \int r^2 n_p(\mathbf{r})\, d\mathbf{r}; \tag{9}$$

$$\langle \mathbf{r}\mathbf{r}' \rangle_{2p} = \int \mathbf{r}\mathbf{r}' n_{2p}(\mathbf{r}, \mathbf{r}')\, d\mathbf{r}\, d\mathbf{r}'.$$

Let us call "zeroth" the nucleon coordinate distribution for which all the distributions

$$n_{\alpha\beta}(\mathbf{r}, \mathbf{r}') = \langle \delta(\mathbf{r} - \mathbf{q}_\alpha)\, \delta(\mathbf{r}' - \mathbf{q}_\beta) \rangle$$

do not depend on α and β; in particular, they do not depend on whether the α-th and β-th nucleons are both protons, both neutrons, or are different.

The functions n_{2n} and n_{pn} which describe the coordinate distribution of two neutrons and of two different nucleons are, in the case of a zeroth distribution, equal among themselves and equal to n_{2p}. Taking this into account, and averaging the square of the Eq. (3) over the nuclear ground state, we find that the following equality is true in the case of a zeroth distribution:

$$\langle r^2 \rangle_p^{(0)} + (A-1) \langle \mathbf{r}\mathbf{r}' \rangle_{2p}^{(0)} = 0. \tag{10}$$

Substituting (10) into (8), we get

$$\langle D^2 \rangle^{(0)} = \frac{e^2}{3} \frac{NZ}{A-1} \langle r^2 \rangle_p^{(0)} \approx \frac{e^2}{5} \frac{NZ}{A-1} R^2. \tag{11}$$

where R is the nuclear radius.

It follows that in the general case the sum rule (2) can be transformed into the form:

$$\int_0^\infty \sigma_{E1}(\nu) \frac{d\nu}{\nu} = \frac{4\pi^2}{5} e^2 \frac{NZ}{A-1} R^2 (1 - \Lambda), \tag{12}$$

$$\Lambda = -[(Z-1)(A-1)/NZ\langle r^2\rangle_p] \times \int \mathbf{r}\mathbf{r}' n_{2p}^{(1)}(\mathbf{r},\mathbf{r}')\,d\mathbf{r}\,d\mathbf{r}', \tag{13}$$

$$n_{2p}^{(1)}(\mathbf{r},\mathbf{r}') = n_{2p}(\mathbf{r},\mathbf{r}') - n_{2p}^{(0)}(\mathbf{r},\mathbf{r}'). \tag{14}$$

In what follows, we are going to assume that the coordinate distribution of a single nucleon, given by the function $n_p(\mathbf{r})$, is the same in the zeroth case and in a non-zeroth case; it follows then that $n_{2p}^{(1)}(\mathbf{r},\mathbf{r}')$ satisfies the condition

$$\int n_{2p}^{(1)}(\mathbf{r},\mathbf{r}')\,d\mathbf{r}' = 0. \tag{15}$$

The previous calculations[6-8] of the quantity $\langle D^2\rangle$ show that the main reason for the deviation of the true coordinate distribution of identical nucleons from the zeroth distribution is the Pauli principle; according to it, the approach to one another of two identical nucleons is appreciably less probable than that of two different nucleons. Therefore, to get the qualitative character of the function $n_{2p}^{(1)}$, it will be sufficient to consider the simplest gas model of the nucleus – so far as this model takes the Pauli principle into account. The result of such an investigation amounts to the following: the function $n_{2p}^{(1)}$ is approximately proportional to $n_{2p}^{(0)}$ everywhere except in a region where the distance between the points $\mathbf{r}$ and $\mathbf{r}'$ is less or of the order of a, a being comparable to the mean internucleonic distance. Considering this region as being small with respect to the nuclear volume (i.e. neglecting the edge effect), we can approximate the function $n_{2p}^{(1)}(\mathbf{r},\mathbf{r}')$ with the help of a δ-function of $\mathbf{r}-\mathbf{r}'$:

$$n_{2p}^{(1)}(\mathbf{r},\mathbf{r}') = \Omega_p\Big[n_{2p}^{(0)}(\mathbf{r},\mathbf{r}') - \delta(\mathbf{r}-\mathbf{r}')\,n_p\Big(\frac{\mathbf{r}+\mathbf{r}'}{2}\Big)\Big]. \tag{16}$$

where Ω_p means (a^3/R^3).

Substituting (16) into (13), we get

$$\Lambda = \Omega_p(Z-1)\,A/N. \tag{17}$$

2. QUADROPOLE TRANSITIONS

The expression of the cross section for quadrupole transitions in the long wave length approximation has the form

$$\sigma_{E2}(\nu) = 4\pi^2 \sum_f{}' \Big(\frac{\nu}{\hbar c}\Big)^3 |Q_{f0}|^2\,\delta(E_f - E_0 - \nu). \tag{18}$$

Q is any of the non-diagonal components of the quadrupole moment operator. To be specific, let

$$Q \equiv Q_{13} = {}^1\!/_2 \sum_\alpha e_\alpha x_\alpha z_\alpha.$$

Using the matrix multiplication rule, we readily get

$$\int_0^\infty \sigma_{E2}(\nu)\,\frac{d\nu}{\nu^2} = \frac{4\pi^2}{(\hbar c)^3}\,\frac{-i\hbar}{2}\langle Q\dot{Q} - \dot{Q}Q\rangle; \tag{19}$$

$$\int_0^\infty \sigma_{E2}(\nu)\,\frac{d\nu}{\nu^3} = \frac{4\pi^2}{(\hbar c)^3}\langle Q^2\rangle. \tag{20}$$

In the derivation of Eq. (20), we have neglected the mean square of the nuclear eigen-quadrupole moment with respect to $(\overline{Q_{00}})^2$, i.e., we have assumed $\langle Q^2\rangle \gg \overline{Q_{00}}^2$. $\overline{Q_{00}}$ is the mean value of the operator Q in the nuclear ground state. The bar means averaging over degeneracy (if any).

It is easy to note that Eq. (19) is analogous to Eq. (1), and Eq. (20) to Eq. (2). This analogy is very useful. Let us first consider the right hand side of Eq. (19). After elementary calculations, we get

$$-(i\hbar/2)\langle Q\dot{Q} - \dot{Q}Q\rangle = (\hbar^2/4m)\,e^2 Z\langle x^2\rangle_p(1+\xi). \tag{21}$$

$\langle X^2\rangle \approx R^2/5$; ξ is a positive quantity which vanishes in the absence of exchange forces. Let us try to obtain the relationship between ξ and the quantity Δ introduced above. For this purpose let us assume some simple expression for the nuclear exchange potential energy U; for instance,

$$U = {}^1\!/_2 \sum_{\alpha,\beta}{}' U_{\alpha\beta}(\mathbf{q}_\alpha - \mathbf{q}_\beta)\,P_{\alpha\beta},$$

where $P_{\alpha\beta}$ is an operator representing the coordinates $\mathbf{q}_\alpha$ and $\mathbf{q}_\beta$ (calculations with such a U are carried out in Ref. 4). Substituting this expression in the sum rule (1) and (19), we get after some calculations

$$\Delta = -\sum_{\alpha\beta} \langle \frac{1}{2\hbar^2}(e_\alpha - e_\beta)^2(z_\alpha - z_\beta)^2 U_{\alpha\beta}P_{\alpha\beta}\rangle \Big/ \sum_\alpha \langle \frac{e_\alpha}{m}\rangle,$$

$$\xi = -\sum_{\alpha\beta} \langle \frac{1}{2\hbar^2}(e_\alpha - e_\beta)^2(x_\alpha z_\alpha - x_\beta z_\beta)^2 U_{\alpha\beta}P_{\alpha\beta}\rangle \Big/ \sum_\alpha \langle \frac{e_\alpha}{m}(x_\alpha^2 + z_\alpha^2)\rangle.$$

Comparing these expressions, one sees that ξ has a tendency to be smaller than Δ by a factor of about $(r_0/R)^2$. This estimate is of course very inaccurate; however, it does not matter for what follows whether we put $\xi = 0$, in the other limiting case, $\xi = \Delta$. To be specific, let $\xi = 0$. Finally

$$\int_0^\infty \sigma_{E2}(\nu)\frac{d\nu}{\nu^2} = \frac{\pi^2}{5}\left(\frac{e^2}{\hbar c}\right)\left(\frac{1}{mc^2}\right)ZR^2. \qquad (22)$$

For the evaluation of the right hand side of Eq. (20), let us first recall that in the evaluation of $\langle D^2 \rangle$ we had to take into account the relationship (3) between the coordinates q_α and Eq. (10), which follows from (3). In particular, we were not able to write the zeroth distribution $n_{2p}^{(0)}(\mathbf{r}, \mathbf{r}')$ in the form of a product of distributions $n_p(\mathbf{r})$ and $n_p(\mathbf{r}')$ because it would have led to a qualitatively incorrect result: the right hand side of the sum rule (4) would have been proportional to Z rather than to ZN/A. In the present case, however, where we have to compute $\langle Q^2 \rangle$, we can consider the coordinates q_α as independent, not taking Eqs. (3) and (10) into account. It is easy to show that the error due to this approximation is of the order of $1/A$. In particular, we will assume that the zeroth distribution $n_{2p}^{(0)}(\mathbf{r}, \mathbf{r}')$ is simply a product of the distribution $n_p(\mathbf{r})$ and $n_p(\mathbf{r}')$. Further the correction for the zeroth distribution is given by formula (16) according to the condition (17) and with the additional assumption on the multiplicativity of

$$n_{2p}^{(0)}(\mathbf{r}, \mathbf{r}').$$

With these assumptions, the expression

$$\langle Q^2 \rangle = {}^1/_4 e^2 [Z\langle x^2 z^2\rangle_p + Z(Z-1)\langle xx'zz'\rangle_{2p}] \qquad (23)$$

becomes equal to

$$\langle Q^2 \rangle = {}^1/_4 e^2 Z \langle x^2 z^2\rangle_p (1 - N\Lambda/A). \qquad (24)$$

Letting $\langle x^2 z^2\rangle_p \approx R^4/35$, , we finally get

$$\int_0^\infty \sigma_{E2}(\nu)\frac{d\nu}{\nu^3} = \frac{\pi^2}{35}\left(\frac{e^2}{\hbar c}\right)(1 - N\Lambda/A). \qquad (25)$$

We see that in this case the correlation has an effect twice as small ($N/A \approx \frac{1}{2}$) as in the case of the sum rule (12) for dipole transitions.

As already mentioned, the function $\Lambda = \Lambda(A)$ can be obtained directly from experiment by substituting the observed value of σ_{E1} into the left hand side of the sum rule (12). However, the errors on the measurements of σ_{E1} are now such that the theoretical values of Λ, calculated in Ref. 7, are probably closer to truth than the experimental ones. The theoretical values of Λ can be approximated with sufficient accuracy by the following formula

$$\Lambda = 0.84(1 + 22/A). \qquad (26)$$

For $A = 50$, $\Lambda \approx 0.6$; for $A = 240$, $\Lambda \approx 0.76$. These values confirm the initial assumption on the smallness of the correlation radius a with respect to the nuclear radius R.

Consider the ratio

$$\bar{\nu}_3 = \int_0^\infty \sigma_{E2}(\nu)\frac{d\nu}{\nu^2} \Big/ \int_0^\infty \sigma_{E2}(\nu)\frac{d\nu}{\nu^3} \qquad (27)$$

$$= 7\frac{(\hbar c)^2}{mc^2}\frac{1}{R^2}\frac{1}{1 + N\Lambda/A} \approx \frac{2.4\cdot 10^2}{A^{2/3}(1 - \Lambda N/A)}.$$

We took $R = 1.1 \times 10^{-13} A^{2/3}$ cm. In the case of a nucleus with $A \approx 50$, Eq. (27) gives $\bar{\nu}_3 \approx 25$ mev, in the case of uranium $\bar{\nu}_3 \approx 9$ mev. Therefore,

$$\bar{\nu}_3 \approx 10 - 20 \text{ MeV}. \qquad (28)$$

Equation (28) gives a lowest bound for the position of the "center of gravity" of the cross section for quadropole transitions. Indeed, the energy ν_0 corresponding to the "center of gravity" is defined by

$$\bar{\nu}_0 = \int_0^\infty \sigma_{E2}(\nu)\,\nu d\nu \Big/ \int_0^\infty \sigma_{E2}(\nu)\,d\nu, \qquad (29)$$

whence $\bar{\nu}_0 > \bar{\nu}_3$.

Hence we conclude that the "center of gravity" of the cross section for quadropole transition is on the right of the dipole resonance, at energies exceeding 10-20 mev.

1 A. B. Migdal, J. Exptl. Theoret. Phys. (U.S.S.R.) **15**, 81 (1945).

2 M. Danos and H. Steiwedel, Z. Naturforsch, **6A**, 217 (1951).

3 M. Danos, Ann. Physik **10**, 265 (1952).

4 I. S. Levinger and H. A. Bethe, Phys. Rev. **78**, 115 (1950).

5 Gell-Mann, Goldberger and Thirring, Phys. Rev. **95**, 1612 (1954).

6 I. S. Levinger and D. C. Kent, Phys. Rev. **95**, 418 (1954).

7 Iu. K. Khokhlov, Dokl. Akad. Nauk SSSR 239 (1954).

8 I. S. Levinger, Phys. Rev. **97**, 122 (1955).

Translated by E. S..Troubetzkoy
16

Inelastic Scattering of 160 mev Pions on Emulsion Nuclei

B. A. Nikol'skii, L. P. Kudrin and S. A. Ali-Zade

(Submitted to JETP editor August 28, 1956)
J. Exptl. Theoret. Phys. (U.S.S.R.) **32**, 48-58 (January, 1957)

The angular and energy spectra of pions inelastically scattered on photographic emulsion nuclei have been obtained. The average energy of pions scattered backwards ($\theta > 90°$) was found to be 64.2 ±3 mev. Inelastic scattering of 160 mev negative pions on emulsion nuclei was calculated by the Monte Carlo method on the assumption that the picture of individual meson-nucleon collisions is valid. The problem of the sensitivity of the results obtained to the assumed characteristics of the interaction of pions with the nucleus is considered in detail. By comparing the calculated results with the experimental data, the average potential energy of the interaction of the pion with the nucleus was determined at $E_\pi = 160$ mev as $V = -(24 \pm 6)$ mev.

INTRODUCTION

THE interaction of high-energy nucleons and pions with the nucleus can be regarded as a convenient tool for studying the properties of nuclei. One can expect that, when the wavelength of the incident particle is less than or comparable with the internucleonic distances in the nucleus, experiments on the interaction of these particles with nuclei will be sensitive to the distribution of nucleons in the nucleus, to the energy spectrum of the nuclear nucleons, and to the interaction potential of the particles in question with the nucleus. In view of the fact that we know too little about the structure of the nucleus, an exact calculation of the interaction of nucleons and pions with the nucleus does not appear to be feasible. Therefore we can establish our conclusions about nuclear properties for the present only on the basis of model representations, the extent of whose validity is determined by comparing the results of calculation with experiment.

One of the possible models for the interaction of the fast particles with the nucleus is the hypothesis of nucleon-nucleon or meson-nucleon collisions in the nucleus [1-3]. There are the more reasons for such a model, the smaller the wavelength of the incident particle is in comparison with the internucleonic distances and the greater the momentum transferred to a nuclear nucleon in a collision. Theoretical estimates indicate that the model of individual collisions of these particles with nucleons of the nucleus possesses adequate validity[2] at an energy $\gtrsim$ 50-100 mev of the nucleons and pions. The results of experiments on the interaction of fast nucleons with heavy nuclei[4-8], on the scattering of fast protons on light nuclei[9-11], and on the production of pions in nuclei by protons[12] lead to the same conclusion. The interaction of fast pions with nuclei has been investigated less fully. In the published work, no quantitative analysis of the experimental results has been carried out; qualitatively, however, the experiments in question do not contradict the picture of individual meson-nucleon collisions in the nucleus. In short, the results of experiments on the interaction of pions of 100-200 mev with nuclei lead to the following[13-22]; 1) pions are efficiently absorbed ny nuclei; 2) in scattering on nuclei pions lose a large part of their energy, which can be explained by their being scattered on the moving nucleons of the nucleus.

Usually experiments on elastic scattering of fast particles by nuclei are described in terms of the optical model. According to this model, the potential energy of the interaction of the particle with the nucleus is assumed to have the form of a square well with real and imaginary parts: $U = V + i\sigma$. The real part V represents the average potential energy of the interaction of the pions (or nucleons) with the nucleus. Obviously the quantity V must be taken into account also in calculating the inelastic interaction of fast particles with the nucleus, inasmuch as the deviation of the average interaction potential brings it about that upon entering the nucleus the particle changes its energy by an amount V.

In the present article the inelastic scattering of 160 mev negative pions by emulsion nuclei is calculated under the assumption that the idea of meson-nucleon collisions in the nucleus is correct; this calculation is compared with experiment.

It is to be noted that the calculation of the interaction of fast pions with the nucleus is presented mainly in comparison with the analogous calculations of the interaction of fast nucleons.

We remark that the calculation of the interaction of fast pions with the nucleus offers the advantage over the analogous calculations for fast nucleons that in this case it is not necessary to consider

the nucleonic part of the intranuclear cascade. The fact that, because of the efficient absorption of pions in the nucleus, pions escaping from the nucleus undergo few collisions with nuclear nucleons, also simplifies the calculation.

1. EXPERIMENTAL RESULTS

In this work a beam of negative pions with an energy $E_\pi = 188 \pm 5$ mev, brought out of the chamber of the synchrocyclotron of the Institute for Nuclear Physics of the Academy of Sciences, USSR, was used. After passing through a deflecting magnet and a collimator the negative pion beam entered an emulsion stack composed of 30 strips of NIKFI type R emulsion, each 395μ thick and 70 mm in diameter. In order to facilitate the following of tracks passing through several emulsion strips, a common coordinate grid with lines about 35μ thick and spaced about 3 mm apart was applied to the emulsion by means of x-rays. During processing, we selected stars so located in the emulsion that the pions which had produced the stars had traveled 4.4 ± 0.9 cm in the emulsion, having lost at the same time 26 ± 6 mev. Thus the experimental results obtained apply to a pion energy of 162 mev.

A total of 1185 interactions of pions of the specified energy with emulsion nuclei was found. Out of these an inelastically scattered charged pion was observed in 323 cases. The interactions of pions with nuclei were found by area scanning the emulsion strips under a magnification of 450 ×. Therefore elastic interactions of pions with nuclei and 0-pronged stars, in which the scattered meson lost less than 80 mev, were not recorded effectively. We also carried out an investigation of inelastically scattered pions escaping from 0-pronged stars and found in scanning a total of 80 meters of beam pion tracks. At the same time it was found that the characteristics of the energy spectrum of pions back-scattered inelastically ($\theta \geq 90°$) do not differ appreciably from the corresponding characteristics of the spectrum of pions escaping from stars with one or more prongs and found by area scanning.

The identification of scattered pions was effected by determining the gradient of the grain density along the track. The energy of the scattered pion was determined from the grain density and from the length of the ionizing range in those cases where the entire pion track was imbedded in the emulsion stack. A graph of grain density vs. pion range for the given emulsion was plotted by following the tracks of pions stopped in the emulsion stack to the place of entry into the stack. Values of dN/dR for pions at $R = 25$ cm and $R = 16$ cm were obtained with great accuracy by measuring the grain density of tracks in the emulsion stack and after traversal of 9 cm of emulsion, respectively. A stack 10 cm in diameter of the same emulsion was used for this purpose.

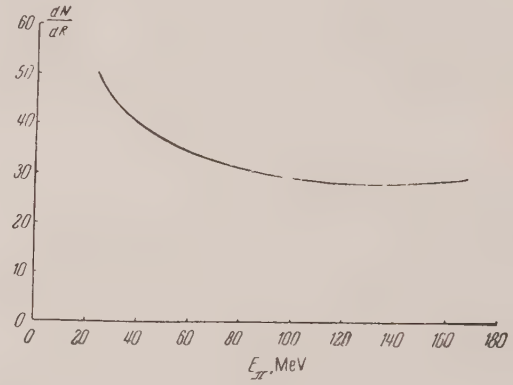

FIG. 1. Grain density *vs.* pion energy. (dN/dR is the number of grains along 80μ.)

A graph of pion energy vs. range in the emulsion was plotted from the data of Fay[23] et al. and of a series of experimental determinations of the range of protons and pions[24-26] in emulsion. For pion energies above 105 mev the graph of $E = f(R)$ was extrapolated in accordance with the calculated data for Cu and Al. The data of Fay et al. used here apply to the Ilford G-5 emulsion; however, as was shown by measuring the lengths of muon tracks in the $\pi \rightarrow \mu$ decay, the stopping power of the NIKFI type R emulsion practically coincides with that of the Ilford G-5 emulsion[27]. The graph of grain density vs. pion energy thus obtained is shown in Fig. 1.

For determining the energy of the scattered pion we selected those events, where the angle between the pion track and the plane of the emulsion did not exceed 30°, inasmuch as for large dip angles the determination of pion energy from grain density gave incorrect results. In accordance with this selection a definite statistical weight, depending on the angle between the tracks of the primary and the scattered pion, was assigned to each event of a scattered pion with a dip angle $\beta \leq 30°$. A statistical weight $k = 1/p$ is assigned to each event, where p is the probability that a particle with a given angle of scattering has a dip angle β (see Appendix).

The energy spectra of pions scattered into the angular interval $\theta = 90°$ to 180° are shown in Fig. 2.

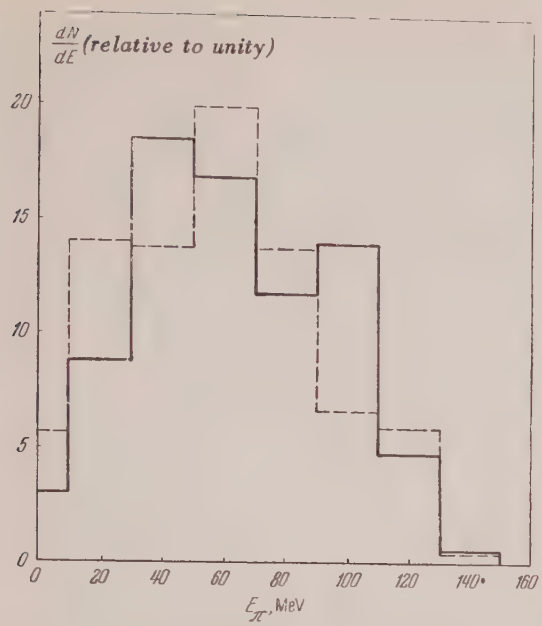

FIG. 2. Energy spectra of pions scattered on emulsion nuclei into the angular interval $\theta = 90^\circ$ to 180°. The experimental spectrum is marked with a solid line, the calculated spectrum by a dashed line.

The indicated pion spectrum has an average energy $E_{exp} = 64 \pm 3$ mev and a half-width

$$\Delta E_{exp} = (\Sigma (\bar{E} - E_i)^2 k_i / \Sigma k_i)^{1/2} = 30.9 \pm 3 \text{ mev}.$$

Here k_i is the statistical weight defined above. The angular distribution of pions scattered inelastically on nuclei is shown in Fig. 3.

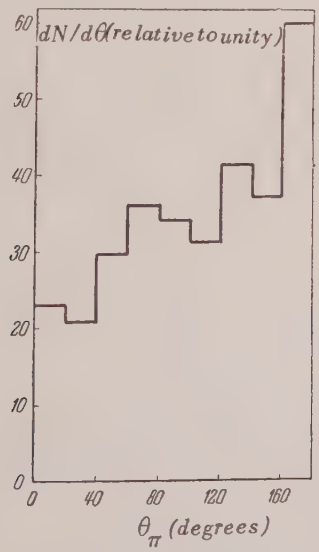

FIG. 3. Angular distribution of pions scattered on emulsion nuclei.

2. CALCULATION OF THE INELASTIC SCATTERING OF 160 MEV NEGATIVE PIONS ON EMULSION NUCLEI

A calculation of the inelastic scattering of pions on nuclei according to the model of individual meson-nucleon collisions can be carried out only under specific assumptions about a set of innacurately known characteristics of the interaction of pions with nuclear nucleons. In particular such characteristics refer to: 1) the angular and energy dependences of the cross sections for meson-nucleon collisions in the nucleus; 2) the parameters of the energy distribution of the nucleons in the nucleus; 3) the average interaction potential of pions with the nucleus.

In order to estimate the effect of the specified parameters of the interaction of pions with the nucleus upon the results of the calculation of the inelastic scattering of 160 mev negative pions on nuclei, a preliminary calculation was performed: the angular and energy spectra of pions that had undergone a single collision with the moving nucleons in the nucleus were computed under different assumptions on the characteristics of the meson-nucleon collisions in the nucleus. The Pauli principle, which forbids collisions in which a nucleon with an energy $E_N \leq 20$ mev or $E_N \leq 30$ mev (depending upon the assumed distribution of nucleons within the nucleus) is formed, was taken into account in the calculation. The results of this calculation are shown in Figs. 4 and 5 and in Table 1.

A comparison is shown in Fig. 4 of the calculated distributions of pions that have undergone a single collision with a nuclear nucleon for the cases of interaction of the pions with a neutron and a proton. Since the scattering cross sections of pions on protons and neutrons have different angular and energy dependences, it follows from Fig. 4 that the results of the calculation of the scattering of 160 mev pions on moving nucleons is not particularly sensitive to the characteristics of the cross sections of the interaction of the pion with nuclear nucleons.

In Fig. 5 there are shown the energy and angular spectra of pions scattered on nuclear neutrons and protons under the assumption that the nuclear nucleons have the momentum distribution of a degenerate Fermi gas with maximum energies $E_N^{max} = 30$ mev and $E_N^{max} = 20$ mev. From Fig. 5 it is seen that the spectra of pions scattered by nucleons are also insensitive to the details of the energy distribution of nucleons within the nucleus.

In the present work it has also been shown that

the angular and energy spectra of pions scattered on nuclear nucleons remain insensitive to the assumed characteristics of meson-nucleon collisions in the nucleus even for lower pion energies (E_π = 70 mev).

The average potential V of the interaction of the pion with the nucleus is related to the change of energy of pions as they cross the boundary of the nucleus. The average energies of pions that have escaped from the nucleus after a single collision with a nuclear nucleon are given in Table 1 for the cases $V = 0$ and $V = -30$ mev. The energy of the incident mesons was taken as $E_\pi = 160$ mev.

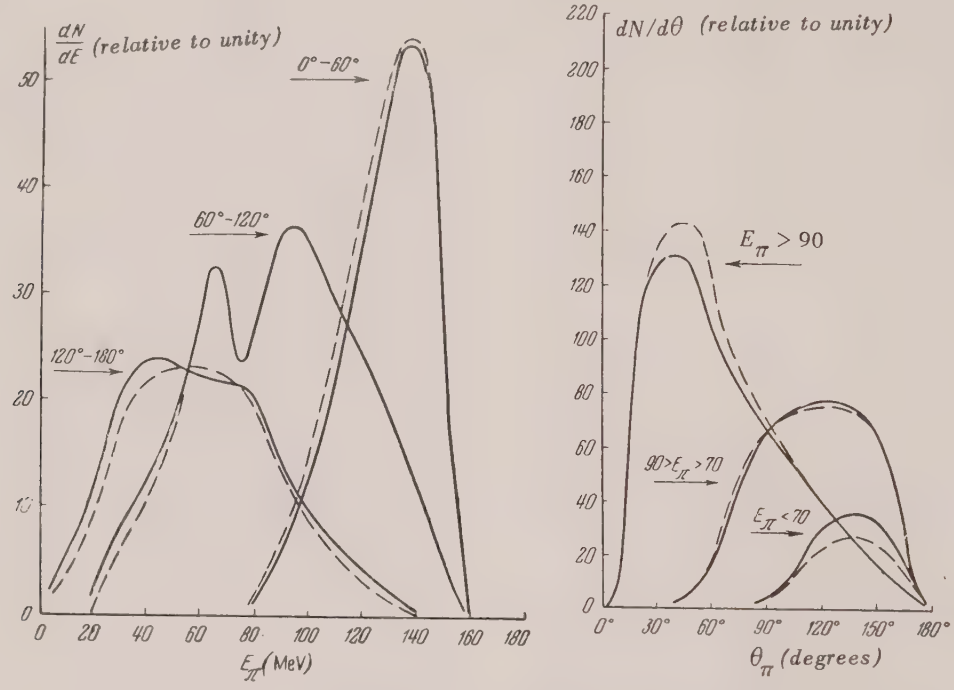

FIG. 4. Comparison of the angular and energy spectra of pions that have undergone a single collision with the nuclear nucleons in the reactions: *1* – (dashed curve) $\pi^- + p \to \pi^- + p$; *2* – (solid curve) $\pi^- + n \to \pi^- + n$. The momentum distribution of the nucleons in the nucleus is that of a degenerate Fermi gas with a maximum energy $E_{max} = 30$ mev.

From Table 1 it is evident that the results of the calculation of inelastic scattering of pions on nuclei are sensitive to the average potential of interaction of the pion with the nucleus. This permits a sufficiently effective determination of the magnitude V by comparing experimental data on inelastic scattering of pions on nuclei with the results of calculation. The insensitiveness of the angular and energy spectra of pions scattered on nuclear nucleons to other inaccurately known parameters of the meson-nucleon collisions in the nucleus makes the problem of determining the magnitude of V sufficiently definite.

TABLE 1

Average energies of pions that have escaped from the nucleus after a single collision with a nucleon of the nucleus.

ϑ_π	0–60°	60–120°	120–180°
$V = 0$	133	105	87
$V = -30$ MeV	128	89	61

The inelastic scattering of 160 mev negative pions by nuclei was calculated by the Monte Carlo method. In the calculation it was assumed that: a) the characteristics of the interaction of pions with nuclear nucleons do not differ from those for free nucleons; b) the momentum distribution of nucleons in the nucleus is that of degenerate Fermi

gas with a maximum energy $E_N^{max} = -30$ mev; c) the quantity V for 160 mev negative pions is taken equal to –30 mev, i.e., in entering the nucleus, a 160 mev π^- meson increases its energy by 30 mev; d) the calculation takes into account the Pauli principle, which forbids collisions in which a nucleon would be formed with an energy ≤ 30 mev.

It was shown above that for the case of the pion-nucleus interaction, the results of calculation are not sensitive to assumptions a) and b). Effects associated with a change in V and also with a change in certain other parameters of the interaction of pions with nuclei will be considered later.

The range of pions between two collisions with nuclear nucleons and also the scattering by this or that angle in collisions with nuclear nucleons was determined in each separate case by the Monte Carlo method.

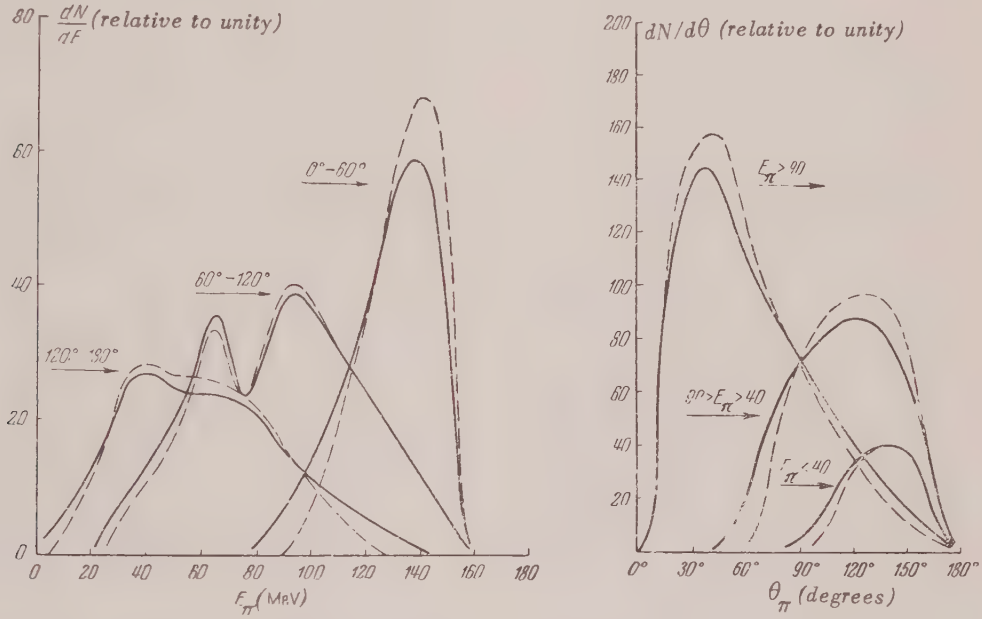

FIG. 5. Energy and angular spectra of pions that have undergone a single collision with the nuclear nucleons, for different momentum distributions of the nucleons in the nucleus. The ratio of the number of neutrons and protons corresponds to that of a nucleus with $A \sim 100$. The solid curves are for a Fermi distribution with $E_{max} = 30$ mev, the dashed curves for $E_{max} = 20$ mev.

A. Range of Pion in Nucleus

The probability that a pion of given energy has a range R in the nucleus is

$$p(R) = \bar{\sigma}\rho e^{-\bar{\sigma}\rho R}, \qquad (1)$$

where $\bar{\sigma}$ is the cross section of the pion-nucleon interaction averaged over the motion of the nucleons and over the ratio of the number of protons and neutrons in the nucleus, and ρ is the density of nucleons in the nucleus. In the present work it was assumed that the nucleon density is the same on the periphery and in the center of the nucleus. Actually the nucleon density in the center of the nucleus, it seems, is larger than on the periphery, which introduces certain changes into the calculated results. These changes will be discussed below.

In the computation of the pion range according to formula (1), the cross sections of the interaction of the pion with nuclear nucleons were replaced by the total cross sections of the interaction of free particles, i.e., the absorption of pions in the nucleus was neglected. The absorption of pions in the nucleus will be discussed in detail in Section D.

Average cross sections of the interaction of negative pions with protons and neutrons of the nucleus were computed by the method described above and are presented in Table 2.

According to the principle of isotopic invariance, the total cross sections of the interaction of neutral pions with nucleons can be written as

$$\sigma(\pi^0 + N) = {}^1/_2 [\sigma(\pi^- + n) + \sigma(\pi^- + p)]. \qquad (2)$$

TABLE 2

Average cross sections of the interaction of pions with nuclear nucleons.

E_π в MeV	30	50	70	90	110	130	150	170	190
$\bar{\sigma}(\pi^- + n)\cdot 10^{27}$ см^2	7.9	19.5	37.2	66.0	98.8	135.1	139.8	168.6	164.1
$\bar{\sigma}(\pi^- + p)\cdot 10^{27}$ см^2	8.3	13.3	18.7	27	37.4	48.9	56.0	58.0	55.9

This relationship obviously holds also for the averaged cross sections.

B. Calculation of the Scattering of Pions on Nuclear Nucleons

In order to determine the energy and scattering angle of a pion after collision with a nuclear nucleon it was necessary in each individual case to transform into the center-of-mass system of the two colliding particles, then to determine the scattering angle by the Monte Carlo method, and finally to find the corresponding scattering angle and the energy in the laboratory system. (The method of this calculation has been described in Ref. 28). In place of the cross sections for the pion-nucleon interaction we took cross sections obtained from the unique system of phase shifts that best fit the experimental results[29].

In calculating the collision of a pion with nuclear nucleons the fact was also taken into account that a collision of a pion and a nucleon is less probable when the directions of motion of both particles coincide as compared with the case when the particles move toward one another. The corresponding change of cross section can be described in the following form:

$$\sigma = \sigma_0\left(1 - \frac{v_N \cos\alpha}{v_\pi}\right). \qquad (3)$$

Here v_N and v_π are the velocities of the nucleon and the pion, and α is the angle between the directions of motion of the nucleon and the pion.

C. Effects Associated with the Change of Potential during Passage of the Pion across the Boundary of the Nucleus

Because the average potential V of the pion-nucleus interaction is different from zero, the pion changes its energy by an amount V, and also the direction of its motion as it passes through the boundary of the nucleus. If the angle of incidence of the pion upon the boundary of the nucleus is sufficiently large, reflection of the particle back into the nucleus may take place. But an exact account of the effect of reflection does not appear feasible since the dependence of the quantity V on the energy can be determined only approximately.

TABLE 3

Average energies of pions going backward ($\theta \geq 90^\circ$) in mev.

Number of collisions	Without reflection	With reflection
1	92.4±3.6	96.1±4.4
2	74.2±3.8	81.7±4.7
3	55.2±4.7	60.1±7.8
4	54.3±2.5	58.1±5.9

Therefore two limiting cases are discussed in the present article: 1) reflection of pions back into the nucleus does not occur on the boundary of the nucleus; 2) reflection on the boundary of the nucleus can take place for pions of any energy under the assumption that $V = -30$ mev.

Average energies of charged pions that have escaped from an emulsion nucleus after one, two, and so forth collisions with nuclear nucleons have been calculated by the Monte Carlo method and are given in Table 3; the absorption of pions in the nucleus was not taken into account.

It is evident from Table 3 that the effect of reflection of pions into the nucleons in crossing the boundary of the nucleus does not change the average energies of inelastically scattered pions substantially.

D. Absorption of Pions in the Nucleus

From experiment it is known that at a pion energy of about 200 mev the number of inelastically scattered charged pions constitutes approximately 30 percent of the number of all interactions

of pions with emulsion nuclei (excluding diffraction scattering)[15]. From this it follows that pions are efficiently absorbed by nuclei. Since the mechanism of pion absorption in the nucleus is unknown, an exact calculation of this process does not appear to be possible.

One of the possible models for the absorption of pions in the nucleus can be constructed on the basis of employing the results on capture of pions in deuterium: $\pi^+ + d \to 2p$. According to this model it is assumed that the cross section of the capture of the pion in a nucleus is proportional to the capture cross section in deuterium:

$$\sigma_{\text{nucleus}} = \gamma\sigma(d), \qquad (4)$$

where the coefficient γ takes into account the probability of the formation of quasi-deuteron states in the nucleus and the Pauli exclusion of certain final states of nucleons in the nucleus. Various authors[16,18,19] estimate that $\gamma \approx 4$. In the calculation of absorption according to this model, the capture of a pion on some part or other of its trajectory in the nucleus is determined by the Monte Carlo method.

It is also possible to assume that each collision of pions with nuclear nucleons is accompanied by the absorption of one and the same fraction α of the pions. The magnitude of α is chosen so that the total number of charged pions coming out of the nucleus under consideration of absorption is equal to the experimental value. In considering the absorption according to this model, the energy spectra of pions coming out of the nucleus after the first, second and so forth collision remain unchanged; only the relative number of pions, that have undergone several collisions up to their escape from the nucleus, decreases.

It is to be noted that under the assumption of the meson-nucleon picture of the interaction of the pion with the nucleus the "deuteron" model of pion absorption seems to be more justified. The assumptions about the nature of pion absorption in the nucleus, made according to the second model, cannot claim any rigorous theoretical basis. The results thus obtained appear to be rejected ones and, as follows from Table IV show only that the energy spectra of pions scattered inelastically by the nucleus are not sensitive to the assumptions about the nature of pion absorption in the nucleus.

In Table IV are given the calculated values of the average energies of pions scattered on emulsion nuclei into the angular interval 90° to 180° for the case of absorption according to the "deuteron" model (I) and for the case of equally probable absorption of pions in every collision (II).

TABLE 4

Average energies of pions in mev with absorption taken into account ($\theta_\pi \geq 90°$).

	With reflection	Without reflection
I	93,2±3,6	88,7±3,0
II	87,2±3,2	84,5±2,7

3. COMPARISON OF THE RESULTS OF THE CALCULATIONS OF INELASTIC SCATTERING OF PIONS BY NUCLEI WITH EXPERIMENTAL DATA

The results of the calculation were obtained on the basis of statistics in 517 cases of interaction of 160 mev negative pions with emulsion nuclei. As the photographic emulsion consists of heavy ($A \sim 100$) and light ($A \sim 14$) nuclei, the calculation includes a computation of the corresponding characteristics for both types of nuclei. From Table 4 it follows that the calculated value of the average energy of the spectrum of pions escaping backward ($\theta \geq 90°$) is given by $(\bar{E}_\pi)_{\text{calc}} = 88 \pm 5$ mev. The quoted error includes the statistical error and a possible spread of values in taking account of reflection and absorption according to the various models. This value of $(\bar{E}_\pi)_{\text{calc}}$ is obtained under the assumption that 160 mev negative pions increase their energy by 30 mev as they enter the nucleus, i.e., $V = -30$ mev. This value of V agrees with the results of experiments on elastic scattering of pions on nuclei (see Table 5). But the exact value of V remains unknown. In the present work, it was shown that a change of the quantity V by 30 mev leads to a change of the average energy of pions scattered backward ($\theta \geq 90°$) by an amount $\Delta E = 7$ mev. Thus, in spite of the inaccurate knowledge of the quantity V at $E_\pi = 160$ mev, the value of $(\bar{E}_\pi)_{\text{calc}}$ obtained appears to be sufficiently definite. The indicated value of $(\bar{E}_\pi)_{\text{calc}}$ applies to the energy spectrum of pions in the nucleus. Upon leaving the nucleus, the pions decrease their energy by the magnitude of the average potential of the pion-nucleus interaction, i.e., by $-V$. Thus by comparing the experimentally found value, $(\bar{E}_\pi)_{\text{exp}} = 64$

± 2.5 mev, of the average energy of pions scattered backward and the magnitude of the calculated energy, $(\bar{E}_\pi)_{calc}$, of pions in the nucleus, it is possible to determine the quantity V for negative pions with an energy $E_\pi = 160$ mev as

$$V = (\bar{E}_\pi)_{exp} - (\bar{E}_\pi)_{calc} = -(24 \pm 6) \text{ mev}.$$

The minus sign implies that the meson-nucleon forces at $E_\pi = 160$ mev are attractive. The absolute value of V is found to be in good agreement with the magnitudes of the average potential of the pion-nucleus interaction obtained in experiments on the elastic scattering of pions on nuclei. The results of these experiments are given in Table 5.

TABLE 5

Values of V obtained from experiments on the elastic scattering of pions on nuclei.

Pion energy mev.	Sign of pion	Nucleus	V	Reference
48	+	C	$-(15 \pm 9)$	[30]
60	+−	He	$-(20 \pm 10)$	[31]
62	−	Photographic emulsion.	−20	[32]
62	+−	C	−18	[19]
80	+	Al	−20	[33]
80	−	Al	−30	[33]
105	+−	He	$-(18 \pm 14)$	[31]
125	−	C	−30	[34]

In Fig. 2 there is shown a comparison of the experimentally found spectrum of pions scattered on emulsion nuclei with the spectrum obtained in the present calculation, where it has been taken into account that the average potential of the interaction with the nucleus of the pions of the specified spectrum is given by $V = -24$ mev. The half-width of the energy spectrum shown in Fig. 2 was computed according to the formula

$$(\Delta E)_{calc} = \sqrt{\Sigma (E - E_i)^2 / (n - 1)} \qquad (5)$$

it turns out to be equal to $(\Delta E)_{calc} = 30.8 \pm 2.6$ mev. This value of $(\Delta E)_{calc}$ agrees well with the value $(\Delta E)_{exp} = 30.9 \pm 2.1$ mev found by experiment. The good agreement of the experimental and theoretical energy spectra of pions scattered on emulsion nuclei indicates that the assumed model satisfactorily describes the interaction of pions with the nucleus.

In calculating the forward ($\theta < 90°$) scattering, the change of density of nuclear nucleons from the center of the nucleus to the periphery has to be considered. A smaller nucleon density on the periphery of the nucleus must lead to an increase of pions coming out of the nucleus at angles $\theta < 90°$ as compared with the results obtained in the present calculation, where it was assumed that the nucleon density in the center and on the periphery of the nucleus is the same. In the performed calculation, the number of pions coming out of the nucleus at angles $\theta < 90°$ constitutes about 30 percent of the total number of pions scattered inelastically by the nucleus, whereas it was found by experiment that this number is about 40 percent.

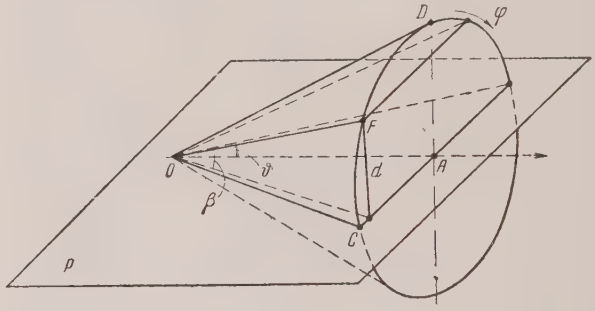

FIG. 6.

The calculation of the pion-nucleus interaction according to the model of individual collisions with nucleons of the nucleus for the case of varying nucleon density presents considerable difficulties and was not carried out in the present work. All the calculated results considered above apply to pions scattered backward ($\theta = 90°$ to 180°), for which the effect of the variation of nucleon density with radius is not noticeable.

In conclusion the authors express gratitude to Professor I. I. Gurevich for a discussion of the results of the work, to Professor M. G. Meshcheriakov for the use of the synchrocyclotron of the Institute for Nuclear Physics of the Academy of Sciences of the USSR, to A. E. Ignatenko and A. I. Mukhin for aid in exposing the emulsion, to G. V. Kolganovii and A. A. Kondrashinii for help in the work, and to D. M. Samoilovich for developing the emulsion.

APPENDIX

In Fig. 6 there is drawn the cone of particles scattered into an angle θ relative to the direction AO of the incident particles. Obviously any azimuthal angle φ is equally probable. In the present case the direction of the primary beam lies in the plane P of the emulsion; therefore the dip angle β of a particle can be measured by the arc CF.

The probability that a particle has a dip angle $\beta \leq \beta_0$ is given by the ratio of the arc CF to the arc CD: $p = CF/CD$. Obviously p decreases with increasing θ.

1 R. Serber, Phys. Rev. **72**, 1114 (1947).
2 G. F. Chew and G. C. Wick, Phys. Rev. **85**, 636 (1952).
3 J. Ashkin and G. C. Wick, Phys. Rev. **85**, 686 (1952).
4 M. L. Goldberger, Phys. Rev. **74**, 1269 (1948).
5 Bernardini, Booth and Lindenbaum, Phys. Rev. **85**, 826 (1952); Phys. Rev. **88**, 1017 (1952).
6 McManus, Sharp and Gellman, Phys. Rev. **93**, 924 (1954).
7 Lees, Morrison, Muirhead and Rosser, Phil. Mag. **44**, 304 (1953).
8 J. Combe, Nuovo cimento Suppl. **3**, No. 2, 182 (1956).
9 O. Chamberlain and E. Segrè, Phys. Rev. **87**, 81 (1952).
10 Cladis, Hess and Moyer, Phys. Rev. **87**, 425 (1952).
11 J. M. Wilcox and B. J. Moyer, Phys. Rev. **99**, 875 (1955).
12 Block, Passman and Havens, Phys. Rev. **88**, 1239 (1952).
13 H. Bradner and B. Rankin, Phys. Rev. **87**, 547, 553 (1952).
14 Bernardini, Booth and Lederman, Phys. Rev. **83**, 1075 (1951).
15 A. H. Morrish, Phys. Rev. **90**, 674 (1953).
16 G. Bernardini and F. Levy, Phys. Rev. **84**, 610 (1951).
17 Minguzzi, Puppi and Ranzi, Nuova cimento **11**, 697 (1954).
18 F. H. Tenney and J. Tinlot, Phys. Rev. **92**, 974 (1953).
19 Byfield, Kessler and Lederman, Phys. Rev. **86**, 17 (1952).
20 A. H. Morrish, Phil. Mag. **45**, 47 (1954).
21 G. Goldhaber and S. Goldhaber, Phys. Rev. **91**, 467 (1953).
22 J. O. Kessler and L. M. Lederman, Phys. Rev. **94**, 689 (1954); Lederman, Byfield and Kessler, Phys. Rev. **90**, 344 (1953).
23 Fay, Gottstein and Hain, Nuovo cimento Suppl. **11**, No. 2,234 (1954).
24 H. Bradner et al., Phys. Rev. **77**, 462 (1950).
25 O. Heinz, Phys. Rev. **94**, 1728 (1954).
26 W. H. Barkas et al.; Phys. Rev. **102**, 583 (1956).
27 V. V. Alpers, R. I. Gerasimova et al.; Dokl. Akad. Nauk SSSR **105**, 236 (1955).
28 L. M. Barkov and B. A. Nikolskii, PTE 2 (1957)
29 deHoffman, Metropolis, Alei and Bethe, Phys. Rev. **95**, 1586 (1954); J. Orear et al., Phys. Rev. **96**, 174 (1954); J. Orear, Phys. Rev. **96**, 176 (1954).
30 A. M. Shapiro, Phys. Rev. **84**, 1063 (1951).
31 E. C. Fowler et al., Phys. Rev. **91**, 135 (1953).
32 A. Minguzzi, Nuovo comento **12**, 799 (1954).
33 Pevsner, Rainwater, Williams and Lindenbaum, Phys. Rev. **100**, 1419 (1955).
34 J. O. Kessler and L. M. Lederman, Phys. Rev. **94**, 689 (1954).

Translated by J. Heberle
7

SOVIET PHYSICS JETP VOLUME 5, NUMBER 1 AUGUST, 1957

Oscillations in a Fermi Liquid

L. D. LANDAU
Institute for Physical Problems, Academy of Sciences, USSR
(Submitted to JETP editor September 15, 1956)
J. Exptl. Theoret. Phys. (U.S.S.R.) 32, 59–66 (January, 1957)

Different types of waves that can be propagated in a Fermi liquid, both at absolute zero and at non–zero temperatures, are investigated. Absorption of these waves is also considered.

THE present paper is devoted to the study of the propagation of waves in a Fermi liquid, and proceeds from the general theory of such liquids developed by the author.[1] These phenomena in a Fermi liquid should be distinguished by a large singularity, connected primarily with the impossibility of propagation in it of ordinary hydrodynamic sound waves at absolute zero. The latter circumstance is already evident from the fact that the path length, and therefore the viscosity of a Fermi liquid, tends to infinity for $T \to 0$, as a result of which the sound absorption coefficient increases without limit.

It is shown, however, that in a Fermi liquid at

absolute zero other waves can be propagated; these differ in nature from ordinary sound, and we shall call them waves of "zero sound".

Initially, theproblem of vibrations in a Fermi liquid was considered by Gol'dman[2] in application to an electron gas with Coulomb interaction between the particles. The problem of a gas with uncharged particles, considered in detail here for liquids, was first considered in the research of Klimontovich and Silin,[3] and later in a series of works of Silin.[4-6] There, the gas was considered to be slightly non-ideal, with an interaction satisfying the conditions of applicability of perturbation theory.

1. VIBRATIONS IN A FERMI LIQUID AT ABSOLUTE ZERO

We begin with the investigation of those vibrations at absolute zero which do not involve the spin characteristics of the liquid. This means that not only the equilibrium distribution function n_0, but also the "perturbing" function

$$n = n_0 + \delta n(\mathbf{p}) \tag{1}$$

is independent of the spin variables. At absolute zero, n_0 is a step function which is broken off at the limiting momentum $p = p_0$. *

The energy of the quasi-particles (elementary excitations) is a function of n, i.e., the form of the function $\epsilon(p)$ depends on the form of $n(p)$. By analogy to (1), we write it in the form

$$\varepsilon = \varepsilon_0(p) + \delta\varepsilon(\mathbf{p}), \tag{2}$$

where the function $\epsilon_0(p)$ corresponds to the distribution $n_0(p)$. The value of $\delta\epsilon$ itself is connected with δn by a formula of the form (see Ref. 1):

$$\delta\varepsilon(\mathbf{p}) = \mathrm{Sp}_{\sigma'}\int f(\mathbf{p}, \mathbf{p}')\,\delta n'\,d\tau', \tag{3}$$

$$d\tau = d^3\mathbf{p}/(2\pi\hbar)^3.$$

Inasmuch as δn is assumed to be independent of the spin variable, the operation Sp is applied only to the scattering amplitude f. But the scalar function $\mathrm{Sp}_{\sigma'} f$ can contain the spin operator σ only in the form of the product $\sigma\,[\mathbf{pp}']$ of two axial vectors: σ and $[\mathbf{pp}']$ (we do not consider expressions containing two products of components of σ, since for spin 1/2, as is well known, they reduce to expressions containing σ in the zeroth or first degree). But this product is not invariant to a time reversal and therefore cannot enter into the invariant quantity $\delta\epsilon$. Thus σ drops out completely and $\delta\epsilon$ is shown to be independent of the spin variable.

The kinetic equation for a Fermi liquid has the form:

$$\frac{\partial n}{\partial t} + \frac{\partial n}{\partial \mathbf{r}}\frac{\partial \varepsilon}{\partial \mathbf{p}} - \frac{\partial n}{\partial \mathbf{p}}\frac{\partial \varepsilon}{\partial \mathbf{r}} = I(n), \tag{4}$$

where $I(n)$ is the integral of collisions between quasi-particles. The number of collisions is proportional to the square of the width of the diffusion zone, so that at absolute zero, $I(n) = 0$. Substituting (1) and (2) in (4), and considering that n_0 and ϵ_0 do not depend on r, we get

$$\frac{\partial \delta n}{\partial t} + \frac{\partial \delta n}{\partial \mathbf{r}}\frac{\partial \varepsilon_0}{\partial \mathbf{p}} - \frac{\partial \delta\varepsilon}{\partial \mathbf{r}}\frac{\partial n_0}{\partial \mathbf{p}} = 0,$$

and assuming δn and $\delta\epsilon$ to be proportional to

$$e^{-i\omega t + i\mathbf{kr}},$$

$$(\mathbf{kv} - \omega)\,\delta n = \mathbf{kv}\frac{\partial n_0}{\partial \varepsilon}\,\delta\varepsilon, \tag{5}$$

where we have introduced the velocity of the quasi-particles $\mathbf{v} = \partial\epsilon_0/\partial\mathbf{p}$. In view of the absence of the δ-function $\partial n_0/\partial\epsilon$ from the right hand side of this equation, there actually enter in them only the values of all quantities taken at the limit $p = p_0$ of the (unperturbed) Fermi distribution. We introduce a new notation for what follows:

$$F = \mathrm{Sp}_{\sigma'} f(\mathbf{p}, \mathbf{p}')\,4\pi p^2 dp/(2\pi\hbar)^3\,d\varepsilon. \tag{6}$$

Then we can write Eq. (3) in the form:

$$\delta\varepsilon = \iint F\,\delta n'\,d\varepsilon'\,do'/4\pi.$$

Here only the $\delta n'$ are functions changing rapidly with ϵ'. Therefore, we can rewrite this expression in the form:

$$\delta\varepsilon = \int F\nu'\,do'/4\pi, \tag{7}$$

where the function

*To avoid excessive complication of our study, we limited ourselves to the simplest and most important caseof an energy spectrum with an occupied region represented by a uniform sphere of radius p_0.

$$\nu(\mathbf{n}) = \int \delta n(\mathbf{p})\, d\varepsilon \tag{8}$$

has been introduced which depends only on the direction n of the vector p, and the function $F(\mathbf{p},\mathbf{p}')$ is taken on the boundary of the (unperturbed) Fermi distribution; here F depends only on the angle χ between p and p′.

We note for what follows that the relation found in Ref. 1, which connects the actual mass m of the particles with the effective mass m^* of the quasi–particles, can, with the help of the function $F(\chi)$ be written in the form

$$\overline{F\cos\chi} = (m^*/m) - 1, \tag{9}$$

where the bar denotes averaging over the directions (in the derivation of this relation, we assume in (6) that $\epsilon = p^2/2m^*$). The equation for the velocity of ordinary sound c can be put in the form

$$\bar{F} = 3mm^*c^2/p_0^2 - 1. \tag{10}$$

Let us substitute (7) in Eq. (5) and integrate the latter over $d\epsilon$. This gives

$$(\mathbf{kv} - \omega)\nu = -\mathbf{kv}\int F\nu\, do'/4\pi.$$

Let us take the direction of k as the polar axis, and let the angles θ, φ define the direction of the momentum p (and the direction of v coinciding with it) relative to this axis. Also, we introduce the propagation velocity $u = \omega/k$ of this wave, and the notation $\eta = u/v$, so that we can finally write the resultant equation in the form

$$(\eta - \cos\theta)\,\nu(\theta,\varphi) = \cos\theta\int F(\chi)\,\nu(\theta',\varphi')\,do'/4\pi. \tag{11}$$

This integral equation defines the principal velocity of propagation of the waves and the form of the function $\nu(\theta, \varphi)$ in them. The latter has the following graphic meaning. The fact that δn is proportional [as is evident from Eq. (5)] to the derivative $\partial n_0/\partial\epsilon$ means that the change of the distribution function for vibrations reduces to the deformation of the boundary of the Fermi surface (a sphere in the undisturbed distribution). The integral of (8) represents the magnitude of the displacement (in energy units) of this surface in the given direction n.

We at once note that it follows from the form of Eq. (11) that the real (only the undamped vibrations are of interest to us) value of η ought to exceed 1, i.e., the propagation velocity of the waves satisfies the inequality

$$u > v. \tag{12}$$

As an example, let us investigate the case in which the function $F(\chi)$ reduces to a constant (we denote it by F_0). The integral on the right hand side of Eq. (11) does not depend on the angles θ, φ in this case. Therefore the desired function ν has the form (we omit the exponential factor):

$$\nu = \text{const}\cdot\cos\theta/(\eta - \cos\theta). \tag{13}$$

The limiting Fermi surface has the form of a surface of revolution, elongated in the forward direction of the propagation of the wave, and flattened in the opposite direction. For comparison, let us point out that the ordinary sound wave corresponds to a function ν of the form $\nu = \text{const}\cdot\cos\theta$, which represents the displacement of the Fermi surface as a whole, without a change in shape.

For the determination of the velocity u, we substitute Eq. (13) in (11) and get

$$\frac{F_0}{4\pi}\int_0^\pi \frac{\cos\theta}{\eta - \cos\theta}\,2\pi\sin\theta\,d\theta = 1.$$

Carrying out the integration, we find the following equation, which determines in implicit form the velocity of the wave for a given value of F_0:

$$\varphi(\eta) \equiv \frac{\eta}{2}\ln\frac{\eta+1}{\eta-1} - 1 = \frac{1}{F_0}. \tag{14}$$

The function $\varphi(\eta)$ decreases monotonically from $+\infty$ to 0 for a change of η from 1 to ∞, always remaining positive. It then follows that the waves under consideration can exist only for $F_0 > 0$. Inasmuch as the function F is proportional to the scattering amplitude, taken with opposite sign (at the angle 0°), of the quasi–particles with one another [(see Ref. 1)], then the latter must be negative, which corresponds to the mutual collision of quasi–particles. However, it must be emphasized that this conclusion applies only to the case F = const. If the function $F(\chi)$ is not constant (and at the same time is not small compared with unity; see below), then propagation of zero sound is in general possible, bor both attractive and repulsive interactions of the quasi–particles.

For $\eta \to \infty$: $\varphi(\eta) \approx 1/3\eta^2$. Therefore, large F_0 corresponds to $\eta = \sqrt{F_0/3}$. In the opposite case of $F_0 \to 0$, we find that η tends toward unity according to the relation

$$\eta - 1 \sim e^{-2/F_0}. \tag{15}$$

The latter case has much more general value. It corresponds to zero sound in an almost ideal Fermi gas for arbitrary form of the function $F(\chi)$. Actually, an almost ideal gas corresponds to a function F which is small in absolute magnitude. It is seen from Eq. (11) that in this case η will be close to unity and the function ν will be significantly different from zero only for small angles θ. On this basis, and being concerned only with this range of angles, we can replace the function F in the integral on the right side of Eq. (11) by its value for $\chi = 0$ (for $\theta \to 0$ and $\theta' \to 0$, $\chi \to 0$ also). As a result, we again recover Eqs. (13) and (15) with the constant F_0 replaced by $F(0)$ (this result coincides with that obtained earlier by Silin[4]).

We note that in a weakly non-ideal Fermi gas, the velocity of zero sound exceeds the velocity of ordinary sound by a factor of $\sqrt{3}$. Actually, for the former, we have $\eta \approx 1$, i.e., $u \approx v$. For the velocity of ordinary sound we get from Eq. (10) (neglecting the term $\overline{F}$ in it and setting $m^* \approx m$): $c^2 \approx p_0^2/3m^2 = v^2/3$

In the general case of an arbitrary dependence of $F(\chi)$, the solution of Eq. (11) is not well defined. In principle, it permits the existence of different types of zero sound, which are distinguished from one another by the angular dependence of their amplitude $\nu(\theta, \varphi)$, and which are propagated with different velocities. Along with the axially symmetric solutions of $\nu(\theta)$, asymmetric solutions can also exist. In these ν has an azimuthal factor $e^{\pm im\varphi}$ (m = integer)

Thus, for a function $F(\chi)$ of the form

$$F = F_0 + F_1 \cos\chi \tag{16}$$

$$= F_0 + F_1(\cos\theta\cos\theta' + \sin\theta\sin\theta'\cos(\varphi - \varphi'))$$

solutions can exist with

$$\nu \sim e^{\pm i\varphi}.$$

Actually, substituting Eq. (16) in (11) and carrying out the integration over $d\varphi'$ (assuming in this case that $\nu = f(\theta)e^{i\varphi}$), we obtain

$$(\eta - \cos\theta) f = \frac{F_1}{4}\cos\theta\sin\theta\int_0^\pi \sin^2\theta' f' d\theta'.$$

Thence,

$$\nu = \text{const} \cdot \frac{\sin\theta\cos\theta}{\eta - \cos\theta} e^{i\varphi}. \tag{17}$$

Conversely, substituting this expression in the equation, we obtain the relation

$$\int_0^\pi \frac{\sin^3\theta\cos\theta}{\eta - \cos\theta} d\theta = \frac{4}{F_1}, \tag{18}$$

which determines the dependence of the propagation velocity on F_1. The integral on the left side of the equation falls off monotonically with increase in the function η. Therefore its maximum possible value is achieved for $\eta = 1$. Computing the integral, we find that the corresponding (the least achieved) value of F_1 is 6. Thus, propagation of the asymmetric wave of the form (17) is possible only for $F_1 > 6$.

Turning to a real Fermi liquid—the liquid He^3—it is reasonable to attempt to approximate the unknown function $F(\chi)$ by the two term expression (16). We can determine the coefficients F_0 and F_1 entering into it by means of the relations

$$F_0 = 3mm^*c^2/p_0^2 - 1, \quad F_1/3 = m^*/m - 1$$

[see Eqs. (9) and (10)], knowing the values of the effective mass m^* and the velocity of ordinary sound c. We can derive the first from experimental data on the temperature dependence of the entropy (in the lowest temperature region). From the data available at present,[7] we get $m^* = 1.43\,m$ (m is the mass of the He^3 atom). For the velocity c, we get 195 m/sec from the data of Walters and Fairbank[8] on the compressibility of liquid He^3. Finally, p_0 is obtained directly from the density of the liquid:

$$p_0/\hbar = 0.76\times10^8 \ \text{см}^{-1}.$$

On the basis of these data, we obtain

$$F_0 = 5.4; \quad F_1 = 1.3. \tag{19}$$

From these values, we can draw a conclusion about the fact that in liquid He^3 the propagation of asymmetric zero sound is impossible. For symmetric zero sound, the solution of the equation with the function $F(\chi)$ from (16) and (19)* leads to the value $\eta = 1.83$, when we obtain $u = v = 1.83 p_0/m^* = 206\ m/\text{sec}$.

The possibility of the propagation of waves in a Fermi liquid at absolute zero means that its energy spectrum can automatically possess a "Bose branch" in the form of phonons with energy $\epsilon = up$. However, one must say that it would be incorrect to introduce corrections corresponding to this branch in the thermodynamic quantities of the Fermi liquid, inasmuch as it has a much higher power of the temperature (T^3 in the heat capacity) than the departures from the approximate theory developed in Ref. 1.

2. VIBRATIONS OF A FERMI LIQUID AT TEMPERATURES ABOVE ZERO

For low, but non–zero, temperatures, mutual collisions of quasi–particles take place in the Fermi liquid. The number of these collisions is proportional to T^2. The corresponding relaxation time (the free path time) is $\tau \sim 1/T^2$. The character of the waves propagated in the liquid naturally depends fundamentally on the relations between their frequency and the reciprocal of the relaxation time.

For $\omega\tau \ll 1$ (which is actually equivalent to the condition of the shortness of the free path length of the quasi–particles in comparison with the wave–length λ), the collisions succeed in establishing thermodynamic equilibrium in each (small in comparison with λ) element of volume of the liquid. This means that we are dealing with ordinary hydrodynamical sound waves, propagated with a velocity c.

If $\omega\tau \gg 1$, then, on the contrary, the collisions do not play essential roles in the process of the propagation of the vibrations, and we will have the waves of zero sound considered in the preceding section.

In both these limiting cases, the propagation of waves is accompanied by a comparatively weak absorption. In the intermediate region, $\omega\tau \sim 1$, the absorption is very strong and isolation of the different types of waves as undamped processes is not possible here.

One can easily obtain the temperature and frequency dependence of the absorption coefficient γ in the region of ordinary sound with the aid of the known formula for the absorption of sound (see Ref. 9, for example), according to which γ is proportional to the square of the frequency and to the viscosity coefficient*. Inasmuch as the viscosity of a Fermi liquid is proportional to $1/T^2$ [10], then we find that

$$\gamma \sim \omega^2/T^2 \quad \text{for} \quad \omega \ll 1/\tau. \tag{20}$$

Absorption in the region of zero sound differs essentially in its character from absorption of ordinary sound. In the latter, the collisions cannot lead to a dissipation of the energy "into the noise" of the distribution, which is changed only by the sound vibrations as such. This is connected with the circumstance already mentioned, that a distribution changed in this fashion remains in thermodynamic equilibrium in each element of the volume. Therefore, the absorption of ordinary sound is connected with the effect of the collisions on the distribution function itself.

In the region of zero sound the collisions lead to absorption "into the background" of the distribution which is changed only by the vibrations themselves, which in this case are not in thermodynamic equilibrium (inasmuch as the form of the limiting Fermi surface is deformed). This change in the distribution function does not depend on the frequency, and therefore the absorption coefficient will not depend on the frequency either. The dependence of γ on the temperature is determined by its proportionality to the number of collisions, i.e.,

$$\gamma \sim T^2 \quad \text{for} \quad \varkappa T/\hbar \gg \omega \gg 1/\tau. \tag{21}$$

The upper limit of the region of applicability of this formula is determined by the inequality $\hbar\omega \ll \varkappa T$ ($\varkappa$ is Boltzmann's constant), which allows a classical consideration of collisions. We recall that the inequality assumed here,

$$\varkappa T/\hbar \gg 1/\tau,$$

i.e.,

$$\hbar/\tau \ll \varkappa T$$

(smallness of the quantum uncertainty of the energy of quasi–particles in comparison with $\varkappa T$), must

*These computations were carried out by A. A. Abrikosov and I. M. Khalatnikov.

*The contribution to γ from second viscosity and thermal conductivity is proportional to a much higher power of T and is therefore inconsiderable.

hold since it is the condition of applicability of everything generally developed in the theory of the Fermi liquid.[1]

The determination of the absorption coefficient of zero sound in the frequency range $\hbar\omega \gtrsim \varkappa T$ requires quantum consideration. The corresponding calculations can be simplified if we develop them in such a way that we express the desired "quantum" absorption coefficient in terms of the "classical" from Eq. (21).

The absorption of sound quanta takes place in the collisions of quasi–particles. If we denote by ϵ_1 and ϵ_2 the energies of the quasi–particles before and after collisions, then at a given frequency ω, they are connected by the law of conservation of energy

$$\varepsilon_1 + \varepsilon_2 + \hbar\omega = \varepsilon_1' + \varepsilon_2'.$$

In addition to the collisions, we must also consider the inverse collisions, which are accompanied by the emission of sound quanta. Taking into consideration the well known properties of the collision probabilities of Fermi particles, we find that the total rate of decrease of the number of sound quanta as a result of collisions is given by the expression

$$\iiiint w(\mathbf{p}_1, \mathbf{p}_2; \mathbf{p}_1', \mathbf{p}_2') \{n_1 n_2 (1 - n_1')(1 - n_2') \quad (22)$$

$$- n_1' n_2' (1 - n_1)(1 - n_2)\}$$

$$\times \delta(\mathbf{p}_1' + \mathbf{p}_2' - \mathbf{p}_1' - \mathbf{p}_2 - \hbar\mathbf{k})$$

$$\times \delta(\varepsilon_1' + \varepsilon_2' - \varepsilon_1 - \varepsilon_2 - \hbar\omega)\, d\tau_1 d\tau_2 d\tau_1' d\tau_2'.$$

The delta functions in the integrand allow the satisfaction of the laws of conservation of energy and momentum.

In the integral (22), the essential values of the energy are only those in the region of diffuseness of the Fermi distribution. In this region, the expressions under the integral sign are changed strongly only by multipliers which contain $n(\epsilon)$. Furthermore, it should be noted that the angular integrals in (22) are practically unchanged in the transition from the "classical" region

$$\hbar\omega \ll \varkappa T,$$

to the "quantum" region

$$\hbar\omega \gg \varkappa T.$$

In view of this fact, it will be sufficient for us to calculate the integral

$$J = \iiiint \{n_1 n_2 (1 - n_1')(1 - n_2') - n_1' n_2' (1 - n_1)$$

$$\times (1 - n_2)\, \delta(\varepsilon_1' + \varepsilon_2' - \varepsilon_1 - \varepsilon_2 - \hbar\omega)\, d\varepsilon_1 d\varepsilon_2 d\varepsilon_1' d\varepsilon_2',$$

taken only over the energy. Then, substituting

$$n(\varepsilon) = [e^{(\varepsilon-\mu)/\varkappa T} + 1]^{-1}$$

and introducing the notation

$$x = (\varepsilon - \mu)/\varkappa T, \quad \xi = \hbar\omega/\varkappa T,$$

we get (omitting the factor T^3)

$$J = \int_{-\infty}^{+\infty}\int\int\int \frac{(1 - e^{-\xi})\, \delta(x_1' + x_2' - x_1 - x_2 - \xi)\, dx_1 dx_2 dx_1' dx_2'}{(e^{x_1} + 1)(e^{x_2} + 1)(1 + e^{-x_1'})(1 + e^{-x_2'})}.$$

In view of the rapid convergence of the integral, the region of integration can be extended from $-\infty$ to $+\infty$.

For integration purposes, we transform to the variables x_1, x_2, y_1, y_2, where $y = x - x'$. Integration over x_1 and x_2 is elementary and gives

$$J = (1 - e^{-\xi})$$

$$\times \int_{-\infty}^{+\infty}\int\int\int \frac{\delta(y_1 + y_2 + \xi)\, dx_1\, dx_2\, dy_1\, dy_2}{(e^{x_1} + 1)(e^{x_2} + 1)(1 + e^{-x_1 + y_1})(1 + e^{-x_2 + y_2})}$$

$$= (1 - e^{-\xi}) \int_{-\infty}^{+\infty}\int\int \frac{y_1 y_2 \delta(y_1 + y_2 + \xi)\, dy_1\, dy_2}{(1 - e^{y_1})(1 - e^{y_2})}$$

$$= -(1 - e^{-\xi}) \int_{-\infty}^{+\infty} \frac{y(\xi + y)\, dy}{(e^y - 1)(e^{-y-\xi} - 1)}$$

$$= \int_{-\infty}^{+\infty} y(\xi + y) \left\{ \frac{1}{e^y - 1} - \frac{1}{e^{y+\xi} - 1} \right\} dx.$$

For calculation of the resulting difference of two diverging integrals, we introduce as an intermediate the finite lower limit $-\Lambda$ and write:

$$J = \int_{-\Lambda}^{+\infty} \frac{y(\xi + y)}{e^y - 1}\, dy - \int_{-\Lambda+\xi}^{+\infty} \frac{y(y - \xi)\, dy}{e^y - 1}$$

$$= 2\xi \int_{-\Lambda}^{\infty} \frac{y\, dy}{e^y - 1} - \int_{-\Lambda+\xi}^{-\Lambda} \frac{y(y - \xi)\, dy}{e^y - 1}.$$

Keeping in mind that we shall transform to the limit $\Lambda \to \infty$, we neglect e^y in the denominator of the second of the integrals. The first we rewrite in the form

$$\int_{-\Lambda}^{\infty} \frac{y\,dy}{e^y-1} = \int_0^{\infty} \frac{y\,dy}{e^y-1} + \int_{-\Lambda}^{0} \frac{y\,dy}{e^y-1}$$

$$= \frac{\pi^2}{6} + \int_{-\Lambda}^{0} \left(\frac{y}{1-e^{-y}} - y \right) dy$$

$$= \frac{\pi^2}{6} + \int_0^{\Lambda} \frac{y\,dy}{e^y-1} + \frac{\Lambda^2}{2}.$$

Carrying out reductions and then transforming to $\Lambda \to \infty$, we finally obtain

$$J = (2\xi\pi^2/3)(1 + \xi^2/4\pi^2).$$

The desired absorption coefficient γ is proportional to J. The coefficient of proportionality between them is so determined that for $\xi \ll 1$, $\gamma = \gamma_{cl}$. We then obtain:

$$\gamma = \gamma_{cl}\,[1 + (\hbar\omega/2\pi\varkappa T)^2] \quad \text{for} \quad \hbar\omega \gg \varkappa T. \tag{23}$$

Considering that $\gamma_{cl} \sim T^2$, we find that in the limit of high frequencies:

$$\gamma \sim \omega^2 \quad \text{for} \quad \hbar\omega \gg \varkappa T, \tag{24}$$

i.e., the absorption coefficient remains proportional to the square of the frequency, but does not depend on the temperature. We note that the transition from the formula for "low" to the formula for "high" frequencies takes place at

$$\hbar\omega \sim 2\pi\varkappa T,$$

(and not $\hbar\omega \sim \varkappa T$).* The result of (24 refers, in particular, to the zero sound of all frequencies at the absolute zero of temperature.

3. SPIN WAVES IN A FERMI LIQUID

In addition to a consideration of zero sound in Sec. 1, which does not involve the distribution of spins, in a Fermi liquid at absolute zero, waves of other types can also be propagated. These we call spin waves.*

In this section, we denote by K the function

$$K = f(\mathbf{p}, \mathbf{p}')\,4\pi p^2\,dp/(2\pi\hbar)^3\,dz, \tag{25}$$

in which the operator Sp is not used. In the calculation of exchange interaction between the quasi-particles, this function contains terms which are proportional to the product $\sigma\sigma'$, i.e., it has the form:[1]

$$K = {}^1\!/_2 F(\chi) + {}^1\!/_2 G(\chi)\,\sigma\sigma' \tag{26}$$

[F coincides with the function (6) used above].

In place of Eq. (11) we have now

$$(\eta - \cos\theta)\,\nu = \cos\theta\,\mathrm{Sp}_{\sigma'} \int F\nu'\,do'/4\pi. \tag{27}$$

In addition to the solutions $\nu(n)$ considered earlier, which do not depend on the spin, this equation also has a solution of the form

$$\nu = \mu(\mathbf{n})\,\sigma. \tag{28}$$

Substituting (26) and (28) in (27), completing the operation Sp and dividing both sides of the equation by σ, we get

$$(\eta - \cos\theta)\,\mu = \cos\theta \int G\mu'\,do'/16\pi. \tag{29}$$

We see that for each of the components of the vector μ, we obtain an equation which differs from (11) only by the replacement of F by $G/4$. Therefore, all the further calculations of Sec. 1 can immediately be applied to the spin waves.

In the real liquid He^3, we can determine from available experimental data on its magnetic susceptibility only the mean value of $\bar{G}$, which was pointed out previously—1.9. Inasmuch as this quantity is negative, then (in view of the results of Sec. 2) it is most probable that the propagation of spin waves in liquid He^3 is not possible. Such a conclusion, however, is in no sense categorical.

In conclusion, I wish to express my thanks to A. A. Abrikosov, E. M. Lifshitz and I. M. Khalatnikov for useful discussions.

*Considering the frequencies $\omega >> \varkappa T/\hbar$, we at the same time assume satisfaction of the inequality

$$\hbar\omega \ll \varkappa T_0$$

(T_0 is the temperature of degeneration of the Fermi distribution). In the opposite case, particles from the "depth" of the Fermi distribution take part in the absorption and all the theory developed here would become inapplicable.

*The equation for spin waves in weakly non-ideal Fermi gas was considered by Silin.[6]

1 L. D. Landau, J. Exptl. Theoret. Phys. (U.S.S.R.) 30, 1058 (1956); Soviet Phys. JETP 3, 920 (1957).
2 I. I. Gol'dman, J. Exptl. Theoret. Phys. (U.S.S.R.) 17, 681 (1947).
3 Iu. L. Klimontovich and V. P. Silin, J. Exptl. Theoret. Phys. (U.S.S.R.) 23, 151 (1952).
4 V. P. Silin, J. Exptl. Theoret. Phys. (U.S.S.R.) 23, 641 (1952).
5 V. P. Silin, J. Exptl. Theoret. Phys. (U.S.S.R.) 27, 269 (1954).
6 V. P. Silin, J. Exptl. Theoret. Phys. (U.S.S.R.) 28, 749 (1955); Soviet Phys. JETP 1, 607 (1955).
7 Abraham, Osborne and Weisntock, Phys. Rev. 98, 551 (1955).
8 G. K. Walters and W. M. Fairbank, Phys. Rev. 103, 263 (1956).
9 L. D. Landau and E. M. Lifshitz, *Mechanics of Continuous Media*, 2nd edition; Moscow, 1954, Sec. 77.
10 I. Ia. Pomeranchuk, J. Exptl. Theoret. Phys. (U.S.S.R.) 20, 919 (1950).

Translated by R. T. Beyer
8

Letters to the Editor

Quantum Field Theoretical Solutions Without Perturbation Theory

V. I. GRIGOR'EV
Moscow Petroleum Institute

(Submitted to JETP editor July 5, 1956)
J. Exptl. Theoret. Phys. (U.S.S.R.) 32, 146-148
(January, 1957)

IN considering processes which take place among systems of bosons and fermions, one can, for instance, split the general transition matrix $U[\sigma]$ into a sum of particular transition matrices $U^{(\xi)}[\sigma]$.

The equation connecting the matrices

$$U^{(\xi)} = U^{(i,j;n,m;k,l)}(U^{(i,j;n,m;kl)}$$

describes a transition accompanied by the absorption of i bosons, n fermions and k antifermions and by the corresponding emission of j, m, l of these particles), given by us earlier[1], makes it possible to obtain exact recurrence relations among the $U^{(\xi)}$; this in turn provides the possibility for analyzing the solution without making use of perturbation theory.

In order to avoid cumbersome expansions, we shall not consider antifermions here. We may then disregard k and l, and set n equal to m. In that case the equation for $U^{(\xi)}$ is considerably simplified (the number of terms on the right-hand of the equation is cut down by a factor of four) and takes the form

$$\begin{aligned}\delta U^{(i,j;n)}/\delta\sigma(x) = {} & N(\bar{u}(x)\gamma u(x)\varphi^{(+)}(x))\,[U^{(i,j-1;n-1)} + U^{(i,j-1;n)} + U^{(i,j-1;n)} \\ & + U^{(i,j-1;n+1)} + U^{(i+1,j;n-1)} + U^{(i+1,j;n)} + U^{(i+1,j;n)} + U^{(i+1,j;n+1)}] \\ & + N(\bar{u}(x)\gamma u(x)\varphi^{(-)}(x))\,[U^{(i-1,j;n-1)} + U^{(i-1,j;n)} + U^{(i-1,j;n)} + U^{(i-1,j;n+1)} \\ & + U^{(i,j+1;n-1)} + U^{(i,j+1;n)} + U^{(i,j+1;n)} + U^{(i,j+1;n+1)}];\quad U^{(i,j;n)} = U^{(i,j;n,n)}.\end{aligned} \tag{1}$$

$u(x)$, $\Phi^{(-)}(x) = (\hbar c/ig)\varphi^{(-)}(x)$ are annihilation operators and $\bar{u}(x)$, $\Phi^{(+)}(x) = (\hbar c/ig)\varphi^{(+)}(x)$ are creation operators for free fermions and bosons. The expression for γ depends on the choice of interaction and meson type. Finally, the fact that $U^{(i,\,j-1,\,n)}$, enters twice in the equation, is linked with the various possible orders of emission and absorption of fermions.

We shall seek a solution of the system (1) for non-stationary problems in the form

$$U^{(i,j;n)} = U^{(\xi)} = \frac{1}{i!\,j!\,(n!)^2} N\int_{\sigma_0}^{\sigma} d_v^{(\xi)}\Lambda^{(\xi)}\{F^{(\xi)}\}\,e^{\{K[\sigma]\}}, \tag{2}$$

where

$$\Lambda^{(\xi)} = \bar{u}(\xi_1)u(\eta_1)\ldots\bar{u}(\xi_n)u(\eta_n) \times \varphi^{(+)}(x_1)\ldots\varphi^{(+)}(x_j)\varphi^{(-)}(y_1)\ldots\varphi^{(-)}(y_i), \tag{3}$$

$$d_v^{(\xi)} = d\xi_1\ldots d\xi_n d\eta_1\ldots d\eta_n dx_1\ldots dx_j dy_1\ldots dy_i,$$

$$\{F^{(\xi)}\} = \left\{\begin{matrix} i,\ j;\ n \\ \xi_1\ldots\xi_n\eta_1\ldots\eta_n x_1\ldots x_j y_1\ldots y_i \end{matrix}\middle|\,\sigma\right\}$$

is a function to be determined. The quantity in the exponential is

$$\begin{aligned}\{K[\sigma]\} = {} & -\int_{\sigma_0}^{\sigma} dz_1\bar{u}(z_1)\gamma u(z_1)\varphi^{(+)}(z_1) \\ & \times\int_{\sigma_0}^{\sigma_1} d\xi\,d\eta\,dy\bar{u}(\xi)\gamma u(\eta)\varphi^{(-)}(y)\left\{\begin{matrix}1,\ 0;\ 1\\ \xi\eta y\end{matrix}\middle|\,\sigma\right\}\Bigg\} \\ & + \Bigg\{\int_{\sigma_0}^{\sigma} dz_1\bar{u}(z_1)\gamma u(z_1)\varphi^{(-)}(z_1) \\ & \times\int_{\sigma_0}^{\sigma_1} d\xi\,d\eta\,dx\bar{u}(\xi)\gamma u(\eta)\varphi^{(+)}(x)\left\{\begin{matrix}0,\ 1;\ 1\\ \xi\eta x\end{matrix}\middle|\,\sigma\right\}\Bigg\}.\end{aligned} \tag{4}$$

The symbol N appearing in front of all terms in (2) denotes the normal product of the operators standing to the right of it. Apart from $\Lambda^{(\xi)}$ the field operators also enter in $\{F^{(\xi)}\}$ and $\{K[\sigma]\}$. Here, however, in contrast to $\Lambda^{(\xi)}$, there appears not the "final" operators, but combinations of non-commuting pairs of operators (0-pairs). Applying the symbol N to these expressions denotes that the operators which enter in them "quasi" commute (anti-commute) with all operators except for these which are included within the same curly brackets. We shall omit the symbol N below, keeping only the curly brackets to denote 0-pairs.

An analysis of Eq. (1) shows that $\{F^{(\xi)}\}$ must have the following form:

$$\{F^{(\xi)}\} = \sum_{q,p,r;\ l} \{[\delta_\tau(\xi_q\eta_p x_r) + \delta_\tau(\xi_q\eta_p y_l)]\,(F_1^{(\xi)})_{\alpha_q\beta_p} + [\delta_\tau(\xi_q x_r) \tag{5}$$

$$+ \delta_\tau(\xi_q y_l)]\,(F_2^{(\xi)})_{\alpha_q} + [\delta_\tau(\eta_p x_r) + \delta_\tau(\eta_p y_l)]\,(F_3^{(\xi)})_{\beta_p} + \delta_\tau(\xi_q\eta_p)\,(F_4^{(\xi)})_{\alpha_q\beta_p}$$

$$+\delta_\tau(\xi_q)\,(F_5^{(\xi)})_{\alpha_q} + \delta_\tau(\eta_p)\,(F_6^{(\xi)})_{\beta_p} + [\delta_\tau(x_r) + \delta_\tau(y_l)]\,F_7^{(\xi)} + F_8^{(\xi)}\}.$$

In the preceeding equation, the expression

$$\delta_\tau(\xi_q x_r);\ \delta_\tau(\xi_q\eta_p y_l) = \delta_\tau(\xi_q\eta_p)\,\delta_\tau(\eta_p y_l)$$

and other similar expressions denote the usual δ-functions, while the index τ is introduced to emphasize the fact that the operators in the integrand of (2) and which depend on the variables entering for example in $\delta_\tau(\xi_q x_r)$ refer to a time which follows all the remaining ones. σ' is a hypersurface lying between σ and σ_0, and which contains the points[2] $\xi_q\eta_p x_r$ or y_l.

The entire expression in the integrand must be symmetric with respect to the permutations $\xi_1 \ldots \xi_n, \eta_1 \ldots \eta_n$, and $x_1 \ldots x_r y_1 \ldots y_1$, which treat equally all particles of interest.

Substituting (2) into the original Eq. (1), and taking Eq. (5) into account, the recurrence relations for the unknown functions $F_1^{(\xi)} \ldots F_8^{(\xi)}$ are easily obtained. These relations are as follows

$$[(F_1^{(\xi)})_{\alpha\beta} \mid \xi_n = \eta_n = x_j = z] = \gamma\,\{F^{(i,j-1;\ n-1)}\}, \tag{6}$$

$$[(F_2^{(\xi)})_\alpha \mid \xi_n = x_j = z] \tag{7}$$

$$= \gamma_{\alpha\beta}\int_{\sigma_0}^{\sigma} dq\,\{u_\beta(z)\,\bar{u}(q)\}\,\{F^{(i,j-1;\ n)}\} \mid \xi_n = q,$$

$$[(F_3^{(\xi)})_\beta \mid \eta_n = x_j = z] \tag{8}$$

$$= \gamma_{\alpha\gamma}\int_{\sigma_0}^{\sigma} dq\,\{\bar{u}_\alpha(z)\,u(q)\}\ \{F^{(i,j-1;\ n)}\} \mid \eta_n = q,$$

$$[(F_4^{(\xi)})_{\alpha\beta} \mid \xi_n = \eta_n = z], \tag{9}$$

$$= \gamma_{\alpha\beta}\int_{\sigma_0}^{\sigma} dq\,[\{\varphi^{(+)}(z)\,\varphi^{(-)}(q)\}\ \{F^{(i+1,j;\ n-1)}\} \mid y_{i+1} = q$$

$$+ \{\varphi^{(-)}(z)\,\varphi^{(+)}(q)\}\ \{F^{(i,j+1;\ n-1)}\} \mid x_{j+1} = q],$$

$$[(F_5^{(\xi)})_\alpha \mid \xi_n = z] = \tag{10}$$

$$= \gamma_{\alpha\beta}\int_{\sigma_0}^{\sigma} dq_1 dq_2\,\{u_\beta(z)\,\bar{u}(q_1)\}\,[\{\varphi^{(+)}(z)\,\varphi^{(-)}(q_2)\}$$

$$\times \{F^{(i+1,j;\ n)}\} \mid \xi_n = q_1;\ y^{i+1} = q_2$$

$$+ \{\varphi^{(-)}(z)\,\varphi^{(+)}(q_2)\}\,\{F^{(i,j+1;\ n)}\} \mid \xi_n = q_1;\ x_{j+1} = q_2],$$

$$[(F_6^{(\xi)})_\beta \mid \eta_n = z] = \tag{11}$$

$$= \gamma_{\alpha\beta}\int_{\sigma_0}^{\sigma} dq_1 dq_2\,\{\bar{u}_\alpha(z)\,u(q_1)\}[\{\varphi^{(+)}(z)\varphi^{(-)}(q_2)\}$$

$$\times \{F^{(i+1,j;\ n)}\} \mid \eta_n = q_1;\ y_{i+1} = q_2 +$$

$$+ \{\varphi^{(-)}(z)\,\varphi^{(+)}(q_2)\}\ \{F^{(i,j+1;\ n)}\} \mid \eta_n = q_1;\ x_{j+1} = q_2],$$

$$[F_7^{(\xi)} \mid x_j = z] = \gamma_{\alpha\beta}\int_{\sigma_0}^{\sigma} dq_1 dq_2\{\bar{u}_\alpha(z)\,u(q_1)\} \tag{12}$$

$$\times \{u_\beta(z)\,\bar{u}(q_2)\}\,\{F^{(i,j-1;\ n+1)}\}\,\xi_{n+1} = q_1;\ \eta_{n+1} = q_2,$$

$$F_8^{(\xi)(\pm)} = \left\{\int_{\sigma_0}^{\sigma} dz_1\bar{u}(z_1)\,\gamma u(z_1)\,\varphi^{(\pm)}(z_1)\right. \tag{13}$$

$$\left.\times \int_{\sigma_0}^{\sigma_1} d\xi_0 d\eta_0 dy_0\bar{u}(\xi_0)\,u(\eta_0)\,\varphi^{(\mp)}(y_0)\right\}\,\{f_{(\pm)}^{(\xi)}(\xi_0 \ldots y_i \mid \sigma\},$$

where

$$\{f_{(+)}^{(\xi)}(\xi_0 \ldots y_i \mid \sigma)\} = \{F^{(i+1,j;\ n+1)}(\xi_0 \ldots y_i \mid \sigma)\} \tag{14}$$

$$- \{F^{(1,0;\ 1)}(\xi_0\eta_0 y_0 \mid \sigma\}\,\{F^{(\xi)}(\xi_1 \ldots y_1 \mid \sigma)\}.$$

These relations yield an exact solution as a function of the interaction constant.

One might have the impression that the presence of the factor $e^{\{K[\sigma]\}}$ leads to a solution in the form of transcendental functions of the operators, so that its practical usage requires a series expansion. This however is not the case, since $\{K[\sigma]\}$

and all other quantities in curly brackets form a single "package".

*In equation (5), $F_k^{(\xi)} = F_k^{(\xi)}(\xi_1 \ldots \gamma_1 | \sigma')$ for K=1, ... 7, and $F_8^{(\xi)} = F_8^{(\xi)}(\xi_1 \ldots \gamma_i | \sigma)$.

1 V. I. Grigor'ev, J. Exptl. Theoret. Phys. (U.S.S.R.) 30, 873 (1956); Soviet Phys. JETP 3, 691 (1956).

Translated by M. A. Melkanoff
23

Concerning the Letter to the Editor by V. A. Krasnokutskii "Light from Aluminum Melts in an Electrolytic Bath"

Z. RUZEVICH
Polytechnic Institute Poland, Vrotslav
(Submitted to JETP editor July 24, 1956)
J. Exptl. Theoret. Phys. USSR 32, 148 (1957)

IN the above mentioned letter to the editor[1], V. A. Kranokutskii discusses an interesting light effect observed during electrolytic oxidation of aluminum or of aluminum melts. However, the author erroneously states that this phenomenon was first discovered by him. Light emission from aluminum electrodes accompanying the formation of oxidation film in electrolytic solutions has been known for several decades, and is described in many monographs devoted to the technical application of anode oxidation of aluminum[2,3]. In addition, Dufford[4] investigated the light emission under discussion in the same electrolytes used by Krasnokutskii and partially obtained similar results. Krasnokutskiis' statement that light emission is not observed in oxide solutions is applicable only to certain acids, while considerable light emission is observed in H_3PO_4 and in different organic acids[4-6]. The influence of different impurities in the aluminum melt on the spectrum of the light was the subject of detail investigations by Guminski[6].

1 V. A. Krasnokutskii, J. Exptl. Theoret. Phys. (U.S.S.R.) 30, 192 (1956); Soviet Phys. JETP 3, 120 (1956).

2 A. Jenny. *Die elektrolytische oxydation des aluminiums and seiner Legierungen* Dresden-Leipzig, 1938.

3 M. Schenk. *Werkstoff aluminum and seine anodische oxydation*, Bern, 1948.

4 R. T. Dufford, J. Opt. Soc. Am. 18, 17 (1929).

5 A. Gunterschultz and H. Betz, Z. Physik 74, 681 (1932).

6 K. Guminskii, Bull. Acad. Pol. Sci. Letters, Ser. A, 145, 457 (1936).

Translated by J. L. Herson
24

Paramagnetic Resonance in Alkali Metals

N. S. GARIF'IANOV
Technical Physics Institute, Kazan Branch, Academy of Sciences, USSR
(Submitted to JETP editor July 20, 1956)
J. Exptl. Theoret. Phys. (U.S.S.R.) 32, 149 (January, 1957)

PARAMAGNETIC absorption resonance due to electron conductivity in metals has been studied by a number of authors[1-4]. We have investigated the dependence of the width of the electron resonance absorption curve on the particle size of metallic lithium containing about 5% impurities of different metals. Measurements were made at frequencies of the oscillating magnetic field of 9350, 400, 225 91 and 35 mcs/s using samples in which the average particle size of lithium varied within wide limits. The method of investigation was described in an earlier work[4].

It was found that the width ΔH of the absorption resonance curve in metallic lithium at room temperature gradually decreases from 20 to 3 Oe with the decrease of the average metal particle size from ~ 50 to $\sim 0.1\mu$.

The width of the curve and the intensity of absorption in samples of lithium with average particle size $\sim 0.1\mu$ remain constant in the frequency range from 9500 to 35 mcs/s and at temperatures from 300 to 90°K. In samples of lithium with larger average size particles the width of the curve also does not depend on the frequency or temperature*, only a distortion in the form of the absorption resonance curve is observed[3,6] which depends on the ratio of the particle size to the depth of the skin layer (see Fig.).

It was successfully shown at the 35 mcs/s frequency that lattice spin relaxation time is increasing with decrease of particle size.

The g-factor value was determined in samples of average particle size of 0.1μ at a 9500 mcs. The value was $g = 2.002 + 0.002$.

In the sodium sample of average particle size 0.1μ and containing 5% impurities, the absorption resonance curve at room temperature has $\Delta H = 110$ Oe, $g = 2.002$ at all investigated frequencies. The

temperature dependence of the width ΔH in this sample is in good agreement with the data in Refs. 2 and 3.

We have not succeeded in trying to detect paramagnetic resonance in the potassium metal sample.

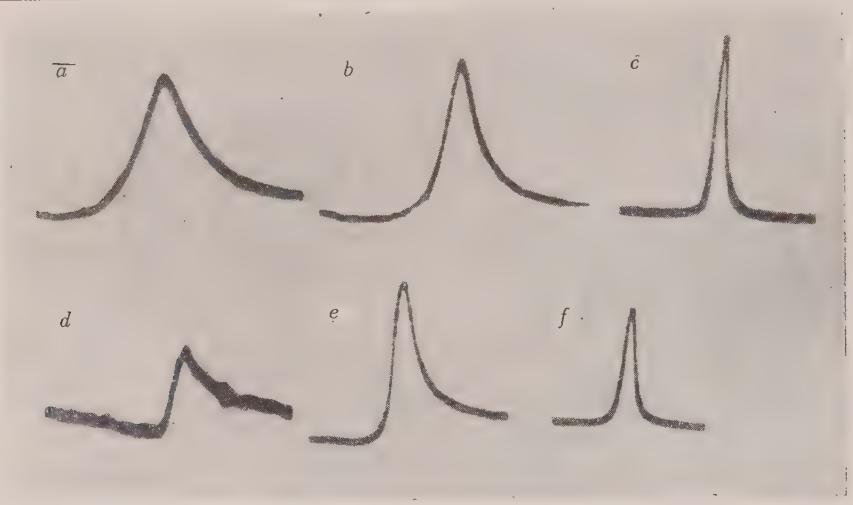

Temperature 300°K; *a*, *b*, *c* 225 mcs/sec; *d*, *e*, *f* – 9500 mcs/sec; size of lithium particles $a \sim 50$; $b \sim 30$; $c \sim 0{,}1$; $a \sim 30$; $e \sim 5$; $f \sim 0{,}1$ μ

* There was observed a widening of the absorption curves in all lithium samples at $T = 463°$K.

1 Griswold, Kip and Kittel, Phys. Rev. **88**, 951 (1952).
2 A. W. Gutowsky and P. J. Frank, Phys. Rev. **94**, 1067 (1954).
3 G. Fehrer and A. F. Kip, Phys. Rev. **98**, 337 (1955).
4 R. A. Levy, Phys. Rev. **98**, 264A (1955).
5 N. S. Garif'ianov and B. M. Kozyrev, J. Exptl. Theoret. Phys. (U.S.S.R.) **30**, 272 (1956); Soviet Phys. JETP 3, 255 (1956).
6 N. Bloemberger, J. Appl. Phys. **23**, 1379 (1952).

Translated by J. L. Herson
25

Energy Spectrum of Cascade Photons in Light Substances

I. P. Ivanenko and M. A. Malkov
Moscow State University

(Submitted to JETP editor July 26, 1956)
J. Exptl. Theoret. Phys. (U.S.S.R.) **32**, 150-151
(January, 1957)

By the method of moments[1-8], it was possible to obtain a fairly complete description of a unidimensional development of an electron-photon cascade shower in light and heavy substances. The method is based on the calculation (with the aid of recurrence formulas) of the moment along the depth t by the distribution function $N(E_0, E^0, t)$ of the number of particles in the shower having energies higher than E^0, in a shower initiated by a primary particle of energy E_0^2.

In Ref. 3, a method was developed for the calculation of the energy spectra of cascade electrons, employing the system of polynomials, orthogonal in the interval $(0, \infty)$. In the present work, a similar method was used for the calculation of the energy spectrum of cascade photons in light substances. The results of the calculation of the number of photons $[N(E_0, E^0, t)]^{p,\Gamma}$ in a shower initiated by a primary electron or a photon in air for certain values of E_0, E^0 and t are given in Tables 1 and 2.

The accuracy of the method of calculation used was investigated in Refs. 3, 5 and 6. In addition, the values of the approximation curves agree, within the limits of 10%, with the values calculated by exact theoretical formulas at $E_0/\beta \gg 1$, where β is the critical energy for a given substance. The energy spectrum at the maximum of the curves is within the limit of 10 or less percent, in agreement with the "equilibrium" spectrum. Therefore, the calculated curves describe the real cascade process with an error of not more than 10 percent.

TABLE 1

$\{N_\Gamma(\varepsilon_0;\varepsilon,t)\}^\Gamma$

ε_0 \ t	0.5	1	2	3	4	5	7	10
				$\varepsilon = 0.11$				
0.6	0,71	0.51	0.26	0.13	0.064	0.032	0.008	0.001
1	0.76	0.58	0.33	0.18	0.10	0.053	0.014	0,002
5	1.12	1.24	1.24	1.00	0.70	0.45	0.155	0.024
11	1.23	1.78	2.45	2.33	1.85	1.30	0.52	0,100
20	1.29	2.24	3.80	4,11	3.57	2,74	1,27	0.295
30	1.50	2.62	4,84	5,72	5.40	4,43	2.30	0.594
50	2.54	3.43	5.92	8,07	8,70	7,93	4.72	1.378
				$\varepsilon = 0.2$				
0.6	0.69	0.48	0.23	0.110	0.053	0.025	0.006	0.001
1	0.72	0.52	0,27	0.140	0.073	0,038	0.009	0,0015
5	1,05	1,07	0,97	0,74	0.50	0,320	0.106	0,016
11	1,14	1,51	1,98	1.78	1.38	0,95	0.35	0,068
20	1.21	1,93	3,11	3,18	2.94	2.25	0.92	0,186
30	1,34	2,26	4,07	4,49	4,13	3.32	1,67	0.42
50	2,02	2.86	4,98	6.48	6,75	5.98	3,45	0.98
				$\varepsilon = 0.6$				
1	0,68	0.46	0,22	0.101	0.047	0.022	0.005	
5	0,85	0.74	0,55	0.37	0.24	0.144	0,045	0.006
11	0.94	1,03	1.12	0,96	0.70	0.46	0.164	0.025
20	0.99	1,33	1,84	1.79	1,44	1,03	0.42	0.084
30	1,02	1.55	2,48	2.62	2,25	1,71	0.78	0.177
50	1,18	1.86	3.36	4.00	3.82	3,16	1.65	0.43
				$\varepsilon = 1$				
5	0,77	0,62	0,40	0.256	0,156	0 090	0.026	0.03
11	0.89	0.88	0,82	0,607	0.428	0 284	0,102	0.018
20	1.02	1.19	1,35	1.22	0.74	0,662	0,275	0,064
30	1,05	1.37	1,86	1 73	1.54	1.03	0.545	0.129
50	1,16	1,72	2.66	2.99	2,69	2,14	1.11	0.150

The curves obtained were used for the calculation of the altitude course of differing in energy photons of the soft component portion, initiated by π^0-mesons. The spectrum of the primary photons was taken from the data by Carlson and others[9]. The calculated and experimental spectra at the height of 45 g/cm^2 differ considerably. This difference, apparently, may be explained by the fact that in Ref. 9 a large number of soft photons was not taken into account.

The authors wish to express their thanks to S. N. Vernov for advice and discussion of the work.

TABLE 2

$\{N_\Gamma(\varepsilon_0, \varepsilon, t)\}^P$

ε_0 \ t	0.5	1	2	3	4	5	7	10
				$\varepsilon = 0.11$				
0.6	0.125	0.14	0.073	0.023	0.007			
1.0	0.28	0.30	0.172	0.060	0.020			
5	1.33	1.67	1.30	0.77	0.405	0.205	0.053	0.009
11	1.98	2.82	2.73	2.10	1.37	0.84	0.295	0.042
20	2.33	3.83	4.73	4.11	3.04	2.05	0.81	0.146
30	2.59	4.63	6.47	6.15	4.90	3.53	1.55	0.327
50	3.01	5.72	9.13	9.76	8.61	6.75	3.36	0.83
				$\varepsilon = 0.2$				
0.6	0.063	0.068	0.036	0.011				
1.0	0.172	0.189	0.105	0.035	0.015			
5	1.09	1.33	0.98	0.538	0.265	0.126	0.032	0.007
11	1.64	2.27	2.16	1.56	1.00	0.591	0.203	0.029
20	1.93	3.07	3.63	3.06	2.21	1.46	0.562	0.096
30	2.16	3.79	5.14	4.75	3.70	2.61	1.11	0.222
50	2.54	4.77	7.35	7.67	6.55	5.03	2.43	0.578
				$\varepsilon = 0.6$				
1	0.025	0.028	0.015	0.008	0.002			
5	0.582	0.69	0.480	0.244	0.108	0.045	0.016	0.003
11	1.00	1.34	1.19	0.80	0.472	0.262	0.079	0.019
20	1.32	1.97	2.12	1.66	1.13	0.70	0.246	0.036
30	1.50	2.45	3.02	2.60	1.91	1.28	0.493	0.087
50	1.66	3.09	4.51	4.37	3.53	2.56	1.12	0.240
				$\varepsilon = 1$				
5	0.382	0.452	0.308	0.152	0.063	0.024	0.004	0.001
11	0.78	1.00	0.83	0.514	0.287	0.152	0.040	0.009
20	1.08	1.53	1.52	1.12	0.732	0.442	0.129	0.027
30	1.28	1.96	2.21	1.80	1.274	0.83	0.299	0.052
50	1.52	2.57	3.38	3.09	2.40	1.69	0.706	0.148

1 G. T. Zatsepin, Dokl. Akad. Nauk SSSR **63**, 243 (1948).
2 S. Z. Belen'kii, J. Exptl. Theoret. Phys. (U.S.S.R.) **19**, 940 (1949).
3 I. P. Ivanenko, J. Exptl. Theoret. Phys. (U.S.S.R.) **32**, 2 (1957); Soviet Phys. JETP **4**, 115 (1957).
4 S. Z. Belen'kii and B. I. Maksimov, J. Exptl. Theoret. Phys. (U.S.S.R.) **22**, 102 (1952).
5 I. P. Ivanenko, J. Exptl. Theoret. Phys. (U.S.S.R.) **30**, 86 (1956).
6 I. P. Ivanenko, Izv. Akad. Nauk SSSR, Ser. Fiz. **19**, 624 (1955).
7 V. Ia. Fainberg, J. Exptl. Theoret. Phys. (U.S.S.R.) **22**, 112 (1952).
8 I. P. Ivanenko, Dokl. Akad. Nauk SSSR **107**, 819 (1956).
9 Carlson, Hooper and King, Phil. Mag. **41**, 701 (1950).

Translated by E. Rabkin
26

Heat Capacity of KCl

T. I. KUCHER
Zhitomir Pedagogical Institute

(Submitted to JETP editor July 27, 1956)
J. Exptl. Theoret. Phys. (U.S.S.R.) **32**, 152
(January, 1957)

WE have calculated the heat capacity of the KCl crystal for 16 temperatures in the range from $T = 10.89°$ to $T = 267.6°$K. In the determination of the heat capacity, the values of the natural frequencies of KCl were used, calculated by the author in previous work[1,2] by taking into account the deformation of the lattice ions, as well as the

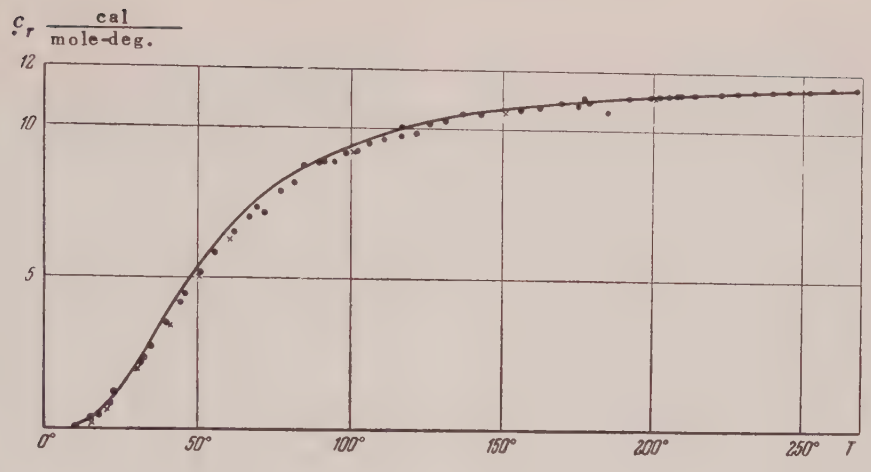

differences in mass of the K and Cl ions. The deformation of the ions was taken into account by the Tolpygo method [3,4].

The results of the calculations are shown in the Figure by the solid curve. On the same curve, in addition to the experimental data[5,6] and the heat capacities taken from the Kaye and Laby[7] and Landolt[8] handbooks, there are also the plotted heat capacities found from the Debye temperatures, determined by Iona[9] for a model of a point lattice and for equal mass of the K and Cl ions; these points are shown by crosses. As is evident from the Figure, it is impossible to express any preference for the present analysis by comparison with the results of Iona. This is associated with the fact that the heat capacity, being an integral value, is not very sensitive to calculation. The fact that at low temperatures the heat capacity was somewhat high indicates a somewhat high value of the parameters a_{11} and a_{22} of the non-electrostatic interaction forces between the ions of KCl, which were taken by the author from Ref. 3.

The author takes this opportunity of expressing his gratitude to K. B. Tolpygo for his constant interest in the work and for valuable comments.

1 T. I. Kucher, J. Exptl. Theoret. Phys. (U.S.S.R.) **32**, No. 3 (1957).

2 K. B. Tolpygo and I. G. Zaslavskaia, Trudy Phys. Inst. Akad. Nauk SSSR, **4**, 71 (1953).

3 K. B. Tolpygo, Trudy Phys. Inst. Akad. Nauk SSSR **6**, 102 (1955).

4 K. B. Tolpygo, Trudy Phys. Inst. Akad. Nauk SSSR **5**, 28 (1954).

5 Clusius, Goldmann and Perlick, Naturforsch, **4a**, 6, 424 (1949).

6 W. H. Keesom and C. W. Clark, Physica **2**, 698 (1935).

7 D. Kaye and T. Laby, *Handbook for Physicists*, IIL, Moscow 1949 p. 160 (Russian translation).

8 L. B. Landolt, 3, part 3 p. 2269.

9 M. Iona, Phys. Rev. 60, 822 (1941).

Translated by E. Rabkin
27

Investigation of γ–Rays from Po–Li and Po–Mg Neutron Sources

Iu. A. Nemilov, A. N. Pisarevskii

(Submitted to JETP editor June 30, 1956)

J. Exptl. Theoret. Phys. (U.S.S.R.) 32, 139–140 (1957)

When lithium and magnesium are bombarded with α–particles of polonium, all (αn) and (αp) reactions are energetically possible with the exception of reactions αn upon Li^6 and Mg^{24}. Gamma rays are formed in the investigated sources as a result of the nucleus, the product of the corresponding reaction, being in an excited state, or because of its further radioactive decay.

The study of the γ–spectra was carried out by means of single or double crystal scintillation spectrometers and utilizing in the measurement system high stability multipliers FEU–12 which were kindly made available to us by G. S. Vildgrube. The resolution (relative width of the line at its half height) for the Cs^{137} 660 kev γ–line was in all cases not greater than 12%. The stability of the measuring system was so high that during the work extending over more than a month the apparatus did not require any additional calibration.

Figure 1 shows the γ–spectrum obtained from the Po–Mg source. The following γ–rays were found: 0.23; 0.8; 1.25; 1.85; 2.3; 4.2 mev. For lines

which were observed on a single crystal spectrometer, attempts made to detect $\eta-\gamma$ coincidences yielded negative results. Neutron–gamma coincidences could not be observed in measurements with the double spectrometer because of its low efficiency.

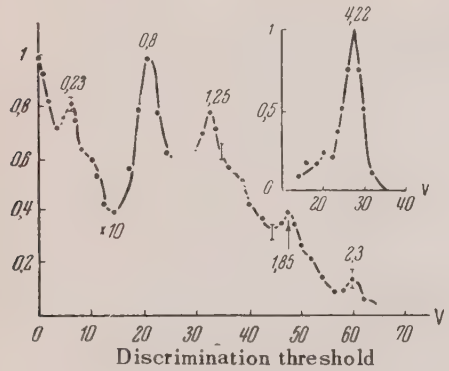

FIG. 1. γ-spectrum (in relative units) of Po-Mg source using a single crystal spectrometer. The γ-line $\sim$ 1 mev is not shown. In the upper right are shown results of measurements with a double spectrometer.

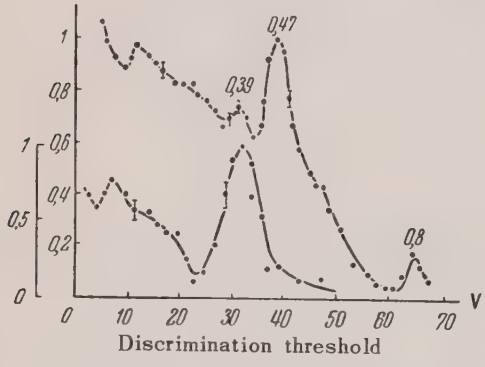

FIG. 2. γ-spectrum of Po-Li source obtained with a single crystal spectrometer. Lower curve: n-γ coincidences. Resolving time for coincidences 2×10^{-7} sec.

The 0.8 mev γ–rays are most likely the known line observed at disintegration of Po^{210} (ref. 1), γ–lines 1.85, 1.25 and 2.3 mev are apparently the result of one of the (αp) reactions. Line 1.85 mev probably corresponds to the disintegration of Al^{28} formed in the reaction (αp) on Mg^{25} (Ref. 2). Gamma rays 1.25 and 2.3 mev are apparently the result of disintegration of Al^{29} (Ref. 3).

Some indirect but quite difinite indications of the existence of γ–rays of the order of 4 mev are contained in Refs. 4–5, In this work we have found, using a double spectrometer, γ–rays of 4.2 mev. These lines may be related to one of the exothermic type (αn) reactions: either to Mg^{25} (αn) Si^{28} with reaction energy $Q = 2.7$ mev or to Mg^{26} (αn) S_i^{29} with $Q = 0.04$ mev, which may lead to the formation of the corresponding nuclei in a state excited to 4.2 mev. From energy considerations, other reactions cannot lead to products of such high state of excitation. For the reasons mentioned above it was impossible to find directly $n-\gamma$ coicidences with the 4.2 mev line. A special verification, using slowed down neutrons, indicated that the detected γ–rays cannot be related to the reaction of the neutron sticking to any material of the equipment.

The inensity of the weak line $\sim$ 1 mev was considerably increased when the measurement crystal CsI (Tl) or NaI(Tl) was surrounded by an I scatterer. It seems to us therefore more reasonable to ascribe this line to the inelastic scattering of neutrons by I rather than to the radiation from the excited state of Al^{28} or Al^{29} as is done in Ref. 4. The energy of the line, 1 mev, agrees well with the energy (1.01 mev), of one of the γ-lines observed in the inelastic scattering of neutrons by I (Ref. 6).

Several assumptions may be stated concerning the origin of the 0.23 mev γ-rays. They are not related to (αn) type reactions, since $n-\gamma$ coincidences did not yield a positive answer. No substantial changes in the intensity of the 0.23 mev line were observed when the measurement crystal was surrounded by the Na or I scatterers; the latter preclude the possibility of accounting for this line by the inelastic scattering of neutrons by the material of the crystal. Possibly these γ-rays are the result of one of the (αp) type reactions mentioned above. The possibility of their occurrence as a result of the excitation of the Mg nuclei by the inelastic scattering of α–particles cannot be rejected.

Figure 2 shows the γ–spectrum of the Po–Li source. Two γ–lines, 0.39 and 0.47 mev can be observed (besides the 0.8 mev γ–line of Po^{210}). The 0.47 mev line is most probably the result of excitation of Li^7 nuclei by the inelastic scattering of α–particles. The obtained γ–ray energy agrees well with results of other investigations.[7-8] When the measurement crystal was surrounded with Na or I scatterers the intensity of the 0.39 mev line practically did not change. Measurements of $n-\gamma$ coincidences indicate coincidence of γ-rays with 0.39 mev neutrons (see Fig. 2). This permits us to conclude that the 390 kev γ-rays are connected with the decay of the excited B^{10} state formed in the reaction Li^7 (αn) B^{10}. Indirect indications of theexistence of such a state of B^{10}

are contained in Ref. 9. No satisfactory explanation has yet been obtained of the origin of the low energy peak in the n–γ coincidence curve (Fig. 2). The 1.5 mev γ– rays for Po–Li previously reported in Ref. 8, have not been observed by us.

1 Siegbahn, Ark. Mat. Astr. Fys, 34A, 15 (1947).
2 K. K. Sheline and N. R. Jonson, Phys. Rev. 90, 352 (1953).
3 Seidlitz, Blueler and Tendam, Phys. Rev. 76, 861 (1949).
4 R. J. Breen and M. R. Hertz, Phys. Rev. 98, 599 (1955).
5 A. Szaly and E. Csongor, Phys. Rev. 74, 1063 (1948).
6 E. A. Wolf, Phil. Mag, 1, 102 (1956).
7 C. W. Li and R. Sherr, Phys. Rev. 96, 389 (1955).
8 K. C. Speh, Phys. Rev. 50, 689 (1936).
9 Hornyak, Lauritsen, Morrison and Fowler, Rev. Mod. Phys. 22, 291 (1950).

Translated by J. L. Herson
19

Concerning the Temperature Dependence of the Magnetic Susceptibility of the Elements

B. I. VERKIN
Physico-Technical Institute, Academy of Sciences, Ukrainian SSR

(Submitted to JETP editor September 10, 1956)
J. Exptl. Theoret. Phys. (U.S.S.R.) 32, 156-157
(January, 1957)

THE experimentally-observed magnetization of a substance is made up of the diamagnetism and paramagnetism of the ionic lattice and the diamagnetism and paramagnetism of the free carriers of charge (for instance the conduction electrons of the metals). Accordingly, one can assume that for the susceptibilities of the elements

$$\chi_{exp} = \chi^{-}_{ion} + \chi^{+}_{ion} + \chi^{-}_{elect} + \chi^{+}_{elect} \qquad (1)$$

(the signs – and + designate the dia- and paramagnetic contributions to the measured susceptibility).

The accepted classification of magnetic substances is based on the sign of the susceptibility measured experimentally. Examination of the experimental data concerning the temperature dependence of the susceptibility of the elements permits us to suggest another method for classifying magnetic materials, based on the character of the temperature dependence of the susceptibility in weak magnetic fields. In line with this proposal, one has to consider four groups of elements, exhibiting 1) paramagnetism which is practically independent of temperature (the alkali and alkali-earth metals), 2) paramagnetism which depends on temperature (the rare earths and the transition metals), 3) diamagnetism which depends on temperature (Be, Mg, Zn, Cd, Hg, Al, Ga. In, Tl, C, Sn, Pb, As, Sb, Bi), and 4) diamagnetism which is independent of temperature (the noble gases, etc.). The character of the temperature dependence of the susceptibility within each group is determined by the predominance of one of the terms in (1). Thus, paramagnetism which is practically temperature-independent indicates the predominance of the paramagnetic contribution of the conduction electrons; temperature-dependent paramagnetism is related to the predominance of the paramagnetic contribution of the ionic lattice; temperature-dependent diamagnetism (as will be shown below) reflects the predominance of the diamagnetic contribution of the conduction electrons; and finally, the magnetic properties of the fourth group of elements indicates the predominance of the diamagnetic contribution of the ionic lattice.

One should pay particular attention to the fact that the elements of the four groups indicated occupy a definite place in the so-called long periodic system of the elements (Fig. 1).* For all metals of the third group, the de Haas-van Alphen effect is observed at low temperatures. With respect to their atomic spectra and the magnetic properties of their crystals, Be and Mg are closer to Zn and Cd than to the alkali-earth metals, and consequently they are situated in the 26th, rather than in the 2nd column of the periodic system. Copper, silver and gold occupy an intermediate position between the transition metals and the elements of the third group; the magnetic properties of sulfur, selenium, tellurium and polonium have been inadequately and insufficiently studied.

The existing theory of the magnetic properties of electrons in metals,[1,3] which includes an explanation of the essential features of the de Haas-van Alphen effect in assuming the existence in these metals of anomalously small groups of electrons, gives the following expression for the constant component of the magnetic susceptibility:[2,3]

$$\chi = \chi_0 (1 - \pi^2/12)(T/T_0)^2 \quad \text{for } T \ll T_0, \qquad (2)$$

$$\chi = {}^2/_3 \chi_0 T_0/T \quad \text{for } T \gg T_0, \qquad (3)$$

where

$$\chi_0 = \frac{\sqrt{2}}{4\pi} \cdot \frac{e^2}{hc^2} \frac{M_i}{\sqrt{m_1 m_2 m_3}} E_0^{1/2} \left[3 \left(\frac{m_{эфф}}{m_0} \right)^2 - 1 \right],$$

and T_0 is the degeneracy-temperature of the electrons comprising the small groups, responsible for the fundamental frequency of the de Haas-van Alphen effect. If $m_{eff} < m_0$, then $x_0 < 0$ and correspondingly $x < 0$.

The temperature dependence of x/x_0 predicted by these relations is presented graphically in Fig. 2. The curves a and b correspond to equations (2) and (3); the curve b is a typical experimental curve for the temperature dependence of x/x_0 for metals of the third group. It is obvious that for $T \ll T_0$ and $T \gg T_0$ the existing theory qualitatively conveys the character of the temperature dependence for the third-group metals. The dependence of their diamagnetic susceptibility on temperature, as well as the de Haas-van Alphen effect, is explained by the presence of the anomalously small groups of electrons with low degeneracy-temperatures. Since m_{eff} is anisotropic, it is clear

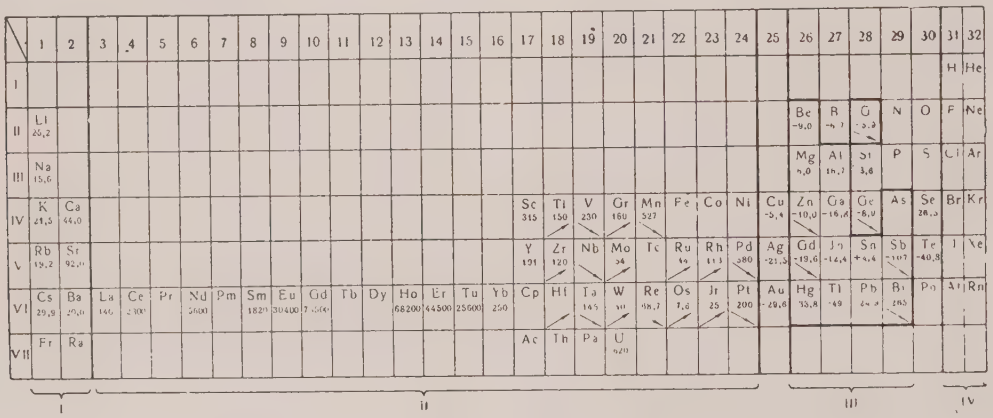

FIG. 1. The location in the periodic table of elements whose susceptibility varies in different ways with temperature. I — paramagnetic substances whose paramagnetism is practically independent of temperature; II — elements whose paramagnetism depends on temperature; III — elements whose diamagnetism increases with decreasing temperature; metals exhibiting the de Haas-van Alphen effect at low temperatures are encircled with heavy lines; IV — diamagnetic materials whose susceptibility is temperature-independent.

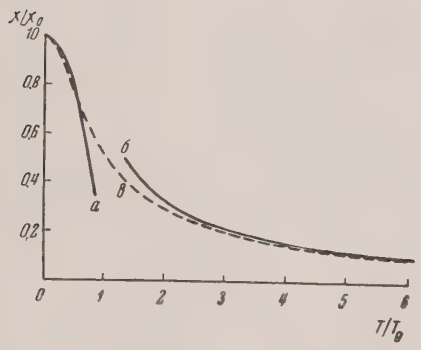

FIG. 2. The temperature dependence of the susceptibility of the conduction electrons in metals: a — theoretical curve for $T \ll T_0$; b — theoretical curve for $T \gg T_0$.

that the temperature dependence of $x_{||}$ and $x_{\perp}$ can be different. We note that the calculated values of the quantity x_0, taken from data for m_1, m_2, m_3, and E_0, obtained from investigations of the de Haas-van Alphen effect, are close to the experimental values. It is necessary to point out that the principle (large) group of electrons with a high degeneracy-temperature gives only an additive constant of the same order of magnitude.

Thus a systematic investigation of the temperature dependence of the magnetic susceptibility of the metals of the third group represents another possible method of studying the energy spectrum of electrons in metals experimentally.

It would also be of interest to look for the de Haas-van Alphen effect in crystals of Ge and in the γ-phase of a series of alloys (for example Cu_5Zn_8) whose susceptibilities exhibit the same temperature dependence as the metals of the third group.

* In Fig. 1 the numerals represent the values of the atomic susceptibilities of the elements at room temperature; the arrows indicate the change of the susceptibility coefficient of each element as the temperature increases.

1 L. D. Landau, see the Appendix to the article by Shoenberg, Proc. Roy. Soc. (London) **A170**, 341 (1939). A. I. Akhiezer, Dokl. Akad. Nauk USSR **23**, 874 (1939). I. M. Lifshitz and A. M. Kosevich, Dokl. Akad. Nauk USSR **96**, 963 (1954).
2 Iu. B. Rumer, J. Exptl. Theoret. Phys. (U.S.S.R.) **18**, 1081 (1948).
3 G. E. Zil'berman, J. Exptl. Theoret. Phys. (U.S.S.R.) **21**, 1209 (1951); **25**, 713 (1953).

Translated by W. M. Whitney
30

Temperature Dependence of the Magnetic Susceptibility of Electrons in Metals

G. E. ZIL'BERMAN AND F. I. ITSKOVICH

(Submitted to JETP editor May 28, 1956)
J. Exptl. Theoret. Phys. (U.S.S.R.) **32**, 158-160
(January, 1957)

WE have investigated the temperature dependence of the magnetic susceptibility x of electrons over a wide range of temperatures in weak magnetic fields, where x is practically independent of H. The necessity of this investigation for the classification of magnetic materials was pointed out to us by Verkin[1]. The following cases were studied: I) only small groups of electrons are present; II) there is, in addition to these small groups, a large group of electrons; III) besides the foregoing there is a large group of holes. The calculation is carried out for a quadratic law of dispersion with respect to the spin paramagnetism and to the anisotropy of the effective masses.

We consider hexagonal crystals like bismuth (for other types of symmetry the results do not differ qualitatively). We make the usual assumption that these crystals have three identical small groups in the form of ellipsoids, the axes of which make an angle of 120° in the plane of the binary axes.

Case I. Carrying out our calculations as in Refs. 2 and 3, we obtain the component x_i (3 is the index of the principal axis) of the three groups referred to:

$$\chi_i = -{}^1/_2 AB_i (kT)^{1/2} F_{-1/2}(\zeta/kT) = -AB_i \sqrt{\zeta_0}\, \mathrm{X} \quad (1)$$

(since $m_i \ll m_0$, where m_0 is the mass of a free electron, we can ignore the spin paramagnetism). In this equation,

$$A = \sqrt{2}\, e^2/6\pi hc^2,\ B_1 = B_2 = 3(m_1+m_2)/2\sqrt{m_1 m_2 m_3},\ B_3 = 3m_3/\sqrt{m_1 m_2 m_3}; \quad (2)$$

$$\chi = {}^1/_2 \sqrt{\theta}\, F_{-1/2}(u); \quad (3)$$

$$\theta = \frac{T}{T_0},\ T_0 = \frac{\zeta_0}{k}, \quad (4)$$

$$\zeta_0 = \zeta|_{T=0} = \left(\frac{nh^3}{16\pi\sqrt{2m_1 m_2 m_3}}\right)^{2/3};$$

$$F_s(u) = \int_0^\infty \frac{x^s dx}{1+e^{x-u}},\quad u = \frac{\zeta}{kT}.$$

The dependence of the chemical potential ζ on temperature is determined from the condition that the concentration n of electrons be constant, which gives

$$\theta = [{}^3/_2 F_{1/2}(u)]^{-2/3} \quad (5)$$

By calculating the function $F_{\pm 1/2}$, we determine from Eqs. (3) and (5) the function $X(\theta)$, which is the desired dependence $X(T)$ in generalized coordinates, and also $\zeta(\theta)/\zeta_0$. For the limiting cases – strong degeneracy and Boltzmann statistics – we obtain

$$\begin{aligned} T \ll T_0 &: \mathrm{X} = 1 - \pi^2\theta^2/12, \\ &\zeta/\zeta_0 = 1 - \pi^2\theta^2/12; \\ T \gg T_0 &: \mathrm{X} = 2/3\theta, \\ &\zeta/\zeta_0 = (3/2)\,\theta \ln[(16/9\pi)^{1/3}\theta^{-1}]. \end{aligned} \quad (3')$$

Curves of $X(\theta)$ and $\zeta(\theta)/\zeta_0$, and also their asymptotic expressions (broken curve), are presented in Fig. 1. A series of metals has just this temperature dependence for x.

Case II. The dependence of the chemical potential ζ' of a large group (we consider its ellipsoid of revolution with $m_1' = m_2' \sim m_3' \sim m_0$) on T is represented here, as it turns out, by the same curve (Fig. 1) as in the preceding case (only the scale is changed; the new reduced temperature $\theta' = T/T_0'$, where $T_0' = \zeta_0'/k$; generally $\zeta_0' \gg \zeta_0$). From the definition of $\zeta(T)$ (for a small group) it turns out that the parameter $\alpha = \zeta_0/\zeta_0' \lesssim 1$.

The overall magnetic susceptibility of the small (X_α) and large groups is equal to

$$\chi_i = -A\sqrt{\zeta_0'}\,[B_i \mathrm{X}_\alpha(\theta') + B_i' \mathrm{X}(\theta')], \quad (6)$$

$$\begin{aligned} B_1' = B_2' &= 1/\sqrt{m_3'} - 3m_1'\sqrt{m_3'}/m_0^2, \\ B_3' &= \sqrt{m_3'}/m_1' - 3m_1'\sqrt{m_3'}/m_0^2, \\ \mathrm{X}_\alpha(\theta') &= \frac{1}{2}\sqrt{\theta'}\, F_{-1/2}\left[u'(\theta') - \frac{1-\alpha}{\theta'}\right]; \end{aligned} \quad (6')$$

$$\theta = \frac{\theta'}{\alpha} \ll 1, \tag{7}$$

$$X_\alpha = \sqrt{\alpha}\left[1 - \frac{\pi^2}{24}(1+\alpha)\theta^2\right]$$

Curves of $X_\alpha(\theta')$ are presented in Fig. 2. If $\alpha \ll 1$, $X_\alpha(\theta')$ has a minimum for $T \sim T_0$ and a weakly-expressed maximum for $T \sim T_0/2$; if $\alpha > \alpha_0 \sim 0.2$, $X_\alpha(\theta')$ decreases monotonically, approaching $X(\theta')$ for $\alpha \sim 1$. For $T \gg T_0'$, $X_\alpha(\theta') = 2/3\,\theta' = X(\theta')$.

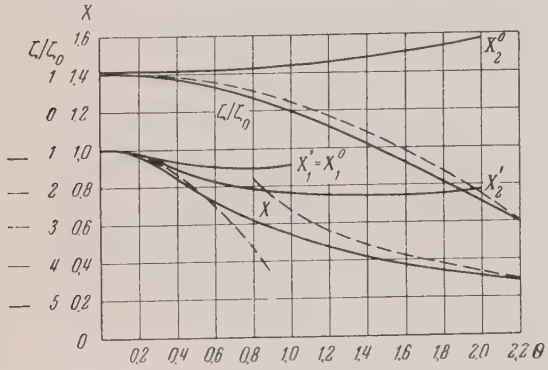

FIG. 1

For the sum of the two terms in (6) there are several possibilities, depending on the values of α and the effective masses (in particular, B_i' can be negative), but for $T \lesssim T_0 \ll T_0'$ the temperature dependence is determined principally by the small groups.

Case III. In this case the total number of particles increases with temperature, but $n_{el} - n_{holes} = \text{const}$. We shall take $n_{el} = n_{holes}$, which gives

$$\gamma^{3/2} F_{1/2}(u') = F_{1/2}\left(\frac{1+\gamma}{\theta'} - u'\right), \tag{8}$$

$$\gamma = \left(\frac{m_1' m_2' m_3'}{m_1^0 m_2^0 m_3^0}\right)^{1/3}$$

Here there appears only a single parameter γ; the mass $m_i^0 \sim m_0$ relates to the assembly of holes, which we also consider in terms of its ellipsoid of rotation around the principal axis. The condition (8) can give a qualitatively different dependence for $\zeta'(T)$ than (5). Namely, $\zeta'(T)$ can not only decrease ($\gamma > 1$), but also increase ($\gamma < 1$), and even stay identically constant ($\gamma = 1$), whereupon the law of the change of ζ' at low T is parabolic, as before; however for $T \to \infty$, $\zeta \sim T$ [compare (3')].

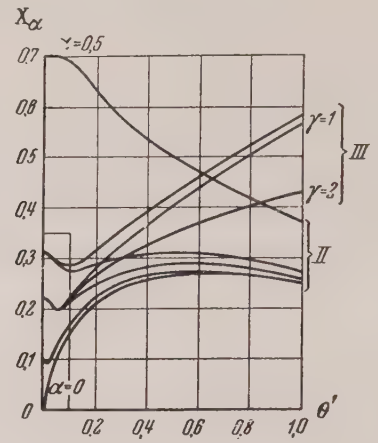

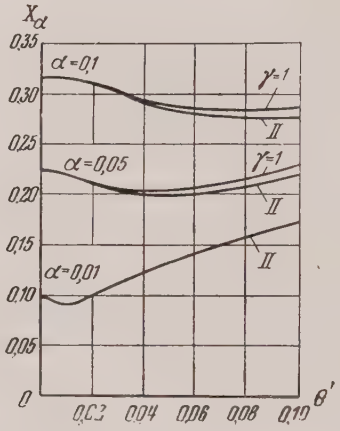

The total magnetic susceptibility is now equal to:

$$\chi_i = -A\sqrt{\zeta_0'}\,[B_i X_{\alpha,\gamma}(\theta') + B_i' X_\gamma'(\theta') - B_i^0 X_\gamma^0(\theta')], \tag{9}$$

where the B_i^0 are determined in the same way as the B_i' (6');

$$X_{\alpha,\gamma}(\theta') = \frac{1}{2}\sqrt{\theta'}\,F_{-1/2}\left[u_\gamma'(\theta') - \frac{1-\alpha}{\theta'}\right]$$
$$X_\gamma'(\theta') = -\frac{1}{2}\sqrt{\theta'}\,F_{-1/2}[u_\gamma'(\theta')], \tag{10}$$
$$X_\gamma^0(\theta') = \frac{1}{2}\sqrt{\theta'}\,F_{-1/2}\left[\frac{1+\gamma}{\theta'} - u_\gamma'(\theta')\right];$$

here $u_\gamma'(\theta')$ is a function determined from (8). For low T:

$$X_{\alpha,\gamma} = \sqrt{\alpha}\left[1 - \frac{\pi^2}{24}\left(1 + \frac{\gamma - 1}{\gamma}\alpha\right)\theta^2\right] \qquad (10')$$

$(T \ll T_0)$;

$$X'_\gamma = 1 + \frac{\pi^2}{12}\,\frac{1-2\gamma}{2\gamma}\,\theta'^2; \qquad (10'')$$

$$X^0_\gamma = \sqrt{\gamma}\left(1 + \frac{\pi^2}{24}\,\frac{\gamma - 2}{\gamma^2}\,\theta'^2\right) \quad (T \ll T'_0).$$

(10') for $\alpha \ll 1$ agrees with (7); the function (10''), depending on γ, can also increase as well as decrease. For high T all three functions (10), and consequently x_i as well (9), increase (for $T \gg T'_0$ they are proportional to $\sqrt{T}$, whereupon $X_{\alpha\gamma} = X^0_\gamma$).

Several representive curves are presented in Fig. 1 for (X_γ', X_γ^0) and in Fig. 2 for $(X_{\alpha\gamma})$. For the sum of these curves (with corresponding coefficients) the various possibilities are even more numerous than in Case II. In particular, one can obtain a curve containing several maxima, similar to the experimental curve of Verkin (4) for Zn. For $T \lesssim T_0 \ll T'_0$ the small groups give the basic temperature dependence, as before.

The authors express their thanks to I. M. Lifshitz, B. I. Verkin and M. I. Kaganov for discussions of this work.

1 B. I. Verkin, J. Exptl. Theoret. Phys. (U.S.S.R.) 32, 156 (1957); Soviet Phys. JETP 5, 117 (1957).

2 G. E. Zil'berman, J. Exptl. Theoret. Phys. (U.S.S.R.) 21, 1209 (1951).

3 G. E. Zil'berman and R. S. Kuznetskii, [Trudy Kh. P. I. (Kharkov Pedagogical Institute) No. 2, 1956].

4 B. I. Verkin and I. F. Mikhailov, J. Exptl. Theoret. Phys. (U.S.S.R.) 24, 342 (1953).

Translated by W. M. Whitney
31

Contribution to the Thermodynamical Theory of Ferroelectrics

I. A. Izhak
Dnepropetrovsk State University

(Submitted to JETP editor September 25, 1956)
J. Exptl. Theoret. Phys. (U.S.S.R.) 32, 160-162
(January, 1957)

FROM the thermodynamical theory of ferroelectrics developed by Ginzburg[1,2], there follows a series of important conclusions concerning the dependence of the dielectric properties of barium titanate on mechanical stress. Strictly speaking, the theory applies only to single-domain monocrystals; however, in the paraelectric region it is expedient to attempt to compare experimental data obtained for polycrystals with the conclusions of the theory. Below we present data which we have obtained for polycrystalline samples of $BaTiO_3$, which corroborate certain conclusions of the thermodynamical theory.

1. The expansion of the thermodynamical potential Φ in the presence of an elastic stress σ_{ik} differs from the analogous expansion in the absence of a stress only in the coefficients α_i for the polarization p_i^2 [3,4]. If there exists only a single compression, along the x-axis, for instance, then for the parallel and perpendicular directions we have respectively:

$$\alpha_1 = \alpha - \varkappa_1\sigma_{xx}, \quad \alpha_2 = \alpha - \varkappa_2\sigma_{xx}, \qquad (1)$$

where $\varkappa_1$, $\varkappa_2$ are the strain coefficients, and α the expansion coefficient in the absence of compression.

It is possible to determine the coefficients α_1 and α_2 from measurements of the dielectric constant:[1,4]

$$\alpha_1 = 2\pi/\varepsilon_{xx}, \quad \alpha_2 = 2\pi/\varepsilon_{yy} \quad (T > \Theta). \qquad (2)$$

In Fig. 1 is shown the experimental behavior of the coefficient α_1 as a function of pressure (unilaterally applied) for various temperatures above the Curie point, calculated from our measurements of the dielectric permittivity for polycrystalline $BaTiO_3$ in a weak field (7 volts/cm) at high frequency (1 Mc/s). It is clear that the linear dependence of α_1 on unilateral pressure, as required by the theory, is well realized over a wide range of pressure, in which

$$\varkappa_1 \approx +\,0.75\cdot10^{-12}\ \text{cm}^2/\text{dyne} \qquad (3)$$

For measurements of ϵ in the direction perpendicular to the axis of compression, the linear dependence is violated for pressures beyond 500 kg/cm^2, but in the region where linearity is preserved,

$$\varkappa_2 \approx -\,0.23\cdot10^{-12}\ \text{cm}^2/\text{dyne} \qquad (4)$$

The values (3) and (4) are smaller than the estimates based on x-ray measurements and the temperature dependence of the spontaneous polari-

zation ($\varkappa_1 \approx +3 \times 10^{-12}$ cm^2/dyne, $\varkappa_2 \approx -1.10 \times 10^{-12}$ cm^2/dyne)[4], but they agree with them in sign and merely agree in magnitude, indicating the possibility of determining the coefficients $\varkappa_1$ and $\varkappa_2$ from dielectric measurements, with the aid of thermodynamical relations.

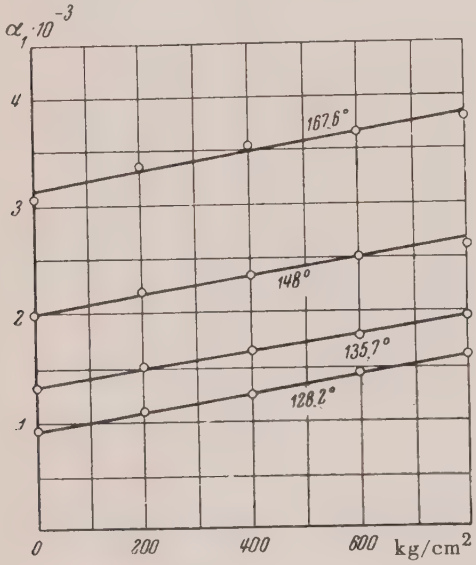

FIG. 1

2. In the thermodynamical theory it is assumed that near the Curie point it is possible to use the expansion

$$\alpha = \alpha'_\theta (T - \Theta) \quad (T > \Theta). \tag{5}$$

The data presented in Fig. 2 show that the coefficient α_θ', determined from the slope of the straight line (5), remains constant over a wide range of temperature and pressure, and thereby confirm the validity of the expansion (5) assumed in the theory. The numerical value of α_θ' for the samples which we investigated was approximately 5.8×10^{-5} deg^{-1}.

3. By treating the data for $\varkappa_1$ and α_θ', obtained experimentally from measurements of the dielectric permittivity, it is possible to estimate the displacement of the Curie point under unilateral compression. Theoretically this displacement is equal to the following:[4]

$$\Delta\Theta \approx -\varkappa_1 \sigma_{xx} / \alpha'_\theta \approx +13 \cdot 10^{-3} \text{ deg} \cdot \text{cm}^2/\text{kg}.$$

From experimental measurements it is approximately equal to 2.8×10^{-3} deg cm^2/kg;[5] that is, it has the same sign and the same order of magnitude as the value calculated from the theoretical formula.

4. Experimental results[5,6] show that the maximum relative change of ϵ under the influence of pressure is observed near the Curie point.

For unilateral compression for $T > \theta$ the theoretical dependence of the relative change of the dielectric permittivity, as measured along the axis of compression, on the temperature is given by the expression

$$\frac{\Delta\varepsilon}{(\varepsilon_{xx})_0} = \frac{\varkappa_1 \sigma_{xx}}{\alpha'_\theta (T - \theta) - \varkappa_1 \sigma_{xx}} \quad \text{or} \quad \frac{(\varepsilon_{xx})_0}{\Delta\varepsilon} \tag{6}$$

$$= -\left(\frac{\alpha'_\theta \theta}{\varkappa_1 \sigma_{xx}} + 1\right) + \frac{\alpha'_\theta}{\varkappa_1 \sigma_{xx}} T = A + BT,$$

where A and B depend on the mechanical stress. Consequently, in the para-electric region the reciprocal of the magnitude of the relative charge of ϵ at constant pressure depends linearly on temperature , but the slope of the straight line is negative ($\sigma_{xx} < 0$) and diminishes in absolute magnitude with increasing pressure. In Fig. 3 are presented the corresponding experimental data, calculated from measurements of ϵ for polycrystalline samples of $BaTiO_3$ in the paraelectric temperature region. As is obvious from these data, the kind of dependence $(\varepsilon_{xx})_0/\Delta\varepsilon = f(T)$ required by the theory is well realized.

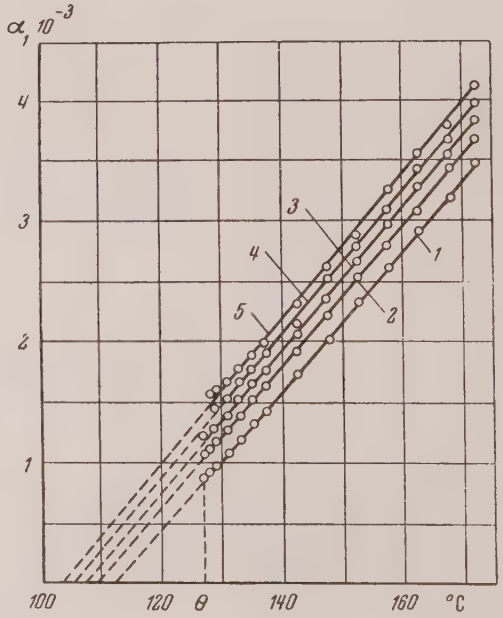

FIG. 2. $1 - p = 0$, $2 - p = 200$ kg/cm^2, $3 - p = 400$ kg/cm^2, $4 - p = 600$ kg/cm^2, $5 - p = 800$ kg/cm^2

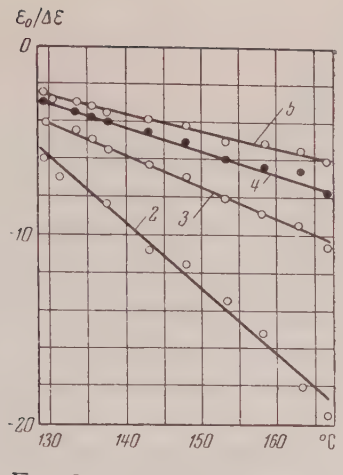

FIG. 3. 2, 3, 4, 5—the same as in Fig. 2.

The comparison which has been made between the conclusions of the theory and the experimental data supports the possibility of applying the theory to polycrystalline $BaTiO_3$, at least in the paraelectric region. Regarding the ferroelectric region, satisfactory agreement between theory and experiment is observed only for temperatures no more than 10-12° below the Curie point.

1 V. L. Ginzburg, J. Exptl. Theoret. Phys. (U.S.S.R.) **15**, 739 (1945).
2 V. L. Ginzburg, Usp. Fiz. Nauk 38, 490 (1949).
3 V. L. Ginzburg, J. Exptl. Theoret. Phys. (U.S.S.R.) **19**, 36 (1949).
4 L. P. Kholodenko and M. Ia. Shirobokov, J. Exptl. Theoret. Phys. (U.S.S.R.) **21**, 1250 (1951).
5 E. V. Siniakov and I. A. Izhak, Dokl. Akad. Nauk SSSR 100, 243 (1955).
6 I. A. Izhak, Izv. Akad. Nauk SSSR Ser. Fiz. **20**, 199 (1956).

Translated by W. M. Whitney
32

On Quantum Effects Occurring on Interaction of Electrons with High Frequency Fields in Resonant Cavities

V. L. GINZBURG AND V. M. FAIN
P. N. Lebedev Physical Institute, Academy of Sciences USSR, and Gor'kii State University
(Submitted to JETP editor September 21, 1956)
J. Exptl. Theoret. Phys. (U.S.S.R.) **32**, 162-164
(January, 1957)

RECENTLY, a number of papers[1-7] were published in which an analysis was made of the quantum effects occurring during the interaction of electrons with high frequency fields in resonant cavities. And in the first place, the dispersion of the kinetic energy or the electron velocity, produced during their passage through the resonator, was calculated. Erroneous deductions are contained in some of the above mentioned papers, however, and in others[4,5,7], classical results were sometimes considered as quantum; quantum-mechanical methods were used for finding expressions, which are simpler, and which in the more general case can be obtained by a classical method. At the same time, the problem of the passage of electrons through resonators is one of the most important in electronics; moreover, the region of high frequencies ω and low temperatures T, when the condition of classicity $\hbar\omega \ll kT$ is disturbed, is acquiring increasingly greater interest. Therefore, we considered it appropriate to discuss briefly the problem which is stated in the title (this is carried out in greater detail in Ref. 8).

We will analyze classically the following problem: a non-relativistic electron enters into the resonator at the instant $t = 0$ with a kinetic energy $K_0 = mv_0^2/2$, and emerges from the resonator at the instant $t = \tau$ with a kinetic energy $K_\tau = mv_\tau^2/2$. Moreover, for simplicity we will consider the electric field E in the resonator along the electron path as homogeneous and directed along its velocity (such a case is completely real). When

$$E = E_1 \cos\omega t + (E_2 + E_0)\sin\omega t, \qquad \text{(a)}$$

we obtain:

$$m\frac{dv}{dt} = eE, \quad v_\tau = v_0 \qquad (1)$$

$$+ \frac{e}{m\omega}[E_1 \sin\omega\tau + (E_2 + E_0)(1 - \cos\omega\tau)].$$

Let now E_1 and E_2 be random values, so that $\overline{E_1} = \overline{E_2} = 0$ and $\overline{E_1^2} = \overline{E_2^2} = \overline{V^2}/d^2$, where d is the path traversed by the electron (thickness of the resonator), and $\overline{V^2}$ is the mean square of the fluctuating voltage; the averaging, which is denoted by the bar, was carried out over the corresponding ensemble of identical systems. As in the papers cited above, we shall also consider the action of the field in the resonator on the electron motion as a small effect, in the strength of which we can limit ourselves to the terms of the e^2 order, and for the time of the electron flight through the resonator we shall assume $\tau = d/v_0$. Then, as can be easily seen,

$$\overline{(\Delta K_\tau)^2} = \overline{K_\tau^2} - [\overline{K}_\tau]^2 = \frac{4e^2 v_0^2}{\omega^2 d^2} \overline{V^2} \sin^2 \frac{\omega\tau}{2} \quad (2)$$

$$= e^2 \overline{V^2} \left[\frac{\sin(\omega\tau/2)}{\omega\tau/2} \right]^2$$

In addition, since $(\overline{\Delta v})^2 \ll v_0^2$, the dispersion of the velocity $\overline{(\Delta v_\tau)^2} = \overline{(\Delta K_\tau)^2} m^{-2} v_0^{-2}$. Under the conditions when $\omega t \ll 1$, $\overline{(\Delta K_\tau)^2} = e^2 \overline{V^2}$, that is, we obtain the expression (for the field constant with time) that is evident from the law of the conservation of energy. If oscillations of various frequencies are present in the resonator, then

$$\overline{(\Delta K_\tau)^2} = e^2 \int_0^\infty \overline{|V_\omega|^2} \left[\frac{\sin(\omega\tau/2)}{\omega\tau/2} \right]^2 d\omega, \quad (3)$$

$$\overline{V^2} = \int_0^\infty \overline{|V_\omega|^2} d\omega.$$

When only one natural oscillation is taken into account, a resonator is equivalent to a circuit consisting of (for example) a series connected resistance R, self-inductance L and capacity C, so that the impedance of the circuit when an emf $\epsilon = ZI$ is applied will be equal to $Z = R + i(\omega L - 1/\omega C)$. In this type of circuit, if we consider the condition of the thermal equilibrium, the spectral density of the fluctuating emf, in accordance with the Nyquist quantum theory[9,10], will be equal to

$$\overline{|\varepsilon_\omega|^2} = \frac{2}{\pi} R(\omega) \left\{ \frac{\hbar\omega}{2} + \frac{\hbar\omega}{e^{\hbar\omega/kT} - 1} \right\}, \quad (4)$$

the density of the square of the current $|I_w|^2 = \overline{|\varepsilon_\omega|^2}/|Z(\omega)|^2$ and the density of the square of the voltage on the condenser

$$\overline{|V_\omega|^2} = \frac{\overline{|\varepsilon_\omega|^2}}{C^2 \omega^2 |Z(\omega)|^2} \quad (5)$$

$$= \frac{\overline{|\varepsilon_\omega|^2}}{R^2 C^2 \omega^2 + (LC\omega^2 - 1)^2}$$

Substituting (4) into (5) and then (5) into (3), we obtain the final expression for $(\overline{\Delta K})_\tau^2$. For a weakly damped resonator with a frequency $\omega_0 = (LC)^{-1/2}$, as can be easily shown, we will obtain from the general expression for $(\overline{\Delta K}_\tau)^2$ (see, for example, Ref. 10):

$$\overline{(\Delta K_\tau)^2} = \frac{e^2}{C(\omega_0)} \left(\frac{\hbar\omega_0}{2} + \frac{\hbar\omega_0}{e^{\hbar\omega_0/kT} - 1} \right) \quad (6)$$

$$\times \left(\frac{2}{\omega_0 \tau} \sin \frac{\omega_0 \tau}{2} \right)^2$$

Senitzky[4] and Weber[7] obtained these results by using the quantum-mechanical theory of perturbations. The corresponding calculations are first, more complex and less clear, and second, are limited by the region of small damping. At the same time, these results hold for any damping of the circuit. A more detailed comparison of the obtained expressions with those given in Refs. 4,7 was carried out in Ref. 8. In the same paper, an analysis was made of the problem under discussion within the frame of canonical formalism, which is limited by the case of weak damping and, obviously, will lead to Eq. (6).

It should be noted also that in quantum-electrodynamic solution of the problem of the electron passage through a resonator, the same as in a number of other cases, the use of the ordinary theory of perturbations is limited (see Ref. 12 and also Refs. 8, 11), and in some cases it becomes necessary to use a more complex procedure of calculations[3, 12] which in the final count leads to essentially classical results.

From formulas (4) – (8) we see that the total quantum effect in the problem of the passage of electrons through a resonator is determined by the account of the quantum fluctuations of the radiation in the resonator and, in particular, of the zero oscillations with the energy $\hbar\omega/2$. In Refs. 4 and 5, it is asserted that there exists also a quantum effect associated with the account of the wave properties of electrons. It can be shown, however, that the dispersion of the electron velocity, as well as the dispersion of the field, calculated in Refs. 4 and 5, and associated with the scattering of the initial position and the momenta of the electrons, can be obtained also as a result of a considerably simpler classical calculation[8]. The single quantum element, moreover, consists in the fact that the initial distributions of the electron velocity and momenta are limited by the ratio of uncertainty. This limitation, however, is apparently completely insignificant in practice, even if we disregard the fact that its existence does not change the assertion of the possibility of purely classical analysis of the electron motion in a resonator within the accuracy with which the calculations were carried out in Refs. 4 and 5.

In conclusion, it should be noted that the portion of the velocity dispersion determined by the zero vibrations, which in the case of (6) is equal to

$$\overline{(\Delta v_\tau)^2} = e^2 \hbar\omega / 2Cm^2 v_0^2, \quad (b)$$

is quite small[8], although it may be of theoretical interest in the analysis of the performance of electronic instruments.

1 L. R. Smith, Phys. Rev. **69**, 195 (1946).
2 D. Gabor, Phil. Mag. **41**, 1161 (1950).
3 I. R. Senitzky, Phys. Rev. **91**, 1309 (1953).
4 I. R. Senitzky, Phys. Rev. **95**, 904 (1954).
5 I. R. Senitzky, Phys. Rev. **98**, 875 (1955).
6 P. S. Farago and G. Marx, Acta Phys. Hung., **4**, 23 (1954); Phys. Rev. **99**, 1063 (1955).
7 J. Weber, Phys. Rev. **94**, 215 (1954); **96**, 556 (1954).
8 V. L. Ginzburg and V. M. Fain, Radiotekhnika i Elektronika **2**, (1957).
9 H. B. Callen and T. A. Welton, Phys. Rev. **83**, 35 (1951).
10 V. L. Ginzburg, Uspekhi Fiz. Nauk **46**, 348 (1952); Fortsch. d. Physik **1**, 51 (1953).
11 V. L. Ginzburg, Dokl. Akad. Nauk SSSR **23**, 773 (1939); **24**, 130 (1939).
12 A. I. Akhiezer and V. B. Berestetskii, *Quantum Electrodynamics*, Sec. 32, GTTI, 1953.

Translated by E. Rabkin
33

On the Problem of K^0 Decays

I. Iu. Kobzarev

(Submitted to JETP editor October 25, 1956)
J. Exptl. Theoret. Phys. (U.S.S.R.) **32**, 180-181 (January, 1957)

IF we assume that in K-meson decays parity is conserved, then from the whole of the experimental data it apparently follows that there exist two mesons τ and θ with spin and parity 0^- and 0^+ respectively. Then it must be supposed that there exists a certain "degeneracy in parity" for the "strange particles"[1]. On the other hand one can assume that there exists only one K meson and that parity is not conserved in the decay interactions[2]. In the present note we point out one possibility for an experimental test of the hypothesis of nonconservation of parity.

We suppose that parity is conserved and consider the decay of a τ^0 meson. The possible decay schemes for it will be

$$\tau^0 \nearrow \pi^+ + \pi^- + \pi^0, \quad \tau^0 \searrow 3\pi^0, \qquad \tau^0 \to \begin{matrix}\mu^\pm \\ e^\pm\end{matrix} + \nu + \pi^\mp.$$

Like the θ^0 meson, the τ^0 meson must represent a mixture of charge-even and charge-odd components

$$\tau^0 = \left(\tau_s^0 + i\tau_a^0\right)/\sqrt{2}\,.$$

τ_s^0 will decay according to all four possible schemes, with the decay $\tau_s^0 \to 3\pi$ being the isotopic analogue of the τ^+ decay.

For τ_a^0 the decay $\tau^0 \to 3\pi^0$ is forbidden, and the decay $\tau^0 \to \pi^+ + \pi^- + \pi^0$ must go into states with orbital angular momentum different from zero and will be suppressed, so that the main decay for it will be

$$\tau_a^0 \to \begin{matrix}\mu^\pm \\ e^\pm\end{matrix} + \nu + \pi^\mp.$$

For both components the lifetime will be of the order of 10^{-7} sec.[3]

The situation is fundamentally changed if we assume that there exists one K meson but that decays occur with nonconservation of parity. In this case the main decay for the K_s^0 component will be $K^0 \to \pi^+ + \pi^-$; this decay is a fast one, so that the lifetime of K_s^0 will be $t \sim 10^{-10}$ sec. The charge-odd component, for which two-meson decay is impossible[4], will decay mainly according to the schemes

$$K^0 \to \begin{matrix}\mu^\pm \\ e^\pm\end{matrix} + \nu + \pi^\mp \quad \text{or} \quad K^0 \to 2\pi + \gamma$$

with lifetime $t \sim 10^{-8}$-10^{-7} sec.

Let us consider the decay curve of $\tau^0 \to \pi^+ + \pi^- + \pi^0$. In the case of conservation of parity, we must observe two slightly separated exponentials with nearly equal lifetimes $t \sim 10^{-7}$ sec. But in the case of nonconservation of parity we must observe together with an exponential of lifetime $t \sim 10^{-8}$-10^{-7} sec a short-lived component with lifetime of the order of 10^{-10} sec.

I express my thanks to I. Ia. Pomeranchuk for a discussion.

1 T. D. Lee and C. N. Yang, Phys. Rev. **102**, 290 (1956).
2 R. P. Feynman, Proc. Sixth Rochester Conference.
3 G. A. Snow, Phys. Rev. **103**, 1111 (1956).
4 M. Gell-Mann and A. Pais, Phys. Rev. **97**, 1387 (1955).

Translated by W. H. Furry
43

Reply to Critical Remarks of I. F. Kvartskhava[1] Concerning our Papers[2-6]

S. V. LEBEDEV
P. N. Lebedev Physical Institute, Academy of Sciences, USSR
(Submitted to JETP editor June 18, 1956)
J. Exptl. Theoret. Phys. (U.S.S.R.) 32, 144–145 (1957)

IN Refs. 2–6, we investigated the dependence of the electrical emission on the energy E released from a metal at currents $i \sim 10^5 - 10^7$ amp/cm^2. Let us review the basic results of these experiments: *a*. The anomalous dependence $R \neq R(E)$ is not observed prior to the beginning of melting of the metal[6]. *b*. Melting begins and ends with the usual values of E and R: $E = W_n + W_{fl}$, $R(W_n) = R_{fl}^s$ $R(W_n + W_{pl}) = R_{fl}^l$.[6,7] *c*. When E reaches the value E_c, the metallic reistance suddenly disappears and the metal explodes[2,5,6,7]. Essentially, E_c increases with the increase of current i. *d*. Near the melting point of the metal, there are observed anomalies of electron emission[3,6] *e*. In lamps with wolfram cathodes, for which the anomalous emission is very high, Langmuir's law does not hold.[4].

Dependence of E_c on i and the anomalous emission could not be attributed to errors. An assumption was therefore made concerning the anomalous condition of the metal. In Ref. 5 a faulty deduction was made that at $i = 5 \times 10^5$ amp/cm^2 the metal does not become liquid at $E = W_n + W_{fl}$. As indicated by the correct interpretation of these experiments, given in Ref. 7, the error made in Ref. 5 is not connected with inaccuracies of R and E measurements.

2. It may seem from Ref. 1 that, in Refs. 2 to 6, we arrived at a conclusion concerning the anomalous dependence of R on $E \leq W_n$ and the breakdown of Ohm's law. But the absence of anomalous R and E at $E \leq W_n$ was established with an accuracy of $\sim 5\%$ in Ref. 6 (pp. 97–100, Fig. 4).

We have never observed deviations from Ohm's law; on the contrary, in Ref. 5, p. 613 and Ref. 6, p. 108, it is noted that the error which lead other experimenters to the deduction concerning the breakdown of this law, is due to inductive distortions of the oscillograms. The same error as in Ref. 1 is unjustifiably ascribed to us, (Ref. 2, p. 630). The assertion of Kvartskhava not withstanding, an induction correction was introduced in Ref. 2 and in the oscillograms Fig. 7 which is indicated on p. 634 of that work.

It should be noted that in Ref. 1 (point 1) our point of view was not formulated correctly. The correct formulation of our conclusions is presented above.

3. Kvartskhava states that our measurements of R and E are incorrect, and that the observed excess energy of the wire at resistance of i is connected with macroscopic movements of the metal and not with internal energy. However, our conclusions are confirmed by new data[7] according to which at $i \geq 5 \times 10^6$ amp/cm^2, the motion of the metal prior to the explosion is not of sufficient duration to disturb the constancy of the cross section along the wire. Therefore the high values and energy of the entire wire enable us to find R and E for $E < E_c$, which has been confirmed by measurements of R_{fl}^s, W_n and W_{fl} for Ni and W[6] and by measurement of R_{fl}^l / R_{fl}^s for Cu.[7]

If the current is switched off at a valve E even a little less than E_c, the wire does not explode and instead disintegrates into drops, the kinetic energy of which $K << E \sim W_n$.[7] Therefore neither the explosion nor the excess energy $\sim W_n$ (of the E_c dependence on i) can be explained on the basis of K. The description of the explosion mechanism in Refs. 1 and 8 (Sec. 4) is in our opinion incorrect.

4. In Ref. 1 there is an attempt to explain the anomalies observed by us of the anode current I_a by the glowing discharge. The author asserts that when discharge takes place along the wire, the relation of the "electronic" I_a to the "ionic" I_i is determined by the ratio of the ion mass to electron mass m_i/m_e and that this relation is observed in our experiments. But as the charge ignites the growth of currents I_i and I_a are limited by the properties of the external links and not by the ratio m_i / m_e (Ref. 3, p. 724). The small value of I_i / I_a measured by us in the absence of discharge* is also not determined by the ratio m_i / m_e, inasmuch as I_i / I_a changes in the course of the experiment and depends on the degassing of the electrodes (Ref. 4, Sec. 2 and Ref. 3, Sec. 3).

5. It is stated incorrectly in Ref. 1 that, at anode voltages $V_a < 1$ kv used by us, the magnetic field of the wire heating current i, should in general lock the anode current I_a as long as there is no discharge along the wire. For the evaluation of the critical anode potential, V_k in Ref. 1 was taken as $i = 10^3$ amp and $i = 10^2$ amp

and the obtained $V_k \approx 100$ *kv* and $V_k \approx 1$*kv*, i.e, $V_k > V_a$. However, in Ref.3, we measured I_a when i passed through zero and remained less than 15 amp. (Ref. 3, Fig. 13) while $V_k \leq 23\ V_k < V_a$. In experiments with $V_a \approx 6v$ condition $V_k < V_a$ is also fulfilled, inasmuch as I_a is here measured with the complete exclusion of current i Ref.4, upper curve, Fig. 3*g*). To a lesser degree this condition is observed in Ref. 6, Sec. 2, where I_a was measured at i = 17 amp, but even in this case

$$V_k < 29\ \text{V} < V_a (62\ \text{V} \leqslant V_a \leqslant 70\ \text{V}).$$

It is obvious that the condition $V_k < V_a$ was maintained during our measurements: besides the anomalous current I_a there is also observed the normal anode current which precedes it and which, according to Ref. 1, cannot take place in the absence of discharge (Ref. 4, Fig. 4, *g*,*h* and Fig. 6, *a*–*h*, where $V_k \approx 90\ V < V_a$). The absence of discharge is insured here because in normal emission Langmuirs' law holds and the $I_a = I_a\ (t)$ curve has a plateau (Ref. 4, p. 496).

Thus, the explanation proposed in Ref. 1 of the anomalous anode current as caused by the discharge, and the explanation of the E_c dependence on i by the macroscopic movement of the metal, are contrary to the results of our experiments. The data contained in Ref. 1 and 8 do not furnish a basis for renouncing the conclusions given above (*a*–*e*).

*During measurements of I_a and I_n the potential difference between the ends of the emitter was maintained below the discharge ignition potential.

1 I. F. Kvartskhava, J. Exptl. Theoret. Phys. (U.S.S.R.) 30, 621 (1956); Soviet Phys. JETP 3, 787 (1956).
2 S. V. Lebedev and S. E. Lhaikin, J. Exptl. Theoret. Phys. (U.S.S.R.) 26, 629 (1954).
3 S. V. Lebedev and S. E. Khaikin, J. Exptl. Theoret. Phys. (U.S.S.R.) 26, 723 (1954).
4 S. V. Lebedev, J. Exptl. Theoret. Phys. (U.S.S.R.) 27, 487 (1954).
5 S. V. Lebedev, J. Exptl. Theoret. Phys. (U.S.S.R.) 27, 605 (1954).
6 L. N. Borodovskaia and S. V. Lebedev, J. Exptl. Theoret. Phys. (U.S.S.R.) 28, 96 (1955); Soviet Phys. JETP 1, 71 (1955).
7 S. V. Lebedev, J. Exptl. Theoret. Phys. (U.S.S.R.) 32, No. 2 (1957).
8 Kvartskhava, Pliutto, Chernov and Bondarenko, J. Exptl. Theoret. Phys. (U.S.S.R.) 30, 42 (1956); Soviet Phys. JETP 3, 40 (1956).

Translated by J. L. Herson
22

Investigation of the Allotropic Transformation $\alpha \rightleftarrows \beta$ Zr with the Aid of an Electronic Projector

A. P. Komar and V. N. Shrednik

Leningrad Physico-Technical Institute, Academy of Sciences, SSSR

(Submitted to JETP editor October 29, 1956)
J. Exptl. Theoret. Phys. (U.S.S.R.) 32, 184 (January, 1957)

THE use of an electronic projector permits a visual observation of phase transformations in metals at crystal particle dimensions of the order of 10^{-4}-10^{-5} cm, with a resolving power of 100-20A. The investigation of transformations in such small crystals has independent interest, since the increased role of surface energy must have an effect at such small dimensions.

The usual Muller[1] electronic projector was used, with a zirconium point, the monocrystalline tip which was the object of investigation. The investigation of zirconium in an electronic projector makes special demands on the quality of the vacuum, since with heating, there is a strong tendency to form oxides, nitrides, and carbides of zirconium which are extremely refractory and nonvolatile, and consequently, are not removed from the surface by heating the point in vacuum.

In spite of the fact that the pressure of the residual gases in the bulb of the projector was less than 10^{-8} mm of mercury, it was not possible to obtain a picture of the autoelectronic emission of a smooth crystal similar to the well known picture of a pure tungsten point.

Crystal particles such as α-Zr (hexagonal close packed lattice), as well as β-Zr (cubic volume-centered lattice) were obtained with corrugations. It is natural to associate the corrugation and the clearly expressed faceting of the crystal with the well-known action of an electric field on the crystal during heating[2]. The faceting of the crystal by faces of the cube {001} and {122} is apparently associated with the intrusion into the surface layer of nitrogen atoms from the residual gases. The nitrogen atoms occupy the spaces between metal atoms, which in addition to smoothing the atomic unevenness, increases the durability of the surface layer.

The following steps were taken for the "purification" of the surface: 1) the layer-by-layer

destruction of the surface by heating the point while a high positive potential was applied to it, with a gradient of 1.4×10^8 V/cm at the surface, and 2) condensation on the surface of the zirconium point of a large quantity of zirconium from an external source in a vacuum of the order of 10^{-8} mm of mercury.

By heating the point above the transformation temperature (862°C), it was easy to form a β-Zr crystal, which during cooling was transformed over the entire volume into a unique α-Zr crystal. The process of $\beta \rightarrow \alpha$ transformation was not always geometrically reversible, because with a repeated rise of temperature, a cubic crystal would

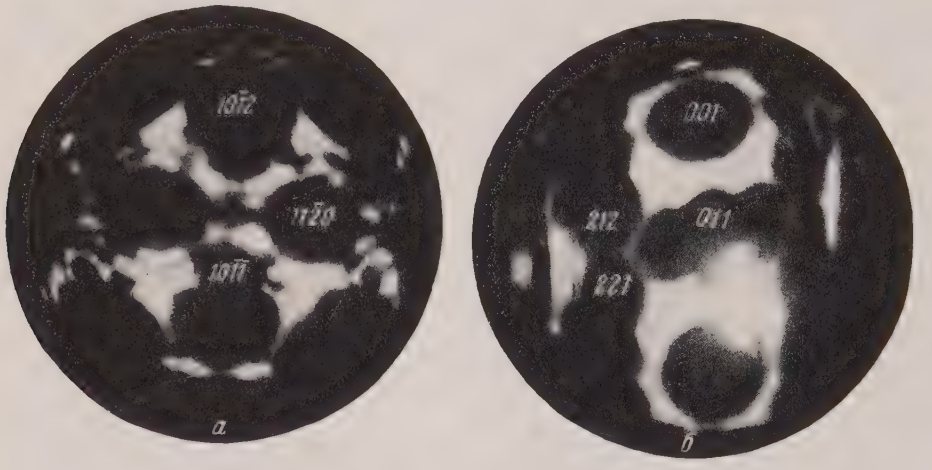

Autoelectronic pictures of zirconium monocrystals at the tip of a point: a – hexagonal crystal. The axis [0001] is vertical in the plane of the figure. $T = 20°C$. Crystal diameter $d_0 = 1.6\mu$; b – cubic crystal. $T = 1060°C$, $d_0 = 3\mu$.

sometimes form with a different orientation than the original. However, in all of the observed cases for the mutual orientation of the crystal the original and new phases satisfied the relations found by Burgers[3] with x-rays

$$\{0001\}_\alpha \parallel \{110\}_\beta \quad \text{and} \quad [11\bar{2}0]_\alpha \parallel [\bar{1}11]_\beta.$$

This allows the possible occurrence of 12 orientations of the new phase for $\beta \rightarrow \alpha$ transitions, and 6 orientations of the new phase for $\alpha \rightarrow \beta$ transitions, corresponding to one orientation of the original phase. But for the observed microcrystals, the experiments showed that as a rule, one (rarely two) of the possible orientations of the new phase was realized. Similar effects were observed by Brock[4] with titanium. It was noted that of the possible orientations, those which lead to the minimum change of surface energy were realized. This is quite natural for crystals of such small dimensions.

A noticeable rise of the transition temperature with an increase of heating duration was observed, associated with absorption by the zirconium of O_2 and N_2 from the residual gases at a pressure lower than 10^{-8} mm of mercury.

A more detailed presentation and discussion of these experiments will be given in the Journal, "Physics of Metals and Metallurgy".

1 E. W. Muller, *Ergebn. exakt. Naturwiss*,. 27, 290 (1953).
2 I. L. Sokol'skaia, J. Exptl. Theoret. Phys. (U.S.S.R) 26, 1177 (1956).
3 W. G. Burgers, *Physica*, 1, 561 (1934).
4 E. G. Brock, *Phys. Rev.* 100, 1619 (1955).

Translated by D. Lieberman
46

On the Question of the Spin and Parity of the τ–Meson

I. S. SHAPIRO, E. I. DOLINSKII AND
A. P. MISHAKOVA
Moscow State University,
Academy of Sciences, USSR
(Submitted to JETP editor October 5, 1956)
J. Exptl. Theoret. Phys. (U.S.S.R.) 32, 173–175
(January, 1957)

A COMPARISON of the experimental data on the energy spectrum and angular distribution of the π–mesons formed in τ^{+-} decay with the theoretical curves of Dalitz[1] leads to the conclusion that the most probable spin and parity values for the τ–meson are 0^-. Dalitz' curves were obtained on the assumption that in the τ–decay the π–mesons are produced in states with the smallest possible orbital angular momenta. Since the correctness of this assumption is not obvious, Marshak[2] pointed out the possibility of securing agreement of the experimental and theoretical data on the energy spectrum of the π–mesons by assuming that the spin and parity of the τ–meson have the values 2^+ and that the mesons are emitted with orbital angular momenta (2,1) and (2,3) (in each of the parentheses, the first number is the relative orbital angular momentum of the two π^+–mesons and the second is the orbital angular momentum of the π^-–meson relative to the center of mass of the two π^+–mesons). In the present paper, we use ideas not previously taken into consideration to show that the experimental data exclude the possibility considered by Marshak. The basis on which we proceed is as follows.

1. We assume that the isotopic spin $I_{3\pi}$ of the system of three π–mesons produced in the τ–decay is equal to 1. This hypothesis, already put forward by several writers (Gell–Mann,[3] Wentzel[4]) follows directly from the Gell–Mann scheme,[5] according to which the τ–meson has isotopic spin

$$I_\tau = 1/2$$

and the slowness of the decay

$$\tau^+ \to \pi^+ + \pi^+ + \pi^-$$

is explained by nonconservation of isotopic spin. It is natural to suppose that the smallest possible change of isotopic spin takes place.

2. We regard the K–mesons that undergo the τ'–decay.

$$\tau'^{\pm} \to \pi^{\pm} + 2\pi^0,$$

as identical with τ–mesons.

3. According to the experimental data*[6–8] the ratio of the probabilities of τ and τ' disintegration is close to 4:

$$W_\tau / W_{\tau'} \approx 4.$$

As has been shown independently by Dalitz[9] and by Berestetskii[10], if the assumptions 1) and 2) are valid the ratio of these probabilities satisfies the equation:

$$W_\tau / W_{\tau'} = (4F + \Phi) / (F + \Phi),$$

where F is a quantity obtained by integrating with respect to the energies of the π–mesons the squares of the absolute values of matrix elements symmetric in the momenta of all π–mesons, and Φ is an analogous quantity obtained from matrix elements symmetric only with respect to the momenta of identical π–mesons. Thus we come to the conclusion that $\Phi \approx 0$, or in other words that the π–mesons are produced in states symmetric in the momenta of all three particles. We note that if this is the case the spectrum of the π^+–mesons from τ' decay must be identical with the spectrum of π^- mesons from τ–decay.** The lower orbital angular momenta corresponding to such states are shown in Table 1, where there are also shown for comparison the orbital angular momenta and types of matrix elements used by Dalitz.

The diagram shows curves for the energy spectrum of the π–mesons calculated from matrix elements of symmetric states with the orbital angular momenta indicated in Table I (for the formulas by which the calculation was done, cf. Ref. 11). The experimental data are shown in the diagram in the form of a histogram representing the total of 492 cases of τ^+–decay* published in the literature.[12–20] As can be seen from the diagram, the curves corresponding to spins and parities 1^+, 1^-, and 2^+ differ markedly from the experimental spectrum. The curve for the case 2^-, although indeed closer in shape to the experimental distribution, agrees with it considerably less well than the curve corresponding to spin and parity 0^-. These conclusions are confirmed by calculations of the quantity χ^2 and the Pearson probability P_{χ^2} which are shown in Table 2.

Summarizing what has been said above, we come to the following conclusions: a) the most probable values of the spin and parity of the τ–meson are the combination 0^-; b) the combinations 1^+, 1^-, and 2^+ must be regarded as practically excluded.

Thus the most probable values of the spin and parity of the τ–mesons turn out to be just the values that lead to the appearance of the so–called "τ– ϑ problem."

In conclusion we express our sincere gratitude to Prof. I. I. Gurevich for an interesting discussion of the results.

TABLE I

Spin and parity of the $\mathcal{T}$-meson	0^-	1^+	1^-	2^+	2^-
Minimal pairs of values (l, l') for symmetric states	$(0,0)\,F$	$(2,1)\,F$	$(4,4)\,F$	$(2,3)\,F$	$\begin{matrix}(0,2)\\(2,0)\end{matrix}\,F$
Minimal pairs of values (l, l') and types of matrix elements used by Dalitz[1]	$(0,0)\,F$	$(0,1)\,\Phi$	$(2,2)\,\Phi$	$(2,1)\,\Phi$	$\begin{matrix}(0,2)\\(2,0)\end{matrix}\,F$

TABLE II*

Spin and parity of the $\mathcal{T}$-meson	0^-	2^-	1^-	1^+	2^+
χ^2	7.53	25.92	68.49	112.32	135.55
P_{χ^2}	0.188	$\sim 10^{-4}$	$< 2\cdot 10^{-16}$	$\ll 10^{-16}$	$\ll 10^{-16}$

*The experimental data are not very exact. In Refs. 6 and 7 the error is not indicated; in Ref. 8, the result

$$W_{\tau'} / W_{\tau} = 0.25 \pm 0.12.$$

is obtained. The analysis of the stability of the results of the present paper with respect to small additions Φ is complicated by interference effects.

**At present there are 34 cases of τ' decay for which the energy of the π^+ meson is known. These data are insufficient, however, for comparison with the theoretical curves because of the small statistical precision.

*After the conclusion of the present work, the writers learned of a paper[21] in which 481 cases of τ^+ decays are collected. The comparison of these experimental data is made, however, with theoretical curves found without taking into account the considerations 1)–3) that are the basis of the present paper.

1 R. H. Dalitz, Phil. Mag 44, 1068 (1954).
2 R. E. Marshak, Notes of the Rochester Conference, 1956.
3 M. Gell–Mann, Notes of the Pisa Conference, 1955.
4 G. Wentzel, Phys. Rev. 101, 1215 (1956).
5 M. Gell–Mann, Notes of the Pisa Conference, 1955.
6 Ritson, Pevsner, Fung, Widgoff and Zorn, S. Goldhaber and G. Goldhaber, Phys. Rev. 101, 1085 (1956).
7 R. W. Birge et al., Proc. of the Pisa Conference, 1955.
8 H. H. Heckman, F.M. Smith et al., Nuovo Cimento 4, 51 (1956).
9 R. H. Dalitz, Proc. Phys. Soc. (London) A66, 710 (1953).
10 V. B. Berestetskii, Dokl. Akad. Nauk SSSR 92, 519 (1953).
11 I. N. Mikhailov, J. Exptl. Theoret. Phys. (U.S.S.R.) 32, No. 2 (1957)
12 Notes of the Pisa Conference, 1955, pp. 22–32.
13 B. T. Feld, A. C. Odian et al., Phys. Rev. 100, 1539 (1955).
14 B. Bhomik, D. Evans et al., Nuovo Cimento 3, 574 (1956).
15 N. N. Biswas and L. Ceccarelli –Fabbrichesi, Nuovo Cimento 3, 825 (1956).
16 R.P. Haddock, Nuovo Cimento 4, 240 (1956).
17 J. Orear, G. Harris et al., Phys. Rev. 102, 1676 (1956).
18 Alpers, Gerasimova, Gurevich et al., Dokl. Akad. Nauk SSSR 105, 236 (1955).
19 Alpers, Gurevich, and Surkova, Dokl. Akad. Nauk SSSR 108, 421 (1956).
20 M. Scharff, Nuovo Cimento 3, 217 (1956).
21 Eisenberg, Lomon and Rosendorf, Nuovo Cimento 4, 610 (1956).

Translated by W. H. Furry
39

Scattering of π–Mesons on Nucleons in Higher Approximations of the Tamm–Dancoff Method

Iu. M. Popov
P. N. Lebedev Physical Institute, Academy of Sciences, USSR

(Submitted to JETP editor September 29, 1956)
J. Exptl. Theoret. Phys. (U.S.S.R.) 32, 169–171 (January, 1957)

IN the Tamm–Dancoff method[1,2] the nucleon–meson equation for the state with isotopic spin $I = 3/2$ is studied in higher approximation than the one used until now. For this purpose, the equations are renormalized and the four–particle approximation is considered. In the equations (written according to the T–D method) for the nucleon–meson and nucleon–two mesons amplitudes (in the Dalitz–Dyson notation[3], for the

$$\langle a_{q\alpha} b_{-qu}\rangle \text{ and } \langle a_{q\alpha} a_{k\beta} b_{-q-kw}\rangle$$

amplitudes, respectively) only those amplitudes (with the number of particles $n \leq 4$ are taken into account) which are found on the right hand sides of the equations for these amplitudes (connected with them by one "step"). The kernels of the resulting equations contain infinities corresponding to the self–energy diagrams of mesons and nucleons, and we always drop these terms from the equations. The system of equations obtained in this manner in the "old" T–D method coincides with the system in the "new" method formulated by Dyson[4] when the amplitudes with "minus" particles are omitted from the latter. In the momentum representation, following Dirac,[5] we are looking for the first of the above–mentioned amplitudes in the following form:

$$\langle a_{q\alpha} b_{-qu}\rangle = \delta(q - q_0) + K_1(qq_0)\,\delta_+(\varepsilon - \omega_q - E_q). \quad (1)$$

Examining the higher approximations of the T–D method, we assume that

$$\varepsilon < m + 2\mu$$

that is to say, no additional mesons are produced and the second amplitude is of the form:

$$\langle a_{q\alpha} a_{k\beta} b_{-q-kw}\rangle = P(\varepsilon - \omega_q - \omega_k - E_{q+k})^{-1} K_2(qkq_0). \quad (2)$$

Taking all the above into account, we obtain the equations for K_1 and K_2

$$K_2(qkq_0) = \int d^3p B(kqp) P(\varepsilon - \omega_p - \omega_k - E_{p+k})^{-1} K_2(kpq_0) + \int d^3p B(qkp) P(\varepsilon - \omega_p - \omega_q - E_{p+q})^{-1} K_2(qpq_0) + iA(qk)[\delta(k - q_0) + \delta_+(\varepsilon - \omega_k - E_k) K_1(kq_0)] + iA(kq)[\delta(q - q_0) + \delta_+(\varepsilon - \omega_q - E_q) K_1(qq_0)]; \quad (3)$$

$$K_1(qq_0) = \int d^3k C(qk)[\delta(k - q_0) + \delta_+(\varepsilon - \omega_k - E_k) K_1(kq_0)] + i\int d^3k L(qk) P(\varepsilon - \omega_q - \omega_k - E_{q+k})^{-1} K_2(qkq_0). \quad (4)$$

$$B(kqp) = \frac{G^2}{2} Q \frac{1}{\sqrt{\omega_q \omega_p}} w_{-q-k}\gamma \times \left(\frac{\Omega^+(-q-k-p)}{\varepsilon - \omega_k - \omega_q - \omega_p - E_{k+q+p}} - \frac{\Omega^-(-q-k-p)}{\varepsilon - E_{q+k+p} - E_{p+k} - E_{q+k} - \omega_k}\right)\gamma v_{-k-p};$$

$$C(qk) = -\frac{G^2}{2} Q \frac{1}{\sqrt{\omega_q \omega_k}} w^*_{-q}\gamma \times \frac{\Omega^-(-q-k)}{\varepsilon - E_k - E_q - E_{q+k}} \gamma u_{-k};$$

$$A(qk) = -iGw^*_{-q-k}\gamma\tau_q v_{-k}/\sqrt{2\omega_q},$$

$$L(qk) = -iGu^*_q\gamma\tau_k w_{-q-k}/\sqrt{2\omega_k},$$

$$\Omega^\pm(p) = [E_p \pm (\alpha p + \beta m)]/2E_p,$$

$$G = g/(2\pi)^{3/2}, \quad Q = (\tau_\gamma\tau_\alpha,\ \tau_\gamma\tau_\beta).$$

The system of equations (3) and (4) contains divergent terms even after removing infinities arising in nuclei. This fact represents the main difficulty in the study of higher approximations of the T–D method for the case of the meson–nucleon equation. We have found such a solution of the non–covariant (three–dimensional) equations (3) and (4) in which the infinities are contained in the functions for the vertex parts and can be removed by renormalization (Itabashi[6] proposed a

similar method of renormalization for covariant equations). The amplitude

$$K_2(qkq_0)$$

can be expressed by the resolvent R_2 of Equation (3) in the following way:

$$K_2(qkq_0) = i\iint d^3q'\, d^3k' R_2(qkq'k')\, A(k'q')\,[\delta(q'-q_0) + \delta_+(\varepsilon-\omega_{q'}-E_{q'})\,K_1(q'q_0)]. \qquad (5)$$

Performing several transformations upon the equation for R_2, analogous to those of Ref. 6, we obtained, after substituting (5) into (4)

$$K_1(qq_0) = \int d^3q' M(qq')\,[\delta(q'-q_0) + \delta_+(\varepsilon-\omega_{q'}-E_{q'})\,K_1(q'q_0)], \qquad (6)$$

$$M(qq') = -[C(qq') + M_1(qq') + M_2(qq') + M_3(qq')]$$

(we omitted from the kernel the term corresponding to the self-energy of the nucleon),

$$M_1(qq') = \Gamma(qq')\,\Gamma'(qq'), \quad M_2(qq') = \int d^3p\,\Gamma(qp) B(pqq')\,\Gamma'(pq'),$$

$$M_3(qq') = \iiiint d^3p\, d^3p'\, dp^{3''}\, d^3p'''\,\Gamma(qp)\, P\frac{B(pqp')}{\varepsilon-\omega_{p'}-\omega_p-E_{p'+p}} R_2(pp'p''p''') \times P\frac{B(p'''p''q')}{\varepsilon-\omega_{p''}-\omega_{p'''}-E_{p''+p'''}}\,\Gamma'(p'''q').$$

The sense of the applied transformation lies in the fact that the infinities contained in the system of equations (3) and (4) are separated in the functions for the vertex parts $\Gamma(qq')$ and $\Gamma'(qq')$:

$$\Gamma(qq') = L(qq')/(\varepsilon-\omega_q-\omega_{q'}-E_{q+q'}) + \int d^3p\,\Gamma(qp)\,B(qpq'), \qquad (7)$$

$$\Gamma'(qq') = A(qq') + \int d^3p B(q'qp)\,\Gamma'(pq').$$

The actual solution of Eqs. (3) and (4) is impossible without separating the angle variables. We shall separate the angles in the equation for

$$K_2(qkq_0)$$

in the case when the total moment of the system—nucleon—two mesons $J = 1/2$, and the angular moments of mesons lie between 0 and 1, which makes it possible to take into account higher approximations for the scattering of pions by nuclei in the S-state. In this way, in the case studied by us, the angular state of two mesons and a nucleon is characterized by the function

$$W_M^{J=1-1/2}(\Omega_1\Omega_2) = \frac{1}{\sqrt{3}} \times \begin{pmatrix} -\sqrt{3/2-M}\; Y_1^{m-1/2}(\Omega_1)\, Y_0^0(\Omega_2) \\ \sqrt{3/2+M}\; Y_1^{m+1/2}(\Omega_1)\, Y_0^0(\Omega_2) \end{pmatrix} \equiv \langle 1_{\Omega_1} 0_{\Omega_2}\rangle_M. \qquad (8)$$

The state of a nucleon and a meson with $l = 0$ is characterized by the function

$$W_M^{1/2}(\Omega) = \frac{1}{\sqrt{3}} \begin{pmatrix} \sqrt{M+1/2}\; Y_0^{M-1/2}(\Omega) \\ \sqrt{-M+1/2}\; Y_0^{M+1/2}(\Omega) \end{pmatrix} \equiv \langle 0_\Omega\rangle_M. \qquad (9)$$

We shall write the amplitudes of K_1 and K_2 as products of functions depending on the absolute value of vectors, and functions depending on the angles

$$K_2(qkq_0) = f_2(qkq_0) \sum_M [\langle 1_q 0_k\rangle_M + \langle 0_q 1_k\rangle_M]\,\langle 0_{q_0}\rangle_M,$$

$$K_1(qq_0) = f_1(qq_0) \sum_M \langle 0_q\rangle_M \langle 0_{q_0}\rangle_M^*. \qquad (10)$$

Making use of the orthogonality of spherical functions with spin, we shall obtain from (3) and (4) a system of equations for the functions f_2 and f_1 which do not contain angle variables (the symbol $\sim$ denotes the independence of angles). The equation for the vertex parts is of the form

$$\tilde\Gamma(qq') = \tilde L(qq') + \int p^2\, dp\,\tilde\Gamma(qp)\,\tilde B(qpq'), \qquad (11)$$

$$\tilde\Gamma'(qq') = \tilde A(qq') + \int p^2\, dp\,\tilde B(q'qp)\,\tilde\Gamma'(pq').$$

We shall introduce new functions:

$$V(zq') = \tilde\Gamma'(zq')/\tilde A(zq'), \quad \Lambda(qz) = \tilde\Gamma(qz)\,\tilde L(qz).$$

For the function

$$V^R(mqq')$$

regularized by the Dalitz–Dyson method,[3] we have

$$V^R(mq0) = 1 + \int dp\,[B_1(moqp) - B_1(moop)]\,V^R(mpo). \qquad (12)$$

When $V^R(mqo)$ is found, we can further find

$$V^R(\varepsilon qq') = V^R(mqo) + W(\varepsilon qq'), \qquad (13)$$

$W(\varepsilon qq')$ satisfies the equation

$$W(\varepsilon qq') = \int dp\,[B_1(\varepsilon q' qp) - B_1(moqp)]\,V^R(mpo) + \int dp\,B_1(\varepsilon q' qp)\,W(\varepsilon pq'o). \quad (14)$$

In an analogous way, the regularized function $\Lambda^R(qq')$ is found. In order to eliminate the complex expressions from the equations for $f_1(qq_0)$, we shall introduce a new function

$$u(q) = f_1(q)\left[1 + \frac{i}{2}\frac{q_0\omega_{q_0}E_{q_0}}{E_{q_0}+\omega_{q_0}}f_1(q_0)\right]^{-1}. \quad (15)$$

After replacing $\tilde{\Gamma}(qq')$ and $\tilde{\Gamma}'(qq')$ by regularized functions $\tilde{\Gamma}^R(qq')$ and $\tilde{\Gamma}'^R(qq')$, the equation for the function $w(q)$ becomes

$$u(q) = \tilde{M}^R(q_0) + \int \frac{(q')^2\,dq'}{\varepsilon - E_{q'} - \omega_{q'}}\,\tilde{M}^R(qq')\,u(q'). \quad (16)$$

The function $w(q_0)$ determines the phase-shift of the scattering of π-mesons on nucleons in the state with isotopic spin $I = 3/2$ by means of the following formula:

$$\delta_S = -\operatorname{arc\,tg}\left[\frac{\pi q_0\omega_{q_0}E_{q_0}}{E_{q_0}+\omega_{q_0}}u(q_0)\right]. \quad (17)$$

The author wishes to express his deep gratitude to Prof. I. E. Tamm for proposing the subject and for his help in its treatment, and also extends his thanks to V. Ia. Fainberg for his advice given in the discussion of the present work.

1 I. E. Tamm, J. Phys. (U.S.S.R.) 9, 445 (1945).
2 S. M. Dancoff, Phys. Rev. 78, 382 (1950).
3 R. H. Dalitz and F.I. Dyson, Phys. Rev. 99, 301 (1955).
4 F.I. Dyson, Phys. Rev. 91, 1543 (1953).
5 P. A. M. Dirac, *The Prinicples of Quantum Mechanics*, 1933.
6 K. I. Itabashi, Progr. Theor. Phys. 12, 585 (1954).

Translated by H. Kasha
37

On the Absolute Value of the Stripping Cross Section and Cross Section for Diffraction Scattering of the Deuteron

I. I. IVANCHIK
P. N. Lebedev Physical Institute, Academy of Sciences, USSR

(Submitted to JETP editor September 21, 1956)
J. Exptl. Theoret. Phys. (U.S.S.R.) 32, 164–165 (January, 1957)

A NUMBER of recent investigations were devoted to the interaction of deuterons with heavy nuclei.[1–5] The cross–section of the diffraction scattering of deuterons on nuclei was calculated in Refs. 3–5, while Ref. 4 treated the case of the diffractive scattering as well. The calculations (for an ideally black nucleus) were effected by seemingly different methods, which, however, can be shown to be essentially identical. Some difference in the final formulas is due to the fact that certain simplifying assumptions of Ref. 4 were too crude.

In Refs. 3 and 4, as well as in usual calculations of the stripping reactions cross–section[6], the wave function of the internal motion in the deuteron is taken as

$$\varphi \sim \exp(-\alpha r)/r,\ \hbar\alpha = \sqrt{M\varepsilon},$$

where M is the nucleonic mass and ϵ is the deuteron binding energy which corresponds to the assumption of a zero radius of the p–n force. The question arises of how a finite force radius would influence the cross sections of the above processes. If we assume a square–well potential of the p–n interaction of radius a and depth U

(where $Ua^2 \sim \pi\hbar^2/2M$),

it is possible to calculate the stripping and diffraction disintegration cross–section by means of the well–known wave function obtained for this case.[7] It is convenient to make use of Glauber's method[5] [see his formulas (5) and (6)]. As the result, we obtain the following expressions for the stripping cross–section σ_{strip} and the diffraction disintegration cross –section σ_{diffr} of deuterons on a black nucleus of radius R:

$$\frac{\sigma_{\text{strip}}}{2\pi R} = \frac{\alpha}{2(1+\alpha a)} \tag{1}$$

$$\times\left[\frac{\cos^2\delta}{4a^2}(1+2\alpha a)+\frac{a^2\cos^2\delta}{\pi+2\delta}(1+2\alpha a)+\frac{a^2}{4}\right],$$

$$\frac{\sigma_{\text{diffr}}}{2\pi R} = \frac{1}{8a}\cdot\left(\frac{4}{3}\ln 2-\frac{1}{3}\right)-\frac{a}{2}\left(\frac{3}{4}-\ln 2\right)$$

$$(\text{for } \alpha a \ll 1). \tag{2}$$

(the exact formula for σ_{diffr} is very cumbersome and for the values of a given in the table yields the same numerical results). In these formulas, δ is determined from the equation

$$\left(\frac{\pi}{2}+\delta\right)\operatorname{tg}\delta = \alpha a.$$

The case $a=0$ corresponds to the usual formula

$$\sigma_{\text{strip}} = \pi R R_d/2 = 0.54\cdot 10^{-13}\, 2\pi R \text{ cm},^2$$

$$\sigma_{\text{diffr}} = \pi R R_d/2\left(\frac{4}{3}\ln 2-\frac{1}{3}\right) = 0.59\,\sigma_{\text{strip}}$$

From the above, numerical computation yields:

$a\cdot 10^{13}$ cm:	0	1	2,82
$(\sigma_{\text{strip}}/2\pi R)\,10^{13}$ cm:	0,54	0,69	0,87
$(\sigma_{\text{diffr}}/2\pi R)\,10^{13}$ cm:	0,32	0,31	0 30

It can be seen that the diffraction scattering cross section is insensitive to the choice of the force radius, while the stripping cross–section is rather strongly dependent on it (for the limiting reasonable choice

$$a = 2.82\cdot 10^{-13} \text{ cm},$$

the result differs by a factor of ~ 1.6). It is possible that this fact can explain the marked discrepancy with the experimentally found cross–section[8] which is larger almost by a factor of three than the one resulting from the equation

$$\sigma_{\text{strip}} = \pi R R_d/2$$

(the effect of the diffraction disintegration is, evidently, contributing essentially to this difference).

1 E. L. Feinberg, J. Exptl. Theoret. Phys. (U.S.S.R.) 29, 115 (1955); Soviet Phys. JETP 2, 58 (1956).

2 A. I. Aliev and E. L. Feinberg, J. Exptl. Theoret. Phys. (U.S.S.R.) 30, 115 (1956); Soviet Phys. JETP 3, 85 (1956).

3 A. I. Akhiezer and A. G. Sitenko, Sc. Pap. Kharkov Univ. 64, 9 (1955).

4 A. I. Akhiezer and A. G. Sitenko, Doklady Akad. Nauk SSSR 107, 385 (1956).

5 R. Glauber, Phys. Rev. 99, 1515 (1955).

6 A. I. Akhiezer and I. Ia. Pomeranchuk, *Certain Problems of the Theory of the Nucleus*, GTTI, Moscow, 1950 p. 137.

7 L. D. Landau and E. M. Lifshitz, *Quantum Mechanics*, GTTI, Moscow, 1948.

Translated by H. Kasha
34

Angular Distribution of the Products of the S^{32} (d,p) S^{33} Reaction

I. B. Teplov, B. A. Iur'ev, and T. N. Markelova

Moscow State University

(Submitted to JETP editor September 24, 1956)
J. Exptl. Theoret. Phys. (U.S.S.R.) 32
165–166 (January, 1957)

THE reactions of the (d,p) type have already been well studied for many light isotopes. For the majority of the nuclei investigated, however, the experiments were carried out for a single value of the incident particle energy. It is of considerable value, in the interest of a more accurate theory of the stripping reaction, to investigate the shape of the angular distribution of the products of such reactions for different energies of incident deuterons. We therefore measured the angular distribution of protons produced in the S^{32} (d,p) S^{33} reaction for 1.8 mev and 3.8 mev deuterons. This reaction was studied earlier by Holt and Marsham[1] for 8.18 mev protons.

The deuterons accelerated in a 72 cm cyclotron bombarded a target of sulphur ($\sim 1\ \mu$ thick) coated on painter's gold. The protons produced in the reaction were registered by nuclear emulsions of the type Ia–2 (100μ thick) placed around the target at the distance of 10 cm.

The angular distribution was measured for two groups of protons, p_0 and p_1, corresponding to the production of the final nucleus in the ground and the first excited states, respectively. The experimental results obtained by us are shown in Figs. 1 and 2, where θ is the angle in the center of mass system and $N(\theta)$ is the number of protons emitted at the angle θ; the dashed lines separate the isotropic part of the angular distribution. The theoretical curves, calculated according to the formula of Bhatia et al.[2] for $R = 6.6\cdot 10^{-13}$ cm

(for this value Holt and Marsham obtained a good agreement with the theory) are shown as well, assuming that in the ground state formation, the neutron is captured with the orbital moment l=2, and in the formation of the first excited state with the orbital moment l=0.

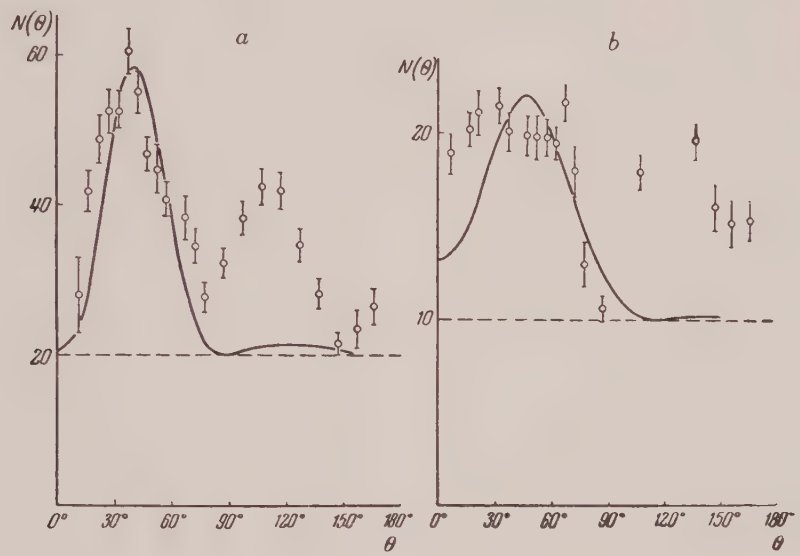

FIG. 1. Angular distributions of the p_0 proton group. Deuteron energy: *a*—3.8 mev; *b*—1.8 mev. The statistical errors are shown. Continuous curves correspond to l=2.

It can be seen that the theoretical curves correctly describe the position of the primary maximum (the small angle maximum) in the distribution of the p_1 protons (Fig.2). In the angular distribution of the p_0 group, the maximum obtained is somewhat wider than the theoretically predicted and is shifted towards smaller angles. This widening and shift of the peak is considerably more pronounced for the 1.8 mev protons than for the 3.8 mev protons. A characteristic feature of the resultant distribution is the presence of relatively large secondary maxima—at about 115° for the p_0 group and 60° for the p_1 group which increase with decreasing energy of incident deuterons. (There are no indications of a secondary peak in the Holt–Marsham distribution; for the case of the non–excited nucleus these authors report the distribution only up to 60 °.) In the angular distribution of the p_1 group, a marked increase for angles close to 180° is also noted.

In order to explain the singularities of the experimental angular distributions obtained by us, it is necessary to take the Coulomb interaction into account, since the effective Coulomb barrier of the S^{32} nucleus for deuterons is equal to 5.1 mev. This, however, shifts the primary maximum towards larger angles and does not bring about the appearance of marked seoondary peaks, as shown by several authors.[3–6] Evidently, a more correct picture could be obtained taking into account not only the Coulomb interaction but the nuclear interaction of the emitted proton with the residual nucleus as well, since it follows from the calculations of Tobocman and Kalos[6] (see also Ref. 7) that the latter interaction should cause the shift of the principal peak towards smaller angles and its narrowing as well as the appearance of secondary maxima of considerable magnitude.

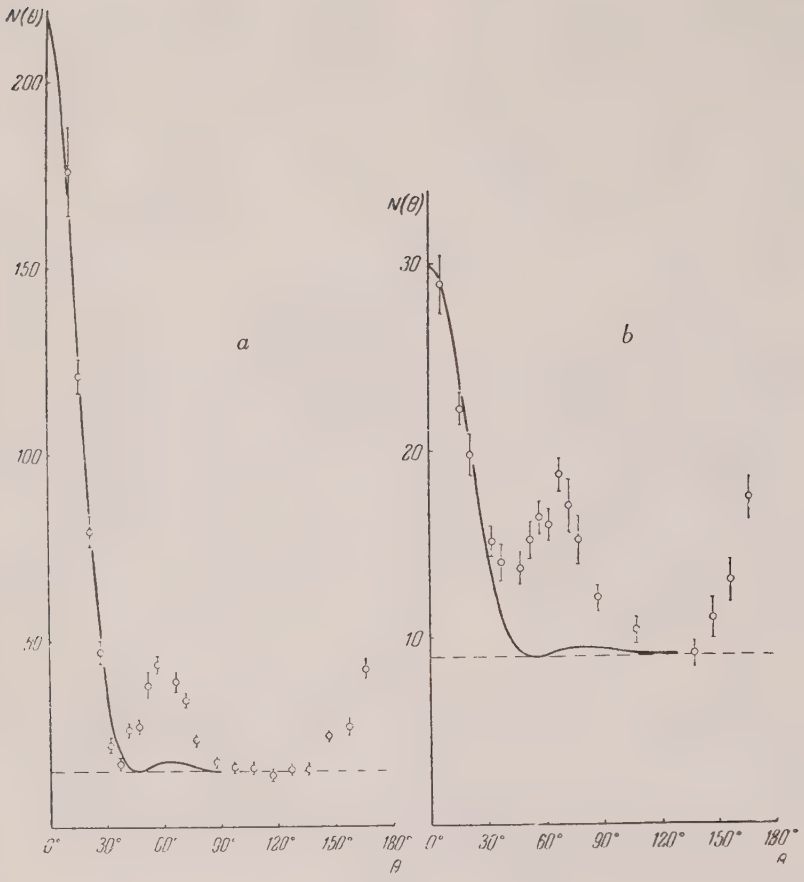

FIG. 2. Angular distributions of the p_1 proton group. Deuteron energy: *a*—3.8 mev; *b*—1.8 mev. Continuous curves correspond to $l = 0$. The scale of the ordinate axis of Figs. 1a and 2a is identical, the same is true for Figs. 1b and 2b.

1 I. R. Holt and T. N. Marsham, Proc. Phys. Soc. (London) A66, 467 (1953).
2 Bhatia, Huang, Huby and Newns, Phil. Mag. 43, 485 (1952).
3 S. T. Butler and N. Austern, Phys. Rev. 93, 355 (1954).
4 J. Yoccoz, Proc. Phys. Soc. (London) A67, 813 (1954).
5 W. Tobocman, Phys. Rev. 94, 1655 (1954).
6 W. Tobocman and N. H. Kalos, Phys. Rev. 97, 132 (1955).
7 J. Horowitz and A. M. L. Messiah, J. Phys. Radium 14, 695 (1953).

Translated by H. Kasha
35

On a Method of Direct Computation of the Nucleon–Nucleon Interaction on the Basis of Experimental Values for the Levels of Light Nuclei

IU. M. SHIROKOV, V. V. BALASHOV AND K. A. TUMANOV

Moscow State University

(Submitted to JETP editor September 29, 1956)
J. Exptl. Theoret. Phys. (U.S.S.R.) 32, 167–168 (January, 1957)

A METHOD is given below for the study of the nucleon–nucleon interaction in nuclei based on the following assumptions: *A*) the forces in nucleus act between pairs of nucleons; *B*) the mean velocity of a nucleon in the nucleus is of the order of 0.1 c or less. Besides these assumptions which are essential for the application of the method, we assume the isotopic invariance of the proper nuclear interaction and neglect the difference in the masses of the proton and the neutron.

The wave function of the nucleus with mass number A is expanded in terms of the products A of single particle eigenfunctions of nucleons in a three–dimensional oscillator well. In this oscillator representation, Schrödinger equations are written down for different nuclei, in which the

matrix elements of nuclear interaction and the coefficients can be eliminated by writing secular equations for the different levels. In the secular equations, only the matrix elements of the nuclear interaction between pairs of particles are unknown, since energy eigenvalues are known from experiment. If the expansion of the wavefunction in terms of the oscillator function converges rapidly, the secular equations can be cut off. The resulting system of the cut–off secular equations is then solved simultaneously for these matrix elements.

The fulfillment of the condition B corresponds to the rapid convergence of the nuclear wave function expansion in terms of the oscillator functions. The oscillator problem consists of finding the minimum value of the expression

$$W = \langle \Delta p^2 \rangle r_0^2 / \hbar^2 + \langle \Delta x^2 \rangle r_0^{-2},$$

proportional to the oscillator energy, where $<. . .>$ denote the mean values in a given state,

$$r_0 = (\hbar / m\omega)^{1/2},$$

ω is the basic oscillator frequency. In a pure oscillator state with the quantum number n, we have

$$W = 2(n + 1/2).$$

If a given state represents a mixture of oscillator states with quantum number n and higher, then

$$W \geqslant 2(n + 1/2).$$

If, on the other hand, it is known that in a certain state $W \approx 1$, then in the expansion of the wave function in terms of oscillator functions, the coefficients with $n > 0$ are small. In general, if

$$W \approx 2(n + 1/2),$$

and all states with quantum number less than n are occupied (in accordance with the Pauli principle), then the only important term in the expansion is the one with quantum number n. The estimation of W for a given nucleus is straightforward. Δx is the nuclear radius, known from experiment, and Δp is obtained from the assumption $v = 0.1$ c (it should be noted that these values of Δx and Δp are subjected to the indetermination relation). The parameter r_0 is chosen in such a way that W is minimum. Calculations for He^4 with

$$\Delta x = 1.2 \cdot 10^{-13} \text{ cm}.$$

yield the value $W \approx 1$. Analogous calculations for heavier elements up to oxygen yield $W \approx 3$. It follows that, in the expansion of the wave functions of H^3, He^3 and He^4 nuclei, only the first oscillator state with $n = 0$ is essential while, for the heavier nuclei up to oxygen, the two first states with $n=0$ and $n = 1$ are essential. The contribution of the other exicted states is small.

The convergence rate of the expansion of the wave function in terms of oscillator functions decreases with the deviation of r_0 from the optimal value for a given nucleus, corresponding to the minimum of W. This optimal value of r_0 varies only slightly for different nuclei:

$$r_0 \sim \sqrt{\overline{\Delta x}} \sim A^{1/6};$$

the expansion of the wave functions of close nuclei can be effected for an oscillator well of the same average width.

Three out of the $3A$ coordinates of the nucleons in a nucleus describe the free motion of the nucleus as a whole. The expansion of a plane wave in terms of oscillator functions diverges and therefore the motion of the system as a whole should be separated before passing to the oscillator representation. The use of Jacobi coordinates makes it difficult to take advantage of the symmetry properties of the wave function. It is more convenient to proceeed as follows: subtract the kinetic energy of the movement of the nucleus as a whole from the total Hamiltonian; the Hamiltonian in the center–of–mass system is then obtained; its eigenfunctions represent the energy levels of the nucleus. In the doubly quantized form, this Hamiltonian is

$$H = \int \psi^+(\mathbf{x}) \frac{\mathbf{p}^2}{2m} \psi(\mathbf{x})\, d\mathbf{x} - \frac{1}{2mA} \left\{ \int \psi^+(\mathbf{x})\, \mathbf{p}\psi(\mathbf{x})\, d\mathbf{x} \right\}^2 - \frac{1}{2} \int \psi^+(\mathbf{x})\, \psi^+(\mathbf{x}')\, V(\mathbf{x} - \mathbf{x}')\, \psi(\mathbf{x}')\, \psi(\mathbf{x})\, d\mathbf{x}\, d\mathbf{x}'.$$

where ψ and ψ^+ are the usual nucleon destruction and creation operators. They are spinors both in the ordinary and in the isotopic space; the interaction

$$V(\mathbf{x} - \mathbf{x}')$$

may contain matrices of both spins. The first two terms in the expression for $\hat{H}$ together represent the kinetic energy operator in the center–of–mass system and can be written in the form

$$-\frac{1}{2A} \int \psi^+(\mathbf{x})\, \psi^+(\mathbf{x}') \frac{(\mathbf{p} - \mathbf{p}')^2}{2m} \psi(\mathbf{x})\, \psi(\mathbf{x}')\, d\mathbf{x}\, d\mathbf{x}'.$$

It should be noted that the operator H commutes with the operators of total momentum and of coordinates of the center–of–mass.

The operators ψ, ψ^+ can be expanded in terms of the oscillator functions

$$\psi_{\mu\nu}(\mathbf{x}) = \sum_{nlm\sigma\tau} b_{nlm\sigma\tau} R_{nl}\left(\frac{r}{r_0}\right) Y_{lm}(\theta, \varphi)\, \chi_\sigma(\mu)\, \chi_\tau(\nu).$$

where n, l and m are the principal, orbital, and magnetic quantum numbers, σ and τ are the projections of the ordinary and isotopic spins. The operators

$$b_{nlm\sigma\tau} \equiv b(q),\ b^+(q)$$

destroy and create nucleons in the state q. In the new representation, the vector of state is given by the sets of functions

$$C_A(q_1, q_2 \cdots q_A),$$

depending on a sets of indices; the Hamiltonian is of the form

$$\hat{H} = \sum_{q_1 q_2 q_1' q_2'} -\frac{1}{2} b^+(q_1)\, b^+(q_2) \langle q_1 q_2 | \hat{H} | q_1' q_2' \rangle b(q_1')\, b(q_2').$$

No assumptions are made about the convergence of the matrix elements

$$\langle q_1 q_2 | \hat{H} | q_1' q_2' \rangle$$

in terms of the oscillator quantum number n. Only a small part of these elements will be independent and non–vanishing; in an interaction between a pair of particles, the total momentum of both particles, the coordinates of their center of gravity, the total moment and the isotopic spin, their projections, and parity are conserved. In order to make use of the above conservation laws, one can express the matrix elements through the matrix elements

$$\langle Q | \hat{H} | Q' \rangle$$

in terms of the oscillator wave functions of the relative motion of the two particles (Q and Q' are the sets of quantum numbers describing the relative motion of the two particles).

The operator $\hat{H}$ (or $\hat{V}$) does not act upon the coordinate of the center–of–mass of two particles

$$(r_1 + r_2)/2.$$

The matrix element

$$\langle Q | \hat{V} | Q' \rangle$$

is diagonal in respect to the total moment and the isotopic spin of the two particles and is independent of their projections. If, in the expansion of the wave functions, we limit ourselves to the first two oscillator states with $n = 0$ and $n = 1$, then there will be only 16 different matrix elements

$$\langle Q | V | Q' \rangle$$

We can hope that it will be possible to describe, by means of these 16 values, the ground and the lower excited states of nuclei up to oxygen. The actual computations in this approximation require the use of computers.

We shall present the results of computation in the most crude approximation ($n = 0$, i.e., all nucleons in the ls state) for the H^3, He^3 and He^4 nuclei. In these approximations, there are only two matrix elements

$$\langle {}^3S_1,\ T = 0 | V | {}^3S_1,\ T = 0 \rangle = A_1;$$

$$\langle {}^1S_0, T = 1 | V | {}^1S_0,\ T = 1 \rangle = A_0,$$

for which we obtained the following system of equations:

$$(3\hbar^2 / mr_0^2) - 3(A_1 + A_0) = -8.49 \text{ mev}, \qquad (H^3)$$

$$(3\hbar^2 / mr_0^2) + (2e^2 / \sqrt{\pi} r_0) - 3(A_1 + A_0) = -7.73 \text{ mev}, \qquad (He^3)$$

$$(9\hbar^2 / 2mr_0^2) + (2e^2 / \sqrt{\pi} r_0) - 6(A_1 + A_0) = -28{,}27 \text{ mev}, \qquad (He^4)$$

This system of three equations contains two unknowns r_0 and $A_1 + A_0$. The equations are satisfied for

$$A_1 + A_2 = 10.83 \text{ mev}, \text{ and } r_0 = 2.27 \cdot 10^{-13} \text{ cm}.$$

The Coulomb energy

$$2e^2 / \sqrt{\pi} r_0$$

equals to 0.716 mev, while the experimental value is 0.764 mev.

1 J. Blatf and V. Weisskopf, *Theoretical Nuclear Physics.*

Translated by H. Kasha
36

Scale Transformation and the Virial Theorem in Quantum Field Theory

Iu. V. Novozhilov
Leningrad State University

(Submitted to JETP editor October 4, 1956)
J. Exptl. Theoret. Phys. (U.S.S.R.) 32, 171–173 (January, 1957)

UNDER the term "scale transformation" we shall understand the transformation of the scale of coordinates, accompanied by an inverse change of the mass scale

$$x_\mu \to \lambda x_\mu; \quad m \to m/\lambda; \quad M \to M/\lambda, \qquad (1)$$

where λ is a real positive number, m is the mesonic mass, and M the nucleonic mass. Neutral meson and nucleon fields will be considered for the sake of simplicity. Two facts pertaining to the group of scale transformations will be noted below: a)the invariance of field equations with respect to this group of transformations and the relations following from this, and b) the virial theorem, deduced by means of scale variations. The variation of the length scale was earlier studied by Fock[1] and then by Demkov[2] in connection with the virial theorem in quantum mechanics. The variation of the scales of length, time and mass for the Dirac equation were studied by Infeld and Schild[3] in gravitational theory.

The field equations for the meson and the nucleon fields are of the form

$$D(x, M)\psi(x, M) \equiv i(\gamma_\mu \partial/\partial x_\mu + M)\psi(x, M) \qquad (2)$$
$$= g\gamma_5 \varphi(x, m)\psi(x, M),$$

$$(\Box - m^2)\varphi(x, m) = -g\bar{\psi}(x, M)\gamma_5\psi(x, M) - 4k\varphi^3(x, m).$$

It is easily seen that Eqs. (2) are invariant under scale transformation (1), if the field operators are transformed according to the formulas

$$\psi'(x, M) = \lambda^{3/2}\psi(\lambda x, M/\lambda);$$
$$\varphi'(x, m) = \lambda\varphi(\lambda x, m/\lambda). \qquad (3)$$

It should be noted that the term containing φ^3 in Eq. (2) is the only non–linear term which can be added to the meson equation without impairing the scale invariance of the field equations. The creation operators

$$a^+, \; b^+, \; c^+$$

and destruction operators a, b, c for free fields, which satisfy the commutation relations

$$\{a^+(\mathbf{p}, M), a(\mathbf{p}', M)\} = \{b^+(\mathbf{p}, M), b(\mathbf{p}', M)\}$$
$$= [c(\mathbf{p}, m), c^+(\mathbf{p}', m)] = \delta(\mathbf{p} - \mathbf{p}')$$

are transformed, according to (1), in the following way:

$$a'^+(\mathbf{p}, M) = \lambda^{-3/2}a^+(\mathbf{p}/\lambda, M/\lambda), \qquad (4)$$
$$c'^+(\mathbf{k}, m) = \lambda^{-3/2}c^+(\mathbf{k}/\lambda, m/\lambda).$$

It follows from the invariance of the field equations with respect to the homogeneous space–time "expansion" $x \to \lambda x$ and the proportional mass construction that the transformation function

$$U_{12} = (\Psi(\sigma_2), \Psi(\sigma_1)),$$

is invariant. $\Psi(\sigma)$ denotes the Heisenberg vector of state, determined by means of the field operators on the space–like surface σ. Indeed, according to the Schwinger action principle

$$\delta U_{12} = i(\Psi(\sigma_2), \; \delta W_{12}\Psi(\sigma_1)) \qquad (5)$$

the variation δU_{12} is determined by the variation of the action operator δW_{12} which, however, does not change under transformation (1). The variated and unvariated actions

$$W'_{12} = \int_{\lambda\sigma_1}^{\lambda\sigma_2} L\left(x', \frac{m}{\lambda}, \frac{M}{\lambda}; \; \psi, \; \bar{\psi}, \varphi\right)dx',$$
$$W_{12} = \int_{\sigma_1}^{\sigma_2} L(x', m, M; \psi, \bar{\psi}, \varphi)\,dx',$$

are equal, if relations (3) are satisfied. In the expression for W_{12}, $\lambda\sigma$ denotes the space–like surface obtained from σ as the result of replacing x by λx.

In the special case when $\sigma_2 \to +\infty$ and $\sigma_1 \to -\infty$, the transformation function U_{12} becomes the scattering matrix $S_{12} = (\Psi_{out}^{(2)}, \; \Psi_{in}^{(1)})$. If we limit ourselves to scattering problems in which Ψ_{out} and Ψ_{in} describe free particles, we can make use of the relations (4). The relation $S'_{12} = S_{12}$ is then equivalent to

$$S_{12}(\mathbf{p}_1 \ldots \mathbf{p}_n; \; \mathbf{p}'_1 \ldots \mathbf{p}'_{n'}; \; m, M) \qquad (6)$$
$$= \lambda^{-3/2(n+n')}S_{12}\left(\frac{\mathbf{p}_1}{\lambda} \ldots \frac{\mathbf{p}_n}{\lambda}; \; \frac{\mathbf{p}'_1}{\lambda} \ldots \frac{\mathbf{p}'_{n'}}{\lambda}; \; \frac{m}{\lambda}, \; \frac{M}{\lambda}\right),$$

where the unprimed values correspond to the initial state, and the primed values to the final one; $\mathbf{p}_i$ is the momentum of the i th particle, and n is the number of particles (nucleons and mesons). For a uniform change of all the masses and momenta of the particles, the transition matrix elements is therefore multipled by the normalization factor

$$\lambda^{-3(n+n')/2}.$$

In the case of the Bethe–Salpeter equation, a relation concerning the kernel Q of the equation follows from the invariance of the field equations with respect to the scale transformation (1). We write the Bethe–Salpeter equation in the form

$$D(x, M_a)\, D(y, M_b)\, f(x, y) = \int Q(x, y;\ x', y';\ M_a, M_b, m)\, f(x', y')\, dx'\, dy',$$

where M_a and M_b are the experimental masses of the particles, and the kernel Q can be regarded as already normalized.

The relation in question is then of the form

$$Q(x, y;\ x', y';\ \lambda m, \lambda M_a, \lambda M_b) = \lambda^{10} Q(\lambda x, \lambda y;\ \lambda x', \lambda y';\ m, M_a, M_b). \tag{7}$$

The Virial Theorem. The invariance of the field equations (2) with respect to the scale transformations (1) is disturbed in the presence of external fields. The variation of the scattering matrix δS_{12} does not vanish in the presence of an external field. In order to find its value we shall make use of the action principle (5). It is evident that, in the absence of an external nucleon field, the variation of a matrix element of the scattering matrix

$$\delta S_{12} = i(\Psi^{(2)}_{\text{out}},\ \delta W_e \Psi^{(1)}_{\text{in}})$$

will be determined by the variation of the part of the action operation W_e, depending on the external meson field φe:

$$W_e = -ig \int \overline{\psi}(x)\, \gamma_5 \varphi_e(x)\, \psi(x)\, dx.$$

The varied action W'_e is obtained from W_e by putting $x = \lambda y$ and the introduction of variated operators $\psi'(y) = \lambda^{3/2} \psi(\lambda y)$ and $\psi(y) = \lambda^{3/2} \psi(\lambda y)$, which yield

$$W'_e = -ig\lambda \int \overline{\psi'}(y)\, \gamma_5 \varphi_e(\lambda y)\, \psi'(y)\, dy.$$

Putting $\lambda = 1 + \epsilon$, where ϵ is infinitesimally small, we find the relation

$$\sum_i^n p_i \frac{\partial S_{12}}{\partial p_i} + \sum_j^{n'} p'_j \frac{\partial S_{12}}{\partial p'_j} + m \frac{\partial S_{12}}{\partial m} + M \frac{\partial S_{12}}{\partial M} + \frac{3}{2}(n + n') S_{12} = \left(\Psi^{(2)}_{\text{out}}, -g \int \varphi\, \gamma_5\, \psi \left[\varphi_e + x_\mu \frac{\partial \varphi_e}{\partial x_\mu}\right] dx\, \Psi^{(1)}_{\text{in}}\right), \tag{8}$$

where the summation is extended on the incident particles (total number n) and the scattered particles (total number n'). The expression under the sign of the integral in the right–hand side of Eq. (8) is of the form typical for the virial theorem. The relation (8) can be therefore regarded as the virial theorem of the quantum field theory.

If we consider the case when we have an external nucleon field $\psi_e(x)$ instead of the external meson field, the nucleon field being characterized by the current

$$j_e = -ig\, \overline{\psi}_e(x)\, \gamma_5 \psi_e(x),$$

we find in an analogous manner that the right–hand side of the equation (8) will be equal to

$$i\left(\Psi^{(2)}_{\text{out}},\ \int \varphi(x) \left[3 j_e(x) + x_\mu \frac{\partial j_e(x)}{\partial x_\mu}\right] dx\, \Psi^{(1)}_{\text{in}}\right). \tag{9}$$

The generalization of the above ideas for the case of other fields is straightforward.

Note added in proof: After the paper had been submitted to the editor, I. M. Shmushkevitch drew the attention of the author to the fact that the scale invariance of the equations of quantum electrodynamics is mentioned in the book of Jauch and Rohrlich.[4] The consequences of this fact and the virial theorem are not, however, studied there.

1 V. A. Fock, Z. Physik 63, 855 (1930).
2 M. N. Demkov, Dokl. Akad. Nauk SSSR 89, 249 (1953).
3 L. Infeld and R. Schild, Phys. Rev. 70, 410 (1946).
4 J. Jauch and F. Rohrlich, *Theory of Photons and Electrons*, Cambridge, Mass, 1955.

Translated by H. Kasha
38

Some New Electrets from Inorganic Dielectrics

A. N. Gubkin and G. I. Skanavi

P. N. Lebedev Physical Institute
Academy of Sciences, USSR

(Submitted to JETP editor September 28, 1956)
J. Exptl. Theoret. Phys. (U.S.S.R.) 32, 140–142 (1957)

It is known that the electret represents an electric analog of the magnet. It is a dielectric characterized by a "constant" electrification with opposite charges at its ends. Usually electrets are obtained by cooling a heated dielectric in an electric field.

No. in order	Material	Dielectric constant and conductivity at room temperature		Maximum current during polarization in Amp.	Surface charge density $\sigma \cdot 10^9$ coul/cm^2					Remarks
		ε	γ, в Ω^{-1} см$^{-1}$		30 min. after polarization	10 days after polarization	30 days after polarization	3 months after polarization	7 months after polarization	
1	$MgTiO_3$	16	10^{-13}—10^{-14}	$4.0 \cdot 10^{-8}$	1.9	1.4	0.5	0.5	0.5	
2	$ZnTiO_3$	22	10^{-12}—10^{-13}*	$3.4 \cdot 10^{-6}$	0.3	0.2	0,3	0.4	нет	
3	$BaO \cdot 4TiO_2$	28	10^{-13}—10^{-14}	$1.6 \cdot 10^{-7}$	1.1	2.8	0.2	1.6	1.4	
4	Bismuth titanate	80	10^{-12}—10^{-13}	$1.2 \cdot 10^{-4}$	10.0	6.8	3.9	4.2	1.8	Samples were polarized at 10 kv/cm*
5	$CaTiO_3$	150	10^{-12}—10^{-13}	$5.0 \cdot 10^{-8}$	5.3	10.5	5.8	9.6	4.2	
6	$SrTiO_3$	175	10^{-10}—10^{-12}	$3.4 \cdot 10^{-7}$	1.7	2.2	0.1	0.7	0.65	
7	Strontium-bismuth titanate	750	10^{-13}—10^{-15}	$7.0 \cdot 10^{-7}$	3.4	0.2	0,8	**	**	Thickness of samples 3.55 mm.
8	$BaTiO_3$	1200	10^{-10}—10^{-12}	$5.9 \cdot 10^{-4}$	15.4	2.0	0.04	1.2	1.1	Samples were polarized at 10 kv/cm
9	Steatite	4—5	10^{-14}—10^{-15}	$3.5 \cdot 10^{-7}$	0,3	2,1	1.5	**	**	
10	Ceramic	4—6	10^{-12}—10^{-13}	$5.0 \cdot 10^{-4}$	none	none	none	**	**	Samples polarized at 10 kv/cm^2
11	Ordinary glass	7—8	10^{-10}—10^{-11}	$1.5 \cdot 10^{-6}$	none	none	none	**	**	Temperature held at 175 °C.*
12	Pyrex glass	5.8	10^{-14}	$1.0 \cdot 10^{-4}$	0.07	none	none	none	none	Temperature held at 50 °C.*
13	Fused quartz	3.7	$<10^{-15}$	$3.5 \cdot 10^{-9}$	none	none	none	none	**	
14	KBr crystals	4.7	10^{-14}	$1.5 \cdot 10^{-5}$	none	none	none	none	**	Sampes polarized at 10 kv/cm

*The values of field intensity and temperature maintained during polarization for a group of materials were limited by their dielectric strength an relation to their thermal conductivity.

**Data have not yet been obtained.

There is a series of published works on the investigation of properties of electrets, obtained from different organic substances.[1,2]

Inorganic substances have been studied very little in this respect, and available information about them is very contradictory. In general electrets of polycrystalline inorganic dielectrics have not been studied, although mention was made of the electret-like behavior of field polarized barium titanate samples[3] in the program of the American Physical Society meeting of 1953.

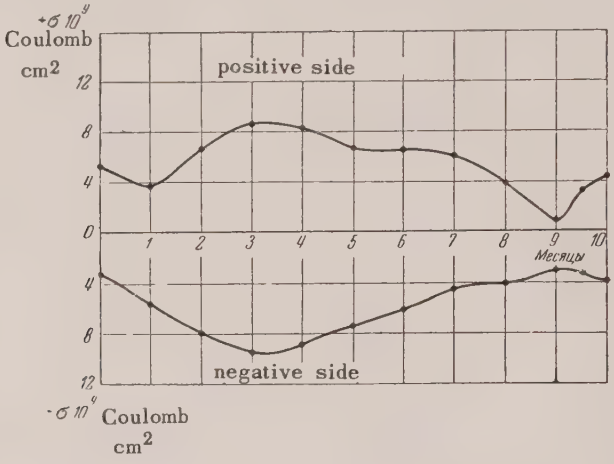

We have first shown that stable electrets, the properties of which are not connected with pyroelectricity, can be obtained from polycrystalline inorganic dielectrics, such as titanates of magnesium, calcium, bismuth, strontium, zinc, strontium-bismuth, from metatitanate of barium, tetratitanate of barium and from steatite.

The following polarization procedure was used to obtain electrets in all cases; the sample was placed in a field of 20 kv/cm, maintained at room temperature for 30 min, raised to 200° C in 2 hours, maintained at this temperature for 2 hours and reduced to 65–90° C in 2 hours. The samples were 5 mm thick and about 60 mm in diamter. The electrodes were brass discs 30 mm in diameter. The surfaces of the samples and electrodes were thoroughly polished. The current was measured during polarization. The polarized samples were wrapped in lead foil and kept in a desicator with $CaCl_2$. Effective surface charge density σ of some electrets was measured by the electrostatic induction method and the signs of the surface charges were determined.

The basic results are shown in the Table. Values of σ in the Table are given only for one side of the electret, namely the one which was facing the minus side* during polarization (the negative side of the electret, the opposite side being positive). The signs of charges at the ends of the studied samples shown in the table coincide with polarity of the voltage applied to the samples during polarization (it is customary to refer to such a charge as "homocharge"), with the exception of pyrex glass, which has charges of opposite polarity (such a charge is called "heterocharge")**

The Figure shows the variation of σ with time for the $CaTiO_3$ electret. Similar curves were obtained for other investigated electrets. Preliminary experiments with $MgTiO_3$ samples indicate that the "life time" of electrets of this dielectric exceeds 1.5 years.

It follows from the data in the Table and the Figure that the surface charge density of the new electrets in all cases reaches the value for electrets made of carnubian wax ($1–2 \times 10^{-9}$ cm); and in some cases considerably exceeds this value (electrets of $CaTiO_3$ and others).

It is characteristic that in polarization without heating the dielectric also acquires homocharges, but they fall off with time much faster than those which were obtained with supplementary heating. Thus values of σ of $CaTiO_3$ samples, obtained without heating were, one month after polarization, 10 times smaller than the corresponding values of σ obtained for samples heated to 200° C. When electrets of magnesium titanate and of steatite are polarized in a 5 kv/cm field a heterocharge is observed, which after a few days is changed to a homocharge and then remains practically constant for a long time. At intensities of less than 5 kv/cm the samples of $MgTiO_3$ samples only a homocharge which slowly drops to zero. If the electrodes are formed by evaporation of silver (there is no layer of air between the elec-

trode and the surface of the electret), then, in the absence of corona discharge from the conducting wires and from the electrodes, there are obtained insignificant charges (exhibit of $ZnTiO_3$) which drop to zero very quickly. An analogous situation is also obtained by the polarizations in a silicon organic liquid.

The work on the study of properties of electrets from inorganic delectrics is continuing at the present time.

The following persons participate in this work: junior scientific assistant V. S. Mitronina, senior laboratory technician A. N. Kalganova and also, in the early phase of this work, P. Ch. Muchamedieva.

*It should be noted that the absolute values of σ on the opposite sides of the electret are nearly equal.

**On the surface of dielectrics of high specific resistance (for example on quartz) there frequently appear, as a result of working the material, friction, etc., surface charges. However, these charges, as a rule, are of relatively small magnitude and are of the same sign at the two ends. Therefore, the error introduced by these changes into the measurements is small.

1 G. Wiseman and E. Linden, Electr. Eng. 72, 869 (1953).
2 F. Gutman, Rev. Mod. Phys. 20, 457 (1948).
3 R. Thickens and R. MacDonald, Phys. Rev. 90, 375 (1953).

Translated by J. L. Herson
20

Dependence of Dielectric Strength of Alkali Halide Crystals on Temperature

E. A. KONORAVA AND
L. A. SOROKINA
P. N. Lebedev Physical Institute, Academy of Sciences, USSR

(Submitted to JETP editor June 28, 1956)
J. Exptl. Theoret. Phys. (U.S.S.R.) 32, 143–144 (1957)

IT has been considered until not so long ago that the dielectric strength at puncture does not depend on temperature. Investigations of recent years[2–6] have shown that the dielectric strength of alkali halides in the region of puncture does not remain constant, and, as reported in all cited references, the temperature dependence of the dielectric strength at constant intensity exhibits a maximum. The results of these investigations do not agree, however, so far as the puncture values for pulsed voltages are concerned. There is also no agreement in the values of the temperature maximum.

In order to refine the existing experimental data, we have investigated the temperature dependence of dielectric strength for puncture KBr and KCl in the temperature interval from −170° to +200° C. Investigations were conducted at constant voltage and with pulses of 10^{-2}, 10^{-4} and 10^{-6} sec duration with the voltage increasing linearly. For constant voltages and 10^{-2} sec pulses, measurements of the voltage applied to the sample were made with an electrostatic voltmeter whose error does not exceed 5%. The cathode ray oscillograph KO–20 was used for recording of the 10^{-4} and 10^{-6} sec pulse amplitudes with the sample voltage applied to the plates of the oscilloscope through a divider. The measurement error in this case did not exceed 10%.

Samples for crystals were prepared from monocrystals KBr and KCl grown by the method of Kiropulos. A cavity was bored in the crystal plates after which, in order to remove mechanical strains, the samples were subjected to a temperature 50 to 70° below the melting point and then to slow cooling at a rate of 1° per minute. After annealing the thickness of the sample in the region of the cavity was reduced, by polishing of the plane surface, to from 0.1 to 0.2 mm and silver electrodes were formed on the surface of the cavity and on the plane surface by evaporation in a vacuum. To guard against cracking the rate of heating and cooling before puncture was made not to exceed 1° per minute.

Figure 1 shows the temperature dependence for KBr. Each point on the curve corresponds to the mean value of dielectric strength based on measurements of 12 to 20 samples. The mean square error did not exceed 8% for constant voltages and 12% for pulses. As shown in Fig. 1, the temperature dependence of the dielectric strength E_{st} at constant voltage exhibits a maximum at 50° C which is smoothed out with decrease of the voltage duration. For pulses of 10^{-6} sec duration there is no maximum, and a gradual increase of the dielectric strength with temperature is observed. In the region below 50° C, the dielectric strength does not depend on temperature for constant voltages and pulses of 10^{-2} and 10^{-4} sec. Figure 2 shows the results of E_{st} temperature dependence measurements for KCl.

The following conclusions can be made on the basis of the present work.

1. It is established that the temperature depen-

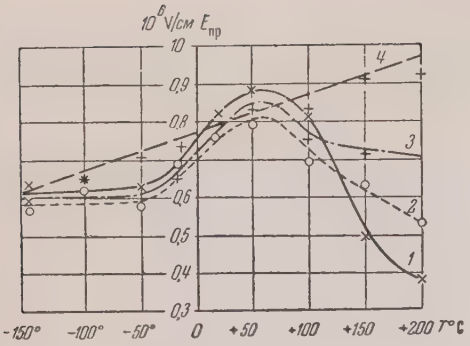

FIG. 1. Temperature dependence of E_{st} for Kbr for various durations of applied voltage: *1*—for constant voltage; *2*—for pulses of 10^2 sec. duration; *3*—for pulses 10^4 sec. durations; *4*—for pulses 10^6 sec. duration

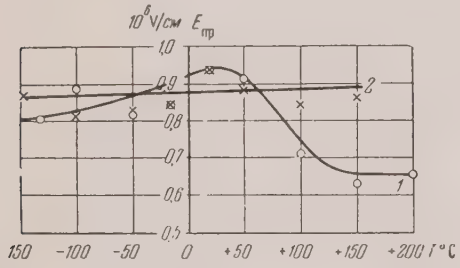

FIG. 2. Temperature dependence of E_{st} for KBr: *1*—for constant voltage, *2*—for pulses of 10^6 sec. duration.

dence of the dielectric strength E_{st} for alkali halide crystals of dielectric voltage exhibits a maximum which is smoothed out as the duration of voltage application is decreased. According to the present theories of electric puncture, which connect the electric breakdown with impact ionization by electrons, there should be observed a gradual growth at constant strength with temperature in the entire temperature range, independent of the duration of voltage application (at any rate for 10^{-6} sec pulses). In Fröhlich's "high temperature" puncture theory,[7] , an effort is made to explain the existence of a maximum in the temperature dependence of E_{st} ; however, it is impossible to explain from the point of view of this theory the fact, that the definitely exhibited maximum at constant voltage is completely absent for pulses of 10^{-6} sec duration.

2. The obtained temperature dependence indicates that the appearance of the maximum is connected with long duration processes taking place in the dielectric upon application of the field. The theory applicable to the explanation of the obtained results is that of Hipple[4] according to which reduction in puncture strength is caused by distortion of the field at the expense of volume charges: at low temperatures negative (electron) charges due to cold possible emission, and at high temperature positive (ionic) changes due to crystal conductivity. It is cathode that at a certain temperature, both charges so compensate each other that the field is relatively undistorted and puncture strength reaches a maximum. Increase of dielectric strength with decrease of applied voltage duration at high temperatures indicates that the time required for the formation of the ionic charge is greater than 10^{-6} sec.

3. The magnitude of the electron volume change apparently depends on the emission velocity of the electrons from the cathode and, therefore, indirectly on the cathode material and condition of the contact surface as well as on the concentration of the electron traps in the crystal, i.e., on the degree of crystal contamination, preliminary heat treatment, etc.

Since it is very difficult to set up identical experimental conditions, it is quite natural to expect differences in the data obtained by different investigators (especially shift of the maximum).

Final conclusions pertaining to the causes of temperature dependence of E_{st} at puncture, it seems to us, can be made by studying the nature of the currents in the prepuncture field region.

The present work was conducted under the supervision of Prof. G. I. Skanavi, to whom the authors express their sincere thanks.

1 Inge, Semenoff, Walter , Z. Physik 32, 373 (1925).
2 R. Buehl, and A. Hippel, Phys. Rev. 26, 941 (1939).
3 A. Hippel and R. Maurer, Phys. Rev. **59**, 820 (1941).
4 A. Hippel and R. Alger, Phys. Rev. 76, 127 (1949).
5 Y. Invishi and T. Svita, J.Phys. Soc. Japan 8, 567 (1953).
6 J. Calderwood and R. Cooper, Proc. Phys. Soc. (London) **66B**, 74 (1953).
7 H. Fröhlich, Proc. Roy. Soc.(London) **A188**, 521(1947).

Translated by J. L. Herson
21

Elastic Small Angle Scattering of Neutrons by Heavy Nuclei

V. S. BARASHENKOV, I. P. STAKHANOV AND IU. A. ALEKSANDROV

(Submitted to JETP editor September 6,(1956)
J. Exptl. Theoret. Phys. (U.S.S.R.) 32, 154–156 (January, 1957)

RECENT investigations of the scattering of fast electrons on hydrogen[1] substantiate the con-

clusions of the meson theory on the extended distribution of electrical charge in the nucleon. This distribution of charge is caused by the "cloud" of charged mesons around the central nucleus—the core. Under the action of the external electrical field the distribution of the electric charge in the nucleon will be changing. In particular, one may expect polarization of the oppositely charged mesons cloud and core in the neutron and the appearance in the neutron of an induced dipole electric moment $p = \alpha E$, which should show up in an anomalous behavior of the differential cross section of the small angle scattering of neutrons by heavy nuclei[2]. If as a first rough approximation we assume that the meson field of the neutron, located in an external electrical field $E = kV/z$, where $k = 1$, can be described by the static equation

$$[\nabla^2 + (e/c\hbar)^2 E^2 z^2]\varphi - (mc/\hbar)^2 \varphi = (4\pi/c) g\delta(r), \quad (1)$$

then the induced dipole electric moment will be given by

$$p = -\frac{e^2 g^2}{\hbar^2 c^2} E \int z^2 \frac{\exp(-2mcr/\hbar)}{r^2} d^3x + O(E^2). \quad (2)$$

From (2) it follows that

$$\alpha(\hbar c/g^2) = (e\hbar/mc^2)^2 \pi/3m = 2{,}1 \cdot 10^{-41}. \quad (3)$$

As a result of electrical polarization the neutron undergoes additional scattering in the coulombic field of the nucleus. The effect of polarization scattering will be greatest when the parameter of collision d is limited by the conditions:

$$R \ll d \ll a, \quad (4)$$

where $R = 1{,}5 \cdot 10^{-13} A^{1/3}$

is the radius of the nucleus;

$$a = 0{,}53 \cdot 10^{-8} Z^{1/3}$$

is the radius of the electron shell. In this case, the energy of the interaction between the neutron and the nucleus has the form:

$$H(r) = U(r) - \mu \frac{iZ}{2r^3}\left(\frac{\hbar e}{mc}\right)^2 \sigma[r\nabla] - \alpha Z^2 e^2 \frac{1}{r^4}. \quad (a)$$

Here the first term is determined by purely nuclear forces, the second term describes the interaction between the magnetic moment of the neutron $\mu\sigma$ and the coulombic field of the nucleus ("Schwinger scattering").[3]

For the evaluation of the magnitude of the polarization scattering the Born approximation was used. At distances greater than R, the nuclear forces decrease rapidly, and from the condition

$$H(\hbar/mv\theta) \ll 2E\theta \quad (5)$$

(m, v and E are the mass, the velocity and the energy of the neutron, scattered at the angle θ)[4] it follows that at

$$\alpha \sim 10^{-39}-10^{-41}\ cm^3,\ Z \sim 50-100,\ 0° < \theta < 15°$$

it is possible to use the Born approximation for energies $E = 10$ mev. On the assumption that the energy of the nuclear interaction U is independent of spin, we will obtain the following expression for the differential cross section of the elastic scattering (cm^2 ·sterad) of a beam of non–polarized neutrons on the nucleus (Z, A):

$$\sigma(\theta) = |f_0(\theta)|^2 + \frac{1}{4}\mu^2\left(\frac{\hbar}{mc}\right)^2\left(\frac{Ze^2}{\hbar c}\right)^2 \operatorname{ctg}^2\frac{\theta}{2} + f(\theta)\,\mathrm{Re} f_0(\theta) + \frac{1}{4} f^2(\theta), \quad (6)$$

where $f_1(\theta)$ is the amplitude of nuclear scattering:

$$f(\theta) = \frac{2m\alpha}{R}\left(\frac{Ze}{\hbar}\right)^2 KR\left(\frac{\sin KR}{K^2R^2} + \frac{\cos KR}{KR} + \mathrm{si}\ KR\right), \quad (b)$$

$$K = 4{,}44 \cdot 10^{12}\sqrt{E}\sin(\theta/2),$$

E is the energy of the scattered neutron in millions of electron volts.

The results of the calculations by Eq. (6) are given in the graph, as well as in the Table, where the relative contribution of the polarization scattering

$$\Delta = (\sigma - \sigma_4)/\sigma$$

is expressed in its dependence on the value of the coefficient of polarizability (for $E = 4$ mev, $\theta = 3°$).* For the nuclear scattering, the solid sphere approximation was used. From the given data it is evident that the polarization scattering, as well as the Schwinger scattering, is manifest in the small angle scattering of neutrons. The range of angles

$$\theta \sim 3° \div 10°,$$

was found to be the most convenient for measurements, where the nuclear scattering is still only

slightly dependent on the angle, and the Schwinger scattering is already negligible. From a comparison with Ref. 2, it follows that α is appreciably smaller than 10^{-39} cm.[3]

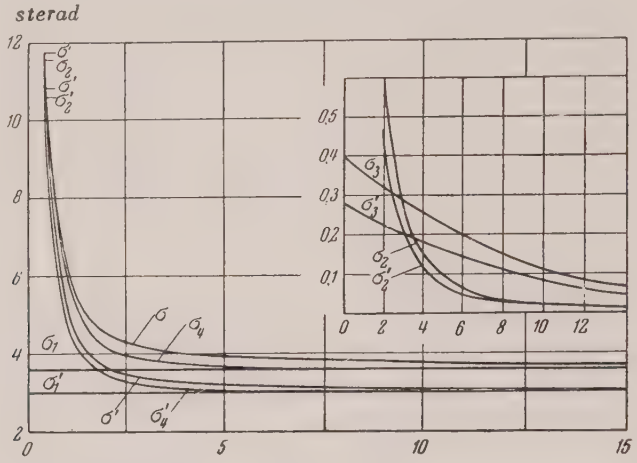

Differential cross section of the elastic scattering of neutrons of energy $e = 4$ mev and $\alpha = 10^{-40}$ cm^3;

$\sigma_1, \sigma_2, \sigma_3$

are the cross sections of the nuclear, Schwinger and polarization scattering on U^{238};

$\sigma_4 = \sigma_1 + \sigma_2$; $\sigma = \sigma_1 + \sigma_2 + \sigma_3$. σ_1', σ_2', σ_3', σ_4', σ'

are the corresponding cross sections of scattering on Pb^{207}

Polarization scattering introduces a considerable contribution into $\sigma(\theta)$ in the scattering of low energy neutrons and it decreases slowly with an increase in the angle θ. Thus, in the scattering

TABLE

α	nucleus		
	Cu^{64}	Pb^{207}	U^{238}
10^{-39}	54	83	88
10^{-40}	1.2	5.9	6.7

on U^{238} of neutrons of energies $E = 0.1$ mev for $\alpha = 10^{-40}$ cm^3, $\Delta = 57\%$ at $\theta = 3^\circ$ and $\Delta = 62\%$ at $\theta = 10.^\circ$ However, in this case for comparison with experiment it is necessary to have a good knowledge of the absolute value of the purely nuclear scattering since the slope of the curve $\sigma(\theta)$ constructed by formula (6) is small and qualitatively the curves $\sigma(\theta)$ and $\sigma_4(\theta)$ are difficult to distinguish. At a neturon energy $E \sim 3-5$ mev it is hoped that one may be able to distinguish these curves qualitatively, all the more, because for the above energies, in any case for Pb, the solid sphere approximation applies inadequately well.[5]

In conclusion we consider it a very pleasant duty to thank I. I. Bondarenko and L. N. Usachev for valuable discussion.

*More exact calculations in the different variants of the meson theory will be published later.

*In the calculations by Eq. (6) it is necessary to take into account that the allowable range of the angles θ and of the energy E is limited not only by the requirement (5), but also by the conditions $KR \ll 1$, $k\alpha \gg 1$, which follows from (4).

1 R. W. McAllister and R. Hofstadter, Phys. Rev. 102, 851 (1956)

2 Iu. A. Aleksandrov and I. I. Bondarenko, J. Exptl. Theoret. Phys. (U.S.S.R.) 31, 726 (1956); Soviet Phys. JETP 4, 612 (1957).

3 J. Schwinger, Phys. Rev. 73, 407 (1948); J.T. Sample, Canad. J.Phys. 34, 36 (1956).

4 N. Mott and G.Massey, "Theory of atomic collisions, IIL Moscow, (1951). (Russian translation).

5 W. D. Whitehead and S. C. Snowden, Phys. Rev. 92, 114 (1953); D. J. Hughes and J. A. Harvey, Heavy Element Cross Sections, presented at Geneva, August, 1955, Addendum to BNL, 325.

Translated by E. Rabkin,
29

Heat Capacity of Laminar Structures at Low Temperatures

E. S. Itskevich and V. M. Kontorovich
Institute of Physico-technical and Radiotechnical Measurements
Institute of Radiophysics and Electronics
Academy of Sciences, USSR

(Submitted to JETP editor October 18, 1956)
J. Exptl. Theoret. Phys. (U.S.S.R.) 32, 175–177 (January, 1957)

It is well known that the heat capacities of laminar and chain structures do not obey the DeBye law $C \sim (T/\theta)^3$ at low temperatures. In the work of I. M. Lifshitz[1,2] it was shown that the deviation from the T^3 law is associated with the special role of bending waves in such structures. The anomalous form of the dispersion law (the relation between the frequency ω add the wave vector K for bending waves leads to an anomalous temperature dependence of crystal energy. In Ref. 2, the dispersion law was obtained for bending waves in strongly anisotropic media, and the corresponding heat capacity of a laminar crystal was calculated. For temperatures at which the interaction between layers may not be neglected ($T \ll \eta\Theta, \zeta\Theta$, where η and ζ are small elastic moduli), the formula for the heat capacity obtained in Ref. 2 may be transformed into the form*

$$Cs^2/A = (\delta/s) + 2\{3K(s) - s\,dK(s)/ds\}, \qquad (1)$$

$$A = Vk\eta^4\pi^2/16a^3\nu^3\zeta, \qquad (2)$$

$$\delta = \zeta\eta/15, \quad s = a'\eta^2\Theta/4\pi\nu aT,$$

where ν is the "transverse stiffness" of the layers ($\nu \sim 1$), a' and a are the atomic distances in the layer and normal to it, and

$$K(s) = \int_0^\infty \frac{t^2 \operatorname{arctg}(t/s)\,dt}{e^{2\pi t} - 1}. \qquad (3)$$

Using an integral representation for $\ln \Gamma(s)$[3], it is easy to show that

$$\frac{dK(s)}{ds} = -\frac{1}{24} - \frac{s^2}{2}\left[\frac{d}{ds}\ln\Gamma(s) - \ln s + \frac{1}{2s}\right]. \qquad (4)$$

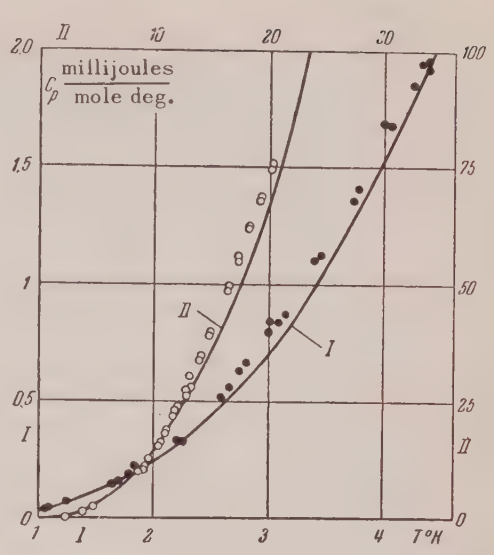

Lattice part of the heat capacity of graphite.[5] *I*—data for the region 1.0–4.4° K. *II*—data for the region 4.0-21.0° K. Solid line—theoretical curve.

In the region of temperatures under consideration, the term

$$\delta/s \approx \zeta T/\eta\Theta \ll 1$$

and may be neglected. From Eqs. (1) and (4) we obtain the precise formula:

$$\frac{1}{A}\frac{d}{ds}(Cs^2) = s^3\frac{d^2}{ds^2}\ln\Gamma(s) - s(s+1) - \frac{1}{6}, \qquad (5)$$

where $d^2\ln\Gamma/ds^2$ is a tabulated function.[4] Thus, in the region of very low temperatures ($T \ll \eta\Theta, \zeta\Theta$) it is easy to tabulate the heat capacity of laminar crystals with the use of one graphical integration.

A comparison with experiment is possible in spite of the fact that the elastic constants in the region of temperatures under consideration are not known for laminar lattices. In fact, for

$$s \to 0: \quad s^2C/A \to 0.0914$$

(the region of quadratic dependence of heat capacity on temperature); and for

$$(T \to 0), \quad s^3C/A \to 1/30$$

(the region of cubic dependence). Determining the combinations of constants required for Eq. (2) by the limiting laws, the entire curve may be constructed.

Until very recently, the necessary experimental data was not available. The data of Keesom and Pearlman[5], which appeared recently, allowed a comparison with experiment for graphite, as shown in

the Figure. Over the entire temperature range, the divergence does not exceed 10–15%, and may be partly due to the error attached to the exclusion of a linear term (electronic contribution to the heat capacity).

It should be noted that Eq. (1), obtained without appealing to models, but on the assumption of strong anisotropy, and yielding satisfactory agreement with experiment for graphite, cannot lay claim to a detailed agreement with experiment for lattices that are not so strongly anisotropic lattices, e.g., laninar halide salts of cadmium.[6] However, in the same way that DeBye's interpolation formula gives good agreement with experiment in the general cases up to $T \sim \theta$, while the precise cubic law ceases to be fulfilled very early, so also in the anisotropic case it may be expected that the interpolation formula obtained by the use of the limiting law of dispersion in Ref. 2 by an integration along k, not to infinity, but to the boundaries of the wave vectors, will give better agreement with experiment at low temperatures and will be applicable to a wide class of laminar structures. This is due to the relatively great stability of the integrals expressing the heat capacity under variations of the dispersion law.[7] and to the considerably greater influence of the upper limit of integration, which is taken into account by cutting off at the boundaries of the wave vectors.

It should be noted that in structures in which the layers differ (for example, in cadmium iodide, in which they are not monatomic and the surfaces of iodine ions facing one another have different positions with respect to the origin in a hexagonal system of coordinates), soft optical branches associated with weak interactions between layers may also contribute to the heat capacity.

The last remark was made by Prof. I. M. Lifshitz. We take this opportunity to thank him for his interest in this work.

*A direct numerical integration of the I. M. Lifshitz formula was performed by N. N. Lazarenko (diploma research, Kharkov State University, 1954). However, the accuracy attained therein is insufficient for comparison with experiment.

1 I. M. Lifshitz, J. Exptl. Theoret. Phys. (U.S.S.R.) 22, 471 (1952).

2 I. M. Lifshitz, J. Exptl. Theoret. Phys. (U.S.S.R.) 22, 475 (1952).

3 E. T. Whittaker and Watson, *Modern Analysis*, Ch. 2.

4 Davis, *Tables of higher mathematical functions*, vol. II, 1935.

5 P. H. Keesom and N. Pearlman, Phys. Rev. 99, 1119 (1955).

6 E. S. Itskevich and P. G. Strelkov, *Thermal capacity of laminated structures*. Proceedings 2nd conference on the Physics of Low Temperatures, Leningrad, June, 1956.

7 I. M. Lifshitz, J. Exptl. Theoret. Phys. (U.S.S.R.) 26, 557 (1954).

Translated by D. Lieberman
40

Investigation of the Excitation Functions for the Reactions $C^{12}(p, pn)C^{11}$ $Al^{27}(p, 3pn)Na^{24}$ and $Al^{27}(p, 3p, 3n)Na^{22}$ in the 150-660 Mev Energy Range

Iu. D. Prokoshkin and A. A. Tiapkin

United Institute of Nuclear Studies

(Submitted to JETP editor October 19, 1956
J. Exptl. Theoret. Phys. (U.S.S.R.) 32, 177-178 (January, 1957)

THE reaction C^{12} (p,pn) C^{11} (1) is widely used for the measurement of proton flux. In connection with this, it is of interest to determine the value of the cross–section for this reaction for various proton energies. The excitation function of the reaction (1) was measured by Aamont and others[1] for energies from the threshold energy up to 340 mev. Comparison of the results of Ref. 1 with the data obtained by Soroko[2] (see Figure) indicate a rapid decrease of the cross–section in the 300–460 mev range. However, the measurements of the ratio of the values of the cross–section at 290 mev and 660 mev revealed[3] that, in this energy range, the value of the cross–section for the reaction (1) decreases much more slowly. The mentioned ratio was found to be

$$\sigma(670) / \sigma(290) = 0\,84 \pm 0{,}03.$$

We therefore concluded it probable that a systematic error ($\sim 15\%$) in the determination of the absolute cross–section in one of the References 1,2 is the real cause of the discrepancy. Results similar to those obtained in Ref. 2 were soon obtained in new investigations[4,5] in the 410–460 mev range. Finally, the cross–sections in the 170–350 mev range were measured with great accuracy by Crandall et al,[6] (see Figure). The values found in Reference 6 are in good agreement with the data of Refs. 2-5. The cross–sections given in Ref. 1 are, evidently, systematically larger by some 15–25%.

The existence of these discrepancies led us to the investigation of the reaction (1) in the 150–660 mev range. In the course of the experiments, a graphite target was placed in the chamber of the

accelerator of the Institute for Nuclear Problems. The decrease in the proton energy was effected by means of varying the distance between the target and the center of the accelerator. The proton flux through the target was determined with an accuracy of about 2% by means of a calibrated thermal battery. The relative activity of the graphite target was measured with a group of proportional counters. The half–life was found to be 20.8 ±0.2 min. The following energy dependence of the cross–section for the reaction (1) was obtained (E_p is the proton energy in mev, $\sigma' = \sigma(E_p)/\sigma(660)$ is the relative reaction cross–section):

E_p:	150	260	290 [3]	350	450	560	660
$\sigma'(C^{11})$:	1,49±0.06	1,23±0.02	1,19±0,04	1,16±0,03	1,03±0.02	0.98±0,02	1,00

These results, normalized for the value of the cross–section at 350 mev[6], are shown in the Figure. The smooth curve is drawn according to the mean of the measurements of Refs. 2,4,5, and 6 and of the present work. (In the region below 150 mev, the results of the relative measurements of Ref. 1 were used). Our data are in a good agreement with those recently published.[7,8]

The excitation functions for the reactions Al^{27} $(p,3pn)$ Na^{24} (2) and Al^{27} $(p,3p3n)$ Na^{27} (3) were also measured by the same method. The results are: Al^{27} $(p, 3pn)$ Na^{24} (2) and Al^{27} $(p, 3p3n)$ Na^{27} (3):

E_p:	150	260	350	450	560	660
$\sigma'(Na^{24})$:	1,10 ± 0,05	1,03 ± 0,03	1,01 ± 0,02	1,02 ± 0,03	0,97 ± 0,02	1,00
$\sigma'(Na^{27})$:	1,20 ± 0,15	1,0 ± 0,1	0,96 ± 0,12	1,0 ± 0,1	1,00 ± 0,07	1,00

The energy dependence found for the reaction (2) is in an agreement with the results of reference 9.

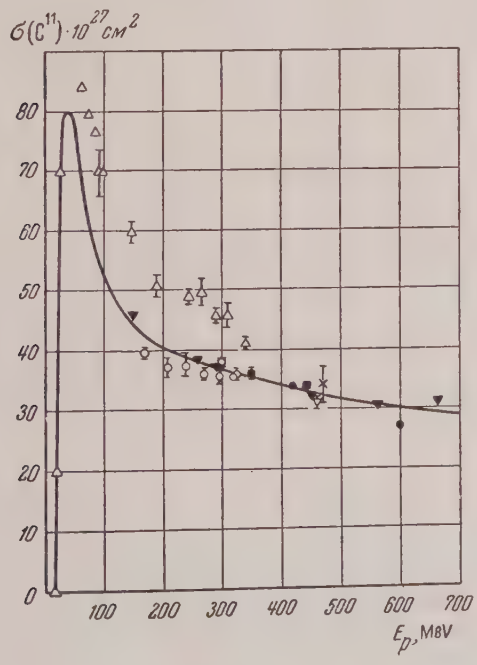

Cross–section for the reaction C^{12} (p,pn) C^{11} for various proton energies according to the data of: △– Ref. 1, ×–Ref. 2, ■ Ref. 4, ● –Ref. 5, ○–Ref. 6, ▽–Ref. 8, ▼–the present work.

Comparison with the results for the reaction (1) shows that the ratio of the cross–section for reactions (1) and (2) decreases smoothly with increasing energy. This does not agree with the results of Ref. 10, according to which the above ratio decreases sharply in the 200–500 mev range . The latter fact leads to the conclusions[10] about the presence of a maximum for the reaction (2) at 500 mev, which is contradicted by our data.

1 Aamont, Peterson and Philips, Phys. Rev. **88**, 799 (1952).

2 L. M. Soroko, Reports of the Institute for Nuclear Problems, 34 (1952); B. V. Gavrilovskii, ibid.

3 Iu. D. Prokoshkin and A. A. Tiapkin, Reports of the Institute for Nuclear Problems, 159 (1954).

4 A. H. Rosenfeld, Phys. Rev. **96**, 1714 (1954).

5 R. L. Wolfgang and G. Friedlander, Phys. Rev. **98**, 1871 (1955).

6 Crandall, Millburn, Pyle and Birnbare, Phys. Rev. **101**, 329 (1956).

7 Burcham, Symonds and Young, Proc. Phys. Soc. London **A68**, 1001 (1955).

8 Rosenfeld, Swanson and Warshaw, Phys. Rev. **103**, 413 (1956).

9 Friedlander, Hudis and Wolfgang, Phys. Rev. **99**, 263 (1955).

10 Chackett, Chackett, Peasbeck, Symonds and Warren, Proc. Phys. Soc. (London) **A69**, 43 (1956).

Translated by H. Kasha
41

Scattering of K Mesons with Change of Intrinsic Parity

V. B. Berestetskii and Iu. A. Bychkov

(Submitted to JETP editor October 25, 1956)
J. Exptl. Theoret. Phys. (U.S.S.R.) 32, 181-183
(January, 1957)

THE analysis of the experimental data on the decay of K mesons[1] leads, with a high degree of probability, to the conclusion that: 1) the spin of K mesons is equal to zero, and 2) K mesons can occur in states with different intrinsic parities, positive (θ mesons) and negative (τ mesons). In collisions of K mesons with nucleons there can occur changes of the intrinsic parities of the former (conversion of mesons into τ mesons and vice versa). For a consideration of some general features of such a process we shall represent the wave function Ψ of the system K meson + nucleon as a combination of two spinors ψ_θ and ψ_τ transforming differently on reflection,

$$\Psi = \begin{pmatrix} \psi_\theta \\ \psi_\tau \end{pmatrix}, \quad I\psi_\theta = \psi_\theta; \quad I\psi_\tau = -\psi_\tau,$$

where I is the operator of reflection.

In the scattering problem Ψ has, as usual, the following form

$$\Psi = u \exp(ik\,\mathrm{n}_0\mathrm{r}) + F(\mathrm{n})\, e^{ikr}/r,$$

where n_0 and n are unit vectors in the directions of the incident and scattered waves, and u and F are the corresponding amplitudes, which like Ψ, are two-spinor quantities. The amplitude F can be written in the form $F = Ru$, where R is a two-rowed matrix (each of its elements is a two-rowed matrix with respect to the spin variables).

If the properties of θ and τ mesons are the same as regards interaction with nucleons, this last relationship holds also for the "parity-conjugate" amplitudes

$$u' = C_p u; \quad F' = C_p F, \quad C_p = \begin{pmatrix} 0 & 1 \\ 1 & 0 \end{pmatrix},$$

where C_p is the operator of parity conjugation introduced by Lee and Yang[2].

Consequently, the matrix R must satisfy the condition $RC_p = C_p R$ and can be written in the form $R = a + bC_p$, where a is a scalar and b is a pseudoscalar (more precisely, corresponding matrices in the spin variables). The amplitude au describes the ordinary scattering (without change of intrinsic parity), and is of a form that is well known from the theory of scattering of spinor waves. Our aim is to find the general form of the amplitude bu that describes the scattering with change of intrinsic parity.

For this purpose we consider the relation between the incident and outgoing waves with definite values of the angular momentum and parity. We write it in the form

$$\Psi^{\mathrm{out}}_{jMg} = S(j, g)\, \Psi^{\mathrm{in}}_{jMg},$$

where j, M, and g are the quantum numbers for the angular momentum, one of its components, and the parity, and S is a two-rowed matrix in the same sense as R. We can write this matrix in the form

$$S(j, g) = \begin{pmatrix} S_{ll} & S_{ll'} \\ S_{l'l} & S_{l'l'} \end{pmatrix}, \quad g = (-1)^l = (-1)^{l'+1},$$

where $l = j \pm \frac{1}{2}$ is the orbital angular momentum of the meson and $l' = j \pm \frac{1}{2}$ is that of the τ meson. By the general symmetry properties of the S-matrix $S_{ll'} = S_{l'l}$.

Furthermore, since

$$\Psi_{jM-g} = C_p \Psi_{jMg},$$

the invariance of the interaction with respect to the parity-conjugation transformation leads to the relation

$$S(j, -g) = C_p S(j, g) C_p^{-1},$$

$$\text{i.e.} \quad S(j, -g) = \begin{pmatrix} S_{l'l'} & S_{ll'} \\ S_{l'l} & S_{ll} \end{pmatrix}.$$

We see that the off-diagonal elements $S_{ll'}$ do not depend on the parity g of the state.

We can now construct the expression for the scattering amplitude bu. For this purpose let us consider the amplitude u of an incident wave with components v, 0 ($a\theta$ meson). To this there correspond ingoing waves of the form

$$\Psi^{\mathrm{in}}_{jMg} = \begin{pmatrix} c\,\Omega_{jlM}(\mathrm{n}) \\ 0 \end{pmatrix} \frac{e^{-ikr}}{r}, \quad c = \frac{2\pi i^l}{k} (\Omega^*_{jlM}(\mathrm{n}_0)\, v),$$

where $g = (-1)^l$ and Ω_{jlM} is a spherical spinor[3].

The outgoing waves will be of the form

$$\Psi^{\mathrm{out}}_{jMg} = \begin{pmatrix} S_{ll}\; c\,\Omega_{jlM}(\mathrm{n}) \\ S_{ll'}\; c\,\Omega_{jl'M}(\mathrm{n}) \end{pmatrix} (-1)^{l+1} \frac{e^{ikr}}{r}$$

and consequently we have

$$bv = \frac{2\pi}{ik} \sum_{jlM} (\Omega^*_{jlM}(\mathrm{n}_0)\, v)\, \Omega_{jl'M}(\mathrm{n}).$$

By making use of the following transformations[3]

$$\Omega_{jl'M}(\mathbf{n}) = \sigma\,\mathbf{n}\,\Omega_{jlM}(\mathbf{n}),$$

$$\sum_M (\Omega^*_{jlM}(\mathbf{n}_0)\,u)\,\Omega_{jlM}(\mathbf{n}) = \frac{1}{4\pi}\left(\alpha_{jl} + \frac{\beta_{jl}}{i\sin\vartheta}[\mathbf{n}_0\mathbf{n}]\sigma\right),$$

$$\alpha_{jl} = (j+1/2)\,P_l(\cos\vartheta),\quad \beta_{jl}$$

$$= \mp P_l^1 \quad \text{for} \quad l = j \mp 1/2,\ \cos\vartheta = \mathbf{n}_0\mathbf{n}$$

(P_l and P_l^1 are Legendre functions), we have

$$\sum_M (\Omega^*_{jlM}(\mathbf{n}_0)\,v)\,\Omega_{jlM}(\mathbf{n}) = \sigma(\mathbf{n}\,r_{jl} + \mathbf{n}_0 q_{jl}),$$
$$r_{jl} = \beta_{jl}/\sin\vartheta;\quad q_{jl} = \alpha_{jl} - \beta_{jl}\,\mathrm{tg}\,\vartheta.$$

Use of well-known relations between Legendre polynomials leads to the equation

$$r_{j,\,j+1/2} + r_{j,\,j-1/2} = q_{j,\,j+1/2}$$

$$+ q_{j,\,j-1/2} = (d/d\cos\vartheta)(P_{j+1/2} - P_{j-1/2}).$$

Inserting all of this into the expression for b, we have finally

$$b = B(\vartheta)\,\sigma\,(\mathbf{n}_0 + \mathbf{n}),$$

$$B(\vartheta) = \frac{1}{2ik}\sum_j S_{j+1/2,\,j-1/2}\frac{d}{d\cos\vartheta}(P_{j+1/2} - P_{j-1/2}).$$

For small momenta we can retain in this expression only the term with $j = 1/2$, corresponding to transitions $s_{1/2} \leftrightarrows p_{1/2}$. Then B does not depend on the angles, and the differential cross-section for scattering with change of intrinsic parity takes the form

$$|b|^2 = \sigma_0(1 + \cos^2\vartheta),$$

where σ_0 is a constant and, according to general properties of the elements of the scattering matrix, $\sigma_0 \sim k^2$. Unfortunately, this dependence of the cross-section on angle and momentum is not sufficient by itself for an experimental singling-out of the process under consideration here, since the differential cross-section for ordinary scattering at small momenta contains an analogous dependence

$$|a|^2 = c_1^2 + c_2^2\cos^2\vartheta,$$

where c_1 and c_2 are constants (the first term corresponds to the s-wave and the second to interference between the s- and p-waves).

From the expression for b it follows that in this type of scattering no polarization of the nucleons occurs. But if the nucleon was polarized before the scattering, then the spin components perpendicular to the vector $n_0 + n$ change sign.

All the preceeding discussion applies also to the scattering of Σ and Λ particles by nuclei of spin 0, if the spin of these particles is equal to ½. The same expressions also describe the processes

$$K + N \to \Sigma + \pi;\quad K + N \to \Lambda + \pi,$$

with the amplitude b in this case referring to the appearance of a hyperon of the same intrinsic parity as the incident K particle (since an odd π meson is produced).

The writers express their sincere thanks to I. Ia. Pomeranchuk for many helpful discussions.

1 R. H. Dalitz, Phil. Mag. **44**, 1068 (1953); Phys. Rev. **94**, 1046 (1954). E. Fabri, Nuova Cimento **11**, 479 (1954). R. P. Haddock, Nuovo Cimento **4**, 240 (1956). C. N. Yang, Report at Rochester Conference, 1956.

2 T. D. Lee and C. N. Yang, Phys. Rev. **102**, 290 (1956).

3 Cf., e.g., A. Akhiezer and V. Berestetskii, *Quantum Electrodynamics*, Moscow 1953.

Translated by W. H. Furry
44

Absorption of γ-Quanta of 500 mev Mean Energy in Lead, Copper and Aluminum

M. D. Baiukov, M. Ts. Oganesian and A. A. Tiapkin

United Institute of Nuclear Studies, Laboratory for Nuclear Problems

(Submitted to JETP editor October 26, 1956)
J. Exptl. Theoret. Phys. (U.S.S.R.) 32, 183 (January, 1957)

WE measured the absorption coefficients of γ-quanta of 500 mev energy in Pb, Cu and Al. γ-quanta from the decay of π^0-mesons produced in the internal phasotron target by protons of 660 mev were registered by a 12 channel-pair γ-spectrometer. The spectrometer was placed at the distance of 23 m from the target. A device, periodi-

cally covering the γ-beam by a lead absorber, was placed before the collimator situated in a 4 meter thick shielding wall 13 meters from the spectrometer. A lead plate in the form of a half-disc, mounted on the reductor axis of an electric motor, periodically covered the γ-beam making 12 r.p.m. The counting of the γ-quanta registered by the spectrometer was done separately for the cases of the completely covered and completely uncovered beam.

For the purpose of the determination of the absorption coefficients of γ-quanta in Cu and Al by means of the same revolving device, the lead absorber was periodically changed by a copper and an aluminum absorber. A frequent change of the absorbers made it possible to carry out the measurements without a monitor and, besides, removed errors due to the time variation of the sensitivity of the spectrometer. The γ-beam, after traversing the collimator, was purified from electrons and positrons by a special magnet.

The values of the absorption coefficients (in cm^2/g) of γ-quanta of the energy $E_\gamma = 500 \pm 50$ mev, obtained in our work, are:

Pb : 0.1115 ± 0.0025; Cu : 0.0510 ± 0.0025;

Al : 0.0295 ± 0.0017.

The absorption of γ-quanta of $E_\gamma = 500$ mev is due basically to electron-positron pair production. The calculation shows that the absorption due to the photoeffect and the Compton effect amounts for Pb to $\sim 0.5\%$, for Cu to $\sim 1.2\%$ and for Al to $\sim 2\%$ of the total absorption cross-section.

The γ-absorption cross-sections obtained by us are in a good agreement with the results of calculations by Davies et al[1].

It should be noted that the results for γ-quanta of 500 mev, which are in agreement with the calculations, were obtained with a lead filter of the thickness 5.55 g/cm^2 permanently placed in the beam. The values of cross-sections obtained without this filter were 10% higher. No influence of such a filter was observed in measurements of the cross-section for 280 mev γ-quanta. The obtained value of the cross-section for 280 mev γ-quanta is in good agreement with Ref. 2. It has not been possible to explain the cause for the higher result for the absorption cross-section of 500 mev γ-quanta in the absence of the additional lead filter.

1 Davies, Bethe and Maximon, Phys. Rev. **93**, 788 (1954).

2 De-Wire, Askin and Blach, Phys. Rev. **83**, 505 (1951).

Translated by H. Kasha
45

A Physical Model of the Hyperon

G. D'ERDI (GYORGI)
Central Physical Research Institute, Cosmic Ray Division, Budapest

(Submitted to JETP editor August 2,1956)
J. Exptl. Theoret. Phys. (U.S.S.R.) 32, 152–154 (January,1957)

IN recent times a number of attempts have been made to reduce the number of particles that are regarded as "elementary" by regarding some of them as compound structures.[1–5] Some proposals of this sort are not in agreement with experiment and with the very successful phenomenological scheme of Gell–Mann, since they lead to charge states that most probably do not exist in nature.[3,5] The one that seems most natural is an early proposal of Goldhaber,[2] which, being applied in the light of our present knowledge, provides the correct charge multiplet of the hyperon and a very attractive picture of the interaction of baryons and heavy mesons.

We assume that hyperons are bound systems* of nucleons and $\bar{K}$–mesons, which, according to Gell–Mann, form a charge doublet $\bar{K}(\bar{K}^0, \bar{K}^-)$. The nucleon and the $\bar{K}$–meson can form singlet and triplet charge states. The singlet state can be identified with Λ°, the triplet with $\Sigma^+, \Sigma^0, \Sigma^-$. The qualitative features of the proposed interaction between K–mesons and nucleons are such that, in agreement with experiment, the binding forces are independent of the charge and depend only on the isotopic spin, the forces being larger for the antiparallel orientation of the isotopic spins. As a model for the Ξ–particle (which we assume to be a doublet) one can take the bound system of a Λ° or a Σ–particle and a $\bar{K}$-meson (doublet of the NKK system). According to the idea being developed here there must exist a hyperon with isotopic spin $T = 3/2$ and with a mass greater than the mass of the Ξ, if the interaction between the Σ and $\bar{K}$–particles is sufficiently strong to form a bound system with parallel isotopic spins. If there is no degeneracy, then there can exist other states with $T = 1/2$ besides the Ξ. For the state with $T = 1/2$ higher than the Ξ and for the components $T_3 = \pm 1/2$ of the state $T=3/2$

there is possible rapid decay to Ξ with emission of a γ–quantum, If the mass difference is large enough, the components $T_3 = \pm 3/2$ can also decay, via a strong interaction, to Ξ and a charged pion.

In connection with our considerations, the question can arise as to why bound systems are not formed of nucleons and $\bar{K}$ (K^+, K^0) particles in analogy with the systems $N\bar{K}$. To account for this, we assume that the interaction energy of the K–meson field and the field of the given nucleon changes its sign on charge conjugation applied to the K–meson variables

$$(K^+ \leftrightarrow \bar{K}^-,\ K^0 \leftrightarrow \bar{K}^0).$$

A similar situation is well known in quantum electrodynamics: the interaction energy of the Dirac field and a given electromagnetic field changes its sign on charge conjugation applied to the variables of the Dirac (for example, electron) field ($e^+ \leftrightarrow e^-$).

Then if the NK forces correspond to attraction, the forces between nucleon and K–particle correpond to repulsion and have the same magnitude.

If the principle of invariance under the parity transformation holds as formulated by Lee and Yang,[6] then the properties of the ϑ and τ particles are identical, except for the intrinsic spatial parity, and we can assume the existence of two-parity –conjugate states of types ($N\vartheta$) and ($N\tau$). The existence of such states has been predicted by Lee and Yang.

The operator of (strong) interaction between $\bar{K}$ and K mesons and nucleons is taken in the form

$$U = G_1 (\bar{\psi}\Omega_N \psi)(\bar{\chi}\Omega_K \chi) + G_2 (\bar{\psi}\tau\Omega_N \psi)(\bar{\chi}\tau\Omega_K \chi). \quad (1)$$

Here ψ is the operator of the nucleon field and χ is that of the K–meson field. Both functions are taken to be isotopic spinors of the first kind in accordance with the proposal of d'Espagnat and Prentki[7] (χ corresponds to the destruction of K^0 and K^+ particles and the creation of $\bar{K}^0$ and $\bar{K}^-\vartheta$); $\bar{\chi}$ has the reverse effect); Ω_N and Ω_K are operators acting on the space and spin coordinates.

The bilinear form of the interaction energy (1) in the operators $\bar{\chi}$ and χ, which is a consequence of the isotopic spinor nature of the K–particles and the postulate of charge invariance,[7] provides for the joint creation of K and $\bar{K}$ particles. If a $\bar{K}$–particle (or more than one of such particles) is created in a bound state with a nucleon, then we have to do with associated productions of types $\rightarrow K\Lambda, K\Sigma, KK\Xi$, predicted by Gell–Mann's theory.

According to our hypothesis the decay $\vartheta \rightarrow 2\pi$ occurs because of a direct weak boson–fermion interaction of the type diccussed by Oneda:[8]

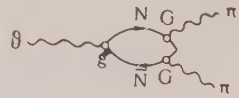

The same coupling with the constant g leads to the decay of the hyperon:

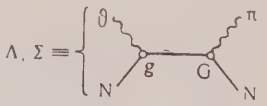

It is easily seen that if our considerations are correct, they provide a physical basis for the phenomenological classification of particles and types of interactions given by Gell–Mann. The "strangeness" quantum number receives a simple interpretation: in our model it is identical with the difference N_k between the number of K–particles and the number of $\bar{K}$ (anti–K) particles. N_K is a constant of the motion for strong interactions. For strong interactions there is conservation of the number ϑ of elementary isotopic fermions, given by the sum of N_K and N_N (number of nucleons minus number of antinucleons). But N_N itself is separately conserved since, according to our conception, all nucleons are elementary baryons, and thus the number of heavy particles (a constant of the motion) is just N_N . Therefore $S = N_K$, is conserved in all fast reactions. The weak interaction of K–mesons with nucleons destroys the conservation of N_K .

The writer is deeply grateful to Prof. I. Kovach and Prof. K. F. Novobatskii, who provided him with the possibility of working in the favorable atmosphere of the Institute of Theoretical Physics of Eötvös University. The writer also thanks his friend G. Marks for advice and discussions.

---

* The situation here is analogous to that occurring in the interaction of electrons. The number of electrons minus the number of antielectrons is conserved as long as only the electromagnetic interaction is considered. But the weak (β-decay) interaction of electrons with nucleons destroys this conservation law.

1 E. Fermi and C. Yang, Phys. Rev. 76, 1739 (1949).
2 M. Goldhaber, Phys. Rev. 92, 1279 (1953).

3 M. Gell-Mann and A.Pais, Proc. Int. Conf. Glasgow, Pergamon Press, 1955.
4 S. Filippov, J. Exptl. Theoret. Phys. (U.S.S.R.) 29, 707 (1955). Soviet Phys. JETP 2, 572 (1956).
5 V. Karpman, J.Exptl. Theoret. Phys. (U.S.S.R.) 30, 781 (1956). Soviet Phys. JETP 3, 754 (1956).
6 T. Lee and C.Yang , Phys. Rev. 102, 290 (1956).
7 B. d'Espagnat and I. Prentki, Nucl. Phys. 1, 33 (1956).
8 S. Oneda and A. Wakasa, Nucl. Phys. 1, 445 (1956)

Translated by W. H. Furry
28

On the Structure of Nucleons

I. E. TAMM
P. N. Lebedev Physical Institute, Academy of Sciences, USSR

(Submitted to JETP editor October 26,1956)
J. Exptl. Theoret. Phys. (U.S.S.R.) 32, 178–180 (January,1957)

COMPARISON of the results of the measurements of the scattering of fast electrons (with energy up to 550 mev) by protons, carried out by Chambers and Hofstadter.[1] with measurements of the interaction of electrons with neutrons[2,3] has led a number of physicists to the conclusion that these data as a whole are in contradiction either with the charge independence of the interaction of π–mesons with nucleons, or else with the foundations of quantum electrodynamics. The purpose of this note is to present arguments against the legitimacy of this sort of conclusions.

The most direct argument in favor of the conclusion mentioned has been formulated by Yennie, Lévy and Revenhall[4]; it reduces to the following. Chambers and Hofstadter have shown that the root–mean-square radius of the electric charge distribution of the proton is close to the value

$$r_p = 0.77 \cdot 10^{-13}\,\text{cm} = 0{,}55\,\hbar/\mu c. \qquad (1)$$

On the other hand, if the interaction of π–mesos with nucleons is charge invariant, then the meson clouds of proton and neutron must be mirror–symmetric (identical charge distributions, but with opposite signs). Therefore if, following Saks, one superposes the charge densities of proton and neutron, their meson charges cancel mutually and we obtain the charge density of the so–called "core" of the nucleus , i.e., the charge density due to the distribution of just the single nucleons and of nucleon pairs:

$$\rho_c(r) = \rho_p(r) + \rho_n(r).$$

Using the above–mentioned experimental data, Yennie et al, found that the root mean square radius of the charge of the core is practically equal to r_p :

$$r_c \sim r_p \sim 0.77 \cdot 10^{-13}\,\text{cm} \sim 3.7\,\hbar/Mc. \qquad (2)$$

It is just this result that is regarded as paradoxical, and for the following reason. If we confine ourselves to the consideration of mesons with energies less than μc^2, then the recoil in the emission of a meson by a "bare" nucleon can be neglected, so that the nucleon must be in the center of the physical nucleon ($r_c \sim 0$), while the radius of the distribution of mesons must be of the order $\hbar/\mu c$, which does not contradict Eq. (1), but does contradict Eq. (2). But in the case of emission of mesons with energies of the order of μc^2, it is necessary to take into account the recoil experienced by the nucleons, and owing to the recoil, the nucleons will be displaced by about the same distance as the mesons; but this distance must be of the order of $\hbar/Mc$. According to Eq. (2), however, r_c is considerably greater than this value.

In my opinion, the argument that has been presented is based, though not obviously, on the idea of weak interaction of mesons with nucleons.

Since in reality this interaction is strong, each meson must be dissociated for an appreciable fraction of the time into a ϑ nucleon–antinucleon pair. Therefore, the distribution of these pairs (which by definition forms part of the core of the nucleon) must be just about the same as the meson distribution itself

$$(r \sim \hbar/\mu c),$$

in accordance with Eq. (2).

It is true that if we confine ourselves to consideration of processes of the type $\pi \to N + \tilde{N} \to \pi$ (where $\tilde{N}$ denotes an antinucleon), then the charge of the nucleon pairs will be distributed in just the same way as the charge of the mesons, and consequently cancels out in the calculation of the quantities p_c and r_c . But measurements by Segrè and others have shown that the cross–section for annihilation of antiprotons on nucleons is very large* (which is quite understandable from the point of view of meson theory). Therefore the antinucleons produced at the mesonic periphery of the physical nucleon will have a large probability of being annihilated with the nucleon located at its center, being created again, and so on. The result is that the charges of all the nucleons and antinucleons (i.e., the charge of the core) is distributed more or less uniformly over the whole

volume of the meson cloud, in agreement with Eqs. (1) and (2).

The ideas that have been explained here also agree entirely with the fact[1] that there are no experimental indications of any concentration of the charge of the proton near its center.

If the total charge of the nucleon is indeed distributed over its whole volume then there cannot be mirror symmetry of the charge distributions even in the peripheral regions of proton and neutron. This, however, does not necessarily have to be in contradiction with the mirror symmetry of their anomalous magnetic moments, since, in view of the difference of the masses of meson and nucleon, these moments are probably mainly due to meson (and not to nucleon) currents, and the meson currents have mirror symmetry owing to the charge invariance.

We take note of one further misunderstanding in connection with the structure of nucleons. In nonrelativistic approximation, the interaction between the electromagnetic field and an (on the whole) neutral particle with spherically symmetric charge distribution (a neutron) is characterized by a potential energy

$$V = -a \operatorname{div} \mathrm{E}. \qquad (3)$$

Foldy[5] pointed out that the experimental value of the constant a for the neutron is very close to the value

$$a_m = (h/2Mc)\,\mu_n$$

(where μ_n is the magnetic moment of the neutron) which corresponds in nonrelativistic approximation to a Dirac particle having a relativistic interaction with the electromagnetic field given by the Pauli term

$$(i/2)\,\mu_n \gamma^\alpha \gamma^\beta F_{\alpha\beta}.$$

According to the latest experimental data[2,3], the difference between a and a_m amounts to only 2 ± 7 percent. Thus there is practically nothing left of the interaction of the neutron with the electric field to correspond to the electric charge in it.

On the other hand, if we estimate this latter part of the interaction, starting from the usual model of the neutron (a small positive core, surrounded by a negative meson cloud of radius of the order $\hbar/\mu c$) this contribution to the quantity a must be several times as large as the whole experimental value of a.

This contradiction is removed if we adopt the model of nucleons described in this note: they contain inside them nucleons and antinucleons distributed according to approximately the same law as the π mesons, an since the total charge of the neutron is equal to zero, the charge density in it is close to zero and the contribution it makes to the value of a must be small.

It is necessary, however, to register the objection that both attempts to estimate the value of the difference $a - a_m$ from a definite model of the neutron are unreliable. In the phenomenological theory

$$a = a_m + a',$$

where the value of the constant a' is entirely arbitrary (in the relativistic theory a' appears in an interaction term

$$a' \gamma_\alpha \partial F^{\alpha\beta} / \partial x^\beta).$$

A direct calculation, starting from a definite (relativistic) model of nucleons, can determine the dependence of the quantity a' on the distribution of charges in the particle. It is hard to foresee the result of these calculations. Thus, for example, from calculations conducted according to meson theory by perturbation method and including the second order in g, it is found [6] that $a' = 0.32\, a_m$. But in any case there is at present no reason to suppose that the so-called zero value of the electrical radius of the neutron (i.e., the equation $a - a_m \approx 0$) is not consistent with charge invariance.

From the point of view of the ideas that have been presented here, theories that do not take into account the production of nucleon pairs by mesons (for example, the theory of Chew and Low) cannot be expected to give a successful explanation of the structure of nucleons. An exact theory of nucleons must also take account of the peculiar properties of the cloud of virtual K-mesons occurring around a nucleon.[7]

---

*According to data presented at the Conference on Theoretical Physics in Seattle in September 1956, this cross-section is equal to 120 to 100 mb at antiproton energies 200 to 500 mev.

1 E. E. Chambers and R. Hofstadter, CERN Symposium, 1956.
2 Hughes, Harvey, Goldberg and Stafne, Phys. Rev. 90, 497 (1953).
3 Melkonian, Rustad, and Havens, Jr. Bull. Am. Phys. Soc. 1, 62 (1956).
4 M. Levy, Report at the Moscow Conference on High-Energy Physics, May, 1956.
5 L. L. Foldy, Phys. Rev. 87, 693 (1952).
6 B. D. Fried, Phys. Rev. 88, 1142 (1952).
7 G. Sandri, Phys. Rev. 101, 1616 (1956).

Translated by W. H. Furry
42

CONTENTS – *continued*

CONTENTS

(*contents continued on inside back cover*)